UNIVERSITÀ DEGLI STUDI DI VERONA

DEPARTMENT OF

Neurosciences, Biomedicine and Movement Sciences

DOCTORAL PROGRAM IN

Applied Life and Health Sciences

WITH THE FINANCIAL CONTRIBUTION OF

Ateneo – University of Verona

Cycle /year (1° year of attendance) XXXVIII / Year 2022

TITLE OF THE DOCTORAL THESIS

CRISPR/Cas9-mediated genome editing: evaluation of different experimental approaches to edit cell lines

S.S.D. BIOS-08/A

Coordinator: Prof. Simone Accordini

Supervisor: Prof. Donato Zipeto

Co-Supervisor: Dr. Alessandra Ruggiero

Doctoral Student: Dr. Mauro Voi

Sommario

La CRISPR/Cas9 è una delle tecnologie di maggior successo usate per l'editing genomico in modelli eucariotici. Il suo meccanismo versatile si basa sull'uso di una guida a RNA (gRNA) disegnata per riconoscere una sequenza target nel genoma e guidare l'enzima Cas9 a tagliare il sito bersaglio. La rottura a doppio filamento (DSB) indotta può essere riparata da meccanismi cellulari come il non-homologous end joining (NHEJ), che può causare l'inserzione o la delezione di nucleotidi. Questo può indurre frameshift, risultando nell'introduzione di un codone di stop prematuro e consentendo il knockout genico. A seconda del gene target, della linea cellulare e dello scopo biologico, l'esperimento CRISPR/Cas9 può richiedere un'attenta ottimizzazione. In questo studio, abbiamo inizialmente utilizzato la tecnologia CRISPR/Cas9 per indurre il knockout di diversi geni in differenti linee cellulari, adottando diverse strategie di knockout a seconda dell'efficienza di trasfezione della linea cellulare target o dello scopo biologico finale. I geni target sono stati selezionati perché coinvolti in pathway tumorali o perché svolgono un ruolo chiave nelle infezioni virali.

Abbiamo effettuato il knockout del gene ACOT8 nella linea cellulare HEK293T, colpendo l'esone 1 con un singolo gRNA, per generare un modello per lo studio dell'infettività di HIV-1 in assenza di ACOT8, una tioesterasi che interagisce con la proteina virale HIV-1 Nef. Gli pseudovirus prodotti in cellule ACOT8-KO hanno mostrato un'infettività significativamente ridotta sulle cellule target, un effetto osservato solo per virus con envelope HIV. La produzione di virus pseudotipizzati con QHO di HIV-1 in cellule ACOT8 KO ritrasfettate con un plasmide ACOT8 ha portato ad un aumento di infettività nelle cellule target a livelli comparabili dello stesso pseudovirus prodotto in cellule WT. Ciò conferma il ruolo specifico di ACOT8 nel mediare la produzione di particelle virali più o meno infettive. In secondo luogo, l'interazione tra ACOT8 e NEF e la conseguente infettività delle particelle virali prodotte sono state valutate con l'aggiunta di plasmidi NEF. Questo ha dimostrato che l'interazione ACOT8/Nef nelle cellule produttrici di virus porta alla produzione di particelle virali più infettive, supportando un ruolo chiave per ACOT8 e ACOT8/Nef nell'infettività di HIV-1.

Abbiamo poi utilizzato la tecnologia CRISPR/Cas9 per identificare il ruolo di alcuni geni coinvolti in pathway tumorali, iniziando da HADHA nelle cellule di cancro al pancreas (PANC-1). Questo gene codifica un enzima mitocondriale coinvolto nel metabolismo lipidico, che è stato rilevato sovraespresso nelle cellule staminali del carcinoma pancreatico. Abbiamo quindi adottato un approccio a due guide per colpire l'esone 1 di HADHA, isolando un singolo clone KO per una linea risultata difficile da trasfettare. Utilizzando il modello HADHA-KO PANC-1, abbiamo osservato che la perdita di HADHA non influisce sulle proprietà staminali del tumore al pancreas, con le cellule staminali di carcinoma pancreatico (PCSCs) HADHA KO che formano tumourspheres più compatte e dense rispetto alle cellule staminali wild-type.

Il knockout genico mediato da CRISPR/Cas9 è stato poi applicato per generare modelli cellulari knockout al fine di valutare il ruolo biologico di geni specifici in altri due tipi di cancro, come melanoma e osteosarcoma. Nel primo caso, abbiamo colpito il gene RUNX2, un fattore di trascrizione sovraespresso nelle cellule di melanoma, in cellule di melanoma murino (B16) con un approccio a singola gRNA e a doppia gRNA. I due diversi setup sperimentali ci hanno permesso di ottenere sia cellule RUNX2 KO, sia cellule con delezione del dominio Runt, essenziale per il legame al DNA. Entrambi i modelli saranno utilizzati per descrivere meglio il ruolo di RUNX2 nella progressione del melanoma.

Nel secondo caso, abbiamo utilizzato CRISPR/Cas9 per colpire FBXW11 nelle cellule di osteosarcoma MG63. Il gene target codifica un'ubiquitina ligasi coinvolta nella degradazione di prodotti cellulari in differenti pathway. Le cellule MG63 hanno richiesto un'attenta ottimizzazione del protocollo CRISPR/Cas9, poiché la trasfezione del plasmide esprimente Cas9/gRNA non ha funzionato su queste cellule. Pertanto, abbiamo utilizzato un plasmide CRISPR più piccolo per trasfettare cellule MG63 precedentemente trasdotte per esprimere stabilmente la proteina Cas9, ottenendo così un moderato aumento dell'efficienza di editing. Infine, abbiamo adottato la trasduzione con virus-like particles (VLP), un sistema non integrativo ed efficiente per la delivery del complesso ribonucleoproteico Cas9/gRNA, consentendoci di aumentare considerevolmente l'efficienza di editing nelle cellule MG63. Dopo la trasduzione con VLP e la conferma della corretta

efficienza di editing su FBXW11, abbiamo isolato un clone MG63 FBXW11 KO che sarà utilizzato come modello per valutare cambiamenti nei pathway molecolari e nella crescita tumorale dovuti all'assenza di FBXW11.

Abbiamo poi lavorato per ottimizzare altre applicazioni della tecnologia CRISPR. In particolare, abbiamo lavorato con la tecnologia del prime editing, un approccio innovativo basato su CRISPR per la prima volta sviluppato nel 2019. La tecnica permette di eseguire modifiche a singolo nucleotide utilizzando un enzima "prime editor", composto da una Cas9 nickasi e una transcrittasi inversa di MMLV, che copia nel genoma l'informazione trasportata da una guida specializzata, chiamata pegRNA. Abbiamo applicato questa tecnologia nel contesto della displasia cleidocranica (CCD), una malattia scheletrica causata da mutazioni nel gene RUNX2. Nel nostro approccio, ne abbiamo dimostrato l'applicazione sulle cellule HEK293T, introducendo la mutazione desiderata (RUNX2, c.505 C>T) in queste linee cellulari, che sono state successivamente utilizzate come modello per esperimenti di prime editing volti a correggere la mutazione. La procedura ha richiesto l'ottimizzazione di diverse condizioni di editing per identificare infine il miglior sistema per introdurre o correggere questa mutazione patogenica.

Abbiamo infine usato la CRISPR/Cas9 per il knockout del gene HLA-C in cellule HEK293T. Le cellule generate sarebbero state poi ri-trasfettate con diversi plasmidi esprimenti HLA-C per creare modelli per investigare la stabilità del complesso HLA-C/beta-2-microglobulina/peptide per i vari allotipi HLA-C. Il nostro scopo era quello di fornire una più accurata classificazione della stabilità di legame con peptidi degli allotipi HLA-C e dimostrare la sua associazione con l'infezione di HIV-1. Nonostante questi esperimenti di setup iniziali, un altro lavoro condotto da Sarkizova et al. aveva già ri-trasfettato allotipi HLA-C in cellule HLA-deficienti e determinato sperimentalmente i peptidi leganti ai diversi allotipi in questione. Abbiamo quindi deciso di utilizzare questi peptidi per analisi bioinformatiche sull'associazione di legame con gli allotipi HLA-C per studiarne la stabilità di legame con peptidi di HLA-C. Per ottenere ciò, abbiamo utilizzato uno strumento bioinformatico (NetMHCpan4.2) per determinare i punteggi di stabilità per i 21 alleli HLA-C umani più frequenti. Questo software ci ha permesso di determinare quantitativamente l'associazione di legame tra gli allotipi HLA-C considerati e

specifici pool di peptidi leganti. Abbiamo poi genotipizzato diversi pazienti HIV-1 positivi per HLA-C e assegnato a ciascun paziente un punteggio di stabilità HLA-C. I nostri risultati hanno dimostrato che i pazienti con rapida progressione all'AIDS e i pazienti con deficit neurologici associati all'HIV-1 mostrano valori di stabilità HLA-C più bassi rispetto ai pazienti con progressione più lenta della malattia e ai pazienti senza deficit neurologici, rispettivamente. Il nostro studio ha confermato il ruolo di HLA-C come un fattore genetico che può determinare diversi esiti dell'infezione da HIV-1.

Abstract

CRISPR/Cas9 is one of the most successful technologies used for genome editing in eukaryotic models. Its versatile mechanism is based on the use of guide RNA (gRNA), designed to recognise a target sequence in the genome and guide the Cas9 enzyme to cut the targeted site. The induced double-strand break (DSB) can be repaired by cellular mechanisms such as non-homologous end joining (NHEJ), which can cause the insertion or deletion of nucleotides. This can induce frameshifts, resulting in the introduction of a premature stop codon and allowing gene knockout. Depending on the target gene, cell line, and biological purpose, the CRISPR/Cas9 experiment may require careful optimisation. In this study, we initially used CRISPR/Cas9 technology to induce the knockout of several genes in different cell lines, adopting different knockout approaches depending on the transfection efficiency of the target cell line or the final biological aim. The target genes were selected because they are involved in tumour pathways or play a key role in viral infections.

We knocked out the ACOT8 gene in the HEK293T cell line by targeting exon 1 with a single gRNA to generate a model for studying HIV-1 infectivity in the absence of ACOT8, a thioesterase interacting with the viral HIV-1 Nef protein. Pseudoviruses produced in ACOT8-KO cells showed significantly reduced infectivity on target cells, an effect that was only observed for viruses with HIV envelopes. The production of HIV-1 QHO-pseudotyped viruses in ACOT8 KO cells re-transfected with an ACOT8 plasmid increased infectivity in target cells to levels comparable to those of the same pseudovirus produced in WT cells. This confirms the specific role of ACOT8 in mediating the production of more or less infectious viral particles. Secondly, the interaction between ACOT8 and NEF, and the resulting infectivity of the viral particles produced, were evaluated with the addition of NEF plasmids. This demonstrated that the ACOT8/Nef interaction in virus-producing cells leads to the production of more infectious viral particles, supporting a key role for ACOT8 and ACOT8/Nef in HIV-1 infectivity.

We then used CRISPR/Cas9 technology to identify the role of certain genes in tumour pathways, starting with HADHA in pancreatic cancer cells (PANC-1). This gene encodes for a mitochondrial enzyme involved in lipid metabolism, which was

found to be overexpressed in pancreatic cancer stem cells. We then used a two-guide approach to target exon 1 of HADHA, isolating a single KO clone for a line that proved difficult to transfect. Using the HADHA-KO PANC-1 model, we observed that loss of HADHA does not affect pancreatic cancer stemness, with the HADHA KO- pancreatic cancer stem cells (PCSCs) forming more compact and denser tumourspheres compared to wild-type pancreatic cancer stem cells.

CRISPR/Cas9-mediated gene knockout was then applied to generate knockout cell models in order to evaluate the biological role of specific genes in two other cancer types, such as melanoma and osteosarcoma. In the first case, we targeted the RUNX2 gene, a transcription factor overexpressed in melanoma cells, in mouse melanoma cells (B16) with a single and dual gRNA approach. The two different experimental setups allowed us to obtain both RUNX2 KO cells and cells deleted for the Runt domain, essential for DNA binding. Both models will be used to better depict the RUNX2 role in melanoma progression. In the second case, we used CRISPR/Cas9 to target FBXW11 in osteosarcoma MG63 cells. The targeted gene encodes a ubiquitin ligase involved in the degradation of cellular products across different pathways. MG63 cells required a careful optimisation of the CRISPR/Cas9 protocol, since transfection of Cas9/gRNA plasmid did not work on these cells. Therefore, we used a smaller CRISPR plasmid to transfect MG63 cells previously transduced to stably express Cas9 protein, thus gaining a moderate increase in editing efficiency. Finally, we adopted transduction with virus-like particles (VLPs), a non-integrating and efficient system for delivering Cas9/gRNA ribonucleoprotein complex, thus allowing us to considerably increase editing efficiency in MG63 cells. After VLP transduction and confirmation of the proper editing efficiency on FBXW11, we isolated an FBXW11 KO MG63 clone that will be used as a model to evaluate changes in molecular pathways and tumour growth due to its absence.

We further worked to optimise other applications of the CRISPR technology. In particular, we worked with the prime editing technology, an innovative CRISPR-based approach first developed in 2019. The technique allows to perform single nucleotide modifications by using a prime editor enzyme, composed of a Cas9 nickase and an MMLV reverse transcriptase, which copies the information carried

by a specialised guide, called pegRNA, into the genome. We applied this technology in the context of cleidocranial dysplasia (CCD), a skeletal disease caused by mutations in RUNX2 gene. In our approach, we demonstrated its application in HEK293T by introducing the desired mutation (RUNX2, c.505 C>T) in these cell lines, which have been subsequently used as a model for prime editing experiments aimed at correcting the mutation. The procedure required the optimisation of different editing conditions to finally identify the best system for introducing or correcting this pathogenic mutation.

We finally used CRISPR/Cas9 to knockout HLA-C gene in HEK293T cells. The generated cell lines would have been re-transfected with different HLA-C-expressing plasmids to create models for investigating the stability of the HLA-C/beta-2-microglobulin/peptide complex for various HLA-C allotypes. Our aim was to provide a more accurate classification of peptide binding stability of HLA-C allotypes and demonstrate its association with HIV-1 infection. Despite these initial experimental setups, another study conducted by Sarkizova et al. had already re-transfected HLA-C allotypes into HLA-deficient cells and experimentally determined the peptides binding to the different allotypes considered. We therefore decided to use these peptides for bioinformatic analyses on the binding association with HLA-C allotypes to further study the stability of the HLA-C complex. To achieve this, we used a tool (NetMHCpan4.2) to determine stability scores for the 21 most frequent human HLA-C alleles. This software allowed us to quantitatively determine the binding association between the considered HLA-C allotypes and specific pools of binding peptides. We then genotyped HIV-1 patients for HLA-C and assigned each patient an HLA-C stability score. Our results demonstrated that patients with rapid progression to AIDS and patients with HIV-1-associated neurological impairment had lower HLA-C stability values than patients with slower AIDS progression to the disease and patients without neurological deficits, respectively. Our study confirmed the role of HLA-C as a genetic factor that can determine different outcomes of HIV-1 infection.

INDEX

Abbreviations

AATD	α1-antitrypsin deficiency
AAV	Adeno-associated virus
ABE	Adenine base editor
ABL	Non-receptor tyrosine kinase Abelson
ACOT8	Acyl-CoA thioesterase 8
AD	Alzheimer's disease
AdV	Adenovirus
AIDS	Acquired immunodeficiency syndrome
APOBEC1	Apolipoprotein B mRNA editing enzyme catalytic subunit 1
AUC	Area under the curve
AuNP	Gold nanoparticles
BA	Binding affinity
BCR	Breakpoint cluster region
BE	Base editor
BER	Base excision repair
Bp	Base pair
CAR-T	Chimeric antigen receptor T-cell
Cas	CRISPR-associated protein
Cascade	CRISPR-associated complex for antiviral defense
CBE	Cytosine base editor
CCD	Cleidocranial dysplasia
CCR5	C-C chemokine receptor type 5
ChIP-seq	Chromatin immunoprecipitation sequencing
CIRCLE-Seq	Circularization for *in vitro* reporting of cleavage effects by sequencing
CML	Chronic myeloid leukemia
Cmr	Cas module RAMP
cOA	Cyclic oligoadenylate
CoASH	Coenzyme A
COL7A1	Collagen type VII alpha 1 chain

COSMID	CRISPR off-target sites with mismatches, insertions, and deletions
Cpf1	CRISPR from *Prevotella* and *Francisella* 1
CPP	Cell-penetrating peptides
CRISPR/Cas	Clustered regularly interspaced short palindromic repeats/ CRISPR-associated genes
CRISPRa	CRISPR activation
CRISPRi	CRISPR interference
crRNA	CRISPR RNA
Csf1	CRISPR-associated protein 1
Csf2	Cas7-like protein
Csm	Cas subtype Mtube
CTL	Cytotoxic T lymphocyte
CXCR4	C-X-C chemokine receptor type 4
dCas9	Deactivated Cas9 or dead Cas9
DECODR	Deconvolution of complex DNA repair
DISCOVER-seq	Discovery of *in situ* Cas off-targets and verification by sequencing
DMD	Duchenne muscular dystrophy
DMEM	Dulbecco's Modified Eagle Medium
DSB	Double-strand break
ECH	Enoyl-CoA hydratase
ecTadA	*Escherichia coli* transfer RNA adenosine deaminase
EL	Eluted ligand
EMT	Epithelial-mesenchymal transition
ER	Endoplasmic reticulum
FACS	Fluorescence-activated cell sorting
FBS	Fetal bovine serum
FBXW11	F-box and WD repeat domain containing 11
Fw	Forward
Gag	Group-specific antigen
GFP	Green fluorescent protein

GMO	Genetically modified organism
gRNA	Guide RNA
HACD	Hydroxyacyl-CoA dehydrogenase
HADHA	Hydroxyacyl-CoA dehydrogenase trifunctional multienzyme complex subunit alpha
HADHB	Hydroxyacyl-CoA dehydrogenase trifunctional multienzyme complex subunit beta
HAND	HIV-associated neurocognitive disorders
HD	Huntington's disease
HDR	Homology-directed repair
HEK	Human embryonic kidney
HEPN	Higher eukaryotes and prokaryotes nucleotide-binding
HER2	Human epidermal growth factor receptor 2
HIV-1	Human immunodeficiency virus type 1
HLA-A	Human leukocyte antigen-A
HLA-B	Human leukocyte antigen-B
HLA-C	Human leukocyte antigen-C
HNH	Histidine-asparagine-histidine motif
HPV	Human papillomavirus
HSF1	Heat shock factor 1
ICE	Inference of CRISPR Edits
IGF1R	Insulin-like growth factor 1 receptor
iMSC	Induced mesenchymal stem cells
INDEL	Insertion/deletion
iPSC	Induced pluripotent stem cells
Kb	Kilobase
KIR	Killer Ig– related receptor
KO	Knockout
KRAB	Krüppel associated box
Lck	Lymphocyte-specific protein tyrosine kinase
LNP	Lipid nanoparticles
LTNP	Long-term non-progressors

LTR	Long terminal repeat
LV	Lentivirus
MD	Molecular dynamics
MeCP2	Methyl-CpG binding protein 2
MiR	MicroRNA
MLH1dn	Dominant-negative MutL Homolog 1
MLV	Murine leukemia virus
MM-GBSA	Molecular mechanics-generalized Born surface area
MMLV	Moloney murine leukemia virus
MMR	Eukaryotic mismatch repair
MN / MegN	Meganucleases
MOI	Multiplicity of infection
MRE11	Meiotic recombination 11
mTOR	Mammalian target of rapamycin
nCas9	Cas9 nickase
Nef	Negative regulatory factor
ngRNA	Nicking guide
NGS	Next-generation sequencing
NHEJ	Non-homologous end joining
NK	Natural killer
NLS	Nuclear localization signal
NMD	Nonsense-mediated mRNA decay
NUC lobe	Nuclease lobe
P	Progressors
PAM	Protospacer adjacent motif
PBMC	Peripheral blood mononuclear cells
PBS	Primer binding site
PCR	Polymerase Chain Reaction
PCSC	Pancreatic cancer stem cells
PD	Parkinson's disease
PDAC	Pancreatic ductal adenocarcinoma
pDNA	Plasmid DNA

PE3ΔRnH	RNase H-deleted PE enzyme
PEG	Polyethylene glycol
pegRNA	Prime editing RNA
PKU	Phenylketonuria
Pol III	RNA polymerase III
Pro	Protease
pre-crRNA	Long precursor RNA molecule
REC lobe	Recognition lobe
Rev	Reverse
RLU	Relative light unit
RNAi	RNA interference
RNF2	RING finger protein 2
RNP	Ribonucleoprotein
RT	Reverse transcriptase
RUNX2	Runt-related transcription factor 2
RuvC	Crossover junction endodeoxyribonuclease domain
RVD	Repeat-variable diresidues
SaCas9	*Staphylococcus aureus* Cas9
SALL1	Spalt-like transcription factor 1
SAM	Synergistic activation mediator
SARS-CoV-2	Severe acute respiratory syndrome coronavirus 2
SCF	SKP1-CUL1-F-box
scFv	Single-chain variable fragment
SD	Standard deviation
SDS3	Sin3A corepressor complex component 3
SDS-PAGE	Sodium dodecyl sulfate polyacrylamide gel electrophoresis
SERPINA1	Serine protease inhibitor, clade A, member 1
sgRNA	Single guide RNA
SITE-Seq	Selective enrichment and identification of tagged genomic DNA ends by sequencing
SpCas9	*Streptococcus pyogenes* Cas9
ssODN	Single-stranded oligodeoxynucleotides

TALEN	Transcription activator-like effector nucleases
TAP	Transporter associated with antigen processing
TBS-T	Tris-Buffered Saline with 0.1% Tween-20
TevopreQ1	Trimmed prequeosine$_1$-1 riboswitch aptamer
TFP	Mitochondrial trifunctional protein
TGF-β	Transforming growth factor-beta
TGF-βR1	Transforming growth factor-beta receptor type 1
TIDE	Tracking of indels by decomposition
TracrRNA	Trans-activating crRNA
U6	U6 small nuclear RNA (snRNA) promoter
UGI	Uracil glycosylase inhibitor
UTR	Untranslated region
VLP	Virus-like particle
VPR	VP64-p65-Rta
VSV-G	Vesicular stomatitis virus G-protein
WB	Western blot
WT	Wild-type
ZFN	Zinc finger nucleases
ZIM3	Zinc finger imprinted 3
β_2m	β2-microglobulin

1. INTRODUCTION

1.1 Introduction to genome editing techniques: pre-CRISPR methods

Genome editing refers to the process of introducing modifications into an organism's DNA, allowing alterations of its genetic sequence (Doudna and Charpentier 2014). The first attempts to modify genomes date back to the 1970s, when researchers managed to integrate genetic information into the yeast genome (Hinnen, Hicks, and Fink 1978). Soon after, the possibility of introducing new genetic elements was also demonstrated in mammalian cell models, as shown by experiments conducted on mouse embryonic stem cells in the late 1980s (Thomas and Capecchi 1987).

Since then, different techniques for genome engineering have emerged, aiming to perform precise genetic modifications, including meganucleases (MNs), zinc finger nuclease (ZFNs) and transcription activator-like effector nucleases (TALENs). Although these approaches have been proven to enable genome editing, they were often characterised by a complex design process and a limited target specificity (Khalil 2020). The real revolution in the field was represented by CRISPR/Cas9 which, originally identified as a bacterial adaptive immune system, has been later engineered and widely used for its versality in introducing precise genetic modifications (Jinek et al. 2012).

Genome editing technologies have contributed significantly to advancements in scientific research, from understanding gene function in basic biology to the development of targeted gene therapies. The continuous improvements and optimisation of these techniques can drive new significant discoveries, contributing to promising applications of gene therapy in different areas, such as cancer research, viral diseases or genetic disorders (Li et al. 2020).

1.1.1 The first genome editing techniques: MNs, ZFNs and TALENs.

The use of designed nucleases has allowed researchers to develop different platforms for genome editing in various cell types and organisms. These technologies exploit these nuclease enzymes and their ability to induce double-

strand breaks in the target genome to induce genetic modifications (Silva et al. 2011).

Before the advent of CRISPR/Cas9 technology, three main nuclease-based approaches were developed, consisting of meganucleases, zinc finger nucleases and transcription activator-like effector nucleases.

Meganucleases (MNs or MegNs), also known as homing endonucleases, are a class of enzymes naturally encoded in the genomes of eukaryotic mitochondria and chloroplasts, as well as in different forms of microbial life. Among the different families classified by sequence and structural motifs, the LAGLIDADG meganucleases were the most used for genome editing purposes. These enzymes assemble as homodimers or monomeric pseudodimers and are able to specifically recognize and cut DNA sequences between 14-40 base pairs. Homing endonucleases have served as a template for the design of new endonucleases that can broaden the enzyme's targeting window (Certo and Morgan 2016; Khalil 2020; Silva et al. 2011; Stoddard 2011).

Zinc finger nucleases (ZFNs) are composed of the assembly of DNA-binding zinc finger domains and a cleavage subunit, connected through a peptide linker. Each zinc finger domain can make contact with approximately 3 bp of DNA in a sequence-specific manner. The cleavage domain has been derived from the restriction enzyme *FokI* and needs to dimerize to induce a double-strand break into the target sequence. For this reason, ZFNs can act only if two zinc finger subunits bind the DNA in the opposite orientation to allow *FokI* dimerization. This modular assembly has enabled the engineering of ZFNs with specific sequence specificities for a wide range of genomic targets (Chou, Leng, and Mixson 2012; Khalil 2020; Urnov et al. 2010).

Conceptually similar to ZFNs, transcription activator-like effector nucleses (TALENs) combine DNA-binding domains with the catalytic module of *FokI* nuclease. The core of this DNA-binding domain is constituted by highly conserved repeated sequences derived from TALE, which are naturally occurring proteins secreted by Xanthomonas bacteria during plant infection to mediate bacterial invasion of host cells. The central region of TALE is fundamental for its DNA recognition properties and is composed of tandem repeats of 33–35 amino acids,

each recognizing a single base pair in the target DNA sequence. Within each repeat, the DNA base specificity is determined by the repeat-variable diresidues (RVDs) located at positions 12 and 13. The decoding of these RVD specificities has enabled the definition of a protein–DNA recognition code, used by researchers to rearrange the order and number of repeats in order to finally customize and reprogram the targeting activity of TALENs (Becker and Boch 2021; Boch et al. 2009; Joung and Sander 2013; Moscou and Bogdanove 2009) (Figure 1).

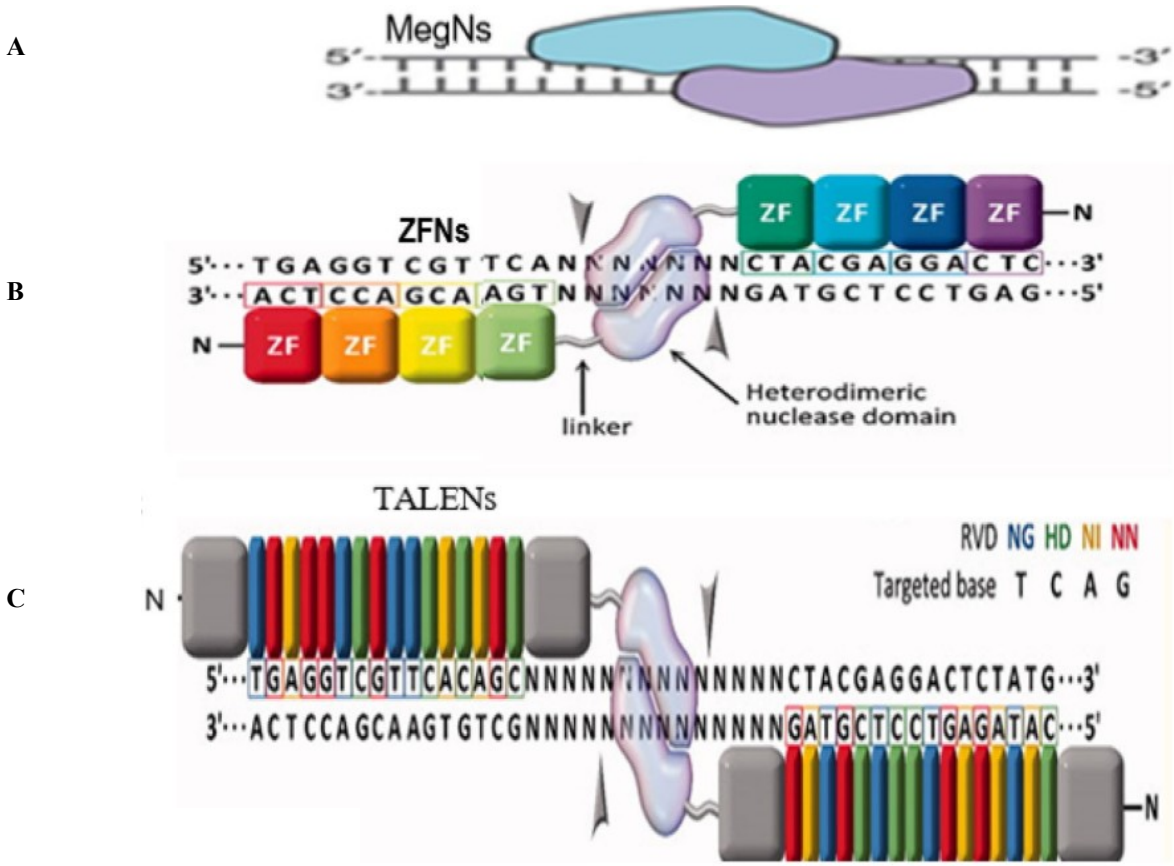

Figure 1. Illustrative diagrams for MNs, ZFNs, TALENs genome editing techniques. *(A) MegNs cleave large DNA sequences as homodimers or monomeric pseudodimers. (B) ZFNs are composed of zinc-finger modules that recognize DNA triplets and the FokI nuclease domain that mediates cutting after dimerization. (C) TALENs are charactesized by tandem repeats with a more flexible and specific cutting design, always mediated by FokI. (Image adapted from Khalil, 2020)***.**

1.1.2 Limitations of these first approaches

As mentioned before, CRISPR/Cas9 technology has represented a significant innovation in the genome editing field, overcoming different limitations of the previous technologies (MNs, ZFNs and TALENs).

Despite the ability to cut large DNA sequences in a highly specific manner, meganucleases are limited in their potential for retargeting. Indeed, the design of new MNs targeting new sequences requires several steps and significant efforts in protein engineering. This is largely due to the tight integration of their DNA-binding and cleavage domains, as well as on the dependence central motif region in the targeted region, thus rendering their customizable design very laborious. In addition, compared to other systems, their editing efficiency depends on the selected MN and can vary considerably between different target loci (Castro et al. 2021; Khalil 2020; Lu et al. 2022; Stoddard 2011).

ZFNs offer the possibility to be assembled with different modules to achieve unique DNA recognition specificities (Gaj, Gersbach, and Barbas 2013). However, the ZF protein-DNA base code is not straightforward, thus making their engineering difficult and time-consuming. Another important drawback lies in the limited target site selection, with suitable sites occurring at an estimated frequency of ~1 per 500 bp. Off-target effects refer to the targeting and cutting of unwanted genomic regions and represent a current issue in the use of ZFNs, since they can arise from their ability to form both homo- and heterodimers, enabling monomers to bind palindromic sequences or sites with partial similarity to their intended half-sites. Furthermore, the context-dependent nature of zinc finger–DNA interactions and the tolerance for mismatches can favour cleavage at unintended genomic loci (Castro et al. 2021; Gupta and Musunuru 2014).

Compared to ZFNs, TALENs are designed to be more specific, leading to fewer off-target effects and reduced cytotoxicity. The variability in the binding affinity and specificity of different RVDs can affect the efficacy of the technique, with some bases that are recognized with high efficiency but inherent degeneracy, and some others recognized with greater specificity but lower binding affinity. Similar to the other genome editing techniques, the overall efficiency can be affected by the cell

type, the choice of the target site, and the duration of the effect (Castro et al. 2021; Khan 2019).

Over the years, different improvements have been performed to overcome the intrinsic limitations of the aforementioned technologies. The production of new engineered meganucleases has expanded the repertoire of targeted natural sequences (Silva et al. 2011). ZFN design has been substantially improved using obligate heterodimeric FokI variants that can reduce off-target events (Miller et al. 2007). Similarly, the use of non-conventional RVDs has ameliorated TALEN performance in the context of multiplex genome editing (Gautron et al. 2017).

Despite these advances, the development of these platforms remains laborious and expensive. CRISPR/Cas9 technology offers a system based on DNA-RNA complementarity and an easier feasibility of reprogramming, effectively overcoming most of the constraints of these previous methods (Jinek et al. 2012).

1.1.3 Overview of the first genome editing applications

From their initial applications to subsequent optimisations, genome editing technologies were utilised in a wide range of fields, from basic research to biomedical and therapeutic interventions. In genetics, these tools have enabled the generation of cellular and animal models, useful to depict gene function within specific disease contexts. In the field of gene therapy, they have been widely used for various applications (Li et al. 2020). Here, some examples of their uses in selected research areas are reported.

In cancer research, mTOR-specific ZNFs conjugated to HER2-targeted cell-penetrating peptides (CPPs) were delivered in cancer cells to inactivate the mTOR locus and to inhibit key cancer pathways, highlighting a relevant role in developing targeted therapies against breast and other cancers (Puria, Sahi, and Nain 2012). Moreover, ZFNs were designed to cleave the BCR-ABL fusion gene, with consequent termination of BCR-ABL protein translation and apoptosis in imatinib-resistant chronic myeloid leukemia (CML) cells (Huang et al. 2018). Notably, in 2015, the biotechnology company Cellectis developed the first cancer cure based on genome editing by applying TALEN technology to engineer donor-derived CAR-T cells by the inactivation of genes causing non-self immune reactions. These

TALEN-modified CAR-T cells were used to treat therapy-resistant acute lymphoblastic leukemia in two children (Qasim et al. 2017).

In the field of viral diseases, genome editing techniques have mainly been applied to modify host cellular genes essential for viral pathogenesis or to target viral genes needed for the infection cycle (Li et al. 2020). In 2008, preclinical studies first demonstrated the anti-HIV potential of the ZFN system by disrupting about 50% of CCR5 alleles in primary human CD4+ T cells. In HIV-infected mice, transfusion with these ZFN-edited CD4+ T cells led to better preservation of native CD4+ T cells and reduced viral loads compared to untreated controls (Perez et al. 2008).

The aforementioned techniques have also found wide use in studies on genetic disorders (Li et al. 2020). For Duchenne muscular dystrophy (DMD), TALEN-mediated targeting of exon 23 of the DMD gene allowed researchers to obtain Dmd^{mdx} rat models, which exhibited significant reduction in muscle strength and spontaneous motor activity (Larcher et al. 2014). In the same context, meganucleases were designed to cut sequences of a dystrophin gene with a frameshift mutation, leading to restoration of the correct reading frame and protein expression (Chapdelaine et al. 2010).

1.2 The CRISPR/Cas system

1.2.1 Discovery and natural function of CRISPR/Cas systems

The acronym CRISPR stands for “Clustered Regularly Interspaced Short Palindromic Repeats” and describes repeated sequences originally identified by Ishino et al. in 1987 in the *Escherichia coli* genome (Ishino et al. 1987). For several years, their role and significance within the bacterium remained unclear. A step forward towards a greater understanding of these sequences was made by Mojica et al., who in a 1993 paper annotated the presence of similar repeated elements in the archaeal genome of *Haloferax mediterranei*, a species which is evolutionarily distant from *E. coli* (Mojica, Juez, and Rodríguez-Valera 1993). In 2007, Barrangou's work on bacterial cultures of *Streptococcus thermophilus* demonstrated that bacteria acquired new sequences (called spacers) from invading bacteriophages

in CRISPR loci. These acquired sequences provide phage-specific resistance and shed light on the role of CRISPR in prokaryotic adaptive immunity, enabling bacteria to "remember" past infections and recognise and counterattack the same bacteriophage upon reinfection (Barrangou et al. 2007).

Despite different initial acronyms, the term CRISPR was definitively coined in 2002 by Jansen, who also described the presence of CRISPR-associated genes, near the repeated CRISPR sequences (Jansen et al. 2002). A CRISPR locus is composed of a leader sequence and a CRISPR array consisting of short repeated sequences interspersed with spacer sequences acquired from invading genetic elements. The leader sequence contributes to regulatory functions, especially in the first phase of CRISPR immunity, and is a conserved, non-coding DNA sequence, with a length of usually hundreds of base pairs, that is found upstream of the CRISPR array. On average, CRISPR repeats are 32 bp long and mostly identical in length and sequence within the same CRISPR locus; most of them possess the ability to form hairpin structures, due to their partially palindromic features. Spacers are also similar in length within the same locus, generally ranging from 26 to 72 bp, but differ in their sequence content (Alkhnbashi et al. 2016; Karginov and Hannon 2010; Karimi et al. 2018). CRISPR-associated (Cas) genes have always been found adjacent to CRISPR loci. These highly polymorphic genes encode different conserved Cas proteins that play a role in various stages of CRISPR immunity (Karginov and Hannon 2010; Karimi et al. 2018) (Figure 2). Prokaryotic CRISPR-based adaptive immunity acts through three main phases: the adaptation phase, in which the host organism is infected by mobile genetic elements, and Cas protein cut short fragments of the invader's genomes, that are then incorporated in the host genome as new spacers; in the second phase of biogenesis, the CRISPR array is transcribed into a long precursor RNA molecule (pre-crRNA) which is subsequently processed by Cas proteins; finally, in the interference phase, the bacterium targets the mature crRNA/Cas complexes to recognize their cognate target in the invader's genome and destroy it (Charpentier and Marraffini 2014).

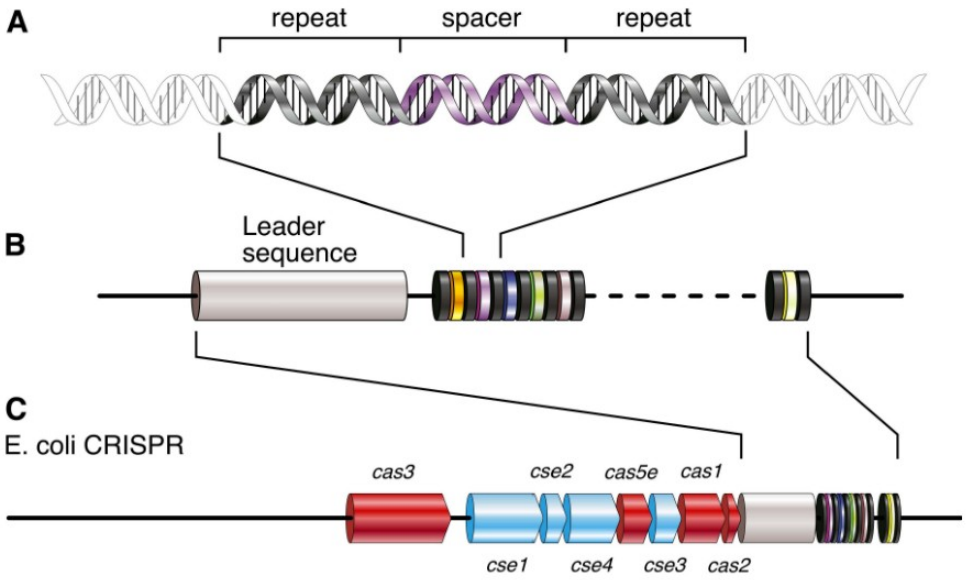

Figure 2. Schematic representation of a CRISPR locus. *A CRISPR locus is composed by a leader sequence followed by an array of repeated sequences interspersed with spacer sequences and is surrounded by CRISPR-associated (Cas) genes. In the image, the E. coli CRISPR locus is shown as an example (Image adapted from Karginov and Hannon, 2010).*

1.2.2 Classification of CRISPR/Cas systems

Based on the organisation and functional composition of Cas proteins, CRISPR/Cas systems are generally divided into two main classes: Class 1 and Class 2. Each class is further divided into three types, each of which comprises several subtypes that are distinguished by their mechanism of action. The effector module comprises Cas genes that are involved in target recognition and cleavage, also known as the interference function (Figure 3). In Class 1 systems, the effector module comprises multiple Cas proteins that mediate the interference stage, whereas Class 2 systems use a single effector protein to exert all these functions (Makarova et al. 2020; Saeed et al. 2025).

Class 1 are the most abundant CRISPR/Cas systems and are classified into type I, type III and IV.

In type I systems, the distinctive signature protein is represented by Cas3 protein that reaches the targeted site to mediate helicase and nuclease activities. Most of the type I subtypes, such as type I-E, require the action of the Cascade complex,

composed by five different Cas proteins. This multisubunit complex acts to mediate target DNA recognition, guided by crRNA, and then recruits Cas3 protein for the cleavage event (Lee and Bae 2016; Saeed et al. 2025).

Type III systems require the action of Cas10 protein and can target both DNA and RNA. In particular, the III-A subtype uses the Csm (Cas subtype Mtube) to target DNA, while RNA is targeted by Cmr (Cas module RAMP) in III-B subtype. Interestingly, in addition to their interference function, type III systems are able to synthesize cyclic oligoadenylate (cOA), which in turn can activate nucleases and transcription factors for a coordinated and time-controlled antiviral response (Rouillon et al. 2018; Saeed et al. 2025).

Type IV is the least understood CRISPR Cas type, generally characterised by the presence of Csf1 protein and Cas7-like protein (Csf2) within the effector complex and by the lack of adaptation modules. This CRISPR Cas type generally includes three subtypes (IV-A, IV-B, and IV-C) characterised by distinct genes and CRISPR-related features (Makarova et al. 2020; Saeed et al. 2025; Taylor et al. 2021).

Class 2 systems are divided into types II and V, which exhibit a DNA interference activity, and type VI, which possesses an RNA cleavage activity. In type II, after incorporation of new spacers from the invading organism into the CRISPR array, the precursor crRNA is transcribed and then processed by Cas9 and a trans-activating crRNA (tracrRNA); the assembled complex (mature crRNA-Cas9-tracrRNA) can recognize and cut the invader's genome upon reinfection. For the intrinsic simplicity of the mechanism of action and the system components, further simplified by the fusion of tracrRNA and crRNA in a chimeric single guide (sgRNA), type II CRISPR/Cas system has been widely adopted in genome editing, as will be described in the next sections (Jinek et al. 2012; Saeed et al. 2025)

The main actor of type V systems is the Cpf1 protein, which induces cuts in the targeted genome by generating sticky ends. Differently from type II, the effector protein (Cpf1) can assemble with crRNA and reach the target site without the action of crRNA (Saeed et al. 2025).

Type VI is characterised by Cas13 protein (also known as C2c2), a RNA endonuclease that assembles with crRNA and performs cutting activity through one

of its two HEPN (higher eukaryotes and prokaryotes nucleotide-binding) domains, while the second one is used to process pre-crRNA into mature RNA molecules. Due to its RNA nuclease activity, the system has been used for various RNA-targeting and RNA-editing applications (Nakagawa et al. 2022; Saeed et al. 2025).

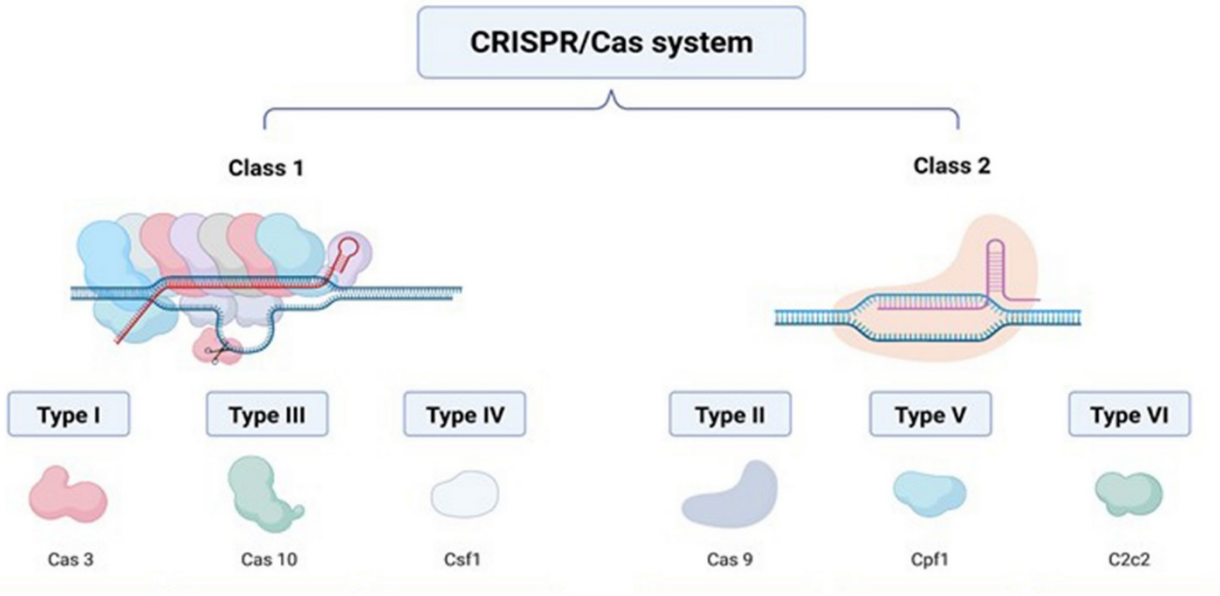

Figure 3. General classification of CRISPR/Cas system. *Class 1 acts through multiple proteins, while class 2 requires the action of a single multi-domain Cas protein. For each type, the generally considered signature molecule is reported. In some other studies, Csf2 is considered the signature molecule for type IV (Taylor et al. 2021). (Image adapted from Aman Mohammadi et al., 2023).*

1.2.3 The three stages of prokaryotic CRISPR-mediated immunity

As previously mentioned, prokaryotic CRISPR adaptive immunity acts in three main stages, namely adaptation, biogenesis (also referred as expression) and interference, that are conserved among the different CRISPR systems but differ in the Cas proteins used by the different microorganisms (Navarro et al. 2025; Selim et al. 2025).

The first stage is adaptation, which is generally driven by the two endonucleases Cas1 and Cas2. During this phase, sequences from invading mobile genetic elements (MGEs) are integrated into the host genome. The original sequence from the invading organism is called a protospacer and becomes a spacer once

incorporated into the CRISPR array. Selecting the target sequence to be incorporated is crucial for the bacterium in order to avoid the recognition of its own regions and finally act only on non-self genomes. This non-self immunity is enabled by a conserved sequence of a few nucleotides (2–5 bp), called the protospacer adjacent motif (PAM), that flanks the protospacer region but is absent near spacers in the CRISPR array (Gleditzsch et al. 2019; Navarro et al. 2025). Cas1-Cas2 form a complex that allows protospacer recognition and acquisition into the host genome by means of the integrase activity of the protein complex. Fragment incorporation occurs at the leader-repeat boundary, followed by the action of DNA polymerases and other ligation complexes that duplicate the first repeat, generating a new copy at the end of the leader sequence. The entire process ensures the proper expansion of the CRISPR array and provides a structural template for the addition of future spacers. The adaptation process generates a genetic memory of the invading organism, thereby being essential for the adaptive functioning of CRISPR immunity (Hille and Charpentier 2016; Navarro et al. 2025).

In the biogenesis phase, a long precursor RNA molecule (pre-crRNA) is transcribed from a promoter in the leader sequence. The pre-crRNA contains both the newly acquired spacer and the pre-existing spacer–repeat units and needs to be cleaved to produce a functional and mature molecule in a process that varies among the different CRISPR systems. For example, in many CRISPR class 1 systems, Cas6 enzyme recognizes and cleaves repeated sequences that form a secondary structure due to their palindromic nature. In type II systems, an additional RNA molecule, as tracrRNA, acts by pairing with crRNA by creating a double-strand RNA molecule, which is then cleaved by RNase III to generate mature molecules (Charpentier et al. 2015; Navarro et al. 2025).

In the interference phase, the final action of the prokaryotic CRISPR mechanism occurs, with the aim of destroying sequences that are complementary to those previously incorporated during the first event of infection. In this step, mature CRISPR RNAs (crRNAs) guide Cas enzymes to recognise, cut and degrade the genome of invading organisms. Recognition occurs through base pairing between the crRNA and the protospacer sequence of the invader, with the presence of the PAM motif that is required in many systems.

The multi-protein Cascade complex acts in Type I CRISPR systems to bind the targeted genetic material and recruit Cas3 for the following interference activity. In type I systems, interference occurs after pairing of the so-called seed region, a 6-8 nucleotides sequence of crRNA that is perfectly complementary to the protospacer. This initial interaction represents the rate-limiting reaction which precedes the entire pairing process and the formation of an R-loop with the displacement of the non-targeted strand. As mentioned before, type II systems require a crRNA-tracrRNA-Cas9 complex for mediating their interference function. The degradation part is mediated by Cas9 catalytic domains, namely HNH that cleaves the strand complementary to crRNA and RuvC that cuts the opposite one (Barrangou and Marraffini 2014; Navarro et al. 2025; Rath et al. 2015).

A simplified representation of these three stages is illustrated in Figure 4.

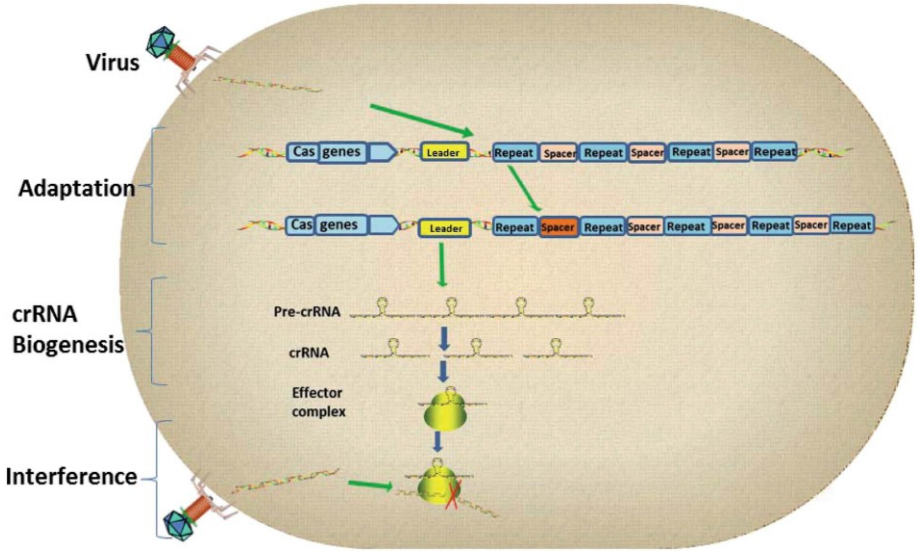

Figure 4. Representation of the three stages of CRISPR immunity. *CRISPR adaptive immunity acts to counteract infections by three stages: adaptation, biogenesis and interference (from Zhang et al., 2018).*

1.2.4 Adaptation of CRISPR/Cas9 for genome editing

Since the discovery of CRISPR as a bacterial defence system capable of recognising invading nucleic acids via complementary RNA and mediating cleavage via Cas proteins, its potential for use as a genome-editing tool in eukaryotes has become apparent. Jinek et al. focused on type II CRISPR, a system based on the use of Cas9 proteins and crRNA-tracRNA complexes to induce cutting in target sequences. Specifically, the crRNA-tracRNA complex is essential for directing Cas9-mediated cleavage, with the tracrRNA first processing the pre-crRNA via RNase III and then orienting the crRNA to bind to the complementary DNA sequence. In this study, the researchers successfully generated a single chimeric RNA molecule by fusing the 3′ end of the crRNA with the 5′ end of the tracrRNA. This demonstrated the ability of the engineered guide to direct Cas9 to efficiently cut target DNA molecules (Jinek et al. 2012).

Based on these observations, Ran et al. developed one of the first protocols to use CRISPR/Cas9 as a genome-editing tool in eukaryotes. The expression of a human codon-optimised Cas9 and a single RNA guide in mammalian cells induces a double-strand break (DSB) at target genomic loci, recognised by Watson–Crick base pairing between the RNA and the target DNA. Following this cleavage, the cell can undergo two main repair mechanisms for this type of damage: non-homologous end joining (NHEJ) and homology-directed repair (HDR). In the first mechanism, the cut DNA strands are rejoined via an error-prone mechanism that can introduce insertions or deletions (INDELs), which can cause frameshift mutations and premature stop codons, resulting in gene knockout. Multiple guides can also be used to mediate genomic deletions at a target locus. Conversely, the HDR system requires an exogenous template in the form of either double-stranded DNA with homology arms flanking the insertion sequence or single-stranded oligodeoxynucleotides (ssODNs). The cell then uses this template to mediate a recombination event at the DSB site, introducing the desired sequence encoded in the template (Ran et al. 2013).

The Cas9 endonuclease has a two-lobe structure comprising the nuclease (NUC) and recognition (REC) lobes. As the name suggests, the nuclease lobe mediates cleavage of the target DNA molecule via two domains: HNH and RuvC. These

domains cleave the complementary and non-complementary strands of the recognised sequence, respectively. In contrast, the REC lobe is essential for recognising cognate target DNA. For cleavage to occur, the recognised target sequence (protospacer) must be followed by a PAM sequence. One of the most widely used Cas9 variants for genome editing is SpCas9, derived from *Streptococcus pyogenes*, which requires an NGG PAM sequence (N indicates any nucleotide). Recognition of the PAM sequence and pairing between the gRNA and the target DNA in the region proximal to the PAM (the "seed region") enable the Cas9 cutting mechanism to function correctly and mediate a double-strand break three bases upstream of the PAM (Le Rhun et al. 2019; Wang, La Russa, and Qi 2016).

Although SpCas9 is a well-characterised and widely used type II endonuclease for CRISPR/Cas experiments, other Cas9 orthologues have been used in this context, offering new specificities in terms of PAM requirements. In particular, SaCas9 from *Staphylococcus aureus* has often been adopted due to its smaller size, which makes it easier to deliver to mammalian cells. It also recognises a distinct PAM sequence (NNGRRT, where R stands for A or G), which allows for new targeting possibilities in the CRISPR editing system. Other Cas9 orthologues used in genome editing applications include those derived from *Neisseria meningitidis* (NmCas9, which recognises the PAM sequence NNNNGATT) and *Streptococcus thermophilus* type 1 (St1Cas9, which recognises the PAM sequence NNAGAAW, where W represents A or T) (Wang et al. 2016).

In conclusion, CRISPR/Cas9 is a relatively simple, versatile and easy-to-engineer genome editing system. The possibility of customising the gRNA to target complementary genomic sequences, as well as the high cutting efficiency of Cas9, represents a real advantage over previous and more laborious technologies (MNs, ZFNs, and TALENs), making this system widely used for gene editing in eukaryotic models (Ran et al. 2013) (Figure 5).

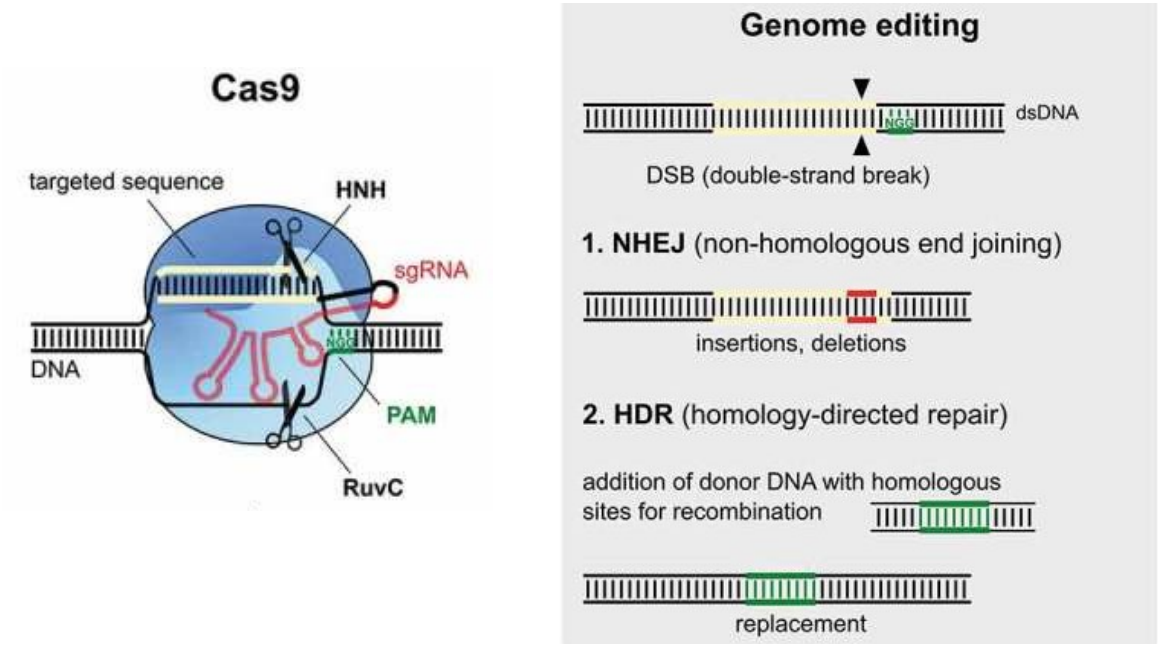

Figure 5. Genome editing mediated by CRISPR/Cas9. *Cas9 protein, complexed with sgRNA, induces a double-strand break in a targeted sequence, which can be repaired by NHEJ or HDR. (Image adapted from Le Rhun et al., 2019).*

1.2.5 General applications and limitations of CRISPR/Cas9

The potential of genome editing using the CRISPR/Cas9 technique has been widely adopted in a variety of fields. In biomedicine, for example, it has entered clinical trials for the treatment of various forms of cancer. This technology is frequently employed to modify pro-tumoural genes in cancer cells. For instance, in cervical cancer caused by the human papillomavirus (HPV), the E6 and E7 oncogenes (expressed by HPV) have been targeted by CRISPR/Cas9 to induce their knockout. In cancer immunotherapy, CRISPR/Cas9 is used to modify T cells to enhance their antitumour activity. In the field of neurodegenerative diseases such as Huntington's disease (HD), Alzheimer's disease (AD) and Parkinson's disease (PD), CRISPR/Cas9 has been a useful tool for improving the understanding of the genetic factors involved and identifying new therapeutic targets. In addition to improving our understanding of molecular pathways, the technology has also been widely adopted in the development of animal models and drug discovery. Moreover, it has been applied in studies on cardiovascular diseases, ocular diseases and inherited

blood disorders. Viral infections have been targeted by CRISPR/Cas9 technology, too. LTR promoter or viral gene of the human immunodeficiency virus-1 (HIV-1) have been targeted in in vitro models, leading to a reduction of HIV-1 biological activity (Du et al. 2023; Saeed et al. 2025).

Other fields of application have been environmental sciences, where CRISPR/Cas9 can be applied with the aim of helping to preserve endangered species or controlling invasive species. In biotechnology and agriculture, the technology has enabled the modification of the DNA of various organisms, leading to the creation of genetically modified organisms (GMOs) with improved traits, such as increased disease resistance or higher yield (Aman Mohammadi et al. 2023; Ansori et al. 2023).

Despite the widespread use of this technology, its major limitations must also be considered. Based on RNA:DNA complementarity, there can be a risk that the gRNA/Cas9 recognises and cuts unwanted regions (off-targets), leading to undesirable effects such as cytotoxicity and unwanted mutations. Furthermore, Cas9 performs a double-strand break in DNA, which can activate p53 response and induce cell death. Other limitations relate to the efficiency and immunogenicity of the delivery methods used to administer CRISPR/Cas9 components (Du et al. 2023; Severi and Akbari 2024).

1.3 Generation of knockout cell lines using CRISPR/Cas9

The advent of CRISPR/Cas9 and its application in generating knockout cell lines has revolutionised the field of genome editing, enabling researchers to explore gene function within different molecular pathways. A CRISPR/Cas9 protocol for generating knockout cell lines requires several steps, including the design of guide RNA, delivery of CRISPR/Cas9 components, and validation of editing events on isolated clones (Hong et al. 2024).

The Cas9 enzyme induces double-strand break (DSB) at the gRNA-targeted region; this genomic damage is recognized by cellular repair mechanisms such as non-homologous end joining (NHEJ), which can lead to the introduction of insertions

or deletions (INDELs), that can cause a frameshift mutation in the gene with the consequent loss of protein expression (Ran et al. 2013).

In this section, we review the fundamental steps, critical for a successful CRISPR/Cas9 experiment, with a particular focus on guide design and the importance to enhance the on-target activity, by avoiding off-target events, as well as the validation strategies for confirmation of successful gene knockout.

1.3.1 gRNA design principles and tools

The single guide (sgRNA) consists of a 20-nucleotide RNA molecule that specifies a target region in the DNA and an invariable scaffold part that allows binding with Cas9. The Cas9 nuclease is guided by the sgRNA to the complementary genomic site, where it recognises it through Watson–Crick DNA:RNA pairing and then exerts a double-strand break. Cleavage, in the form of double-strand break, occurs three base pairs upstream of the PAM sequence on both DNA strands (Jinek et al. 2012; Ran et al. 2013).

The correct design of the sgRNA (or gRNA) requires several preliminary rules to obtain a functional and effective molecule. For a complete knockout, the gRNA/Cas9 complex must target a common coding exon in order to avoid the partial knockout of only some isoforms (Mohr et al. 2016). The nucleotide sequence composing the gRNA must also be taken into account, as too high or too low GC content can lead to poor gRNA performance (Doench et al. 2014). Intramolecular interactions in the gRNA can lead to secondary structures, finally affecting the nucleotide accessibility in the gRNA/Cas9 complex. In this context, nucleotides 18-20 of the gRNA sequence have been found to be important to be accessible for an effective editing (Hiranniramol et al. 2020). Since for CRISPR/Cas9 experiments, gRNAs are often expressed in constructs under the control of a RNA Polymerase III (Pol III) promoter (like the U6 promoter), a good functioning of the machinery also relies on transcription efficiency. For this reason, an additional guanine (G) is preferentially added as first nucleotide at the 5’ terminus of the gRNA, as Pol III promoters preferentially initiate transcription with this nucleotide. In addition, poly-T tracts (as TTTT), that act as termination signals for the Pol III transcription, are

generally avoided from gRNA design (Gao, Herrera-Carrillo, and Berkhout 2018; (Ran et al. 2013).

The gRNA efficiency, generally referred to as on-target activity, is a crucial factor determining a successful knockout experiment. On-target describes the ideal interaction between the gRNA/Cas9 complex and the pre-established DNA target, while off-target events involve the binding to similar target DNA regions that were not intentionally selected for the desired modification. When designing the guide, maximising its on-target activity while minimising off-target effects is a priority concept on which the specific cutting activity of the gRNA will depend (Doench et al. 2014, 2016; Motoche-Monar et al. 2023).

Several online computational tools have been developed to evaluate the aforementioned gRNA design principles and adapt them to different CRISPR/Cas9 systems. These tools continually evolve their computational structures through updates to machine learning techniques and neural networks (Motoche-Monar et al. 2023). Among the different features, these tools are able to evaluate key parameters in gRNA design, such as secondary structure, GC content, PAM compatibility, on-target activity and potential mismatches with non-intended genomic sites. Many of them also include the possibility to design guides for different organisms, gene editing modalities (knockout, knock-in, activation) or CRISPR nucleases (as Cas9, Cpf1/Cas12a, Cas13). Some widely used CRISPR gRNA design platforms include CHOPCHOP, CRISPROR, E-CRISPR and Cas-Designer, all offering user-friendly features and scoring systems for a complete evaluation and proper gRNA design (Hwang, Song, and Bae 2021; Liu, Zhang, and Zhang 2020).

1.3.2 Analysis and validation of knockout efficiency

Generally, after delivery of CRISPR/Cas9 components, cells are subjected to clonal isolation in order to derive single clones characterised by precise editing events. Experimentally, the isolation is usually performed by limiting dilution cloning or fluorescence-activated cell sorting (FACS) (Hong et al. 2024). After obtaining single clones, different methods can be adopted for validation of gene knockout. At the sequence level, knockout events are defined by frameshift mutations that can introduce a premature stop codon, often leading to mRNA degradation through

nonsense-mediated mRNA decay (NMD) pathway (Van Campenhout et al. 2019). To identify these genomic events, DNA is extracted from clones and then subjected to PCR on the gRNA-targeted region. PCR amplicons are then analysed by Sanger sequencing to detect editing events (Kahaki et al. 2024). Sanger sequencing can also detect homozygous editing events, but it cannot properly decipher heterozygous modifications. For this reason, different computation tools, such as TIDE, ICE, DECODR and SeqScreener, have been developed to analyse CRISPR/Cas9-induced indels. Among these, DECODR provided the most accurate results, being able to deconvolute also wide regions of inserted and deleted sequences. Alternatively, heterozygous allelic events can be discriminated by TOPO cloning, followed by sequencing. In this time-consuming procedure, the PCR amplicons are cloned into the TOPO vector, followed by bacterial transformation and sequencing of isolated colonies (Aoki et al. 2024; Giuliano et al. 2019). For more accurate sequencing results, even if more expensive, next-generation sequencing (NGS) can also be employed to detect CRISPR-derived mutations (Ran et al. 2013). At the protein level, the Western blot (WB) technique represents the crucial validation for a CRISPR/Cas9 experiment. Indeed, WB allows the specific detection of a protein within a sample, thus enabling the confirmation of gene knockout in the CRISPR-edited samples when the target protein expression is absent, compared to control samples. Moreover, as mentioned before, FACS can allow the isolation of knockout cells by negative selection of cells not expressing a targeted surface protein, encoded by the CRISPR/Cas9-inactivated gene (Giuliano et al. 2019).

1.3.3 Off-target prediction and analysis

The seed region refers to the PAM-proximal region where DNA strand separation and DNA:RNA hybridisation begin. It has been suggested that this region is important for Cas9 specificity, even though sequence-dependent specificity has been observed within the 20-nt gRNA. Taking this into account, mismatches between the gRNA and the target DNA are generally better tolerated in the PAM-distal region, thereby increasing the likelihood of off-target effects, while

mismatches near the PAM are generally less tolerated (Hsu et al. 2013; Wang et al. 2016).

The high similarity between the gRNA sequence and an unintended non-target DNA sequence is the primary cause of off-target events, thus driving Cas9 cutting despite the presence of mismatches or gaps within the DNA:RNA heteroduplex. The generated and unwanted cuts can ultimately lead to undesired and unexpected outcomes in CRISPR/Cas9 experiments (Motoche-Monar et al. 2023).

Over the years, the evaluation of off-target effects has become critical, particularly in the field of translational medicine. For this reason, a series of methods based on *in silico* prediction and experimental validation (further classified as cell-free, cell culture-based, or in vivo detection methods) have been developed.

Among the cell-free methods to detect CRISPR/Cas9 off-target events, SITE-Seq and CIRCLE-Seq rely on exposure of genomic DNA to Cas9/gRNA complexes, followed by sequencing of the resulting cleaved DNA. In particular, in the first approach, biotinylated-streptavidin reaction is used to enrich cleaved DNA ends before sequencing, while in CIRCLE-Seq, DNA is sheared and then circularized before being linearized by gRNA/Cas9 cutting.

A popular cell culture-based method for detecting unintended cleavage sites is GUIDE-Seq. In this technique, CRISPR/Cas9 components are delivered into cells together with double-stranded oligonucleotides (dsODN) of a known sequence. After Cas9 cutting, these dsODNs are integrated into the related cutting sites and act as templates for targeted PCR amplification and subsequent sequencing of the cleaved fragments.

Finally, among the *in vivo* detection tools, DISCOVER-seq identifies off-target events by recruitment of the DNA damage repair protein MRE11 on double-strand break sites, followed by ChIP-seq analysis (Cameron et al. 2017; Guo et al. 2023; Tsai et al. 2015, 2017; Wienert et al. 2019).

Potential off-target events can also be preliminarily evaluated by in silico tools. Some bioinformatic tools, such as COSMID, also allow a scoring of the different off-target sites, based on the mismatch position relative to the PAM, while others, such as Cas-OFFinder and CasOT, just provide a list of off-target sites. In this case, validation of predicted off-target events is usually accomplished by PCR

amplification and sequencing of the putative off-target regions to verify their integrity (Bao et al. 2021).

1.4 Delivery methods

Delivery of CRISPR/Cas9 components is a critical step for a successful CRISPR/Cas9 experiment. For this reason, since its initial development, several efforts have been made to optimise and find delivery methods that can target the widest range of cell lines or tissues (Severi and Akbari 2024).

Before describing the various delivery methods, it is important to mention the three ways in which the CRISPR/Cas9 machinery can be delivered: plasmid DNA (pDNA), RNA, and ribonucleoprotein (RNP).

Plasmid DNA, which contains the expression cassettes for Cas9 and sgRNA, is a stable, low-cost format that leads to long-term expression of the CRISPR components. However, this prolonged persistence, along with the chance of genomic integration, could increase the likelihood of off-target effects. The large size of plasmid DNA can also hinder its delivery into difficult-to-transfect systems.

The mRNA form of Cas9, after entering the target cells, can be directly translated to form a complex with sgRNA that acts with faster kinetics than the plasmid form. However, mRNA suffers from stability issues that can lead to easier degradation of the molecule. To address this, chemical modifications are often added to improve overall stability.

In the last form, RNP, Cas9 protein is pre-assembled with sgRNA before delivery into target cells. This form does not require translation and transcription, but it only needs a nuclear localization signal (NLS) to enter the nucleus and induce genome editing in a rapid way, thus decreasing the occurrence of off-target events. A major drawback of the RNP complex remains its high cost (Liu et al. 2023; Taha, Lee, and Hotta 2022).

These different forms can be delivered using different approaches, which can generally be classified into physical, biological and chemical methods (Taha et al. 2022). Among the physical methods, a widely adopted technique in CRISPR/Cas9 experiments is electroporation, which is based on the application of a high electric

field to increase the permeability of the cell membrane. Despite its relative straightforward use, electroporation can induce cell death, thus requiring a careful optimisation of voltage and current when applied to different cell types. Microinjection is another and more sophisticated physical method that directly injects CRISPR components into target cells. The approach has no size limitation for the delivered molecule and can be directly followed under the microscope. Despite these advantages, microinjection can target only one cell at a time and requires highly qualified technical expertise.

Sonoporation is a physical method that co-injects microbubbles and cargo molecules and exploits ultrasound waves to generate pores in the cell membranes, through which cargo can enter the cell.

Among biological methods, viral vectors have been widely used for their effectiveness in delivering CRISPR components, with adeno-associated virus (AAV), adenovirus (AdV) and lentivirus (LV) vectors being among the most commonly used. Adeno-associated viral (AAV) vectors can carry genomes up to approximately 4.7 kb, making it necessary to split SpCas9 and the gRNA into two different vectors, or to use smaller versions of Cas9. These vectors have been widely used in studies on animal models, while clinical applications have encountered significant challenges. In particular, the main limitations concern the immune response caused by the administration of these viral vectors and reported liver toxicity, especially when administered at high doses. Although they do not generally integrate into the host genome, the risk of genomic integration cannot be ruled out due to the possible combination with the CRISPR/Cas9 transgene. Furthermore, persistent expression of Cas9 can lead to undesirable off-target effects. Adenoviral vectors are characterised by high transduction efficiency and lead to a transient expression of CRISPR/Cas9 components, as they remain as episomal DNA. The main issue, which has greatly limited their clinical application, regards the high immunogenicity. In contrast to the two vectors described above, lentiviral vectors can accommodate a viral RNA genome of up to 9 kb, which is then reverse transcribed into DNA and integrated into the host chromosome.

Lentiviral vectors have been used in *ex vivo* gene therapies, while the main limitation of their *in vivo* use concerns the stable integration of the CRISPR/Cas9

system, which can lead to undesirable effects, such as insertional mutagenesis (Du et al. 2023; Liu et al. 2017, 2023; Taha et al. 2022).

Other more innovative biological methods consist of using virus-like particles (VLPs). These vehicles are composed of the main viral proteins, as capsid and envelope, but lack the viral genome, thus ensuring no integration into the host genome. VLPs can deliver Cas9/gRNA RNP in a transient and efficient way, by operating in a rapid manner and avoiding persistence of CRISPR/Cas9 components in the cell, thereby reducing off-target effects. Different virus-like particle systems have been developed and the most widely used include Nanoblades, VesiCas, Gesicle and NANOmedic.

Nanoblades are produced by transfecting HEK293T cells with plasmids encoding for: MLV Gag-pro-pol, which are required for assembly of the viral particle; Gag-Cas9, a fusion protein separated by a proteolytic site that will be cleaved by MLV protease to release the functional Cas9 enzyme; sgRNA, which will assemble with Cas9 to form the RNP complex for mediating genome editing; VSV-G, the viral glycoprotein envelope required to ensure broad tropism.

In the VesiCas system, VLPs are produced by transfecting HEK293T cells with plasmids encoding for Cas9, gRNA and VSV-G. Differently from the Nanoblades, VesiCas depend on the passive assembly of viral structures to incorporate the Cas9 protein complexed with the gRNA.

Gesicle represents another and more sophisticated form of VLP, based on dimerization-driven assembly of Cas9.

Finally, NanoMEDIC system utilizes two recruiting mechanisms for Cas9 and gRNA, as chemically induced dimerization for Cas9 and HIV-1 packaging signal for gRNA (Kostyushev et al. 2020; Lotfi et al. 2023; Mangeot et al. 2019; Taha et al. 2022).

Another biological delivery method is represented by cell-penetrating peptides (CPPs), which are short peptides that can be fused or conjugated with cargo molecules and have been used to deliver CRISPR RNP (Taha et al. 2022).

Chemical-based delivery methods, such as gold nanoparticles (AuNP) and polymer and lipid-based nanoparticles, are also widely used in CRISPR/Cas experiments.

AuNPs are generally easy to synthesize and offer high loading capacity, allowing for the delivery of RNP by leveraging a simple endocytosis-mediated cellular uptake.

Cationic lipid-based delivery, as represented by commercial reagent Lipofectamine3000, is a valuable and efficient solution for in vitro experiments, but its use in *in vivo* applications is limited due to high toxicity. This issue can be solved by the use of lipid nanoparticles (LNP), a more complex and multi-composed vehicle that integrates different lipidic components. In detail, for an efficient and safer delivery of CRISPR components, it uses an ionizable lipid that becomes cationic after entry to induce cargo molecule release, a PEG-lipid to enhance stability, and helper phospholipid and cholesterol for mediating the fusion process and improving structural stability (Lotfi et al. 2023; Taha et al. 2022). Figure 6 shows a summary of the described CRISPR delivery systems.

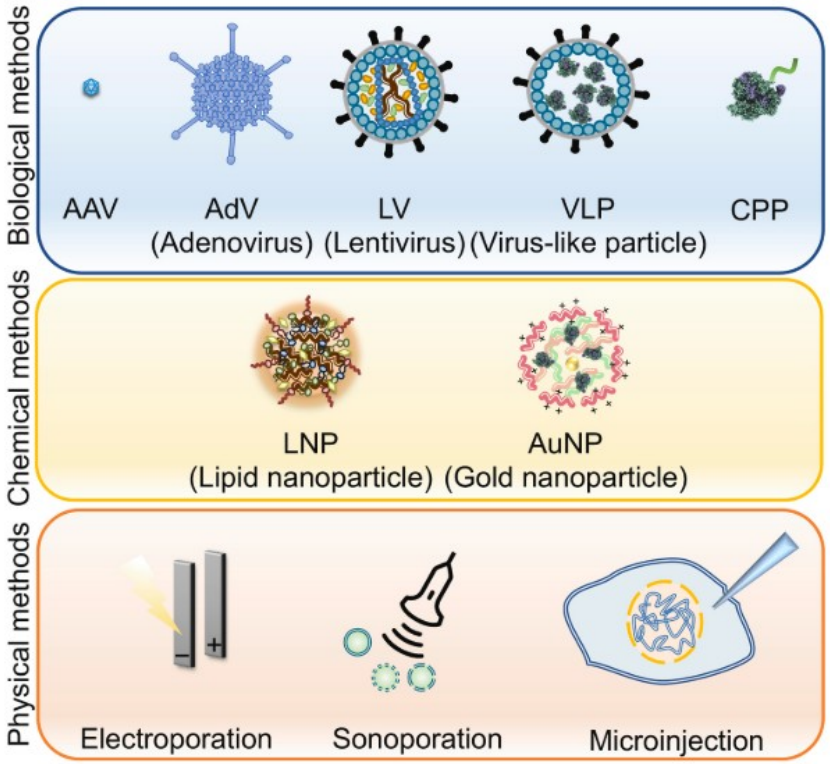

Figure 6. Summary of the main delivery systems for CRISPR components. *The delivery methods can be summarized into biological, chemical and physical methods. (Image from Taha, Lee and Hotta, 2022).*

1.5 CRISPR-based precision editing

1.5.1 Base editing: cytosine and adenine base editors

First attempts at precise genome editing using CRISPR were leveraged on homology-directed repair (HDR). After cutting by Cas9 and double-strand break induction, HDR machinery can intervene and use a homologous template to repair the damage. This strategy can utilize an exogenously provided donor template (in the form of double-stranded or single-stranded DNA) to guide sequence correction or modification. Despite the large possibilities of introducing targeted genomic modifications, this mechanism is mainly active in G2/S phases of the cell cycle and generally inefficient in postmitotic cells (Liao et al. 2024; Ran et al. 2013). Following this, other CRISPR-based platforms for precise genome editing were subsequently developed.

Different from HDR-based CRISPR knock-in, base editing represents an innovative CRISPR-based strategy without requiring double-strand break or a homologous template, opening the way to new potential applications in genetic medicine, as well as new therapeutic possibilities for individuals affected by genetic disorders (Xu et al. 2024). Komor et al. first developed base editing technologies by fusing catalytically inactive Cas9 (dCas9) with a cytidine deaminase enzyme. Coupled with a gRNA, this fusion protein could be programmed to target and mediate the substitution of cytosine (C) for thymine (T). dCas9 lacks nuclease activity but retains the ability to bind to DNA guided by the RNA guide; the cytidine deaminase enzyme then deaminates the cytosine to uracil (U), which is subsequently recognized by the cell's repair machinery and replaced by thymine (T). In their initial paper, the researchers optimised several versions, ranging from BE1 to BE3, to enhance base editing efficiency. In brief, BE1 involved the fusion of the cytidine deaminase domain of rat APOBEC1 to dCas9 via a 16-residue XTEN linker, enabling it to induce a C to T substitution from positions 4 to 8 within the protospacer (the sequence recognised by the gRNA). The second version, BE2, added a uracil glycosylase inhibitor (UGI) domain to the C-terminus of the dCas9-APOBEC1 fusion to better fix the induced substitution by impeding base excision repair (BER), which can otherwise revert the U:G heteroduplex to C:G. Significant

improvements were achieved with BE3, which replaced dCas9 with a Cas9 nickase. BE3 introduces a single-strand nick on the non-edited strand (the G-containing strand opposite the deaminated U), thereby stimulating eukaryotic mismatch repair (MMR) pathways to preferentially replace the nicked strand. This process incorporates an A opposite the U, effectively fixing the desired C→T conversion (Choe and Musunuru 2021; Komor et al. 2016).

This class of enzymes, later called cytosine base editors (CBEs), preceded the second major class of enzymes for base editing, namely the adenine base editors (ABEs), which were developed soon after and can convert an adenine (A) into a guanine (G). For this class of enzymes, the reaction consists of the deamination of adenine to inosine, which can pair with cytosine and be subsequently replicated as G. Based on the fusion of Cas9 nickase with *Escherichia Coli* transfer RNA adenosine deaminase (ecTadA), Gaudelli et al. optimised a series of ABEs by protein engineering and mutagenesis experiments. One of their final versions, ABE7.10, efficiently achieved a conversion of A•T base pairs into G•C of approximately 50% in human cells with a minimal percentage of indel rates, and an editing activity window ranging from positions 4 to 7 in the protospacer sequence (Gaudelli et al. 2017).

By exploiting Cas9 nickase fused to deaminase enzymes, base editing does not induce double-strand breaks (DSBs) in DNA, which could activate p53-mediated cellular responses (Haapaniemi et al. 2018). It is also simpler than HDR-mediated CRISPR knock-in, which, as mentioned before, requires a donor template to introduce the desired genetic modification and remains relatively inefficient and dependent on cell cycle phase (Smirnikhina et al. 2022). Collectively, base editing provides a platform for mediating all four possible transition mutations. CBE and ABE mechanisms are shown in Figure 7.

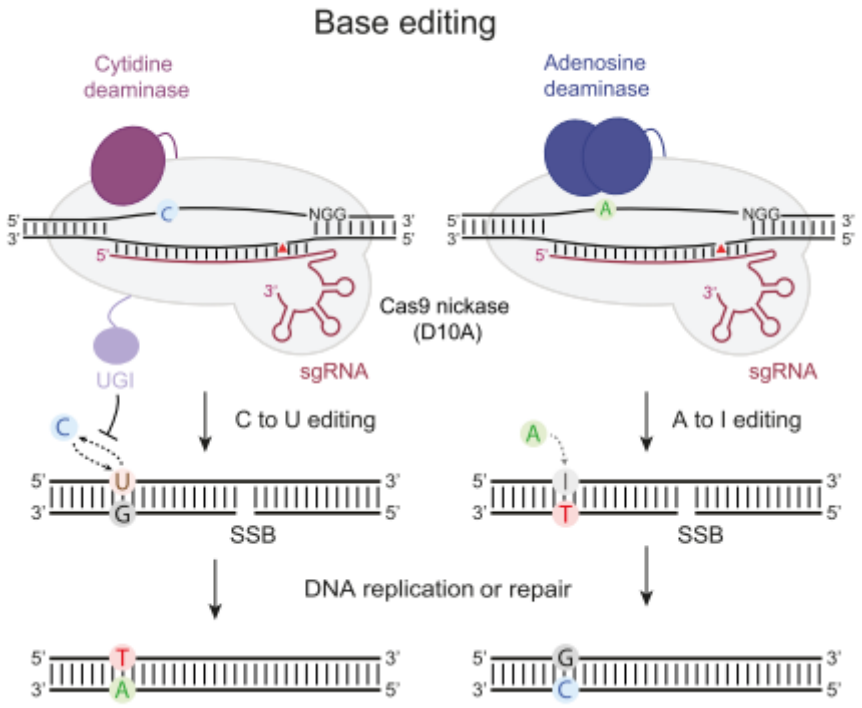

Figure 7. Schematic representation of base editing*. Mechanisms of CBE, that convert a C to a T, and ABE, that mediates the conversion of an A to G, are shown.*

1.5.2 Prime editing: mechanism and different strategies

Prime editing was initially defined as a "search-and-replace" genome editing technology able to introduce targeted deletions, insertions and all 12 types of base-to-base conversions. Prime editing essentially comprises two elements: a prime editor (PE) enzyme consisting of a Cas9 nickase (nCas9, H840A) fused with a reverse transcriptase from the Moloney murine leukemia virus (MMLV-RT), and a prime editing RNA (pegRNA) that comprises a spacer sequence, a Cas9 binding scaffold, an RT template carrying the desired modification, and a primer binding site (PBS). The PE is guided by the spacer sequence of the pegRNA on a target DNA locus; after hybridization of the spacer with the target DNA strand, the Cas9 nickase nicks the PAM-containing strand by exposing a 3′-hydroxyl group (3'-OH). The resulting 3′-single-stranded DNA (ssDNA) hybridizes with the PBS, further allowing the associated RT to extend the strand by copying the information encoded by the RT template. At this point, the redundant single-stranded DNA flaps are

formed: one 5’ flap containing the non-edited DNA sequence and a 3’ flap carrying the desired genetic modification. Although exact complementarity of the 5' flap is favoured, this strand is generally more susceptible to degradation by nucleases, ultimately leading to its excision and hybridization and ligation of the 3' flap. The resulting heteroduplex can be resolved by DNA repair or replication, by copying information from the edited strand to the unedited strand, finally resulting in the permanent incorporation of the desired mutation (Anzalone et al. 2019; Doman et al. 2022). The prime editing mechanism is summarized in Figure 8.

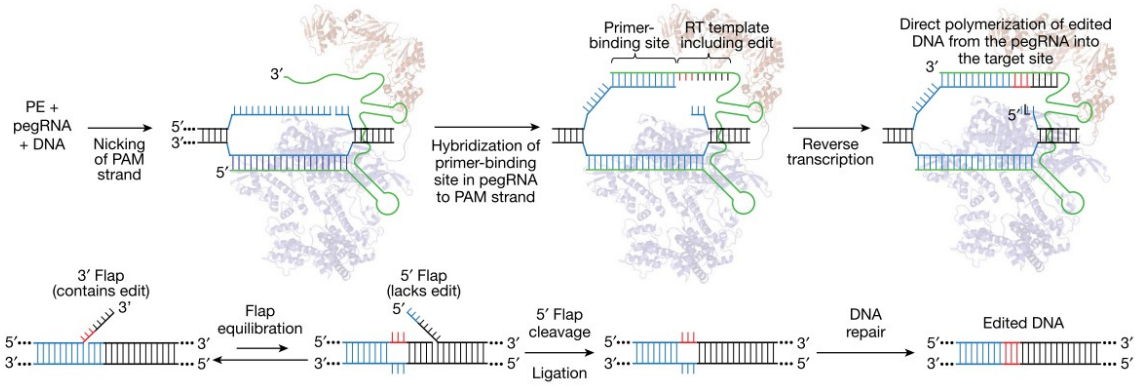

Figure 8. Schematic representation of prime editing mechanism. *Prime editing acts through a prime editor enzyme, composed by a Cas9 nickase fused to a reverse transcriptase. The Cas9 nickase mediates a nick on the pegRNA-targeted site, while the reverse transcriptase allows to copy the genetic information encoded in the pegRNA 3’-extension. Finally, cellular DNA repair mechanisms complete the installation of the desired modification. (Image adapted from Anzalone et al., 2019).*

The first prime editor version (PE1) utilised the WT form of Moloney murine leukemia virus reverse transcriptase, while the subsequent version (PE2) introduced five mutations to increase the overall efficiency and stability of the RT enzyme. During the prime editing mechanism, DNA mismatch repair (MMR) can intervene to revert the nicked heteroduplex after 3’ flap annealing or after ligation to restore the wild-type sequence. In order to impede these events, different strategies have been developed. PE3 uses a second gRNA, called nicking guide (ngRNA), to enable Cas9 to introduce a second nick on the opposite strand to the edited strand. This approach biases MMR repair outcomes towards cellular replacement of the nicked non-edited strand, leading to an increased editing efficiency compared to PE2.

Concurrent nicks, the one introduced by Cas9-pegRNA and the second by the Cas9-ngRNA, can predispose the cell to the formation of indel byproducts. To avoid this, PE3b strategy uses a nicking guide that can only perfectly match the edited sequence, thereby allowing nicks only after the edit is incorporated. Better performance of the prime editing machinery was also reached by transient expression of an engineered MMR-inhibiting protein (MLH1dn), thus leading to the development of PE4 (PE2 + MLH1dn) or PE5 strategies (PE3 + MLHdn1) (Chen et al. 2021; Chen and Liu 2023; Doman et al. 2022).

Compared to the first version of prime editing, substantial improvements were also performed on pegRNA, aiming preferentially to stabilize its structure. The incorporation of structural RNA motifs, such as the so-called trimmed prequeosine$_1$-1 riboswitch aptamer (tevopreQ1), to the 3' terminus of pegRNAs protects them from 3' exonuclease degradation and improves the structural stability. The resulting engineered pegRNA (epegRNA) contributed to increasing the prime editing efficiencies (Nelson et al. 2022).

1.5.3 Base and prime editing: improvements, applications and current limitations

Several engineering efforts have been made to improve the overall editing activity of base and prime editing, addressing needs in on-target efficiency and limited off-target effects. For base editing, Richter et al. developed ABE8e, a more processive enzyme, that has been successfully applied in recessive dystrophic epidermolysis bullosa (RDEB) patient-derived fibroblasts, by correcting the c-5047 C>T mutation in COL7A1 gene, with high efficiency and no detectable DNA and RNA off-target events (Richter et al. 2020; Sheriff et al. 2022). During the development of the different base editor versions, the need to expand their targeting scope led to the combination of cytosine and adenine deaminases with engineered Cas9 variants recognizing alternative PAM sequences, such as the SpCas9-NG variant (Nishimasu et al. 2018). In addition, bystander edits can arise due to the presence of multiple editable cytosines or adenines in the target site, thus leading to the undesired conversion of non-targeted nearby nucleotides (Rees and Liu 2018). In this context, the development of NG-ABE9e version, characterised by a narrowed

editing window, showed enhanced on-target editing activity and reduced bystander mutations compared to the previous NG-ABE8e (Tu et al. 2022).

From the beginning, the main challenges with prime editing were the large size of the prime editor enzyme and the low editing efficiency. The Prime Editor 6 (PE6) system introduces several modifications in the Cas9 and RT to improve various aspects of prime editing technology. These include a smaller size for more effective delivery, improved specificity and editing activity, and enhanced performance in challenging cell types such as T cells and primary cells (Doman et al. 2023; Lee, Kweon, and Kim 2025). From the pegRNA side, a recent innovation regards the use of the La protein, which is an RNA-binding factor that protects transcripts from degradation by exonucleases. In particular, fusing the prime editor enzyme to the N-terminal RNA-binding domain of the La protein allows La to bind to and stabilise polyuridine sequences at the 3′ end of the pegRNA. The resulting system, PE7, produced considerable improvements in MMR-proficient cell lines such as HeLa and U2OS, compared to previous editing systems (Yan et al. 2024).

In mice, prime editing has been successfully used to treat α1-antitrypsin deficiency (AATD) by targeting a G-to-A substitution in the SERPINA1 gene. In this context, the use of an NLS-optimised PE2 plasmid increased targeted correction by 3.1-fold compared to the PE2 strategy. Additionally, in a Pah^{enu2} mouse model of phenylketonuria (PKU), adenoviral delivery of an RNase H-deleted PE enzyme (PE3ΔRnH) achieved up to 17.4% correction of the Pah mutation. The correction was also associated with therapeutic benefits as a reduction in blood phenylalanine and no technical-related issues, such as off-target effects or liver inflammation (Zhao et al. 2023).

1.6 Other CRISPR-related approaches

1.6.1 CRISPR activation

The CRISPR activation (CRISPRa) system uses a catalytically inactive Cas9 (dCas9), which, when fused with activator domains, can be directed by a guide RNA (gRNA) to recognise specific promoter or enhancer regions and activate gene

transcription. This approach does not rely on double-strand breaks but exploits the DNA-binding ability of Cas9 to modulate transcription through specific activator domains (Gilbert et al. 2014). One of the first used activator domains was VP64 (derived from herpes simplex protein VP16) and VP160 (ten copies of VP16). Following these single-component activators, new activators were developed by fusing multiple domains to increase the resulting transcriptional activation. These include VPR, a hybrid tripartite activator constituted by VP64-p65-Rta that, when fused to dCas9 and coupled with 3 or 4 sgRNA, showed enhanced activation of endogenous target genes compared to VP64. Other activators were represented by Suntag, a system that uses a peptide repeat that binds copies of VP64 via a single fragment antibody (scFv), and by SAM (Synergistic Activation Mediator) system, that extends dCas9-VP64 by recruiting additional activator domains, p65 and HSF1, via a modified sgRNA using an MS2 stem-loop structure. An integration of SAM and Suntag elements generated TREE, one of the most recent platforms to achieve even higher activation levels (Chavez et al. 2015; Clark et al. 2024).

1.6.2 CRISPR interference

Similarly to CRISPRa, CRISPR interference (CRISPRi) exploit DNA-binding ability of dCas9 (devoid of nuclease activity) to silence genomic regions, specified by gRNA. In this case, dCas9 alone has been demonstrated to be enough for transcriptional inactivation of target genes, due to steric hindrance of the dCas9/gRNA complex on the targeted site. Indeed, by targeting different genomic regions (promoter or coding regions), the system can interfere with RNA polymerase, preventing the binding of transcription factors and the initiation of transcription, or by blocking its activity, thereby stopping the transcription elongation (Qi et al. 2013). To achieve a more effective transcriptional repression, dCas9 has often been fused to transcriptional repressors, such as the well-known Krüppel Associated Box (KRAB) repressor domain from Kox1, that were demonstrated to increase the efficiency of CRISPRi by recruiting proteins affecting the chromatin structure. Subsequent studies also identified a suitable targeting window (from -50 to +300bp relative to the transcription start site) to achieve good silencing results (Gilbert et al. 2013, 2014). Other repressor systems include the

dCas9- KRAB-Methyl-CpG Binding Protein 2 (MeCP2), which enhances transcription repression by recruiting additional co-repressors; the ZIM3 dCas9-KRAB, which uses a more potent KRAB domain; and the most recent dCas9-SALL1-SDS3, which can recruit other chromatin-modifying enzymes, such as histone deacetylases, to achieve a stronger transcriptional inhibition (Alerasool et al. 2020; Mills et al. 2022; Yeo et al. 2018).

1.6.3 High-throughput CRISPR screening

Among the various uses of the CRISPR system, CRISPR screening immediately attracted particular interest, given its ability to interrogate the function of a wide range (or even the totality) of genes. CRISPR screening, in the form of knockout, activation, and interference, has allowed researchers to explore complex biological questions in a high-throughput manner. Two main versions of CRISPR screening have been developed: the pooled and arrayed approach. In a pooled screening, cells are transduced with a pooled library of sgRNA at low multiplicity of infection (MOI) to ensure that cells do not receive more than one sgRNA-expressing vector. A selection is then applied to isolate specific phenotypes, followed by deep sequencing to identify enriched or depleted sgRNAs. On the other hand, arrayed screens are performed in multi-well plates, where a different sgRNA-targeting gene is delivered in each well, thus allowing a more precise identification of genotype-to-phenotype perturbations. CRISPRko and CRISPRi screening have shown advantages over the previous RNA interference (RNAi) screen, which often suffer from variability and off-target issues, while CRISPRa has largely substituted cDNA overexpression libraries, which usually lead to unphysiological target overexpression and are costly to produce. One of the recent arrayed CRISPR libraries uses plasmids encoding 4sgRNA, achieving high levels of gene perturbations, with potential applications in the discovery of new gene candidates in the investigated molecular pathways (Agrotis and Ketteler 2015; Joung et al. 2017; Yin et al. 2025).

1.7 Besides CRISPR genome editing: investigation of HLA-C stability by *in silico* approaches

1.7.1 HLA-C molecule: role and genetic diversity

The human leukocyte antigen C (HLA-C) is a highly polymorphic gene encoding the α (heavy) chain of the major histocompatibility complex class I (MHC-I). Together with β2-microglobulin (β_2m) and an antigenic peptide, the complex plays a central role in immune defence (Figure 9) (Parham, 1988; Kulpa and Collins, 2011). Along with the other HLA classical Class I molecules (HLA-A and HLA-B), HLA-C presents peptides derived from cytosolic proteins to $CD8^+$ cytotoxic T lymphocytes (CTLs), enabling the recognition and elimination of intracellular pathogens. In addition, HLA-I molecules can act as a ligand for killer Ig–related receptors (KIRs) on natural killer (NK) cells, aiming at counteracting pathogens that tend to reduce HLA-I expression to escape immune recognition (Kulpa and Collins, 2011; Rasmussen et al., 2014).

HLA-C molecules display lower cell surface expression compared with HLA-A and HLA-B (Blais, Dong, and Rowland-Jones 2011). The binding of miR-148a to the 3' UTR of the HLA-C gene results in reduced HLA-C protein expression levels. HLA-C alleles presenting substitutions in the microRNA binding site contribute to a higher surface expression. This differential expression has also been associated with a better or worse control of HIV-1 viral load, in case of highly or poorly expressed HLA-C alleles, respectively (O'Huigin et al. 2011). The limited surface expression has also been linked to a dihydrophobic signal present in the HLA-C cytoplasmatic tail, which causes accelerated molecule internalization and intracellular degradation (Schaefer et al. 2008).

The poor surface expression of HLA-C also correlates with its intrinsic assembly properties, since HLA-C heavy chains have been demonstrated to be less efficiently associated with β2m (Neefjes and Ploegh 1988). Additionally, HLA-C molecules display more selective peptide-binding preferences, which result in prolonged association with the transporter associated with antigen processing (TAP) in the endoplasmic reticulum (ER). Consequently, many molecules are retained and

degraded in the ER, with a reduction of stable complexes that reach the surface (Blais et al. 2011; Neisig, Melief, and Neefjes 1998).

Although to a lesser extent than HLA-A and -B, HLA-C exhibits a high level of gene polymorphism. It has already been established that the expression of HLA-C also varies in relation to the allele considered. Kaur et al. demonstrated that variations in exons 2 and 3, encoding antigen-binding α1 and α2 domains of MHC Class I heavy chain, determine variations in membrane expression. These differences are due to structural variations in the peptide-binding cleft, which changes the range of peptides bound by each HLA-C molecule and the consequent efficiency of complex assembly (Kaur et al. 2017).

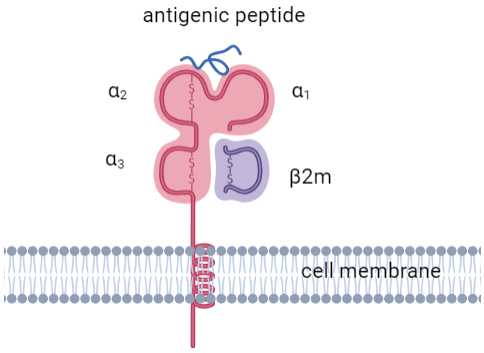

Figure 9. MHC-I complex. *HLA-C molecule (in red) is expressed on cell membrane and binds with β2-microglobulin (β2m) and an antigenic peptide. Image created with Biorender.*

1.7.2 *In vitro* and bioinformatic approaches to study HLA-C allele stability

Genetic diversity, differential expression and specific peptide binding properties are all factors influencing HLA-C complex stability. This concept, defined as the ability to form and maintain stable membrane HLA-C/β_2m/peptide complexes, varies among the different HLA-C allotypes. The high number of HLA alleles has also made it difficult a complete characterisation of the stability of the different HLA-C/peptide complexes *in vitro.* Pulse-chase experiments by Sibilio et al. demonstrated allele-specific differences in the post-assembly stability of HLA-C molecules. Variants such as HLA-C*05, *06, and 08 showed a stronger binding with β2-microglobulin binding with a resulting increased complex stability, while

alleles like HLA-C*04 and *07 exhibited weaker β_2m association and reduced stability with a consequent higher proportion of free heavy chains (Parolini et al. 2018; Sibilio et al. 2008).

CRISPR/Cas9 technology has primarily been used in other contexts, primarily to study the immunological roles of HLA molecules. Hong et al., for example, used CRISPR/Cas9 to disrupt the HLA-A, HLA-B and HLA-C genes simultaneously, generating an HLA Class I-null HEK293T cell line. These cells were subsequently transduced with single HLA class I alleles together with co-stimulatory molecules to create artificial antigen-presenting cells (APCs), demonstrating that these engineered cells could effectively present antigens and selectively activate tumour antigen-specific $CD8^+$ T cells (Hong et al. 2017).

Another study, conducted by Xu et al., utilized CRISPR/Cas9 to disrupt HLA genes in iPSCs, aiming to generate immunocompatible donor cell lines. The study highlights critical aspects in the design of a CRISPR/Cas9 experiment for HLA gene knockout, including the need to identify gRNAs that can specifically target individual alleles present in target cells, thereby avoiding off-target effects resulting from the high similarity between different HLA genes (Xu et al. 2019).

Sarkizova et al. experimentally identified the peptides binding to the most frequent HLA class I molecules, including several HLA-C allotypes. To do this, they used mass spectrometry on B721.221 cells lacking endogenous HLA and engineered to express single HLA class I alleles. This strategy allowed them to characterise a large repertoire of eluted peptides. The resulting dataset contributed to the development of HLAthena, a high-performance bioinformatic tool for predicting peptide/HLA interactions (Sarkizova et al. 2020).

Over the years, several computational tools have been developed to predict and estimate the binding affinity between HLA and peptides (Wang, Kurgan, and Li 2023). Among these, NetMHCpan has been widely used in various contexts, including recent studies investigating the possibility of developing new vaccines, being used as a system to identify immunodominant class I–restricted epitopes from SARS-CoV-2 and influenza virus proteins (Elalouf et al. 2023; Khairkhah et al. 2020). NetMHCpan 4.0 used the integration of binding affinity and mass spectrometry-eluted ligand data to predict HLA Class I/peptide interactions (Jurtz

et al. 2017), while version 4.1 was based on a larger training dataset and a more advanced neural network, resulting in more accurate and biologically relevant estimates of antigen presentation (Reynisson et al. 2021).

The most recent version, NetMHCpan 4.2, available in 2025, offers several significant improvements. It includes a larger training dataset, expands MHC Class I coverage, and incorporates new features in the algorithm, such as amino acid deletion modelling. Like previous versions, the new version consistently provides an EL (eluted ligand) score that quantitatively describes the likelihood of a peptide being naturally processed and presented on an MHC Class I molecule, thus offering a more biologically relevant measure than binding affinity (BA) alone. In addition to the conventional BA+EL prediction mode, the tool now offers specialised modes tailored to pathogen and tumour neoepitopes, enabling more biologically relevant predictions (Nilsson et al. 2025).

The calculation of the EL-score on the NetMHCpan server can therefore be used to derive a measure of the stability of the HLA-C/peptide complexes. By determining this score for a wide range of peptides binding to a specific allotype, it is possible to deduce the strength of association of the various HLA allotypes with their own peptide pools. Other tools have been developed to provide more direct measures of stability, such as NetMHCstabpan (Rasmussen et al. 2016), but these have been trained on data from only a few alleles, meaning that most HLA-C alleles are not covered by these data.

1.7.3 HLA-C genotyping and correlation with infectious diseases

The presence of a high number of different HLA-C alleles has often been linked to the concept of genetic susceptibility to viral infections (Blackwell, Jamieson, and Burgner 2009). In particular, the stability and expression levels of different HLA-C can influence the response to certain viral infections, such as HIV-1. High HLA-C expression levels have been shown to contribute to more effective control of HIV-1 infection, primarily due to an enhanced cytotoxic CD8+ cell antiviral response (Apps et al. 2013). At the same time, being correlated to expression levels, the concept of stability plays an important role in modulating viral infectivity. Parolini et al. demonstrated that, following HIV-1 infection of PBMCs derived from

healthy donors genotyped for either stable or unstable alleles and supernatant collection, the resulting infectivity on target cells revealed significant differences, with higher levels of infectivity in supernatants from donors carrying unstable alleles. Consistently, virions produced by 721.221-CD4 cells transfected with HLA-C*07, previously characterised as unstable allele, displayed significantly greater infectivity than those produced by the same cells transfected with the stable HLA-C*06 allele (Parolini et al. 2018).

The study by Stefani et al. provided stronger evidence for the association between HLA-C complex stability and viral infection outcomes. The researchers performed HLA-C genotyping on a cohort of treatment-naïve HIV-1-positive patients displaying different rates of progression to AIDS. The study showed that individuals with unstable HLA-C alleles progressed to AIDS significantly faster than those with stable alleles (Stefani et al. 2022).

HLA-C genetic variability has also been associated with HIV-associated neurocognitive disorders (HAND). Unstable HLA-C alleles, presenting a weaker binding stability with β_2m /peptide, can lead to increased levels of free β2-microglobulin (β_2m) in the cerebrospinal fluid, thus promoting neuroinflammation and neuronal damage (Zipeto et al. 2018). Furthermore, the HLA-C*07 allele has specifically been associated with an increased incidence of HAND in HIV-positive patients (Pons-Fuster et al. 2024).

An association between HLA-C and the severity of viral infections has also emerged in the context of SARS-CoV-2. Specifically, analysis of a Spanish Mediterranean Caucasian cohort revealed that certain HLA-C alleles, such as HLA-C*08:02, HLA-C*12:03 and HLA-C*16:01, were associated with a milder course of COVID-19. These alleles can induce a more efficient antiviral immune response by forming a greater number of stable HLA-C/β_2m/peptide complexes. In contrast, other less expressed and less stable alleles can be linked to an ineffective response and risk of severe disease outcomes (Vigón et al. 2022).

2. MATERIALS AND METHODS

2.1 Buffer and solution

Laemmli Buffer	50mM Tris-HCl pH 6.8 6% v/v glycerol 3% v/v β-mercaptoethanol 1% w/v SDS 0.001 % w/v bromophenol blue
RIPA buffer	50mM Tris-HCl pH 7.5 150mM NaCl 2mM EDTA 1mM PMSF 1% v/v Triton X-100 1% v/v Sodium deoxycholate Protease inhibitors cocktail (Roche)
Running Buffer	25mM Tris 192mM Glycine 0.1% w/v SDS
Transfer buffer	25mM Tris 192mM Glycine 0.1% w/v SDS 20% v/v methanol
TBS-T	20mM Tris 150mM NaCl 0.1% v/v Tween-20 pH 7.6

TAE	40 mM Tris 20 mM Acetic acid 1 mM EDTA

2.2 Cell culture

Human embryonic kidney (HEK) 293T cells were purchased from the American Type Culture Collection (ATCC) and cultured in Dulbecco's Modified Eagle Medium (DMEM, Euroclone), supplemented with 10% fetal bovine serum (FBS, Euroclone), 1% L-glutamine (Euroclone) and 1% penicillin/streptomycin (Euroclone), at 37 °C under humidified atmosphere of 5% CO_2. Cells were washed with 1X Phosphate Buffered Saline (PBS, Euroclone) and splitted using 1X trypsin/EDTA (Euroclone). For prime editing experiments, HEK293T were provided by Prof. Marianne Carlon and cultured in Dulbecco's Modified Eagle Medium + Glutamax ™ (Gibco ™), supplemented with 8% fetal bovine serum (FBS, Euroclone), and 0.1% gentamicin (Euroclone), at 37 °C under humidified atmosphere of 5% CO_2. Cells were washed with 1X Phosphate Buffered Saline (PBS, Euroclone) and splitted using 1X trypsin/EDTA (Euroclone).

The HeLa derived TZM-bl cells were provided by EU Programme EVA Centre for AIDS (NIBSC) and cultured in Dulbecco's Modified Eagle Medium (DMEM, Euroclone), supplemented with 10% fetal bovine serum (FBS, Euroclone), 1% L-glutamine (Euroclone) and 1% penicillin/streptomycin (Euroclone), at 37 °C under humidified atmosphere of 5% CO_2. Cells were washed with 1X Phosphate Buffered Saline (PBS, Euroclone) and splitted using 1X trypsin/EDTA (Euroclone).

PANC-1 PDAC cells were provided by Prof. Ilaria Dando's Laboratory and grown in RPMI 1640 (Gibco), supplemented with 10% FBS (Euroclone) and 50 μg/ml gentamicin sulphate (Gibco), at 37 °C under humidified atmosphere of 5% CO_2. Cells were washed with 1X Phosphate Buffered Saline (PBS, Euroclone) and splitted using 1X trypsin/EDTA (Euroclone).

Mouse melanoma B16 cells were kindly provided by Prof. Maria Teresa Valenti and cultured in Dulbecco's Modified Eagle Medium (DMEM, Euroclone), supplemented with 10% fetal bovine serum (FBS, Euroclone), 1% L-glutamine

(Euroclone) and 1% penicillin/streptomycin (Euroclone), at 37 °C under humidified atmosphere of 5% CO_2. Cells were washed with 1X Phosphate Buffered Saline (PBS, Euroclone) and splitted using 1X trypsin/EDTA (Euroclone).

Osteosarcoma MG63 cells were kindly provided by Dr. Maria Teresa Valenti and cultured in Dulbecco's Modified Eagle Medium (DMEM, Euroclone), supplemented with 10% fetal bovine serum (FBS, Euroclone), 1% L-glutamine (Euroclone) and 1% penicillin/streptomycin (Euroclone), at 37 °C under humidified atmosphere of 5% CO_2. Cells were washed with 1X Phosphate Buffered Saline (PBS, Euroclone) and splitted using 1X trypsin/EDTA (Euroclone).

2.3 Plasmids

The pSpCas9(BB)-2A-Puro (PX459) V2.0, psPAX2, pVSV-G, lentiCas9-Blast, and B52_puro_empty_gRNA were purchased from Addgene.

The pEGFP plasmid was obtained from Clontech.

pCMV-dR8.91 and pCSFLW were purchased from Addgene.

The plasmid expressing HIV-1 envelope proteins was purchased from EU Program EVA Centre for AIDS (NIBSC).

HIV-1-LAI Nef (Nef-LAI) and HIV-1-SF2 Nef (Nef-SF2) plasmids were provided by Prof. Massimo Pizzato (CIBIO, Trento, Italy).

The ACOT8 plasmid was provided by S. Benichou (Institut Cochin de Genetique Moleculaire, France).

ACOT8 mutant plasmid, called ΔPAK-ΔPK, was generated by our research group, as described by Serena *et al.*, 2016.

PcDNA6.2 (Invitrogen) plasmids expressing different HLA-C alleles (C*01/02/03/04/05/06/07/08/12/16) were engineered by HLA-C RT PCR.

For prime editing experiments, pU6-tevopreq1-GG-acceptor, pU6-pegRNA-GG-acceptor, and pCMV-PE2 were kindly provided by Prof. Marianne Carlon. For virus-like particles (VLPs) production, pBS-CMV-MLV-gag-pol, pCMV-MMLVgag-3xNES-Cas9, pBluescriptSKII+ U6-sgRNA(F+E) empty and VSV-G plasmids were kindly provided by Prof. Marianne Carlon, too.

2.4 sgRNA design and cloning

SgRNAs were designed using the CHOPCHOP (https://chopchop.cbu.uib.no/) or CRISPRscan (https://www.crisprscan.org/gene/) tools. According to Zhang's protocol (Ran et al. 2013), forward and reverse oligonucleotides were ordered (BMR genomics) after addition of overhangs, annealed and cloned into proper recipient vectors. After transformation into TOP10 competent bacteria, sgRNA-encoding plasmids were extracted and purified by MIDIprep (QIAGEN). Correct insertion of the sgRNAs was confirmed by Sanger sequencing (BMR genomics). Table 1 lists the ordered oligonucleotides and their corresponding recipient vectors.

TARGET GENE	sgRNA (s)	Expressing vector (s)
ACOT8 *Exon 1*	Fw: CACCGCGGTCGTGACCAAGACGCTA Rev: AAACTAGCGTCTTGGTCACGACCGC	Px459 v2.0
HADHA *Exon 1*	gRNA_1_fw: CACCGGGCAGGCCTCACCTCGGGAG gRNA_1_rev: AAACCTCCCGAGGTGAGGCCTGCCC gRNA_2_fw: CACCGGGAAGGCAGAAAAGCGGCTG gRNA_2_rev: AAACCAGCCGCTTTTCTGCCTTCCC	Px459 v2.0
RUNX2 *Exon 4*	gRNA_1_fw: CACCGCCCATCTGGTACCTCTCCGA gRNA_1_rev: AAACTCGGAGAGGTACCAGATGGGC gRNA_2_fw: CACCGAAATCTCAGATCGTTGAACC gRNA_2_rev: AAACGGTTCAACGATCTGAGATTTC	Px459 v2.0
FBXW11 *Exon 1*	Fw: CACCGGCTGCTGCGCGGGGAGAGCG Rev: AAACCGCTCTCCCCGCGCAGCAGCC	Px459 v2.0
FBXW11 *Exon 2*	Fw: CACCGGTGGCTAGGCTGCGCCAACC Rev: AAACGGTTGGCGCAGCCTAGCCACC	Px459 v2.0
FBXW11 *Exon 5*	Fw: CACCGTTCTTTCGTACCTGGATGCC Rev: AAACGGCATCCAGGTACGAAAGAAC	Px459 v2.0
FBXW11 *Exon 7*	Fw: CACCGTGGACGACACAACTTGCAG Rev: AAACCTGCAAGTTGTGTCGTCCAC	B52_puro_empty_gRNA; pBluescriptSKII+ U6-sgRNA(F+E) empty
FBXW11 *Exon 4*	gRNA_1_fw: CACCGCTTGATCTGATTCAGACCAC gRNA_1_rev: AAACGTGGTCTGAATCAGATCAAGC gRNA_2_fw: CACCGCTGTGATCGTCTCCAGAAAG gRNA_2_rev: AAACCTTTCTGGAGACGATCACAGC	pBluescriptSKII+ U6-sgRNA(F+E) empty

HLA-C Exon 2	Fw: CACCGACACAGAAGTACAAGCGCC Rev: AAACGGCGCTTGTACTTCTGTGTC	pBluescriptSKII+ U6-sgRNA(F+E) empty

Table 1. sgRNA design and recipient vectors. *SgRNAs, in the form of forward and reverse oligonucleotides, are reported in column 2. Overhangs are highlighted in green. Targeted genes (and exons) and recipient vectors are shown in column 1 and 3, respectively.*

2.5 Guide design for prime editing

PegRNA and ngRNA were designed using PRIDICT 2.0 online software (https://www.pridict.it/). Oligos for the pegRNA spacer, the 3' extension, and the ngRNA spacer were ordered both for introducing the RUNX2 (c.505C>T) mutation and also to correct it. Oligos were annealed and then ligated into the corresponding linearized vectors, along with the annealed scaffold oligonucleotides, in a Golden Gate assembly reaction. Briefly, for pegRNA, 30ng of pU6-tevopreq1-GG-acceptor (digested with BsaI enzyme) was incubated with annealed pegRNA protospacer, annealed pegRNA 3'extension, and phosphorylated annealed sgRNA scaffold. For ngRNA, 30ng of pU6-pegRNA-GG-acceptor (digested with BsaI enzyme) was incubated with annealed ngRNA protospacer and two annealed sgRNA scaffolds (with the first one phosphorylated). For both the reactions, T4 DNA ligase (NEB), 10X T4 DNA ligase buffer (NEB) and BsaI (ThermoFisher) were added and this setup was followed: 5 min at 16°C and 5 min at 37°C for 8 cycles, followed by 15 min at 80°C, then hold at 12°C. The resulting plasmids were transformed into *E. coli* DH5α competent cells, followed by colony isolation, miniprep of three selected colonies, Sanger sequencing verification, and subsequent maxiprep. Table 2 reports the different oligos used as pegRNA or ngRNA spacer, 3' extensions, and scaffold. Table 3 reports the composition of the different ligation conditions.

Oligo name	Oligo sequence	Editing purpose
RUNX2_e3_spA/B	Fw: CACCGAAAATTATTCTGCTGAGCTCGTTTA Rev: CTCTTAAACGAGCTCAGCAGAATAATTTTC	Mutation correction (C>T) and insertion (T>C)
RUNX2_RTT_1A	Fw: GTGCAGAGGCATTCCgGAGCTCAGCAGAATAATT Rev:CGCGAATTATTCTGCTGAGCTCcGGAATGCCTCT	Mutation correction (C>T)
RUNX2_RTT_2A	Fw:GTGCGCAGAGGCATTCCgGAGCTCAGCAGAATAA Rev:CGCGTTATTCTGCTGAGCTCcGGAATGCCTCTGC	Mutation correction (C>T)
RUNX2_RTT_3A	Fw:GTGCGAGGCATTCCgGAGCTCAGCAGAATAA Rev: CGCGTTATTCTGCTGAGCTCcGGAATGCCTC	Mutation correction (C>T)
RUNX2_ng1_e3_A/B	Fw: CACCGCCCATCTGGTACCTCTCCGAGTTTA Rev: CTCTTAAACTCGGAGAGGTACCAGATGGGC	Mutation correction (C>T) and insertion (T>C)
RUNX2_ng2_e3_A/B	Fw: CACCGAGACCTACCTCGTCCACTCGTTTA Rev: CTCTTAAACGAGTGGACGAGGTAGGTCTC	Mutation correction (C>T) and insertion (T>C)
RUNX2_e4_sp_1B	Fw: CACCGTCATAACAGCAGAGGCATTCGTTTA Rev: CTCTTAAACGAATGCCTCTGCTGTTATGAC	Mutation insertion (T>C)
RUNX2_RTT_1.1B	Fw: GTGCTGAGCTCtGGAATGCCTCTGCT Rev: CGCGAGCAGAGGCATTCCaGAGCTCA	Mutation insertion (T>C)
RUNX2_RTT_2.1B	Fw: GTGCTGCTGAGCTCtGGAATGCCTCTGCTGTT Rev: CGCGAACAGCAGAGGCATTCCaGAGCTCAGCA	Mutation insertion (T>C)
RUNX2_RTT_1.2B	Fw: GTGCAGAGGCATTCCaGAGCTCAGCAGAATAATT Rev: CGCGAATTATTCTGCTGAGCTCtGGAATGCCTCT	Mutation insertion (T>C)
RUNX2_RTT_2.2B	Fw: GTGCGAGGCATTCCaGAGCTCAGCAGAATAA Rev: CGCGTTATTCTGCTGAGCTCtGGAATGCCTC	Mutation insertion (T>C)
RUNX2_ng1_e4_B	Fw: CACCGACTGTGGTTACTGTCATGGGTTTA Rev: CTCTTAAACCCATGACAGTAACCACAGTC	Mutation insertion (T>C)
RUNX2_ng2_e4_B	Fw: CACCGAGAGGTACCAGATGGGACTGGTTTA Rev: CTCTTAAACCAGTCCCATCTGGTACCTCTC	Mutation insertion (T>C)
F+E_COM	Fw:AGAGCTATGCTGGAAACAGCATAGCAAGTTTAAATAAGG CTAGTCCGTTATCAACTTGGCTGAATGCCTGCGAGCATCCCA CCCAAGTGGCACCGAGTCG Rev: gcacCGACTCGGTGCCACTTGGGTGGGATGCTCGCAGGC ATTCAGCCAAGTTGATAACGGACTAGCCTTATTTAAACTTGC TATGCTGTTTCCAGCATAG	Scaffold sequence
FE_COM_H1	Fw: AGAGCTATGCTGGAAACAGCATAGCAAGT TTAAATAAGGCTAGTCCGTTA Rev: TTGATAACGGACTAGCCTTATTTAAACTT GCTATGCTGTTTCCAGCATAG	Scaffold sequence
FE_COM_H2	Fw: TCAACTTGGCTGAATGCCTGCGAGCATCC CACCCAAGTGGCACCGAGTCGGTGC Rev: AAAAGCACCGACTCGGTGCCACTTGGGTGGG ATGCTCGCAGGCATTCAGCCAAG	Scaffold sequence

Table 2. Oligo name and design for pegRNA and ngRNA. *For RUNX2 mutation correction or insertion, pegRNA and ngRNA spacer, 3' extensions and scaffold sequences*

are reported in the form of forward and reverse oligonucleotides in column 2. Overhangs are highlighted in green.

Condition	Vector	Spacer	Scaffold	3'-extension/scaffold
1A	pU6-tevopreq1-GG-acceptor	e3_spA/B	F+E_COM	RTT_1A
2A	pU6-tevopreq1-GG-acceptor	e3_spA/B	F+E_COM	RTT_2A
3A	pU6-tevopreq1-GG-acceptor	e3_spA/B	F+E_COM	RTT_3A
4A	pU6-pegRNA-GG-acceptor	ng1_e3_A/B	FE_COM_H1	FE_COM_H2
5A	pU6-pegRNA-GG-acceptor	ng2_e3_A/B	FE_COM_H1	FE_COM_H2
6B	pU6-tevopreq1-GG-acceptor	e4_sp_1B	F+E_COM	RTT_1.1B
7B	pU6-tevopreq1-GG-acceptor	e4_sp_1B	F+E_COM	RTT_2.1B
8B	pU6-tevopreq1-GG-acceptor	e3_spA/B	F+E_COM	RTT_1.2B
9B	pU6-tevopreq1-GG-acceptor	e3_spA/B	F+E_COM	RTT_2.2B
10B	pU6-pegRNA-GG-acceptor	ng1_e4_B	FE_COM_H1	FE_COM_H2
11B	pU6-pegRNA-GG-acceptor	ng2_e4_B	FE_COM_H1	FE_COM_H2

Table 3. The different ligation conditions. *From the ordered oligos, 11 ligation reactions were prepared.*

2.6 Off-target prediction and analysis

Off-target were identified by COSMID (https://crispr.bme.gatech.edu/) web tools. The top-ranked predicted off-target sites were amplified by PCR on the extracted DNA and compared to wild-type sequences to verify the presence of unwanted mutations. Table 4 reports the PCR primers and the features of the selected off-target sites with respect to the wild-type sequence.

Target gene and gRNA	Off-target site features	PCR primers
HADHA_ gRNA_1	Chr. 5, 2 mismatches, 1 deletion	Fw: CAGGTAAAATGAAGTGCAGGG Rev: TTGAGGTGTTGAGTTAATGAGG
HADHA_ gRNA_1	Chr.16, 2 mismatches, 1 deletion	Fw: CAACAACGACAAAATGGTTGAG Rev: TTGCCCAAGCCTGAAAAG
HADHA_ gRNA_2	Chr.19, 3 mismatches	Fw: ATTCCCCAGAGATGTTGCCG Rev: CTCGTCGAGCCTTACCTGTC
HADHA_ gRNA_2	Chr. 10, 3 mismatches	Fw: TGCGTTCGCTACATACAAGGT Rev: ACCATAAACAAAGCAGCGGG

Table 4. Off-target sites and PCR primers. *Column 1 reports the considered genes and gRNAs, column 2 shows the features (mismatches and/or insertions or deletions) with respect to the wild-type sequence, column 3 reports the PCR primers for off-target site amplification.*

2.7 Killing curve

For PANC-1 and MG63 cells, a killing curve was performed by seeding $1 * 10^5$ cell in a 12-well plate (Sarstedt). The day after, different antibiotic (puromycin for PANC-1; puromycin and blasticidin for MG63) concentrations were added. 3 days after starting of selection, cells were trypsinized and counted. Table 5 reports the different antibiotic concentrations for the killing curves of the considered cell lines.

Antibiotic	Concentration (µg/ml)	Cell type
Puromycin	5 – 4.5 – 4 – 3.5 – 3 – 2.5 – 2	PANC-1
Puromycin	3 – 2.5 – 2 – 1.5 – 1 – 0.5	MG63
Blasticidin	8 – 7 – 6 – 5 – 4	MG63

Table 5. Killing curve conditions for the considered cell types.

2.8 Transfection

HEK293T cells were transfected using the TransIT®- LT1 Transfection Reagent (Mirus Bio), following the manufacturer's protocol. For prime editing experiments,

HEK293T were transfected with jetPRIME® transfection reagent (Polyplus), following the manufacturer's protocol.

MG63 cells were transfected with TransIT®- LT1 Transfection Reagent LT1 (Mirus Bio), Lipofectamine™ 3000 Transfection Reagent (Invitrogen) and Lipofectin™ Transfection Reagent (Invitrogen), following the manufacturer's protocol. MG63-Cas9 cells were transfected with in-house prepared calcium phosphate solutions.

PANC-1 cells were transfected with TransIT®- LT1 Transfection Reagent LT1 (Mirus Bio), Lipofectamine™ 3000 Transfection Reagent (Invitrogen) and nucleofected with AmaxaTM Cell Line NucleofectorTM Kit C, following the manufacturer's protocol.

B16 cells were transfected with Lipofectamine™ 3000 Transfection Reagent (Invitrogen), following the manufacturer's protocol.

Following transfection and selection, single clones were isolated by seeding 0.3 cells/well in three 96-well plates**.**

2.9 Pseudovirus production and infectivity assays

For pseudoviral production, 0.5 * 10^6 HEK293T cells are seeded in 6-well plates. Cells are then transfected with 1000ng of pCMV-dr8.91, 1250ng of pCSFLW and 2000ng of HIV-1 or VSV-G envelopes. 16-18 hours after transfection, the medium was changed. 48 hours after medium change, virus-containing medium is harvested and centrifuged at 1200rpm for 5 minutes. Supernatant is then filtered with a 0.45 µm filter. Pseudoviruses are then concentrated by using through Amicon® Ultra Centrifugal Filters with 50 kDa molecular weight cutoff (MWCO) (MilliporeSigma, Merck KGaA), by centrifuging at 2000g for 10minutes. Aliquots are then stored at -80°C.

Before pseudovirus quantification, an infectivity test is performed to confirm the efficiency of viral production. First, 50 µl of the concentrated pseudoviruses are added to wells of a 96-well plate, followed by addition of 50ul of medium. 20.000 target cells/well are then plated in 96-WP (100 µl/well). DEAD-dextran was added to the cell mixture to increase the viral infectivity, at a volume ratio of 1:187.5 (DEAE-dextran:cell suspension). 48 hours after infection, cells were treated by

using the Britelite™ Plus Reporter Gene Assay System (PerkinElmer), according to the manufacter's instructions, and the resulting luciferase activity (RLU) was measured at the Victo 3 luminometer (PerkinElmer).

One Wash™ Lentivirus Titer Kit, HIV-1 p24 ELISA (Origine) was then used to calculate the pg/ml of p24 capsid protein in the concentrated pseudoviruses, according to the manufacturer's instructions. After quantification, infectivity experiments were performed as described above, by using 625 pg of quantified p24/well and a 1:5 dilution of the viral stock. For each condition, four technical replicates were performed.

2.10 Generation of Cas9-expressing cells

$2*10^6$ HEK293T cells were seeded in 10cm dish. After 24 hours, cells were transfected with 5µg Lenti-Cas9, 3.75µg pspax2, 1.25µg VSV-G by calcium phosphate in DMEM (w/o antibiotics). The day after, the medium was changed with complete DMEM. 48hours after medium change, supernatant containing Cas9-lentiviral particles was harvested, centrifuged at 1400rpm for 5 minutes and filtered with 0.45µm filter. Target cells were infected at different multiplicities of infection (MOI) to optimise transduction efficiency, followed by selection with appropriate concentrations of blasticidin.

2.11 Virus – like particles (VLP) production and cell transduction

Virus-like particles (VLPs) were produced by transfecting HEK293T cells by linear PEI with pBS-CMV-MLV-gag-pol, pCMV-MMLVgag-3xNES-Cas9, pBluescriptSKII+ U6-cloned sgRNA(F+E) and VSV-G plasmids, according to the ratio described in Mangeot *et al.*, 2019.

VLPs were concentrated through Amicon® Ultra Centrifugal Filters with 100 kDa molecular weight cutoff (MWCO) (MilliporeSigma, Merck KGaA) and resuspended in Optimem (0% FBS, 50 µg/ml gentamicin).

For cell transduction, cells were counted, pelleted by centrifugation, and resuspended in 50 µL of VLP-containing medium. Following an incubation at room temperature for 10 minutes, the cells were plated in the appropriate culture vessels.

2.12 DNA extraction, PCR and sequence analysis

Genomic DNA was extracted using the Monarch ® Genomic DNA Purification Kit (New England BioLabs). All the CRISPR-targeted exons were first amplified through PCR, in a final concentration of 1X Wonder Taq Buffer (Euroclone), 0,6 µM forward and reverse primers (BMR Genomics); 0,05 U Wonder Taq (Euroclone). The primer pairs used are listed in Table 6. PCR products were purified through a PCR Purification kit (Norgen Biotek) and submitted for Sanger sequencing (BMR genomics). CRISPR/Cas9 knockout events were analysed using the DECODR (https://decodr.org/) or ICE (https://ice.editco.bio/) tools, while prime editing events were analysed using EditR (https://moriaritylab.shinyapps.io/editr_v10/). For HADHA KO, the pcDNA™3.1/V5-His TOPO® TA Expression Kit (Invitrogen) was used to determine the editing events.

TARGET GENE	PCR PRIMERS
ACOT8	Fw: CAGTCAAGATCAAGTTTCTGCC Rev: TGTATGTCTCCGCGTCTTCC
FBXW11 (EXON 4)	Fw: CCAAAGAAATGCTGCCTCAC Rev: GACTAATTTGAGGACACAGACC
FBXW11 (EXON 7)	Fw: ACACTGAGAGCTGCCAAGAT Rev: GAAGCAACGCCAAAGTCTGA
HADHA	Fw: AGTTGGGGAGTTAGGAAGCC Rev: CTCCACTGCTGTCCTCTTCA
RUNX2 (*MOUSE*)	Fw: AGGGAAGGAGATGCTACTTCG Rev: ATTCCCGCAGACAGCCTAAC
RUNX2 (HUMAN)	Fw: AGTGGCATCACAACCCATACA Rev: AGAAAAACACTCAACTTCATCTGG
HLA-C (EXON 2)	Fw: GGAGATGGGGAAGGCTCCCCACT Rev: AGCGAGGGGCCCGCCCGGCGA

Table 6. Target gene and PCR primers to amplify the gRNA-targeted region.

2.13 Western blot analyses

Proteins were extracted using RIPA buffer and quantified with the Coomassie Plus Bradford Protein Assay Reagent (Thermo Scientific) using a spectrophotometer (Eppendorf). Protein samples were mixed with Laemmli buffer and resolved by SDS–PAGE on acrylamide gels. Proteins were then transferred onto a PVDF membrane (GE Healthcare), blocked with 5% milk in TBS-T, and incubated overnight with the specific primary antibody. For the detection of ACOT8 and

Lamin-B1, anti-mouse and anti-rabbit secondary antibodies, respectively, were diluted 1:3000 in 5% milk TBS-Tween buffer and incubated for 1 hour at room temperature. For the detection of HADHA, the anti-mouse IgGκ BP-HRP secondary antibody was diluted 1:1500 in the same buffer and incubated for 1 hour at room temperature. Amido Black staining was used as a loading control.
For the detection of RUNX2, an anti-rabbit secondary antibody was diluted 1:3000 in 5% milk TBS-Tween buffer and incubated for 1 hour at room temperature.
For the detection of Cas9 and ACTIN, anti-mouse and anti-rabbit secondary antibodies, respectively, were diluted 1:3000 in 5% milk TBS-Tween buffer and incubated for 1 hour at room temperature.

2.14 Primary antibodies

The anti-ACOT8 monoclonal murine antibody (Santa Cruz Biotechnology) was used at a 1:500 dilution in 5% non-fat dry milk, 1X TBS, 0,1% Tween-20.
The anti-Lamin-B1 monoclonal rabbit antibody (Cell Signaling Technology) was used at a 1:1000 dilution in 5% non-fat dry milk, 1X TBS, 0,1% Tween-20.
The anti-HADHA monoclonal murine antibody (Santa Cruz Biotechnology) was used at a 1:200 dilution in 5% non-fat dry milk, 1X TBS, 0,1% Tween-20.
The anti-RUNX2 monoclonal rabbit antibody (Cell Signaling) was used at a 1:1000 dilution in 5% non-fat dry milk, 1X TBS, 0,1% Tween-20.
The anti-Cas9 monoclonal murine antibody (Santa Cruz Biotechnology) was used at a 1:1000 dilution in 5% non-fat dry milk, 1X TBS, 0,1% Tween-20.
The anti-ACTIN monoclonal murine antibody (Santa Cruz Biotechnology) was used at a 1:200 dilution in 5% non-fat dry milk, 1X TBS, 0,1% Tween-20.

2.15 Analysis of HLA-C peptide binding stability

Peptides binding to the 21 most frequent human HLA-C allotypes (Table 7) were experimentally identified through mass spectrometry analysis by Sarkizova et al. (Sarkizova et al. 2020). From the initial dataset, we selected only 8-12aa peptides, since this corresponds to the preferential binding range for MHC-I complexes (Karnaukhov et al. 2022). Netmhcpan4.2 server ((https://services.healthtech.dtu.dk/services/NetMHCpan-4.2/) was used with

default parameters to determine the eluted ligand (EL) score for each HLA-C-peptide pool interaction. A ranking of peptides specifically binding the proper HLA-C allotype was then established according to their EL score and then expressed as percentiles (% Ranking). Finally, EL score versus % Ranking curves were generated for each allele, and the area under the curve (AUC) was calculated to define a stability score for each of the considered HLA-C allotypes.

HLA-C Allotype	Frequency in the human population
C*01:02	0.085
C*02:02	0.028
C*03:02	0.025
C*03:03	0.056
C*03:04	0.091
C*04:01	0.112
C*04:03	0.019
C*05:01	0.026
C*06:02	0.062
C*07:01	0.069
C*07:02	0.131
C*07:04	0.015
C*08:01	0.045
C*08:02	0.020
C*12:02	0.032
C*12:03	0.020
C*14:02	0.025
C*14:03	0.015
C*15:02	0.034
C*16:01	0.024
C*17:01	0.019

Table 7. List of the considered human HLA-C allotype and their frequency.

2.16 HIV-1 patient cohorts

Two groups of HIV-1 infected patients were selected for our analysis.

The first cohort included HIV-1 treatment-naïve subjects presenting a different degree of AIDS progression, with 47 patients classified as progressors (P; >10,000 copies HIV genome/mm^3, and ≤200 CD4+ T lymphocytes/mm^3) and 37 patients classified as long-term non-progressors (LTNPs; <10,000 copies HIV genome/mm^3, and ≥400 CD4+ T lymphocytes/mm^3). All participants provided informed consent, and the study was approved by the relevant institutional review boards and ethics committees in Brazil. Major details on the enrolled cohort are described in Stefani et al. (Stefani et al. 2022).

The second cohort was composed of HIV-1 patients presenting or not neurocognitive impairment, as referred by the HIV-1 associated neurocognitive disorder (HAND) diagnosis, defined according to the Frascati criteria (Antinori et al. 2007). Specifically, 41 HIV-1 patients were cognitively normal (HAND-), while 16 patients reported neurocognitive deficits (HAND+). Patients reporting subjective cognitive complaints were included in the first group, in line with current international recommendations. All participants provided informed consent, and the study was approved by the Institutional Ethics Committee of Verona and Rovigo, Italy (#2459 CESC), in accordance with the Declaration of Helsinki.

2.17 HLA-C genotyping and determination of patient-specific stability scores

We extracted DNA from peripheral blood lymphocytes of HIV-1 patients and performed allele-specific polymerase chain reaction (AS-PCR) followed by Sanger sequencing to determine HLA-C allotypes, as previously described (Stefani et al. 2022). The HLA-C classification proposed by Shen et al. was adopted as the reference for conducting HLA-C genotyping (Shen, Parks, and Smith 2023). Accordingly, a set of HLA-C allotypes was selected for first digit typing since rarer allotypes generally cluster within the same subgroup, while another group was typed at the second digit mainly through sequencing of the region between exons 2–3 of the HLA-C gene and alignments using the Immuno Polymorphism Database (IPD https://www.ebi.ac.uk/ipd/index.html). Table 8 reports the set of HLA-C

allotypes typed at the first or second digit. Only for C*12 and C*16, AS-PCR allowed us to define them as 12:03 and 16:01, respectively.

For determining a patient-specific stability score, after HLA-C genotyping, the multiplication of the stability scores (previously determined by AUC) of the corresponding allotypes was performed. For HLA-C*14, where the two most common allotypes (C*14:02 and C*14:03) have similar frequencies and belong to the same subgroup, we applied a frequency-weighted mean, according to the frequency of HLA-C alleles reported by Sarkizova et al. (Sarkizova et al. 2020). The same approach was used when second-digit genotyping was not possible due to insufficient DNA. For HLA-C*12, we assigned the stability score of the other frequent allotype (C*12:02 when C12 typing did not match C*12:03). Finally, for all the alleles typed at the first-digit resolution, we used the score of the most frequent allotype.

HLA-C allele	Genotyping resolution
C*01, C*02, C*05, C*06, C*12, C*14, C*15, C*16, C*17	First-digit typing
C*03, C*04, C*07, C*08	Second-digit typing (for C*03: C*03:02, C*03:03, C*03:04; for C*04: C*04:01, C*04:03; for C*07: C*07:01, C*07:02, C*07:04; for C*08: C*08:01, C*08:02).

Table 8. HLA-C alleles and the adopted genotyping resolution.

2.18 Molecular dynamics (MD) simulations

Molecular dynamics (MD) simulations were performed on five human HLA-C allelic variants (HLA-C*03:04, C*04:01, C*05:01, C*06:02, and C*07:02) using single point-mutated peptides introduced with the 'Mutate Residue' tool in the Maestro Workspace (release 2021–2, Schrödinger, LLC, New York, NY, USA). The systems were prepared using the ff19SB force field, immersed in TIP3P water, and energy-minimized to allow the HLA-C/β_2m complex to adapt to the new peptide sequences (Mark and Nilsson 2001; Tian et al. 2020). Three independent

replicas per system were then run for 300 ns MD simulations in Amber24. Trajectories were clustered using Amber24's cpptraj tool to identify dominant conformations (Roe and Cheatham 2013). MM-GBSA analysis was then applied to quantify the pairwise binding energy contributions within HLA/β_2m complexes.

2.19 Statistical analysis

For ACOT8 experiments, four biological replicates were performed and readout was performed in four technical replicates for each biological sample. For comparison between the different experimental conditions, a two-tailed Mann–Whitney U test was used. A p-value < 0.05 was considered statistically significant. For HIV-1 patients, comparisons between HLA-C stability scores of the independent patient groups (LTNP vs P; HAND- vs HAND+) were performed using the two-tailed Mann–Whitney U test. A p-value < 0.05 was considered statistically significant.

3. AIM OF THE THESIS

The aim of this present thesis work is the application and methodological optimisation of CRISPR/Cas9 technology to study the function of single genes, specific domains, or point mutations in different biological contexts. In particular, this genome editing technique has been applied in different areas, namely the analysis of genes involved in HIV-1 virus-host interaction, the study of genes or functional domains associated with cancer pathways (such as pancreatic cancer, melanoma, and osteosarcoma), and the characterisation of single-nucleotide variants causing genetic disorders, such as cleidocranial dysplasia.

To achieve these goals, the central theme of the thesis was the development of methodological strategies to obtain efficient gene knockout and gene editing, both in easy-to-manipulate cell lines and in hard-to-transfect systems. This involved using and comparing different delivery systems for CRISPR/Cas9 technology, from conventional plasmid transfection to the use of virus-like particles for safer and more efficient delivery. Through this process, in this thesis work, we generated new *in vitro* edited cell lines that are useful for clearly depicting gene function in the associated molecular contexts.

This work has also incorporated significant *in silico* methods to complement and advance CRISPR technology, with the aim of studying gene relevance in a clinical setting, such as the impact of HLA-C stability on different outcomes of HIV-1 infection.

4. RESULTS

4.1 Successful examples of knockout of single genes in easy-to-transfect cells

4.1.1 Generation of ACOT8 KO HEK293T

ACOT8 is an acyl-CoA thioesterase mainly localized in peroxisomes and involved in lipid metabolism. Its enzymatic activity relies on the hydrolysis of fatty acyl-CoA esters, such as myristoyl-CoA and palmitoyl-CoA, into Coenzyme A (CoASH) and the corresponding free fatty acids, thereby maintaining a correct balance of intraperoxisomal acyl-CoA/CoASH levels (Ishizuka et al. 2004; Palmeira et al. 2019). Enzyme characterisation in mouse and rat models showed that the enzyme possesses a broad substrate specificity, hydrolysing nearly all tested acyl-CoA esters by recognizing the CoA moiety rather than the acyl chain. Furthermore, an increase in peroxisomal proliferation was observed after ACOT8 overexpression in murine and human T cells, thus highlighting its potential role also in peroxisome biogenesis (Hunt, Siponen, and Alexson 2012). The role of this protein has attracted greater attention since researchers discovered that it interacts with the HIV-1 Nef protein (Liu et al. 1997; Watanabe et al. 1997). HIV-1 is an enveloped virus composed by two single-stranded RNA molecules, belonging to the Lentivirus genus (family Retroviridae) and is the main cause of AIDS, a severe immune deficiency characterised by a progressive and severe depletion of CD4+ cells and a greater susceptibility to opportunist infections and neoplasm development (Février, Dorgham, and Rebollo 2011).

The negative regulatory factor (Nef) is a small HIV-1 accessory protein that plays key roles in promoting viral infections and pathogenesis. Nef can ensure an efficient viral spread by antagonizing the action of cellular proteins, such as Tetherin, that would otherwise inhibit the release of viral particles. Nef also acts in the regulation of surface membrane proteins, specifically contributing to the downregulation of MHC-I and CD4 molecules. This action finally results in immune evasion and prevents superinfection of already infected cells, thereby enhancing viral propagation (Lamers et al. 2012; Manrique et al. 2017; Palmeira et al. 2019). The N-terminal myristoylation of the Nef protein has been shown to be essential for its activity, enabling the viral protein to be anchored to the plasma membrane and

adopt an open conformation required for the interaction with targeted cellular proteins (Palmeira et al. 2019; Udenwobele et al. 2017). According to Serena et al., interaction between Nef and ACOT8 would prevent Nef cleavage by steric hindrance, thereby increasing the stability of Nef and preventing its degradation (Serena et al. 2016). Another proposed mechanism is that ACOT8 is addressed by Nef to the cell membrane, leading to an increase of ACOT8 activity with resulting depalmitoylation of Lck, a binding partner of the CD4 cytoplasmatic tails, necessary for maintaining CD4 at the cell surface. The resulting dissociation of the CD4–Lck complex contributes to CD4 internalization (Lazarow 2011; Palmeira et al. 2019).

To better elucidate the role of ACOT8 and its interaction with NEF in HIV-1 infectivity, we started with the generation of an HEK293T ACOT8 KO cell model by CRISPR/Cas9 technology (Figure 10A). Exon1 of ACOT8 was selected as a suitable target region for gRNA/Cas9-mediated knockout. After gRNA cloning into a Cas9-expressing plasmid, HEK293T cells were transfected and then selected with 0.5 μg/ml puromycin. Single clones were isolated and editing events were verified by Sanger sequencing of the PCR-amplified gRNA-targeted region. All isolated clones exhibited editing events, presenting heterozygous or homozygous CRISPR/Cas9-induced indels, thus confirming the high efficiency of the technique aided by the easy transfectability of the HEK293T cell line (Figure 10B). A clone (named A3) showing a homozygous frameshift deletion of 5bp in the targeted region was selected for further experiments (Figure 10C). Absence of the ACOT8 protein expression on the isolated A3 clone was confirmed by Western blot analysis, with lamin B1 used as housekeeping control (Figure 10D).

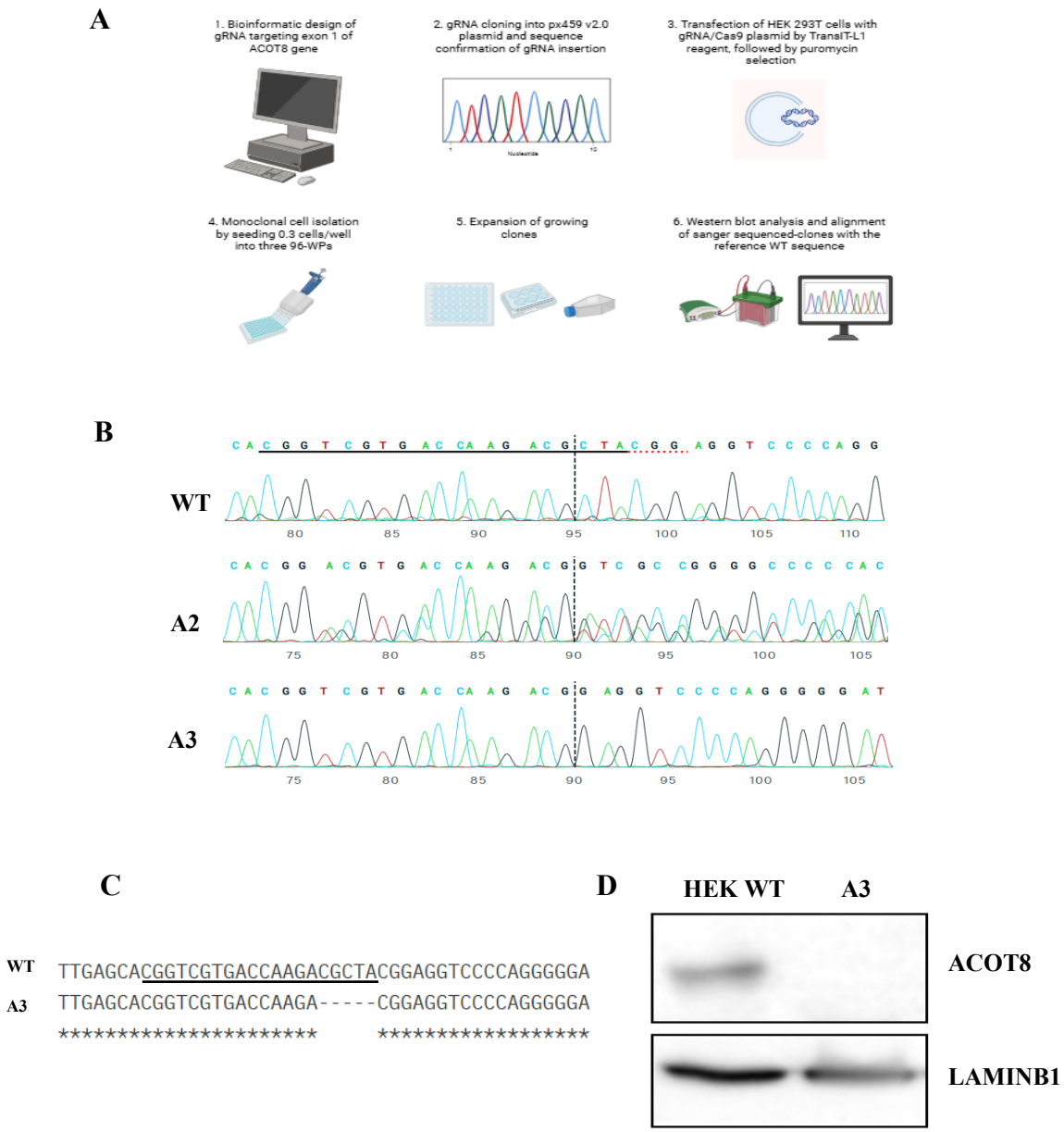

Figure 10. CRISPR/Cas9 generation of ACOT8 KO HEK293T cells. *(A) Workflow of CRISPR/Cas9 procedure to knockout ACOT8 gene in HEK293T cells (image created with BioRender). (B) Sanger sequencing chromatograms showing examples of heterozygous (in A2 clone) or homozygous (in A3 clone) CRISPR/Cas9-induced editing events in the isolated clones, in comparison with the WT sequence. In the WT sequence, the gRNA sequence is shown with a black horizontal line, the cut site with a vertical black dashed line, the PAM with a horizontal red dotted line (image adapted from Synthego Performance Analysis, ICE Analysis. 2019. v3.0. Synthego) (C) Alignment of ACOT8 gene for A3 and WT sequences, showing a 5bp-deletion in the gRNA-targeted region of A3 clone (image adapted from Clustal Omega Multiple Sequence Alignment). gRNA sequence is presented with a black horizontal line. (D) Western blot of A3 clone with respect to WT cells, showing absence of ACOT8 protein band.*

4.1.2 Investigating ACOT8 in HIV-1 infectivity

HEK293T ACOT8 KO cells were first used to assess the effect of ACOT8 absence on HIV-1 infectivity. To this aim, lentiviral-based pseudoviruses carrying different types of HIV-1 envelopes (QHO, RHPA, AC10 and LA1) were produced in HEK293T packaging cells, both ACOT8 KO and WT. A p24-normalized amount of harvested pseudoviruses was used to infect target cells (TZM-bl). Results showed that HIV-1 pseudoviruses produced in ACOT8 KO were less infective compared to the same viruses produced in WT cells, as determined by RLU infectivity values. This significant reduction effect was not observed with viruses pseudotyped with the VSV-G envelope, thus confirming a specific role of ACOT8 in supporting HIV-1 infectivity (Figure 11).

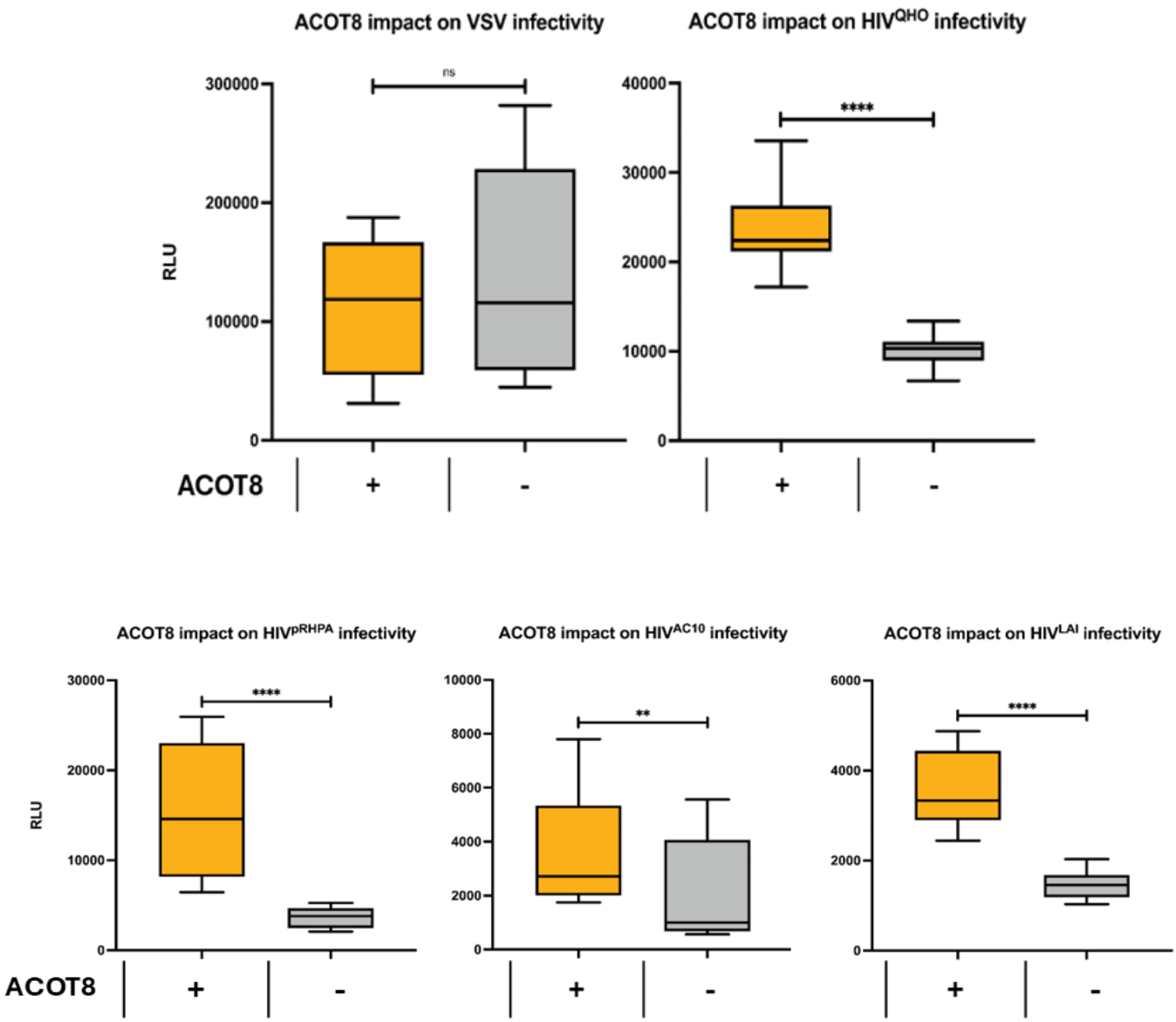

Figure 11. ACOT8 impact on HIV-1 infectivity. *Pseudoviruses bearing different HIV-1 envelopes were produced in HEK WT (ACOT8+) and HEK KO (ACOT8-) cells and used to infect target cells. Luciferase RLU values showed reduced viral infectivity for viruses produced in HEK293T ACOT8 KO, compared to the WT counterpart. No reduction in infectivity was observed when VSV-G pseudotyped viruses were produced in HEK293T ACOT8 KO or HEK WT cells.*

To confirm that the reduced infectivity was specifically due to the absence of ACOT8, we re-introduced ACOT8 plasmid in KO cells to restore ACOT8 expression at physiological levels, as confirmed by Western Blot analysis (Figure 12A-B). QHO-pseudotyped viruses were then produced in HEK WT, ACOT8 KO and ACOT8 rescued cells and then used to infect target cells. Infectivity levels, after viral production in cells with a restored ACOT8 expression, showed comparable values to pseudoviruses produced in HEK WT cells, while the virus produced in ACOT8 KO cells was confirmed to be less infectious (Figure 12C).

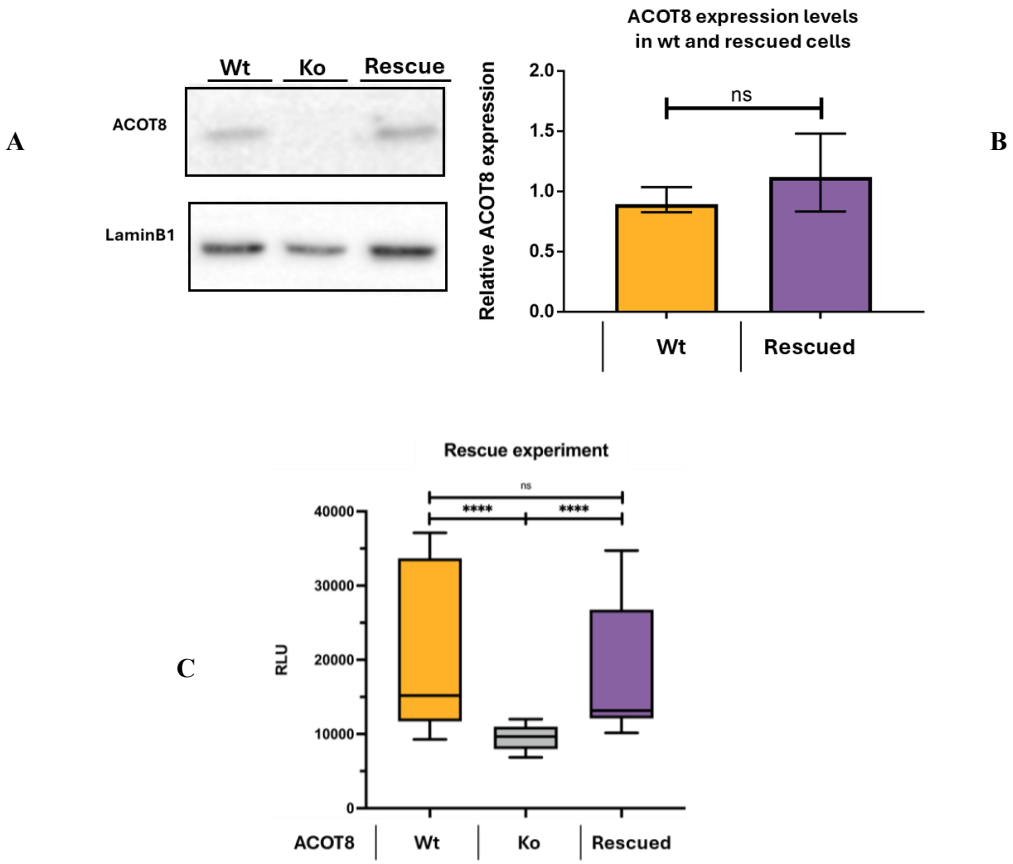

Figure 12. ACOT8 rescued expression restores HIV-1 infectivity. *(A-B) ACOT8 KO cells were transfected with ACOT8 plasmid, thus restoring physiological levels of ACOT8 expression, as shown by Western blot analysis. (C) QHO-pseudotyped viruses produced in ACOT8-rescued cells showed infectivity levels comparable to those produced in WT cells.*

4.1.3 Investigation of ACOT8/Nef interaction and resulting HIV-1 infectivity

Since the previously produced viral particles did not express Nef protein, to assess the role of the ACOT8/Nef interaction in the context of HIV-1 infectivity, we introduced two additional Nef-expressing plasmids: Nef-LAI, which maintains its interaction with ACOT8, and Nef-SF2, which harbors mutations preventing its binding with ACOT8 (Serena et al. 2016). In the following experiment, QHO-viral particles were produced in ACOT8 KO cells, transfected or not with ACOT8 plasmid and with one of the different Nef plasmids, and used to infect target cells, as described before. As previously shown, restoration of ACOT8 plasmid led to an increased in infectivity levels. The addition of Nef-LAI, interacting with ACOT8, in virus-producing cells further enhances the resulting infectivity values. The use of a Nef-expressing plasmid, NEF-SF2, not interacting with ACOT8, restored infectivity values comparable to those observed in ACOT8-rescued cells (Figure 13A).

To confirm this observation, we also used a mutant form of ACOT8, called ΔPAK-ΔPK, that carries deletions abolishing its binding to Nef (Serena et al. 2016). Following the same approach as previously described, QHO-viral particles were produced in ACOT8 KO cells and in cells that had been transfected with either the ΔPAK-ΔPK ACOT8 plasmid or one of the different Nef plasmids, and then used for the infection experiment. The addition of the mutant ACOT8 plasmid to the virus-producing cells led to an increase in infectivity on target cells with respect to cells without ACOT8 expression. Co-expression of mutant ACOT8 and NEF-LAI or NEF-SF2 did not result in further increases of infectivity (Figure 13B). Taken together, these results indicate that the ACOT8–Nef interaction contributes to a further and significant increase in HIV-1 infectivity, suggesting a possible additive effect to the ACOT8 expression alone.

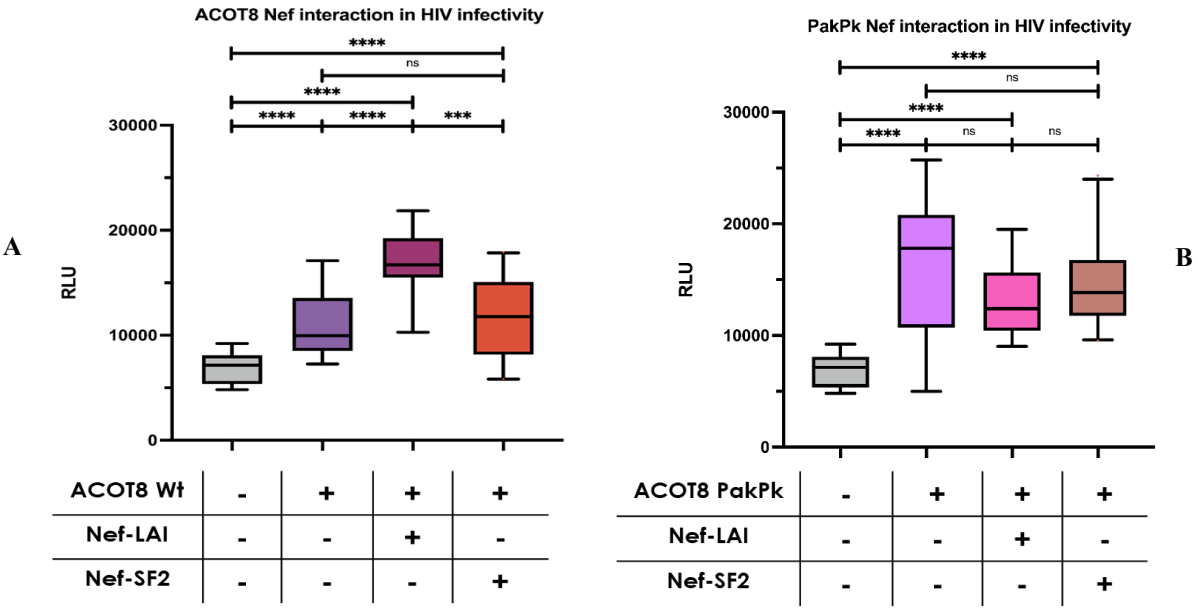

Figure 13. ACOT8/Nef interaction further promotes HIV-1 infectivity*. (A) ACOT8 KO cells were transfected with ACOT8 plasmid and one of the two Nef-expressing plasmids (NEF-LAI, interacting with ACOT8; NEF-SF2 not interacting with ACOT8). Interaction between ACOT8 and LAI in the virus-producing cells led to more infectious QHO-viral particles. (B) ACOT8 KO cells were transfected with the ACOT8 mutant plasmid (here named PakPk; not interacting with Nef) and one of the two Nef-expressing plasmids (NEF-LAI and NEF-SF2). In the absence of ACOT8-Nef interaction in the producing cells, no further increase in infectivity was observed.*

4.1.4 Generation of RUNX2 KO and Runt-deleted melanoma B16 cells

RUNX2 (Runt-related transcription factor 2) is a key transcription factor regulating osteogenesis, with prominent roles in osteoblast differentiation and chondrocyte hypertrophy (Hojo 2023). RUNX2 is generally expressed into two main isoforms, whose expression is driven by two different promoters and alternative splicing events. The DNA-binding activity of RUNX2 transcription factor is mediated by a highly conserved 128-aa region, called Runt domain (Dalle Carbonare, Innamorati, and Valenti 2012). In cancer, a correlation is often observed between elevated levels of RUNX2 and poor prognosis. For example, in breast cancer, higher RUNX2 expression contributes to increased Wnt and TGF-beta signalling and is associated with the more aggressive triple negative phenotype (Ferrari et al. 2013; Wysokinski, Blasiak, and Pawlowska 2015). In gastric cancer, RUNX2 contributes to the

overexpression of the chemokine receptor CXCR4, thereby promoting invasion and metastasis (Guo et al. 2016). Also in melanoma, RUNX2 was found to be more expressed in cancer cells compared to nevic melanocytes (Boregowda et al. 2014). Melanoma is an aggressive and heterogeneous cancer that primarily affects melanocytes, leading to a high mortality rate due to its metastatic properties, which make treatment difficult (Dhanyamraju and Patel 2022). Deiana et al. demonstrated that ablation of the Runt-domain in melanoma cells led to reduced Epithelial Mesenchymal Transition (EMT) properties, along with impaired cell growth and migration (Deiana et al. 2018). Accordingly, subsequent studies from the same research group concluded that RUNX2 plays a role in several molecular pathways contributing to the induction of bone metastasis associated with melanoma (Deiana et al. 2020).

Based on these studies, we aimed to use the CRISPR/Cas9 technology to target the RUNX2 gene in mouse melanoma B16 cells, by adopting two different approaches. The first CRISPR/Cas9 strategy utilized a unique guide RNA (gRNA) to target exon 4 of the RUNX2 gene, aiming to induce a knockout (KO) of the RUNX2 gene. In the second approach, the additional use of a second gRNA targeting exon 4 enabled the induction of a specific in-frame deletion of the Runt domain. The generation of these two complementary CRISPR/Cas9-engineered cell models will contribute to better dissecting the functional contribution of RUNX2 in melanoma, addressing emerging needs in therapy resistance and tumour progression. These cells will be further employed in *in vivo* studies in syngeneic B16 melanoma mouse models, to assess the biological and functional impact of RUNX2 in melanoma growth and metastasis.

After cloning the first gRNA-targeting RUNX2 in the Cas9-expressing plasmids, mouse melanoma B16 cells were transfected using this single guide approach. The transfected and selected bulk population presented a transfection efficiency of 70.6 %, after analysis with the DECODR tool, confirming a good transfectability of this melanoma cell line. Clones were then isolated and editing events were analysed by Sanger sequencing and DECODR analysis. Among the isolated clones, five showed frameshift-inducing editing events (Table 9). In particular, clone A13 presented a homozygously edited sequence with +1 insertion (C) resulting in a

premature stop codon on the coding sequence of exon 4 and was selected for further analysis (Figure 14).

Clone name	Editing event
A3	+1 bp, +1bp
A10	+ 1bp, -1 bp
A13	+ 1bp
A21	-1 bp, -13 bp
A31	-1 bp, -23 bp

Table 9. Editing events on the B16 clones. *Different mouse melanoma B16 cells were isolated and tested for Sanger sequencing. Among five selected clones, A13 clone showed an insertion of a C nucleotide in homozygosity.*

VVALGRGTRWDCGYRHGRE--

Figure 14. Alignment of B16 WT and A13 and protein translation for A13. *A13 shows a +1bp (nucleotide C) insertion in the gRNA-targeting region (underlined), resulting in a premature stop codons (in red).*

For the dual gRNA-approach, an additional gRNA was used along with the previous one in order to generate an in-frame deletion of 108-bp in the Runt domain. Similar to the previous approach, after transfection and selection, single clones were isolated and screened by PCR to identify clones harbouring the expected deletion in the targeted region. After Sanger sequencing, three clones (L13, L25 and L34) were confirmed to carry a 108-bp homozygous deletion in the exon 4 of RUNX2 gene and are hereafter referred as Runt-deleted clones (Figure 15).

Figure 15. Alignment of the Runt-deleted clones with WT sequence. *The sequence of clones presenting a 108-bp homozygous deletion in the Runt-domain are shown in the second lane, while wild-type (WT) sequence is reported on the top. The deleted region is indicated by the red dashed line. The target sites of the two gRNAs are highlighted by black rectangles, with PAM underlined in red.*

Both single-guide and dual-guide generated clones were tested by Western Blot (Figure 16). As expected, the A13 clone does not show RUNX2 protein expression. Interestingly, no RUNX2 protein band is present in L13, L25 or L34, despite a lower deleted band should be expected. The used antibody, indeed, is monoclonal and recognizes an epitope located outside the deleted region. It may be hypothesized that the deletion of this region, part of a functional domain as Runt, could lead to the production of a non-functional protein that is then degraded. To better understand these possibilities, another antibody targeting a different epitope should be tested to visualise the lower band.

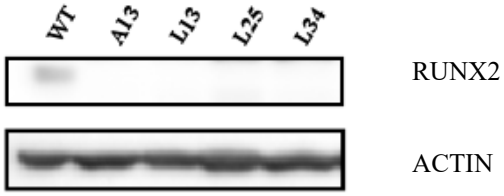

Figure 16. Western blot of RUNX2 KO and Runt-deleted clones. *A13 clone does not express RUNX2 protein, as expected. L13, L25 and L34 clones, harbouring an in-frame deletion, do not show any RUNX2 protein band, despite a lower band should be expected.*

4.2 Optimisation of CRISPR/Cas9 protocol in hard-to-transfect cells

4.2.1 Generation of HADHA KO PANC-1 cells

Pancreatic ductal adenocarcinoma (PDAC) is the most common form of pancreatic cancer and is one of the deadliest malignancies worldwide. The tumor, which originates from the exocrine cells of the organ, causes symptoms that are often detected only at advanced stages, making early diagnosis and treatment particularly difficult (Sarantis et al. 2020). A small subset of cells within the tumor, known as pancreatic cancer stem cells (PCSCs), plays a critical role in tumor initiation, progression, metastasis, and resistance to therapy, thereby representing a challenging target in pancreatic cancer treatment (Ercan, Karlitepe, and Ozpolat 2017).

The HADHA (hydroxyacyl-CoA dehydrogenase trifunctional multienzyme complex subunit alpha) gene encodes for the α subunit of the mitochondrial trifunctional protein (TFP) and intervenes in the last steps of fatty acid β-oxidation, a fundamental metabolic pathway that generates energy from breaking down fatty acids molecules**.** TFP is located on the inner mitochondrial membrane and acts through HADHA, responsible for enoyl-CoA hydratase (ECH) and hydroxyacylCoA dehydrogenase (HACD) activities, and its partner subunit, HADHB, with a thiolase activity (Liang et al. 2018). Under hypoxic conditions, pancreatic cancer cells experience a change in metabolism to meet their energy demands, including an increase in uptake of fatty acids (Wang et al. 2022). Consistently, Di Carlo et al. found that HADHA was overexpressed in PCSCs (Di Carlo et al. 2021).

These findings suggest that HADHA could represent a promising therapeutic target in pancreatic cancer. To further support this hypothesis, we utilized CRISPR/Cas9 to knockout HADHA in a well-established pancreatic cancer cell line, PANC-1, to better understand its role in the stemness of the pancreatic cancer.

To generate knockout cells, we adopted a multi-guide CRISPR/Cas9 approach by selecting two gRNAs targeting exon 1 of the HADHA gene. Before performing knockout experiments, we assessed the transfection efficiency in PANC-1 cells. In order to do that, we evaluated different transfection approaches (Lipofectamine

3000, TransIT-LT1, and nucleofection) by visualizing the fluorescence signal after transfecting a GFP plasmid into PANC-1 cells. All three methods resulted in low fluorescence intensity, indicating that PANC-1 cells are generally hard to transfect with conventional transfection procedures. Despite low efficiency, Lipofectamine3000 seemed to give the highest proportion of GFP-positive cells (Figure 17).

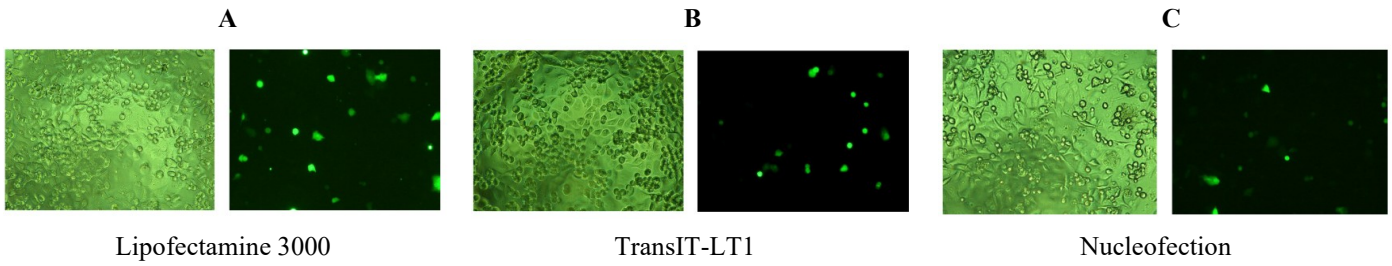

Figure 17. Evaluation of different transfection approaches by GFP delivery. *Lipofectamine3000 (A) showed higher transfection efficiency than TransIT-LT1 (B) and nucleofection (C) in PANC-1 cells. For each panel, brightfield is shown on the left and GFP fluorescence on the right.*

Starting from these results, we aimed at optimising transfection of CRISPR/Cas9 components in PANC-1 cells, by testing different Lipofectamine3000-based conditions. Following transfection of two Cas9/gRNA-encoding plasmids and puromycin selection, only conditions 6 (1.5:4:1, ratio Lipofectamine 3000 –p3000 –DNA, with 5 µg DNA) and 8 (1.25:2:1, ratio Lipofectamine 3000 –p3000 –DNA, with 3 µg DNA) exhibited a good percentage of surviving cells, while the other conditions showed high cell death rates. Since conditions 7 and 9 showed a low percentage of surviving cells, they were pooled together as a unique cell population (Table 10).

CONDITION	LIPOFECTAMINE RATIOS	DNA AMOUNT	RESULT
1	3:2:1	2,5 µg	No cell survival
2	2,5:2:1	3 µg	No cell survival
3	1,5:2:1	5 µg	No cell survival
4	3:4:1	2,5 µg	No cell survival
5	2,5:4:1	3 µg	No cell survival
6	1,5:4:1	5 µg	Good cell survival
7	1,5:2:1	2,5 µg	Poor cell survival
8	1,25:2:1	3 µg	Good cell survival
9	0,75:2:1	5 µg	Poor cell survival
Untransfected	-	-	No cell survival

Table 10. The different Lipofectamine-based conditions for PANC-1 transfection*. In each volumetric ratio (second column), the first value indicates the amount of Lipofectamine 3000 reagent, the second value to the amount of p3000 reagent, and the third value to the amount of DNA. The total DNA quantity, where the two gRNA/Cas9 plasmids were added in equal amount, is expressed in µg (third column). Results, in terms of cell survival, are shown in the last column.*

After cell recovery, cells from conditions 6, 8 and 7/9 were subjected to single cell cloning in order to isolate HADHA KO PANC-1 clones. Western Blot analysis allowed the identification of a clone (C8E12) with no detectable HADHA protein expression (Figure 18A). Sanger sequencing of the gRNAs-targeted region revealed a mixed signal with overlapping peaks (Figure 18B). To allow an accurate reading of the signal, we used the TOPO® TA Expression kit to clone PCR amplicons into a vector, followed by bacterial transformation and sequencing of plasmids extracted from the isolated colonies. The analysis showed that CRISPR/Cas9 led to a heterozygous editing of the target region, with a 124-bp frameshift deletion on the first allele removing part of exon 1 and intron 1 and a 78-bp deletion on the second allele disrupting almost entirely exon 1, including the disruption of the start codon and Kozak sequence, as shown in the alignment in Figure 18C. A multi-guide approach can be a more effective approach to achieve gene knockout, but it can also lead to an increased chance of off-target effects. To investigate this aspect, we used a bioinformatic tool (COSMID) to select the two most probable off-target sites for each gRNA. Sequencing of these off-target regions revealed no unintended editing events, thus excluding the occurrence of unwanted CRISPR/Cas9-induced off-target effects at the most probable sites (Figure 18D).

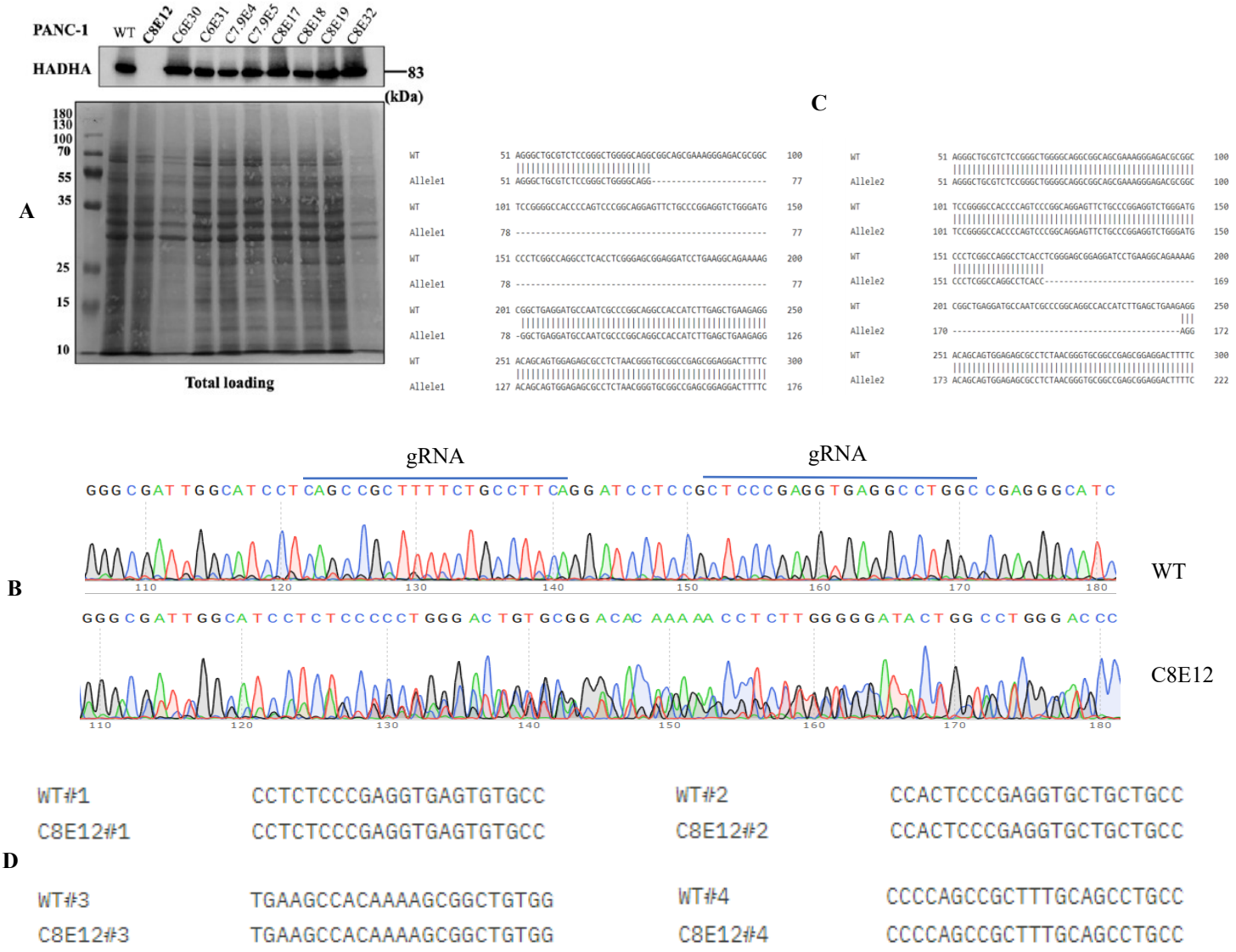

Figure 18. Generation of HADHA KO PANC-1 cell line. *(A) Western blot analysis showing the absence of HADHA protein expression in the C8E12 clone. (B) Sanger sequencing of the gRNAs-targeted region of PANC-1 WT and C8E12 clone (sequencing from reverse strand). C8E12 sequence shows a double peak and an unreadable signal. Sequences corresponding to the two gRNAs are underlined. (C) Alignment of the WT sequence with sequences obtained from TOPO TA cloning of the C8E12 PCR product. Two representative sequences were present in the analysed bacterial colonies, thus allowing the clear discrimination of the editing events on each allele. Allele 1 of the C8E12 clone 1 shows a 124bp-deletion, while allele 2 has a 78bp-deletion with respect to WT sequence. (D) Alignment of off-target sites of the C8E12 clone with the corresponding WT sequences. No off-target events occurred in these selected most probable off-target sites.*

4.2.2 HADHA role in the pancreatic cancer stemness

To investigate the role of HADHA in pancreatic cancer stemness, parental (P) PANC-1 cells were first cultured in a specific "stem selective medium" to obtain pancreatic cancer stem cells. Induction of dedifferentiation on the HADHA KO clone showed that loss of HADHA does not impair the stemness of the pancreatic cancer cell line; indeed, the C8E12 clone retained its ability to grow in suspension and remain undifferentiated.

A microscopic analysis at different time points showed that, while P cells seemed not to be affected by HADHA KO, KO-PCSCs tend to form more compact tumourspheres, with larger aggregated structures than the WT-PCSCs. As shown in Figure 19, the morphological structures formed by the KO cells appear denser, with cell boundaries that are almost indistinguishable.

Based on these preliminary observations, the generation of a HADHA KO PANC-1 cell line could represent a starting point to evaluate the role of HADHA in the context of pancreatic cancer and its stem cell component. In particular, the generated cell model could be used to better depict the effect of HADHA absence on PCSC proliferation, tumour migration and therapy resistance, thus providing valuable insights into its potential as therapeutic target in pancreatic cancer.

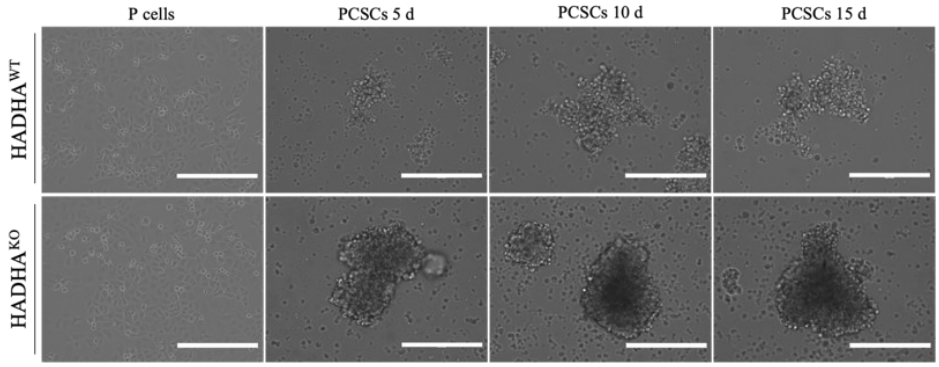

Figure 19. Bright-field microscopic images of WT and HADHA KO P cells and PSCSs. *Upon induction of dedifferentiation, HADHA KO-PCSCs maintained stem-like morphological features and exhibited the formation of larger tumourspheres with respect to WT-PSCSs. Cells were imaged at different days (5,10,15) after induction.*

4.2.3 Plasmid transfection efficiency on MG63 cells for FBXW11 knockout

FBXW11, also called β-TrCP2, is an F-box protein (FBXW subfamily) that takes part in the SCF complex, a well-characterised ubiquitin E3 ligase involved in targeted substrate degradation. By recognising generally phosphorylated substrates and targeting them for ubiquitin-mediated degradation, the F-box proteins contribute to the regulation of several cellular pathways, both in normal and pathological conditions (Tekcham et al. 2020). For example, in cancer, FBXW11 has been shown to be involved in different tumour-associated outcomes. The overexpression of the FBXW11 gene has been observed in colorectal cancer, resulting in an increase in cell proliferation and migration, as well as promoting the stem cell-like features of cancer cells. Consequently, in mouse models injected with FBXW11-knockdown cells, a significant reduction in tumor growth and liver metastasis was achieved (Yao et al. 2021).

Osteosarcoma cells, as MG63, show lower FBXW11 protein, while maintaining higher mRNA levels compared to normal osteoblasts, probably due to an increased expression of miR-221 that targets FBXW11 for degradation. Reduced FBXW11 protein correlates with elevated β-catenin (target of FBXW11), a critical factor linked to tumor progression (Dalle Carbonare et al. 2023).

Based on these preliminary results, we hypothesized that the complete absence of FBXW11 could better depict its role in osteosarcoma-related cancer pathways. For this reason, we designed a CRISPR-mediated knockout strategy targeting the FBXW11 gene to directly assess the functional consequences of its depletion in osteosarcoma cells and to better understand how FBXW11 loss contributes to tumorigenic phenotypes.

MG63 are generally described as hard-to-transfect with plasmid DNA, as previously demonstrated by Fouriki et al., that adopted magnetic nanoparticles to significantly enhance GFP-plasmid delivery (Fouriki et al. 2014). To assess transfection efficiency, we tested GFP delivery with different transfection reagents. In particular, we transfected 3μg of GFP plasmid (3.4 Kb)/well in 6-well plate, by testing Lipofectamine3000, *Trans*IT®-LT1 (Mirus) and Lipofectin. For the experiment, we used a 2.5:1, 2:1, 3.3:1 reagent:DNA ratio for Lipofectamine3000, Mirus, Lipofectin, respectively. As shown in Figure 20, the highest GFP

transfection efficiencies were obtained for Lipofectamine3000 and *Trans*IT®-LT1 (Mirus) reagents, while a poor efficiency was observed for Lipofectin.

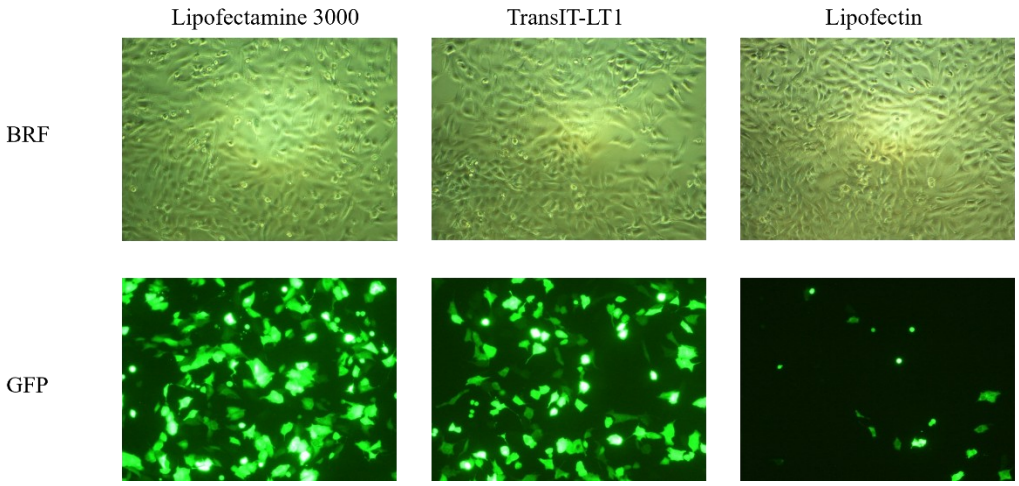

Figure 20. GFP delivery on MG63 cells by different transfection reagents. *Lipofectamine3000 and TransIT-LT1 showed the best transfection efficiency, while Lipofectin yielded poor fluorescence signal. Brightfield (BRF) images are on top, while fluorescence (GFP) images are on the bottom.*

Next, a killing curve was performed to determine the minimal amount of puromycin to kill the majority (about 95%) of MG63 cells. Different puromycin concentrations, expressed in µg/ml, were tested. After two days of selection, cells were counted and cell number of the treated conditions was compared to the one of the control condition (no treated with puromycin). Puromycin concentration of 1.5 µg/ml was selected as the lowest puromycin concentration suitable for MG63 selection (Figure 21).

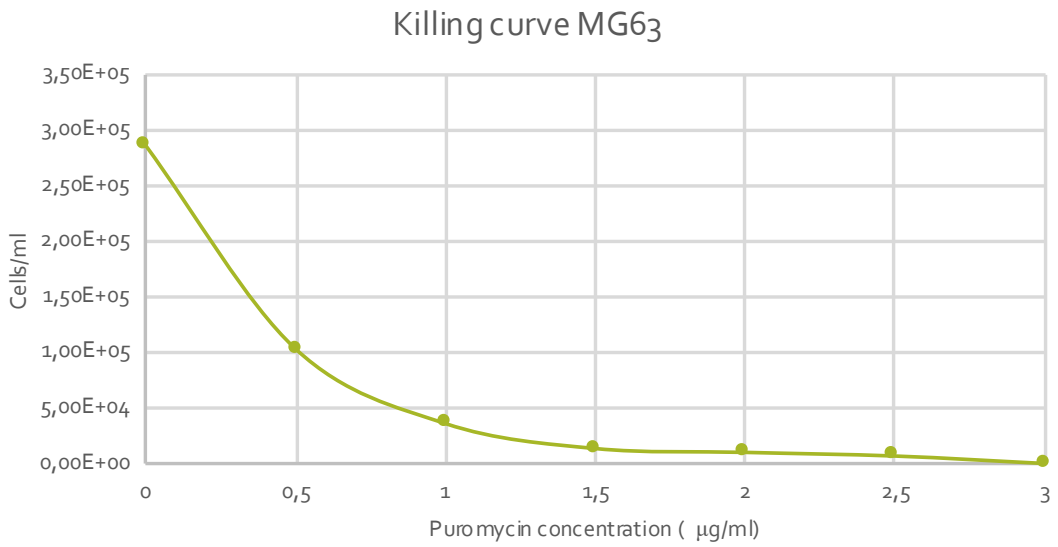

Figure 21. Puromycin killing curve on MG63 cells. *Different puromycin concentrations (0- 0.5 – 1 – 1.5 – 2 – 2.5 – 3 µg/ml) were tested on MG63 cells to determine the lowest concentration capable of killing the majority of cells.*

TransIT-LT1 transfection was adopted to deliver three gRNA/Cas9 plasmids targeting exon 1, 2 and 5 of FBXW11 gene. Following transfection, selection with puromycin (1.5 µg/ml) led to high cell mortality in both transfected and non-transfected conditions, probably indicating poor transfection efficiency. To confirm transfection efficiency and presence of editing events on the polyclonal transfected cell line, genomic DNA was extracted and amplified by PCR for the three different targeted exons. PCR amplicons were then purified and used for Sanger sequencing. The sequencing results showed no CRISPR/Cas9-induced editing events in the targeted regions (Figure 22).

To rule out the possibility that the guide design was inappropriate for inducing editing events in the target loci, we applied the same protocol on HEK293T cells, a more easily transfectable cell line. Sequencing results showed editing in each of the regions targeted by the guides, confirming their correct design and appropriate action (Figure 22). This data confirms that MG63 lines are difficult to transfect with standard transfection reagents, despite relatively good transfection outcomes with GFP. The main reason for this is likely to be the larger size of the Cas9/gRNA plasmid (>9 Kb) compared to the GFP plasmid.

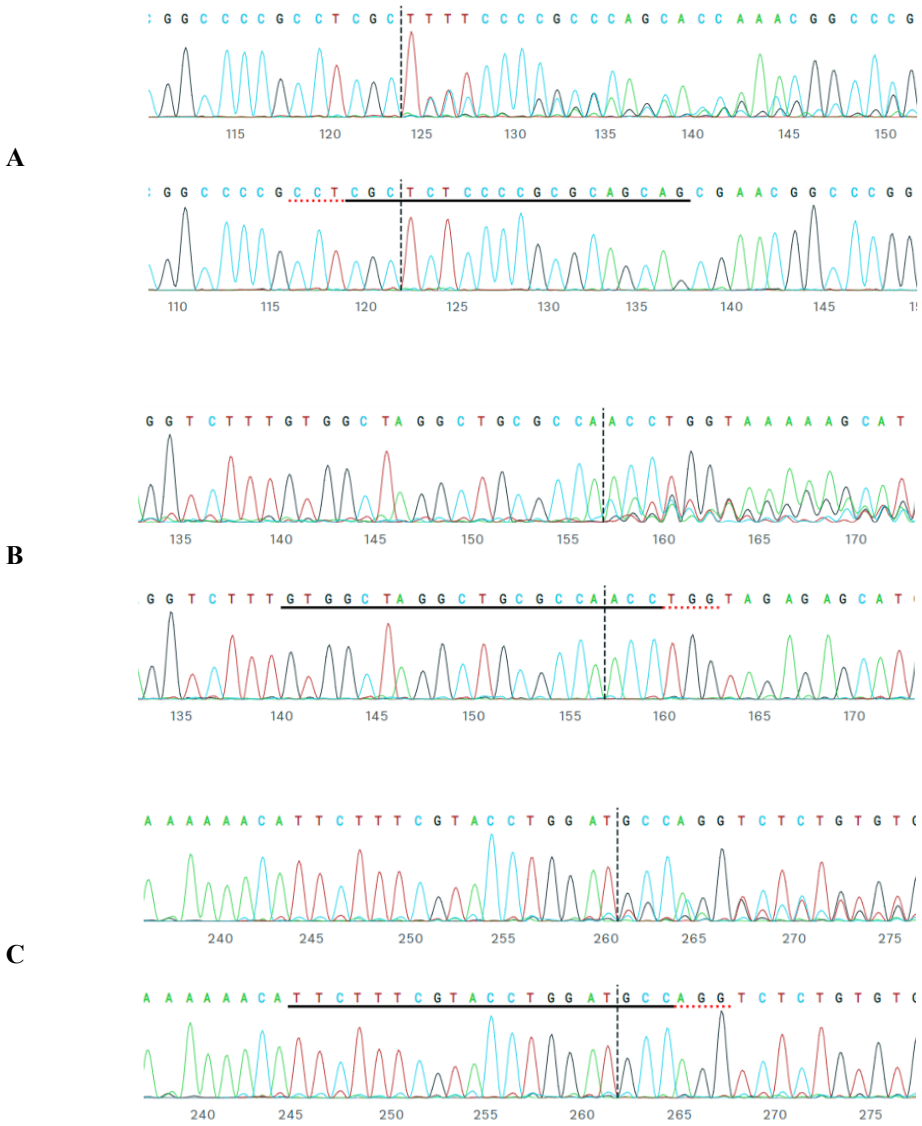

Figure 22. Sanger sequencing on polyclonal MG63 and HEK293T, after transfection. *No editing events were observed for MG63 cells, while HEK293T cells appear with double peaks corresponding to editing events. For each panel (A, B, C) corresponding to the different gRNA-targeted regions, HEK293T sequencing results are shown on the top, MG63 on the bottom. For each region, gRNAs are underlined.*

4.2.4 Generation of Cas9-MG63 cells and transfection with a smaller plasmid

Since the large size of the plasmid can negatively affect transfection efficiency in MG63 cells, we decided to use a smaller plasmid (B52_puro, 4 kb) to deliver the

CRISPR/Cas9 components. In this case, the B52_puro plasmid carries only the gRNA (up to two) and maintains the puromycin resistance gene. To deliver Cas9, we chose to transduce MG63 cells with a lentiviral vector encoding Cas9 in order to generate a stable line expressing Cas9, which could be used with the appropriate guide to perform a knockout experiment. After transduction, the cells were selected with blasticidin (encoded by the Cas9-expressing vector) to select a cell population expressing Cas9. Again, the optimal concentration of blasticidin was determined by a killing curve by testing different doses of antibiotic (Figure 23). After transduction and cell selection with 5 µg/ml blasticidin, Cas9 expression was verified and confirmed by Western Blot (Figure 24).

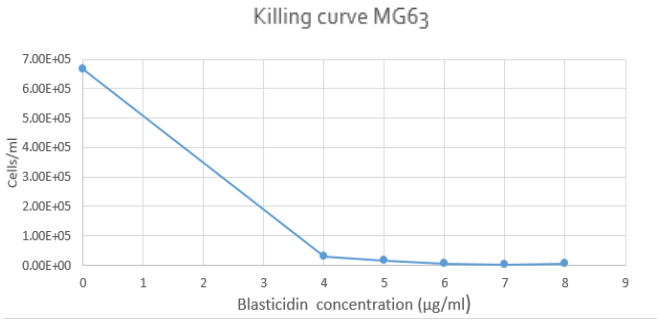

Figure 23. Blasticidin killing curve on MG63 cells. *Different blasticidin concentrations (from 0 to 8 µg/ml) were tested on MG63 cells to determine the lowest concentration for MG63 selection.*

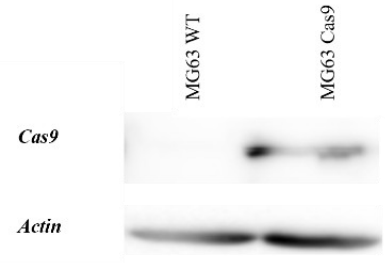

Figure 24. Western blot analysis on MG63-Cas9 cells. *After transduction and blasticidin selection, Cas9 expression was confirmed in MG63-Cas9 cells by Western blot. Actin was used as housekeeping control.*

For this new FBXW11 KO CRISPR/Cas9 experiment, we decided to use another gRNA, targeting exon 7 of the FBXW11 gene, that was already validated for FBXW11 knockout in other studies (Jin et al. 2024; Kainulainen et al. 2016). After cloning this gRNA into B52_puro, the resulting plasmid was used to transfect MG63-Cas9 cells by calcium phosphate. After two rounds of puromycin selection at a lower concentration (1 µg/ml), transfected cells showed better survival than untransfected ones. To assess transfection efficiency on the transfected polyclonal cells, DNA was extracted and PCR-amplified with primers spanning the gRNA-targeting region of exon 7 of FBXW11 gene. Unlike previous results, knockout efficiency (represented by the percentage of frameshift modifications) was 15.7%, confirming that the use of a smaller plasmid on a Cas9-expressing cell can transfect challenging cell lines as MG63, albeit still at a low performance. Sanger sequencing of the edited region, compared to the WT, is shown in Figure 25.

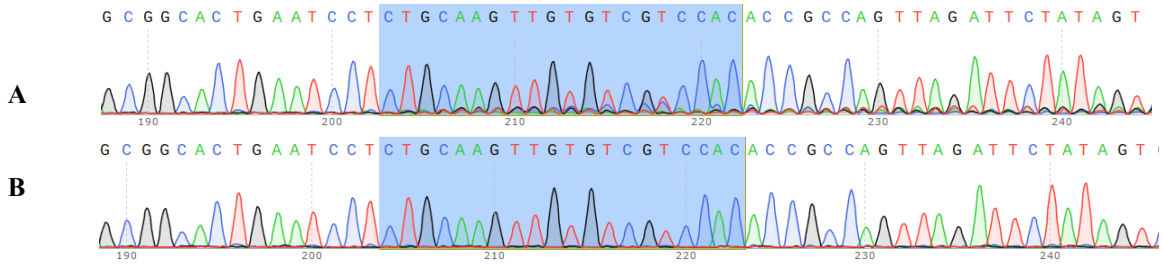

Figure 25. Editing efficiency on the polyclonal cell line after CRISPR/Cas9 transfection. *The transfected MG63 cell line showed a modest editing efficiency (A), represented by the appearance of double peaks in the gRNA-targeted region of exon 7 of FBXW11 gene, with respect to the WT (untransfected) counterpart (B).*

4.2.5 Generation of FBXW11 KO MG63 cells via virus-like particles (VLP) transduction

Although the use of a smaller plasmid has made it possible to achieve CRISPR/Cas9-induced editing on MG63-Cas9, the percentage was still quite low, making it difficult to isolate KO clones. Furthermore, the integration and the consequent prolonged expression of Cas9 can lead to toxicity in the cell line, making it less suitable for subsequent studies. For this reason, we decided to adopt

another strategy, based on the use of virus-like particles (VLPs). VLPs are virion-resembling structures that do not carry a viral genome, thus avoiding genetic integration in the host genome. These particles can deliver Cas9/gRNA ribonucleoprotein complexes in an efficient and rapid way, without the need of selecting cells after transduction. VLPs were produced by transfecting HEK293T with VSV-G, Gag-pol, Gag-Cas9 and sgRNA-encoding plasmids. In order to compare editing efficiency with previous results, we delivered VLPs targeting exon 7 of FBXW11 gene. After transduction, genomic DNA was analysed for editing events by DECODR software, as described previously. Editing results showed a knockout efficiency of 67.5 %, with a 4-fold increase compared to previous results (Figure 26). The total percentage of genomic modifications for VLP delivery reached 83.4 % (the sum of 67.5 % frameshift and 15.9 % non-frameshift events), with the remaining 16.6 % representing unedited (wild-type) sequence. In contrast, the previous approach still showed a larger unmodified wild-type fraction of 77.8%, together with an editing efficiency of 22.2% (15.7% frameshift and 6.5% non-frameshift events).

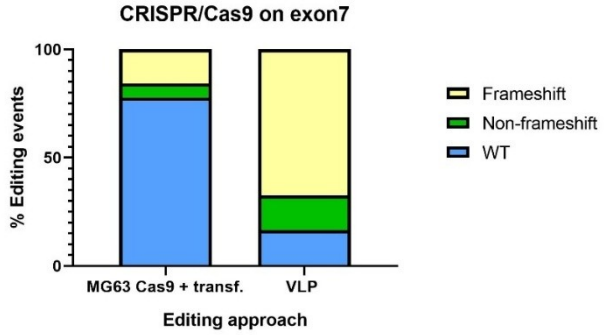

Figure 26. VLP transduction targeting exon 7 of FBXW11 gene. *Compared to previous editing approach (transfection of MG63 Cas9 with a smaller plasmid), VLP-mediated CRISPR/Cas9 delivery achieved greater editing efficiency on the same targeted exon.*

To assess whether the combined use of two guides could result in a more efficient editing on MG63 cells, with the aim of generating a target deletion causing a frameshift, we performed two VLPs productions carrying guides targeting exon 4 of FBXW11. In order to optimise the transduction protocol, we transduced different cell numbers (10000 – 40000 – 80000) with the same amount of VLP. The simultaneous delivery of two gRNAs resulted in higher editing efficiencies,

especially in the condition with a lower cell number. As shown in Figure 27, transduction of 10000 cells led to almost 100% of knockout efficiency, with no remaining unedited (wild-type) sequence, demonstrating that the dual-gRNA knockout approach, mediated by VLP, is the most effective and safe CRISPR/Cas9 approach on difficult-to-transfect cells, such as MG63 cells.

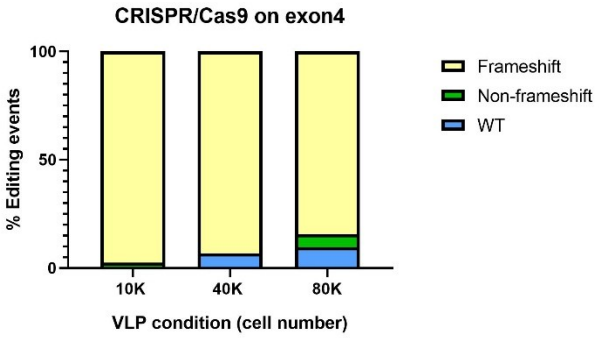

Figure 27. VLP transduction targeting exon 4 of FBXW11 gene. *Different cell numbers (10000 – 40000 – 80000) were transduced with the same amount of VLPs carrying both guides targeting exon 4 of FBXW11. Lower cell density (10K) resulted in the highest editing efficiency, as represented by the greater percentage of frameshift editing events.*

From the best performing condition (10K cells), monoclonal isolation was then performed in order to obtain FBXW11 KO MG63 clones. We finally isolated a FBXW11 KO clone (named J6), characterised by a frameshift deletion of -65bp on the gRNAs-targeted region of exon 4 of FBXW11 gene (Figure 28).

```
J6      AAGATGTTCCACAAATTCCACTTGATCTGATTCAGAC----------------------   217
UT      AAGATGTTCCACAAATTCCACTTGATCTGATTCAGACCACTGGTCAAAATATTTAATACA   230
        ************************************

J6      ------------------------------------------TCTGGAGACGATCACAGA   235
UT      CAAGTCTTTTTCTTTTTGATAGTTTCCTTCTGATGGCCTCTTTCTGGAGACGATCACAGA   290
                                                  ******************
```

Figure 28. Sequence alignment of the edited clone. *Alignment of J6 (FBXW11 KO MG63 clone) with the UT (untransfected) sequence shows a frameshift deletion of -65bp in the edited clone. The two gRNAs are underlined.*

4.3 Prime editing applied to single-nucleotide variants

4.3.1 Design of prime editing strategy in the context of CCD

Cleidocranial dysplasia (CCD) is a rare autosomal dominant disorder affecting skeletal development. The disease, whose prevalence is estimated to be 1 in one million individuals, is generally associated with clavicular hypoplasia, open fontanelles, short stature, and dental anomalies (Dhiman et al. 2014; Mundlos 1999). CCD is caused by mutations in the RUNX2 (Runt-related transcription factor 2) gene, which encodes a transcription factor essential for bone development and osteoblast differentiation. Variants are classified as either in-frame or null mutations, with a correlation between the genetic location of the mutation and the clinical skeletal features (Thaweesapphithak et al. 2024). In CCD patients, early treatments are generally dedicated to favour tooth eruption, while combined surgical-orthodontic and orthognathic interventions can be adopted in adult age to ensure functional dentition and an ameliorated facial profile (Zhu et al. 2018). CRISPR/Cas9 has already been utilized for gene correction in CCD-derived IPSCs cells. The edited cells, generated by CRISPR-mediated homologous recombination through a donor template, showed better osteogenic properties both *in vitro* and in a rat model (Saito et al. 2018).

Therefore, CRISPR-based technologies can open new possibilities to therapeutically intervene in genetic disorders such as cleidocranial dysplasia (CCD). More recently, the emergence of prime editing offers a powerful approach for targeted correction of mutations without the need for exogenous donor templates or the introduction of double-strand breaks, which are known to cause undesired cellular outcomes. Furthermore, prime editing has been shown to reduce off-target effects compared to traditional CRISPR/Cas9 system (Anzalone et al. 2019). To test the applicability of prime editing in the context of CCD, we focused on a previously characterised pathogenic variant in the RUNX2 gene (c.505C>T) (Dalle Carbonare et al. 2025). The mutation, located on exon 4 of the gene, causes a missense substitution (R169W) in the RUNT domain of the RUNX2 protein. Analysis of mRNA expression patterns in CCD-derived cells revealed an altered expression profile of mRNA involved in osteogenesis, such as an up-regulation in

transforming growth factor beta 1 (TGF-β1), TGF-b receptor 1 (TGF-βR1) and insulin-like growth factor 1 receptor (IGF1R) mRNA levels. Moreover, RUNX2-mutated induced mesenchymal stem cells (iMSCs), upon osteogenic differentiation, exhibited a deregulation of RUNX2 expression levels compared to wild-type cells, thus confirming the impact of the mutation on the regulation of osteogenic pathways (Dalle Carbonare et al. 2025).

Prime editing represents a suitable strategy to correct disease-causing mutations, as those causing cleidocranial dysplasia. In parallel, the technology has been employed to generate isogenic cell models, which can be particularly useful in contexts where accessibility to patient-derived cells can be limited (Cerna-Chavez et al. 2025). To address both aspects, we designed a prime editing strategy to firstly introduce the c.505C>T RUNX2 mutation and then to correct it.

We chose to adopt both the PE2 and PE3 strategies, by including different pegRNA and ngRNA design combinations, in order to select the most performing editing conditions (Table 11). For correcting the c.505C>T RUNX2 mutation, we selected a unique spacer sequence and combined it with three different 3′ extensions. For the PE3 strategy, two additional ngRNAs were designed and paired with each pegRNA. For inserting the mutation, we designed two different spacers, each coupled with two distinct 3’ extensions, and each pegRNA was then combined with two different ngRNAs in PE3 strategy. Finally, we had a total of 9 different conditions (3 PE2 + 6 PE3) and 12 different conditions (4 PE2 + 8 PE3) for correcting and inserting the RUNX2 mutations, respectively. A representation of pegRNA and ngRNA targeting exon 4 of RUNX2 for both correcting and inserting the mutation is shown in Figure 29.

The corresponding oligos were cloned through Golden Gate assembly in recipient plasmids. After transformation, for each assembled plasmid, three colonies were subjected to plasmid DNA miniprep and Sanger sequencing was used to verify correct insertion events. Among 33 screened colonies, 26 showed correct insert ligation (78.8%), 4 presented mutations (12.1%) and 3 lacked the insert (9.1%). Correct plasmids were then extracted by maxiprep and used to transfect target cells.

A

Condition	gRNA	sequence	RTT	PBS	Distance to edit
1A	pegRNA	Spacer #1: GAAAATTATTCTGCTGAGCTC	15	15	3
2A	pegRNA	Spacer #1: GAAAATTATTCTGCTGAGCTC	17	13	3
3A	pegRNA	Spacer #1: GAAAATTATTCTGCTGAGCTC	14	13	3
4A	ngRNA	ngRNA #1: GCCCATCTGGTACCTCTCCGA	-	-	69
5A	ngRNA	ngRNA #2: GAGACCTACCTCGTCCACTC	-	-	-67

B

Condition	gRNA	sequence	RTT	PBS	Distance to edit
8B	pegRNA	Spacer #1: GAAAATTATTCTGCTGAGCTC	15	15	3
9B	pegRNA	Spacer #1: GAAAATTATTCTGCTGAGCTC	14	13	3
4A	ngRNA	ngRNA #1: GCCCATCTGGTACCTCTCCGA	-	-	69
5A	ngRNA	ngRNA #2: GAGACCTACCTCGTCCACTC	-	-	-67

C

Condition	gRNA	sequence	RTT	PBS	Distance to edit
6B	pegRNA	Spacer #2: GTCATAACAGCAGAGGCATTC	12	10	4
7B	pegRNA	Spacer #2: GTCATAACAGCAGAGGCATTC	15	13	4
10B	ngRNA	ngRNA #3: GACTGTGGTTACTGTCATGG	-	-	-35
11B	ngRNA	ngRNA #4: GAGAGGTACCAGATGGGACTG	-	-	-50

Table 11. Design of prime editing strategy. *(A) Design of pegRNA and combined ngRNA to be used for correcting the RUNX2 mutation. (B-C) Design of pegRNA and ngRNA to be used for inserting the RUNX2 mutation. Each condition was assigned a different code.*

A

B

C

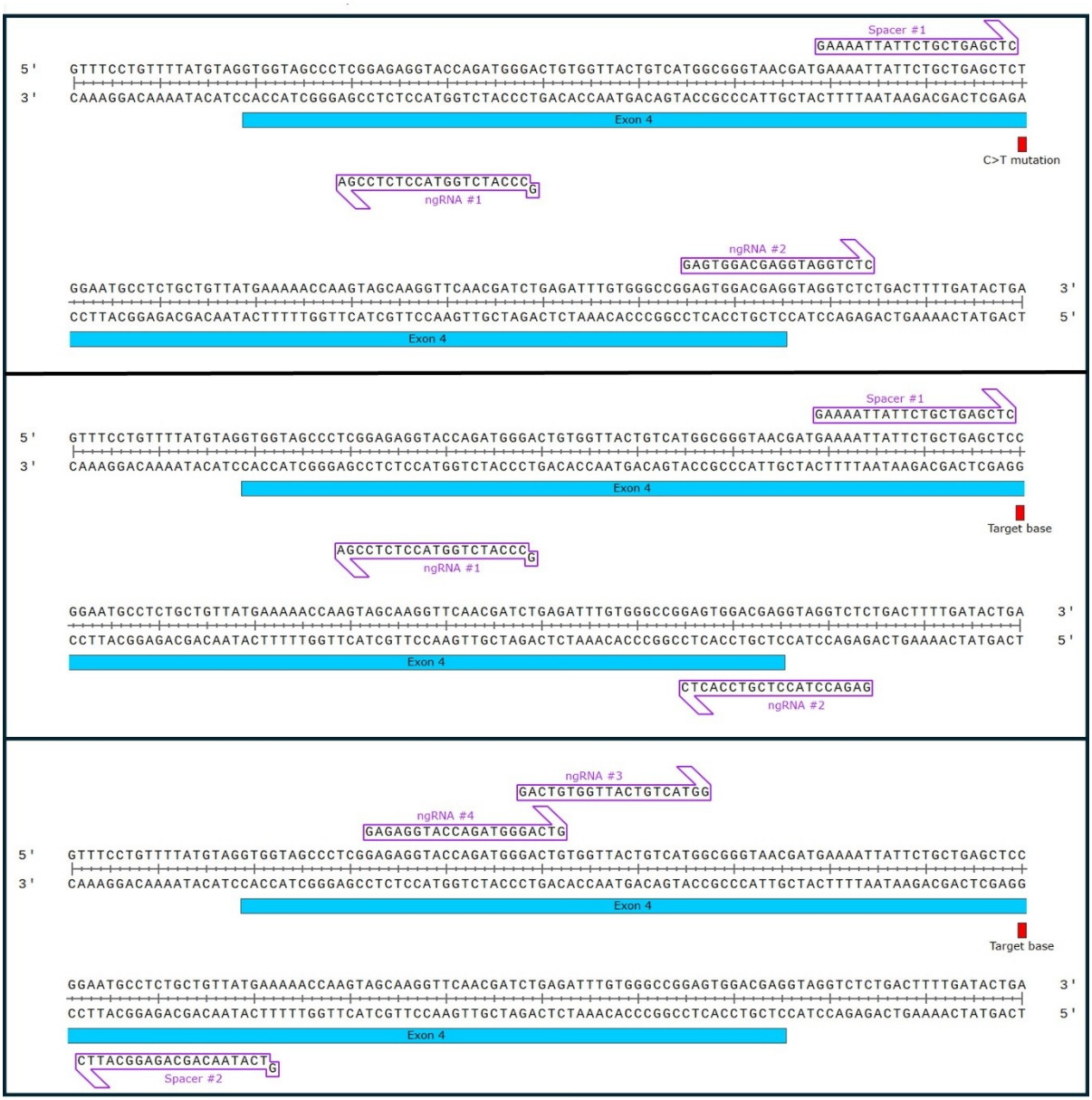

Figure 29. Prime editing on exon 4 of RUNX2 gene. *(A) Representation and location of the unique spacer and the two ngRNAs used to correct the C>T mutation. (B-C) The same was done for the two spacers and corresponding ngRNA used for inserting the C>T mutation. Images were generated using the SnapGene® software (from Dotmatics; available at snapgene.com).*

4.3.2 Generation of HEK293T carrying the c.505C>T RUNX2 mutation

Before moving on to clinically relevant cell types, we first optimised the prime editing strategy for the introduction of the c.505 C>T RUNX2 mutation in HEK293T cells.

As mentioned before, cells were transfected with 12 different combinations of plasmids corresponding to either the PE2 strategy (prime editor plasmid + pegRNA plasmid) or the PE3 strategy (prime editor plasmid + pegRNA plasmid + ngRNA plasmid). Following genomic DNA extraction and sequencing of the target region, editing efficiency was assessed using the EditR software to quantify the introduction of the desired mutation.

In general, addition of ngRNA (PE3) allowed us to obtain higher editing efficiency compared to PE2 conditions, as expected. Among all the tested conditions, pegRNA 8B/9B coupled with ngRNA 5A achieved an average editing efficiency, represented by the introduction of a T, of 45% and 42%, respectively (Figure 30A). Sanger sequencing data showed clearly the appearance of a double peak (C/T) on the target site, thus confirming the insertion of the desired mutation (Figure 30B).

These results demonstrated the applicability of prime editing for introducing the mutation into HEK293T cells. We then generated single clones (n = 11) from conditions 8B/5A and 9B/5A, successfully isolating both homozygous (n=5, 45.4%) and heterozygous (n = 2, 18.2 %) clones for the RUNX2 mutation, as well as wild-type clones (n = 4, 36,4 %) (Figure 30C-D).

Therefore, we established isogenic HEK293T clones carrying either the homozygous or heterozygous form of the mutation of interest, providing a cellular model on which to test the efficiency of prime editing for correcting the mutation.

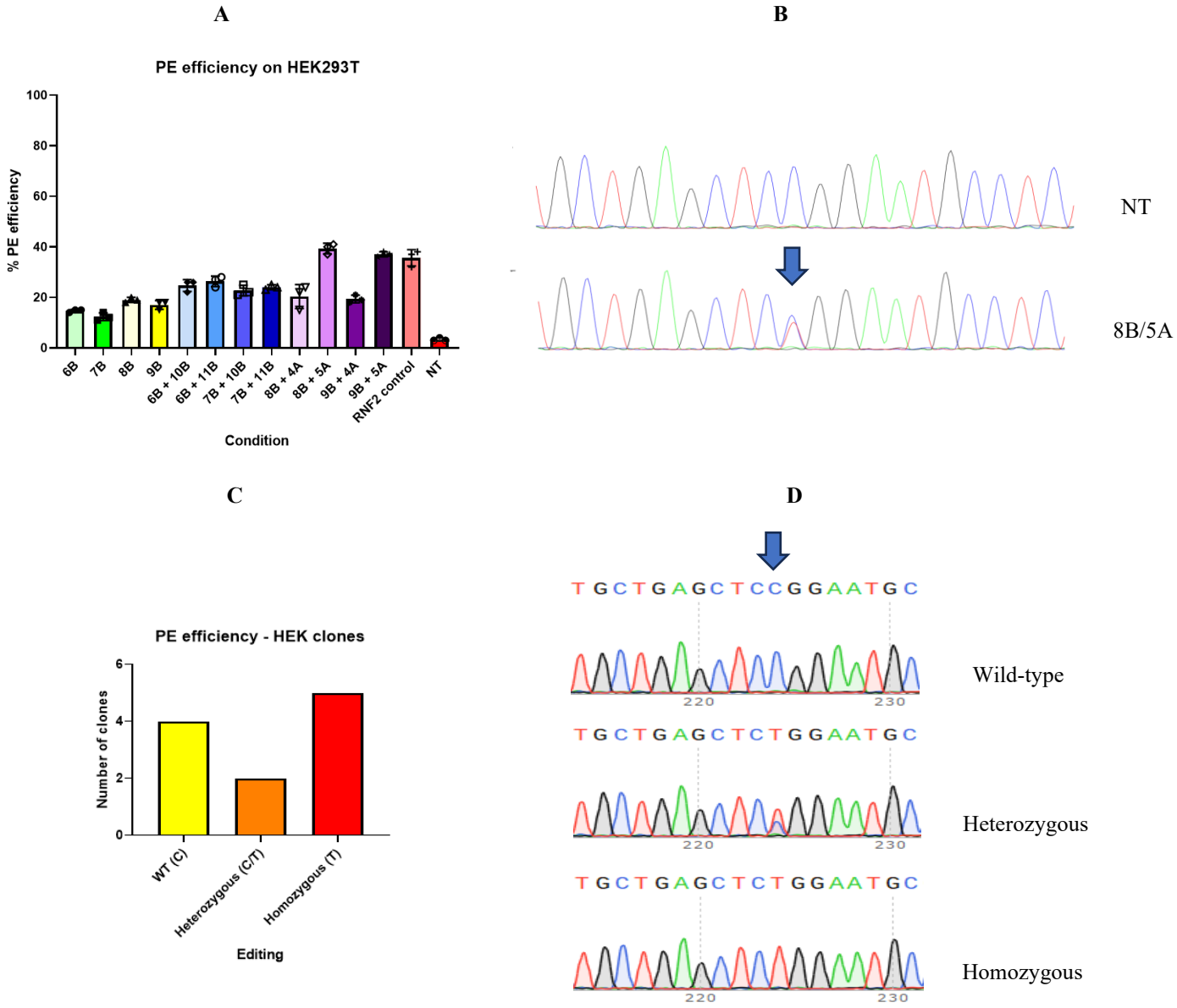

Figure 30. Prime editing efficiency to introduce the RUNX2 mutation. *(A) Efficiency on HEK293T cells of the different editing conditions. The different pegRNAs (6B, 7B, 8B, 9B) were used alone (PE2) or in combination with ngRNA (PE3). A pegRNA/ngRNA pair targeting RNF2 gene was included as positive control for editing, while non-transfected (NT) cells were used as negative control. Bars represent the mean ± standard deviation (SD) from three biological replicates. (B) Representative Sanger data from condition 8B/5A, showing the best editing efficiency with respect to NT. (C-D) Screening of HEK clones (n=11) with representative Sanger data, illustrating the proportion of editing events: wild-type (WT), heterozygous (C/T), homozygous (T).*

4.3.3 Correction of RUNX2 mutation in HEK293T cells

Starting from previously isolated HEK293T clones carrying the c.505 C>T mutation, we tested the feasibility of our prime editing design to correct back this pathogenic variant. We chose to apply a total of 9 prime editing conditions on both a homozygous mutant clone (named C#5) and a heterozygous clone (named C#12). Analysis of the editing results confirmed that the PE3 strategy generally outperforms PE2. In particular, the combination of pegRNAs 1A, 2A, 3A with ngRNA 5A achieved the highest editing efficiencies (Figure 31). For the heterozygous clone, the ~35% baseline observed for the C nucleotide in Clone 12 is primarily attributable to the aneuploid nature of HEK293T cells, which frequently present more than two copies of specific genomic loci. In this context, the consistent ~1:2 ratio between edited and wild-type alleles suggests the presence of three copies of the *RUNX2* locus, where a 33.3% frequency would be expected. Minor deviations from the theoretical 50:50 C/T heterozygous ratio can also be due to technical factors, such as PCR amplification bias or inherent sequencing-related limitations. Interestingly, nicking guide 5A is included in the design for both the introduction and the correction of the targeted mutation, resulting in the superior editing outcomes in both cases. The ngRNA 5A and the other selected ngRNAs follow a PE3 (or PE3a) strategy rather than PE3b, which is generally associated with higher editing efficiencies. During the design phase, available PE3b-ngRNA candidates for the *RUNX2* locus were either unavailable or had low efficiency scores, leading to a preference for high-performing PE3 ngRNAs. In conclusion, by identifying the most effective conditions, we managed to optimise the prime editing design for the correction of the c.505 C>T RUNX2 mutation in HEK293T cells.

A

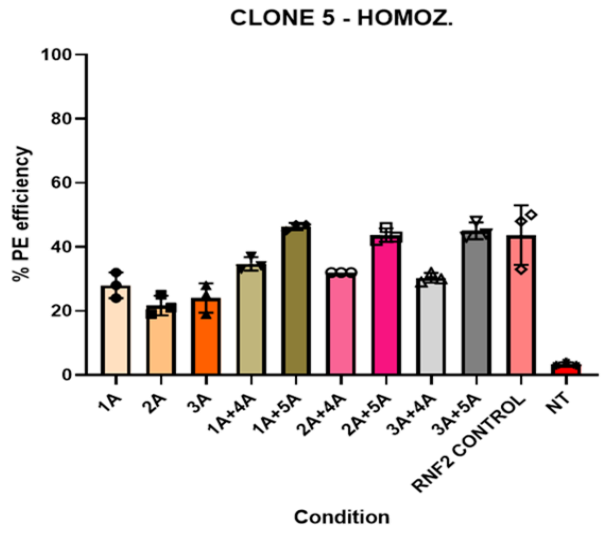

B

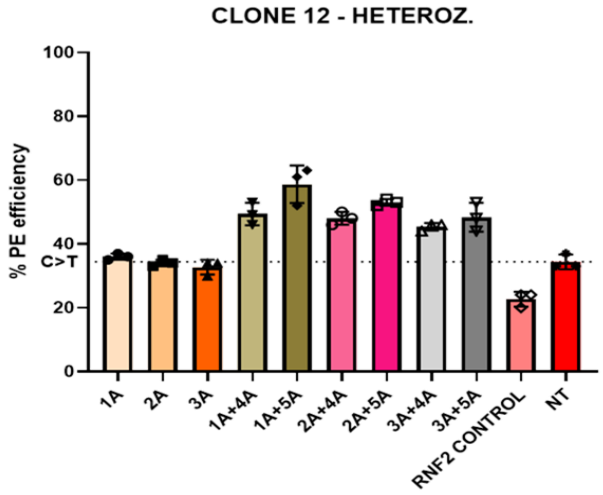

Figure 31. Correction of RUNX2 mutation on mutated HEK293T cells by prime editing. *(A). Editing efficiency on HEK293T clone (C#5) homozygous for the RUNX2 mutation. (B) Editing efficiency on HEK293T clone (C#12) heterozygous for the RUNX2 mutation. The dotted line represents the experimental heterozygous baseline of clone C#12 (~35% C>T frequency). The different pegRNAs (1A, 2A, 3A) were used alone (PE2) or in combination with ngRNA (PE3). A pegRNA/ngRNA pair targeting RNF2 gene was included as positive control for editing, while non-transfected (NT) cells were used as negative control. Bars represent the mean ± standard deviation (SD) from three biological replicates.*

4.4 From *in vitro* CRISPR genome editing to *in silico* approaches: investigation of HLA-C stability

4.4.1 CRISPR/Cas9 to knockout HLA-C gene in HEK293T cells

The HLA-C molecule assembles in a trimeric complex on the cell membrane together with beta-2 microglobulin (β_2m) and an antigenic peptide, playing a key role in immune defence (Kulpa and Collins 2011). The stability of this complex, defined as the strength of the binding between HLA-C and the peptide/β_2m, can influence the immune response, particularly in the case of viral infections. More unstable alleles tend to dissociate more frequently from β_2m/peptide, thus resulting in the generation of HLA-C free chains, while more stable alleles are more present in the heterotrimeric form. Due to the high degree of polymorphism of the HLA-C gene, many alleles are present, each of which may present a different degree of stability. Parolini et al. observed that HIV-1 virions produced in cells with unstable alleles were more infectious than those produced in cells with stable alleles. This is probably due to the higher percentage of free HLA-C molecules capable of interacting with the HIV-1 envelope, which leads to advantageous modulation of infectivity (Parolini et al. 2018). Subsequent studies have followed this line of investigation, by genotyping samples from HIV-1 patients at different stages of HIV-1 progression and showing that patients progressing faster towards AIDS were characterised by the presence of unstable HLA-C alleles. The study was conducted by assigning a binary, non-quantitative classification (stable or unstable) to the stability of HLA-C. This was based on studies that measured stability using antibodies which either did or did not bind to the trimeric complex, as well as defining stability of certain alleles according to phylogenetic proximity (Parolini et al. 2018; Sibilio et al. 2008; Stefani et al. 2022).

To deeply investigate the stability of different HLA-C allotypes and its relevance HIV-1 infection, we initially designed a VLP-mediated CRISPR/Cas9 experiment to rapidly and efficiently generate a HEK293T cell line knockout for HLA-C gene. As expected, the VLP-induced knockout was quite high (71%), as shown by analysis using ICE Synthego software (Figure 32).

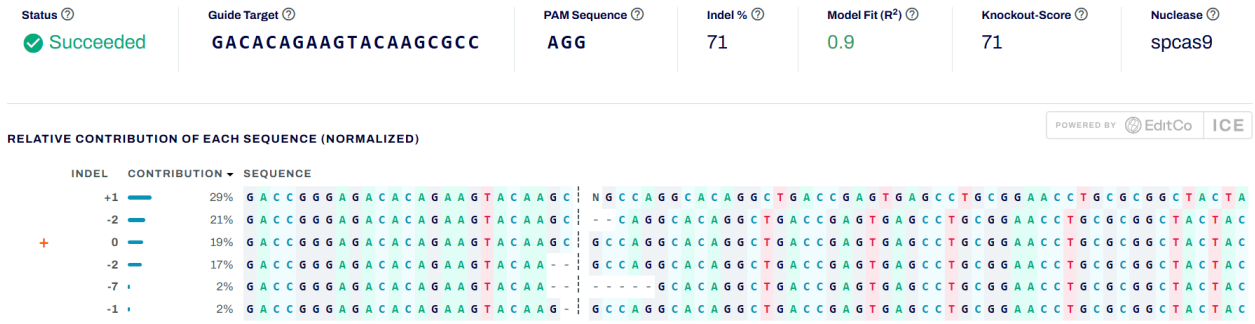

Figure 32. Quantification of CRISPR/Cas9-induced knockout for HLA-C gene. *HEK293T cells were transduced with virus-like particles (VLP) delivering CRISPR/Cas9 components to target exon 2 of HLA-C gene. The knockout efficiency on the targeted exon was quantified by ICE Synthego online tool, after Sanger sequencing of the gRNA-targeted region.*

We constructed different HLA-C expressing plasmids, including several HLA-C allelic variants, such as C*01, C*02, C*03, C*04, C*05, C*06, C*07, C*08, C*12, C*16 to be transfected on the generated HLA-C KO HEK293T cell line to restore the expression of individual HLA-C alleles. After generating lines that stably express the different HLA-C alleles of interest, dissociation kinetics would have been tested using flow cytometry analysis with an antibody that recognises free chains, preceded by acid washing to induce dissociation, in order to obtain a measure of the stability of the HLA-C/peptide/β_2m complex for the different HLA-C variants.

While proceeding, we became aware that Sarkizova et al. already adopted a similar approach. Specifically, their research group conducted a mass spectrometry analysis to identify peptides that bind to various HLA-C allotypes after re-transfecting the HLA-null B721.221 cell line with different HLA-C alleles (Sarkizova et al. 2020). Therefore, as our experimental workflow would have been time-consuming and challenging, and has already been addressed in the literature, we decided to adopt an *in-silico* approach to characterise the peptide-binding stability of the different HLA-C variants and investigate its associations in the context of HIV-1 infection.

4.4.2 Computational characterisation of binding stability of HLA-C allotypes with specific peptides

Starting from the dataset of HLA-C binding peptides identified by Sarkizova et al., we used this pool of experimentally identified peptides to study the binding stability of the 21 most common human HLA-C allotypes. To achieve this, we adopted a computational approach using the NetMHCpan-4.2 tool, which enabled us to calculate the binding affinity of various analysed peptides with their HLA-C allotype. The tool provides an EL (eluted ligand) score that quantitatively determines the binding affinity between the peptide and the HLA-C molecule, as well as the likelihood that the peptide will be processed and presented on the cell membrane by the corresponding HLA-C allotype. We calculated and ranked the EL-score values for each peptide that specifically binds to a different HLA-C allotype. This ranking was then expressed in percentile form (% Ranking) to account for the varying number of peptides for each allele. We plotted the ranked EL-score values against their percentile ranking to create curves. We then calculated the area under the curve (AUC) to determine a stability value for each allotype. Figure 33 shows the set of stability curves representing the binding of the different allotypes to their respective peptide pools. As we can observe, allele 05:01 shows the strongest binding stability for most peptides, while allele 07:04 shows significantly weaker binding values. It is interesting to observe how the stability curves of different subtypes, such as 08:02 and 08:01, differ significantly, with 08:02 being one of the most stable and 08:01 being one of the least stable. Most of the HLA-C allotypes present intermediate stability values. Figure 33B shows the separated curves, for each allotype, by indicating also the AUC value. The applied methodology allowed us to give a defined stability score for each HLA-C allotype, based on binding values calculated on experimentally identified peptides.

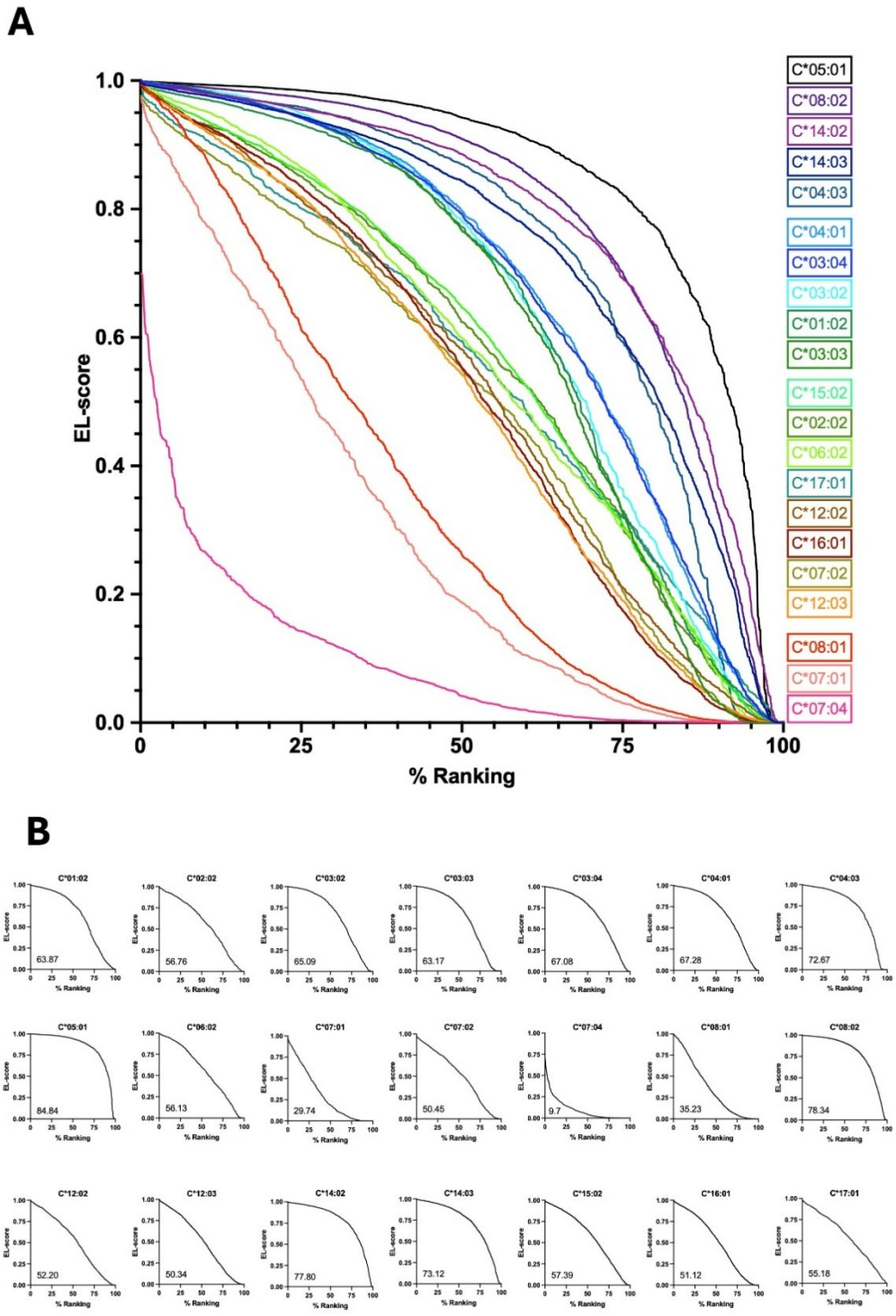

Figure 33. Stability curves of the most common human HLA-C allotypes. *Stability curves were drawn by plotting EL-score, calculated on Netmhcpan4.2, for each HLA-C allotype for the corresponding binding peptides, against the percentile of peptide ranking position. Area under the curve was then calculated to determine a stability score for each HLA-C allotype. Curves are shown overlapped (A) or separated with the reported stability score (B).*

4.4.3 HLA-C complex stability by molecular dynamics

To confirm that the HLA-C complex stability is determined by interactions with the peptide, molecular dynamics (MD) simulations were performed to define binding energies in the HLA-C/ β_2m /peptide complex. To accomplish this, we selected two random 9-mer peptides for five HLA-C allotypes, for which crystal structures were available. Computational analysis allowed the identification of the residues involved in the interaction between the selected peptide and the HLA-C/β_2m complex. Three recurrent β_2m residues (Trp80, Phe76, Trp61) were found to be involved in this interaction, and their energetic contribution was analysed. These β_2m amino acids show similar binding free energy values (ΔG, expressed in kcal/mol) across the different HLA-C/peptides tested (Table 12). This result confirmed that β_2m consistently interacts with the HLA-C heavy chain, thus indicating that the stability of the overall complex is determined by the bound peptide.

Allotype	Peptide	β_2m residue	ΔG [kcal/mol]
C*03:04	QATMPHLSM	Trp80	-10.1
		Phe76	-5.8
	TITDIISAL	Trp80	-10.5
		Phe76	-5.7
C*04:01	YHDKNIVLL	Trp80	-10.7
		Phe76	-4.7
	TFESLVAKL	Trp61	-9.4
		Phe76	-5.2
C*05:01	NLDQPPAFF	Trp80	-9.3
		Phe76	-5.6
	NAEAKITKL	Trp 61	-10.3
		Phe76	-5.5
C*06:02	FKMTIPLLV	Trp80	-11.7
		Phe76	-6.1
	VYYLKNREV	Trp80	-9.8
		Phe76	-6.5
C*07:02	LRHPVCVEL	Trp80	-10.4
		Phe76	-5.8
	FYRVTTEQY	Trp80	-10.7
		Phe76	-5.6

Table 12. Binding free energies of β_2m residue for different HLA-C/peptide complexes. *Two random peptides, shown in column 2, were selected for the five HLA-C considered. Binding free energies (ΔG, kcal/mol) of the β_2m residues involved in the interaction were determined.*

4.4.4 Association between HLA-C stability and HIV-1 progression and HIV-1 related neurocognitive disorders

After determining the stability values of the considered HLA-C allotypes, thus overcoming the previous binary classification, we proceeded to study the HLA-C stability in the context of HIV-1 infection. Two cohorts of HIV-1-positive patients were examined: the first group consisted of individuals with rapid or slow disease

progression, and the second group consisted of individuals with or without HIV-1-related neurocognitive impairment. Each patient was genotyped for HLA-C allele at the first digit resolution. For some HLA-C allotypes, a more specific genotyping at the second digit was performed to determine more accurate stability values, as described in the Materials and Methods section. A stability score was then determined for each patient based on their HLA-C genotype by multiplying the stability scores calculated from the area under the curve (AUC) of the corresponding allotypes, following the rules described in the Materials and Methods section.

Our analysis showed that patients showing rapid progression to AIDS (called progressors, P) exhibited significantly lower HLA-C stability values ($p=0.0143$) than patients with slower progression to AIDS, referred as long-term non-progressors (LTNP). Furthermore, HIV-1 patients with associated neurocognitive deficits (HAND+) also had statistically lower HLA-C stability scores ($p=0.0221$) than cognitively normal patients (HAND-) (Figure 34).

Our study confirms and enriches previous studies, allowing us to define a more rigorous definition of HLA-C stability and associate it with various outcomes of HIV-1 infection, such as progression or the presence of neurocognitive impairment. This study was recently published in Frontiers in Immunology (*Voi M, Sangalli A, Milano EG, De Martinis C, Orlandi E, Tamburin S, Mantovani E, Federico A, Lanzafame M, Lattuada E, Arganaraz GA, Da Silva BCM, Da Silva Duarte AJ, Casseb J, Arganaraz ER, Malena M, Albani M, Ruggiero A, Romanelli MG, Valenti MT, Grazioso G and Zipeto D (2025) Computational characterization of peptide binding stability to HLA-C allotypes and its association with HIV-1 infection progression and HIV-1 related neurocognitive impairment. Front. Immunol. 16:1703026. doi: 10.3389/fimmu.2025.1703026).*

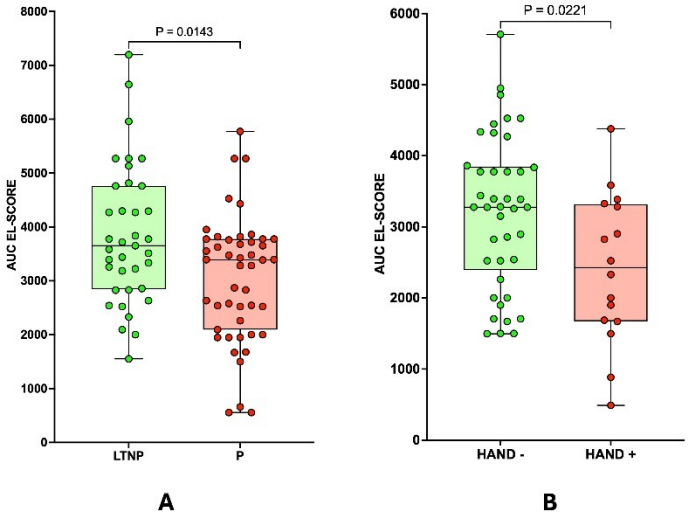

Figure 34. HLA-C stability scores of HIV-1 patients and association with HIV-1 progression and HIV-1 related neurocognitive impairment. *(A) HIV-1 patients with a rapid disease progression (P) exhibit lower stability scores than LTNP. (B) HIV-1 patients presenting neurocognitive impairment (HAND+) were associated with lower stability scores than HAND-. For statistical analysis, the two-tailed Mann-Whitney U test was used, with $p < 0.05$ considered statistically significant.*

5. DISCUSSION

CRISPR/Cas9 is an efficient and relatively simple genome editing technology, which enables gene knockout, aiming at characterising gene function in tumour pathways, viral infections and other cellular processes.

After identification of the target gene and the corresponding cell line, a CRISPR experiment begins with the design of the guide RNA in order to induce a specific gene knockout. This is a fundamental step in achieving good efficiency of the system and requires adherence to specific design rules. Nowadays, updated and user-friendly online software (CHOPCHOP, CRISPRscan, etc) can facilitate this process by identifying the most suitable guides to achieve optimal editing efficiency, by maximising the on-target activity while minimising off-target activity. The next step consists of the evaluation of the appropriate method to deliver the CRISPR/Cas9 components.

For the knockout (KO) of ACOT8 in HEK293T cells, the knockout of HADHA in PANC-1 cells, and the knockout of RUNX2 in B16 cells, transfection was performed using classic polymeric or lipid-based transfection reagents with a large plasmid (9 kb) encoding both Cas9 and the RNA guide. This delivery method optimally transfects HEK293T and B16 cells, allowing for the easy isolation and verification of KO clones.

PANC-1 cells showed lower transfection efficiency, as demonstrated by previous GFP transfection experiments that showed poor transfection of the cell line. Despite this, optimisation of the transfection protocol allowed us to obtain an HADHA KO line. However, the only KO clone showed a heterozygous sequence, composed of complex and mixed editing events that could not be accurately deconvoluted by sequence analysis software, such as ICE and DECODR. For this reason, in order to unambiguously characterise the sequence of the isolated KO clone, we used TOPO cloning to discriminate between individual allelic events. This is a more time-consuming procedure, but it was necessary in this case to ensure the correct interpretation of the results. While the double-guide approach on PANC-1 cells aimed to create a large deletion on exon 1 useful to induce HADHA knockout, the double-guide approach on exon 4 of RUNX2 in B16 cells was specifically designed to induce an in-frame deletion of the Runt domain. Despite confirmation of

homozygous in-frame deletion by Sanger sequence analysis, a lower band of RUNX2 protein was not visualised in Western blot, probably due to protein degradation after removal of a functional domain or lack of recognition by the antibody used to detect the protein product carrying the deletion. For this reason, to rule out a possible experimental artifact, the protein extracts from the Runt-deleted clones will be retested with a different antibody.

For the KO of FBXW11 in MG63 cells, we used classical plasmid transfection as a first-line approach, as performed for the previous cell lines, but no editing events were detected. Since the transfectability of a line may also depend on the size of the transfected plasmid, we decided to transfect MG63 cells with a smaller plasmid, encoding only the guide RNA and puromycin resistance cassette. In order to perform this approach, we first generated Cas9-expressing cells through transduction with VSV-G pseudotyped lentiviral particles, which allowed for high-efficiency delivery into target cells and subsequent integration of the genetic material encoding Cas9, whose expression was confirmed by Western blot. This approach leads to constitutive expression of Cas9, which is only active in the presence of the gRNA, which can be provided via transfection or another delivery strategy for its transient expression. Compared to other systems (e.g., LentiCRISPR v2) that integrate both Cas9 and gRNA, the generation of a Cas9-expressing line could be advantageous in reducing off-target effects. This experimental setup allowed us to achieve a moderate editing efficiency, but still low. To increase efficiency, we tried using virus-like particles (VLPs) to deliver the CRISPR RNP complex in a rapid and efficient way, without integration into the genome. Transduction via VLP proved to be the most efficient approach for difficult-to-transfect cell lines, such as MG63, ultimately allowing us to isolate an FBXW11 KO clone.

Before proceeding with downstream functional studies, it is good practice to validate the knockout cells by ensuring that no off-target events occurred in the generated knockout cell models. For the HADHA KO project, a bioinformatic tool was used to identify the two top-ranked predicted off-target sites, which were then amplified by PCR and sequenced to exclude the presence of unwanted mutations in

the KO clone. In the case of ACOT8 KO, its specific effect was validated by re-transfection of the ACOT8 plasmid in ACOT8 KO cells to restore the phenotype. HEK293T ACOT8 KO cells were then used to produce HIV-1 pseudoviruses and infect target cells, demonstrating that ACOT8 absence leads to the production of less infectious viral particles, whereas the presence of ACOT8 and its interaction with HIV-1 Nef protein leads to the production of more infectious viral particles. Since ACOT8 is involved in lipid metabolism, and can be delivered by Nef to the plasma membrane, subsequent studies will evaluate the effect on the lipid composition of virions produced in the different cell lines under examination (WT, ACOT8 KO, ACOT8 rescued and ACOT8 rescued + NEF).

In the HADHA knockout project involving PANC-1 cells, we obtained preliminary results indicating that the KO cells retained the capacity to dedifferentiate into stem cells and form larger tumourspheres than WT-induced stem cells. Further investigation of the effect of HADHA absence on pancreatic cancer stem cell (PCSC) proliferation, chemoresistance and tumour migration is required to understand its role in PCSC biology and its potential as a therapeutic target in pancreatic cancer.

Regarding the generation of RUNX2 KO and Runt-deleted melanoma cell lines, the resulting cells will be injected into mice to evaluate RUNX2 contribution to tumour proliferation, cell migration, and metastasis formation. FBXW11 KO MG63 cells will subsequently be used to improve the understanding of the role of FBXW11 in osteosarcoma.

Prime editing is an innovative technology that enables all 12 base conversions to be performed and insertions or deletions to be introduced into the target sequence. The prime editing mechanism involves a series of cellular events that can incorporate the desired mutation, but can also revert the sequence to wild type (WT), thereby reducing editing efficiency in certain circumstances. Therefore, a careful design of the prime editing conditions is essential, including the design of the pegRNA, choice of the editing approach, and transfection efficiency of the targeted cell line. In this study, we focused on a point mutation in the RUNX2 gene that causes cleidocranial dysplasia. To optimise the conditions for correcting this mutation, we first needed a cell model carrying the mutation of interest. For this purpose, we used

the HEK293T cell line as a starting model to validate our system and apply the prime editing protocol to first generate a cell model carrying the mutation.

After generating clones carrying the mutation of interest both in homozygosity and in heterozygosity, we tested the efficiency of our prime editing design in correcting back this pathogenic mutation in these clones. We tested different conditions in both cases, involving either a different pegRNA design or the inclusion of ngRNA in combination. As expected, approaches involving ngRNA (PE3) were markedly more efficient than those using pegRNA alone (PE2). After optimising the conditions for introducing and correcting mutations, we will aim to apply these editing conditions to more challenging patient-derived cell lines, as induced mesenchymal stem cell lines (iMSCs). These iMSCs will be then subjected to osteogenic differentiation in order to evaluate the effect of introducing or correcting the mutation in a relevant cell or organoid context.

The final project presented in this thesis work focuses on studying the stability of HLA-C alleles and its association with HIV-1 infection. In this case, we first used CRISPR-Cas9 to knockout the HLA-C gene in HEK293T by the VLP delivery approach and constructed HLA-C expressing plasmids to be used for transfecting knockout cells and evaluating the binding stability of individual HLA-C allotypes. However, Sarkizova et al. utilised a similar approach and derived a list of HLA-C binding peptides by mass spectrometry investigation. Based on this, we used an updated bioinformatic software (NetMHCpan4.2) to obtain quantitative measures of the binding affinity between different HLA-C allotypes and the pool of specific binding peptides determined by Sarkizova et al. (Sarkizova et al. 2020). We then derived specific stability scores for each of the considered HLA-C allotype. Using this new, more accurate classification of HLA-C stability, we genotyped for HLA-C two cohorts of HIV-1 patients: one with varying degrees of progression towards AIDS, the other with or without HIV-1 related neurological deficits. These new stability measurements enabled us to assign an HLA-C stability score to each patient and assess that lower scores (i.e. less stable alleles) were associated with patients with a rapid progression towards AIDS or presenting neurological impairment. This analysis confirmed HLA-C as a genetic factor to be considered in personalised HIV-1 infection management and treatment, as it can be potentially

relevant for the identification of subjects who are more susceptible to increased risk of rapid disease progression or the development of neurocognitive deficit. We will next analyse other HIV-1 patient cohorts to validate these results and determine if HLA-C is associated with the same or other outcomes of HIV-1 infection.

6. BIBLIOGRAPHY

Agrotis, Alexander, and Robin Ketteler. 2015. “A New Age in Functional Genomics Using CRISPR/Cas9 in Arrayed Library Screening.” *Frontiers in Genetics* 6(SEP):1–15. doi: 10.3389/fgene.2015.00300.

Alerasool, Nader, Dmitri Segal, Hunsang Lee, and Mikko Taipale. 2020. “An Efficient KRAB Domain for CRISPRi Applications in Human Cells.” *Nature Methods* 17(11):1093–96. doi: 10.1038/s41592-020-0966-x.

Alkhnbashi, Omer S., Shiraz A. Shah, Roger A. Garrett, Sita J. Saunders, Fabrizio Costa, and Rolf Backofen. 2016. “Characterizing Leader Sequences of CRISPR Loci.” *Bioinformatics (Oxford, England)* 32(17):i576–85. doi: 10.1093/bioinformatics/btw454.

Aman Mohammadi, Masoud, Mariana Rocha Maximiano, Seyede Marzieh Hosseini, and Octavio Luiz Franco. 2023. “CRISPR-Cas Engineering in Food Science and Sustainable Agriculture: Recent Advancements and Applications.” *Bioprocess and Biosystems Engineering* 46(4):483–97. doi: 10.1007/s00449-022-02842-5.

Ansori, Arif Nm, Yulanda Antonius, Raden Jk Susilo, Suhailah Hayaza, Viol D. Kharisma, Arli A. Parikesit, Rahadian Zainul, Vikash Jakhmola, Taru Saklani, Maksim Rebezov, Md Emdad Ullah, Nikolai Maksimiuk, Marina Derkho, and Pavel Burkov. 2023. “Application of CRISPR-Cas9 Genome Editing Technology in Various Fields: A Review.” *Narra J* 3(2):e184. doi: 10.52225/narra.v3i2.184.

Antinori, A., G. Arendt, J. T. Becker, B. J. Brew, D. A. Byrd, M. Cherner, D. B. Clifford, P. Cinque, L. G. Epstein, K. Goodkin, M. Gisslen, I. Grant, R. K. Heaton, J. Joseph, K. Marder, C. M. Marra, J. C. McArthur, M. Nunn, R. W. Price, L. Pulliam, K. R. Robertson, N. Sacktor, V. Valcour, and V. E. Wojna. 2007. “Updated Research Nosology for HIV-Associated Neurocognitive Disorders.” *Neurology* 69(18):1789–99. doi: 10.1212/01.WNL.0000287431.88658.8b.

Anzalone, Andrew V., Peyton B. Randolph, Jessie R. Davis, Alexander A. Sousa, Luke W. Koblan, Jonathan M. Levy, Peter J. Chen, Christopher Wilson, Gregory A. Newby, Aditya Raguram, and David R. Liu. 2019. “Search-and-

Replace Genome Editing without Double-Strand Breaks or Donor DNA." *Nature* 576(7785):149–57. doi: 10.1038/s41586-019-1711-4.

Aoki, Kanae, Mai Yamasaki, Riku Umezono, Takanori Hamamoto, and Yusuke Kamachi. 2024. "Systematic Comparison of Computational Tools for Sanger Sequencing-Based Genome Editing Analysis." *Cells* 13(3). doi: 10.3390/cells13030261.

Apps, Richard, Ying Qi, Jonathan M. Carlson, Haoyan Chen, Xiaojiang Gao, Rasmi Thomas, Yuko Yuki, Greg Q. Del Prete, Philip Goulder, Zabrina L. Brumme, Chanson J. Brumme, Mina John, Simon Mallal, George Nelson, Ronald Bosch, David Heckerman, Judy L. Stein, Kelly A. Soderberg, M. Anthony Moody, Thomas N. Denny, Xue Zeng, Jingyuan Fang, Ashley Moffett, Jeffrey D. Lifson, James J. Goedert, Susan Buchbinder, Gregory D. Kirk, Jacques Fellay, Paul McLaren, Steven G. Deeks, Florencia Pereyra, Bruce Walker, Nelson L. Michael, Amy Weintrob, Steven Wolinsky, Wilson Liao, and Mary Carrington. 2013. "Influence of HLA-C Expression Level on HIV Control." *Science (New York, N.Y.)* 340(6128):87–91. doi: 10.1126/science.1232685.

Bao, X. Robert, Yidan Pan, Ciaran M. Lee, Timothy H. Davis, and Gang Bao. 2021. "Tools for Experimental and Computational Analyses of Off-Target Editing by Programmable Nucleases." *Nature Protocols* 16(1):10–26. doi: 10.1038/s41596-020-00431-y.

Barrangou, Rodolphe, Christophe Fremaux, Hélène Deveau, Melissa Richards, Patrick Boyaval, Sylvain Moineau, Dennis A. Romero, and Philippe Horvath. 2007. "CRISPR Provides Acquired Resistance against Viruses in Prokaryotes." *Science (New York, N.Y.)* 315(5819):1709–12. doi: 10.1126/science.1138140.

Barrangou, Rodolphe, and Luciano A. Marraffini. 2014. "CRISPR-Cas Systems: Prokaryotes Upgrade to Adaptive Immunity." *Molecular Cell* 54(2):234–44. doi: 10.1016/j.molcel.2014.03.011.

Becker, Sebastian, and Jens Boch. 2021. "TALE and TALEN Genome Editing Technologies." *Gene and Genome Editing* 2(March):100007. doi: 10.1016/j.ggedit.2021.100007.

Blackwell, Jenefer M., Sarra E. Jamieson, and David Burgner. 2009. “HLA and Infectious Diseases.” *Clinical Microbiology Reviews* 22(2):370–85, Table of Contents. doi: 10.1128/CMR.00048-08.

Blais, Marie Eve, Tao Dong, and Sarah Rowland-Jones. 2011. “HLA-C as a Mediator of Natural Killer and T-Cell Activation: Spectator or Key Player?” *Immunology* 133(1):1–7. doi: 10.1111/j.1365-2567.2011.03422.x.

Boch, Jens, Heidi Scholze, Sebastian Schornack, Angelika Landgraf, Simone Hahn, Sabine Kay, Thomas Lahaye, Anja Nickstadt, and Ulla Bonas. 2009. “Breaking the Code of DNA Binding Specificity of TAL-Type III Effectors.” *Science (New York, N.Y.)* 326(5959):1509–12. doi: 10.1126/science.1178811.

Boregowda, Rajeev K., Oyenike O. Olabisi, Walid Abushahba, Byeong-Seon Jeong, Keneshia K. Haenssen, Wenjin Chen, Marina Chekmareva, Ahmed Lasfar, David J. Foran, James S. Goydos, and Karine A. Cohen-Solal. 2014. “RUNX2 Is Overexpressed in Melanoma Cells and Mediates Their Migration and Invasion.” *Cancer Letters* 348(1–2):61–70. doi: 10.1016/j.canlet.2014.03.011.

Cameron, Peter, Chris K. Fuller, Paul D. Donohoue, Brittnee N. Jones, Matthew S. Thompson, Matthew M. Carter, Scott Gradia, Bastien Vidal, Elizabeth Garner, Euan M. Slorach, Elaine Lau, Lynda M. Banh, Alexandra M. Lied, Leslie S. Edwards, Alexander H. Settle, Daniel Capurso, Victor Llaca, Stéphane Deschamps, Mark Cigan, Joshua K. Young, and Andrew P. May. 2017. “Mapping the Genomic Landscape of CRISPR-Cas9 Cleavage.” *Nature Methods* 14(6):600–606. doi: 10.1038/nmeth.4284.

Van Campenhout, Claude, Pauline Cabochette, Anne Clémence Veillard, Miklos Laczik, Agnieszka Zelisko-Schmidt, Céline Sabatel, Maxime Dhainaut, Benoit Vanhollebeke, Cyril Gueydan, and Véronique Kruys. 2019. “Guidelines for Optimized Gene Knockout Using CRISPR/Cas9.” *BioTechniques* 66(6):295–302. doi: 10.2144/btn-2018-0187.

Di Carlo, Claudia, Bebiana C. Sousa, Marcello Manfredi, Jessica Brandi, Elisa Dalla Pozza, Emilio Marengo, Marta Palmieri, Ilaria Dando, Michael J. O. Wakelam, Andrea F. Lopez-Clavijo, and Daniela Cecconi. 2021. “Integrated

Lipidomics and Proteomics Reveal Cardiolipin Alterations, Upregulation of HADHA and Long Chain Fatty Acids in Pancreatic Cancer Stem Cells." *Scientific Reports* 11(1):1–13. doi: 10.1038/s41598-021-92752-5.

Castro, Nicolás González, Jan Bjelic, Gunya Malhotra, Cong Huang, and Salman Hasan Alsaffar. 2021. "Comparison of the Feasibility, Efficiency, and Safety of Genome Editing Technologies." *International Journal of Molecular Sciences* 22(19). doi: 10.3390/ijms221910355.

Cerna-Chavez, Rodrigo, Alba Ortega-Gasco, Hafiz Muhammad Azhar Baig, Nathan Ehrenreich, Thibaud Metais, Michael J. Scandura, Kinga Bujakowska, Eric A. Pierce, and Marcela Garita-Hernandez. 2025. "Optimized Prime Editing of Human Induced Pluripotent Stem Cells to Efficiently Generate Isogenic Models of Mendelian Diseases." *International Journal of Molecular Sciences* 26(1). doi: 10.3390/ijms26010114.

Certo, Michael T., and Richard A. Morgan. 2016. "Salient Features of Endonuclease Platforms for Therapeutic Genome Editing." *Molecular Therapy* 24(3):422–29. doi: 10.1038/mt.2016.21.

Chapdelaine, P., C. Pichavant, J. Rousseau, F. Pâques, and J. P. Tremblay. 2010. "Meganucleases Can Restore the Reading Frame of a Mutated Dystrophin." *Gene Therapy* 17(7):846–58. doi: 10.1038/gt.2010.26.

Charpentier, Emmanuelle, and Luciano A. Marraffini. 2014. "Harnessing CRISPR-Cas9 Immunity for Genetic Engineering." *Current Opinion in Microbiology* 19:114–19. doi: 10.1016/j.mib.2014.07.001.

Charpentier, Emmanuelle, Hagen Richter, John van der Oost, and Malcolm F. White. 2015. "Biogenesis Pathways of RNA Guides in Archaeal and Bacterial CRISPR-Cas Adaptive Immunity." *FEMS Microbiology Reviews* 39(3):428–41. doi: 10.1093/femsre/fuv023.

Chavez, Alejandro, Jonathan Scheiman, Suhani Vora, Benjamin W. Pruitt, Marcelle Tuttle, Eswar P R Iyer, Shuailiang Lin, Samira Kiani, Christopher D. Guzman, Daniel J. Wiegand, Dmitry Ter-Ovanesyan, Jonathan L. Braff, Noah Davidsohn, Benjamin E. Housden, Norbert Perrimon, Ron Weiss, John Aach, James J. Collins, and George M. Church. 2015. "Highly Efficient Cas9-Mediated Transcriptional Programming." *Nature Methods* 12(4):326–

28. doi: 10.1038/nmeth.3312.

Chen, Peter J., Jeffrey A. Hussmann, Jun Yan, Friederike Knipping, Purnima Ravisankar, Pin Fang Chen, Cidi Chen, James W. Nelson, Gregory A. Newby, Mustafa Sahin, Mark J. Osborn, Jonathan S. Weissman, Britt Adamson, and David R. Liu. 2021. *Enhanced Prime Editing Systems by Manipulating Cellular Determinants of Editing Outcomes*. Vol. 184.

Chen, Peter J., and David R. Liu. 2023. "Prime Editing for Precise and Highly Versatile Genome Manipulation." *Nature Reviews. Genetics* 24(3):161–77. doi: 10.1038/s41576-022-00541-1.

Choe, Dongwook C., and Kiran Musunuru. 2021. "Base Editing: A Brief Review and a Practical Example." *Journal of Biomedical Research* 35(2):107–14. doi: 10.7555/JBR.34.20200003.

Chou, S. T., Q. Leng, and James Mixson. 2012. "Zinc Finger Nucleases: Tailor-Made for Gene Therapy." *Drugs of the Future* 37(3):183–95. doi: 10.1358/dof.2012.037.03.1779022.

Clark, Teleri, Matthew A. Waller, Lipin Loo, Cesar L. Moreno, Christopher E. Denes, and G. Gregory Neely. 2024. "CRISPR Activation Screens: Navigating Technologies and Applications." *Trends in Biotechnology* 42(8):1017–34. doi: 10.1016/j.tibtech.2024.02.007.

Dalle Carbonare, Luca, Macarena Gomez Lira, Arianna Minoia, Jessica Bertacco, Silvia Orsi, Angela Lauriola, Veronica Li Vigni, Alberto Gandini, Franco Antoniazzi, Donato Zipeto, Monica Mottes, Lekhana Bhandary, Daniele Guardavaccaro, and Maria Teresa Valenti. 2023. "Expression of FBXW11 in Normal and Disease-Associated Osteogenic Cells." *Journal of Cellular and Molecular Medicine* 27(11):1580–91. doi: 10.1111/jcmm.17767.

Dalle Carbonare, Luca, Giulio Innamorati, and Maria Teresa Valenti. 2012. "Transcription Factor Runx2 and Its Application to Bone Tissue Engineering." *Stem Cell Reviews and Reports* 8(3):891–97. doi: 10.1007/s12015-011-9337-4.

Dalle Carbonare, Luca, Arianna Minoia, Alberto Gandini, Francesca Cristiana Piritore, Cristina Patuzzo, Lucrezia Ceretti, Anna Vareschi, Antonino Aparo, Mattia Cominacini, Giovanni Malerba, Maria Grazia Romanelli, Joao

Pessoa, Daniele Guardavaccaro, Franco Antoniazzi, and Maria Teresa Valenti. 2025. “Unraveling RUNX2 Mutation in a Cleidocranial Dysplasia Patient: Molecular Insights into Osteogenesis and Proteostasis.” *Genes & Diseases* 12(4):101449. doi: 10.1016/j.gendis.2024.101449.

Deiana, Michela, Luca Dalle Carbonare, Michela Serena, Samuele Cheri, Francesca Parolini, Alberto Gandini, Giulia Marchetto, Giulio Innamorati, Marcello Manfredi, Emilio Marengo, Jessica Brandi, Daniela Cecconi, Antonio Mori, Maria Mihaela Mina, Franco Antoniazzi, Monica Mottes, Natascia Tiso, Giovanni Malerba, Donato Zipeto, and Maria Teresa Valenti. 2018. “New Insights into the Runt Domain of RUNX2 in Melanoma Cell Proliferation and Migration.” *Cells* 7(11):1–16. doi: 10.3390/cells7110220.

Deiana, Michela, Luca Dalle Carbonare, Michela Serena, Samuele Cheri, Simona Mutascio, Alberto Gandini, Giulio Innamorati, Pamela Lorenzi, Michela Cumerlato, Jessica Bertacco, Franco Antoniazzi, Maria Grazia Romanelli, Monica Mottes, Donato Zipeto, and Maria Teresa Valenti. 2020. “A Potential Role of RUNX2- RUNT Domain in Modulating the Expression of Genes Involved in Bone Metastases: An In Vitro Study with Melanoma Cells.” *Cells* 9(3). doi: 10.3390/cells9030751.

Dhanyamraju, Pavan Kumar, and Trupti N. Patel. 2022. “Melanoma Therapeutics: A Literature Review.” *Journal of Biomedical Research* 36(2):77–97. doi: 10.7555/JBR.36.20210163.

Dhiman, Neeraj Kumar, Akhilesh Kumar Singh, Naresh Kumar Sharma, and Chandresh Jaiswara. 2014. “Cleidocranial Dysplasia.” *National Journal of Maxillofacial Surgery* 5(2):206–8. doi: 10.4103/0975-5950.154838.

Doench, John G., Nicolo Fusi, Meagan Sullender, Mudra Hegde, Emma W. Vaimberg, Katherine F. Donovan, Ian Smith, Zuzana Tothova, Craig Wilen, Robert Orchard, Herbert W. Virgin, Jennifer Listgarten, and David E. Root. 2016. “Optimized SgRNA Design to Maximize Activity and Minimize Off-Target Effects of CRISPR-Cas9.” *Nature Biotechnology* 34(2):184–91. doi: 10.1038/nbt.3437.

Doench, John G., Ella Hartenian, Daniel B. Graham, Zuzana Tothova, Mudra Hegde, Ian Smith, Meagan Sullender, Benjamin L. Ebert, Ramnik J. Xavier,

and David E. Root. 2014. “Rational Design of Highly Active SgRNAs for CRISPR-Cas9–Mediated Gene Inactivation.” *Nature Biotechnology* 32(12):1262–67. doi: 10.1038/nbt.3026.

Doman, Jordan L., Smriti Pandey, Monica E. Neugebauer, Meirui An, Jessie R. Davis, Peyton B. Randolph, Amber McElroy, Xin D. Gao, Aditya Raguram, Michelle F. Richter, Kelcee A. Everette, Samagya Banskota, Kathryn Tian, Y. Allen Tao, Jakub Tolar, Mark J. Osborn, and David R. Liu. 2023. “Phage-Assisted Evolution and Protein Engineering Yield Compact, Efficient Prime Editors.” *Cell* 186(18):3983-4002.e26. doi: 10.1016/j.cell.2023.07.039.

Doman, Jordan L., Alexander A. Sousa, Peyton B. Randolph, Peter J. Chen, and David R. Liu. 2022. *Designing and Executing Prime Editing Experiments in Mammalian Cells*. Vol. 17. Springer US.

Doudna, Jennifer A., and Emmanuelle Charpentier. 2014. “Genome Editing. The New Frontier of Genome Engineering with CRISPR-Cas9.” *Science (New York, N.Y.)* 346(6213):1258096. doi: 10.1126/science.1258096.

Du, Yimin, Yanfei Liu, Jiaxin Hu, Xingxing Peng, and Zhenbao Liu. 2023. “CRISPR/Cas9 Systems: Delivery Technologies and Biomedical Applications.” *Asian Journal of Pharmaceutical Sciences* 18(6):100854. doi: 10.1016/j.ajps.2023.100854.

Elalouf, Amir, Tomer Kedarya, Hadas Elalouf, and Ariel Rosenfeld. 2023. “Computational Design and Evaluation of MRNA- and Protein-Based Conjugate Vaccines for Influenza A and SARS-CoV-2 Viruses.” *Journal of Genetic Engineering and Biotechnology* 21(1):120. doi: 10.1186/s43141-023-00574-x.

Ercan, Gulinnaz, Ayfer Karlitepe, and Bulent Ozpolat. 2017. “Pancreatic Cancer Stem Cells and Therapeutic Approaches.” *Anticancer Research* 37(6):2761–75. doi: 10.21873/anticanres.11628.

Ferrari, Nicola, Laura McDonald, Joanna S. Morris, Ewan R. Cameron, and Karen Blyth. 2013. “RUNX2 in Mammary Gland Development and Breast Cancer.” *Journal of Cellular Physiology* 228(6):1137–42. doi: 10.1002/jcp.24285.

Février, Michèle, Karim Dorgham, and Angelita Rebollo. 2011. “CD4+ T Cell Depletion in Human Immunodeficiency Virus (HIV) Infection: Role of

Apoptosis." *Viruses* 3(5):586–612. doi: 10.3390/v3050586.

Fouriki, A., M. A. Clements, N. Farrow, and J. Dobson. 2014. "Efficient Transfection of MG-63 Osteoblasts Using Magnetic Nanoparticles and Oscillating Magnetic Fields." *Journal of Tissue Engineering and Regenerative Medicine* 8(3):169–75. doi: 10.1002/term.1508.

Gaj, Thomas, Charles A. Gersbach, and Carlos F. 3rd Barbas. 2013. "ZFN, TALEN, and CRISPR/Cas-Based Methods for Genome Engineering." *Trends in Biotechnology* 31(7):397–405. doi: 10.1016/j.tibtech.2013.04.004.

Gao, Zongliang, Elena Herrera-Carrillo, and Ben Berkhout. 2018. "Delineation of the Exact Transcription Termination Signal for Type 3 Polymerase III." *Molecular Therapy. Nucleic Acids* 10:36–44. doi: 10.1016/j.omtn.2017.11.006.

Gaudelli, Nicole M., Alexis C. Komor, Holly A. Rees, Michael S. Packer, Ahmed H. Badran, David I. Bryson, and David R. Liu. 2017. "Programmable Base Editing of T to G C in Genomic DNA without DNA Cleavage." *Nature* 551(7681):464–71. doi: 10.1038/nature24644.

Gautron, Anne-Sophie, Alexandre Juillerat, Valérie Guyot, Jean-Marie Filhol, Emilie Dessez, Aymeric Duclert, Philippe Duchateau, and Laurent Poirot. 2017. "Fine and Predictable Tuning of TALEN Gene Editing Targeting for Improved T Cell Adoptive Immunotherapy." *Molecular Therapy. Nucleic Acids* 9:312–21. doi: 10.1016/j.omtn.2017.10.005.

Gilbert, Luke A., Max A. Horlbeck, Britt Adamson, Jacqueline E. Villalta, Yuwen Chen, Evan H. Whitehead, Carla Guimaraes, Barbara Panning, Hidde L. Ploegh, Michael C. Bassik, Lei S. Qi, Martin Kampmann, and Jonathan S. Weissman. 2014. "Genome-Scale CRISPR-Mediated Control of Gene Repression and Activation." *Cell* 159(3):647–61. doi: 10.1016/j.cell.2014.09.029.

Gilbert, Luke A., Matthew H. Larson, Leonardo Morsut, Zairan Liu, Gloria A. Brar, Sandra E. Torres, Noam Stern-Ginossar, Onn Brandman, Evan H. Whitehead, Jennifer A. Doudna, Wendell A. Lim, Jonathan S. Weissman, and Lei S. Qi. 2013. "CRISPR-Mediated Modular RNA-Guided Regulation of Transcription in Eukaryotes." *Cell* 154(2):442–51. doi:

10.1016/j.cell.2013.06.044.

Giuliano, Christopher J., Ann Lin, Vishruth Girish, and Jason M. Sheltzer. 2019. "Generating Single Cell-Derived Knockout Clones in Mammalian Cells with CRISPR/Cas9." *Current Protocols in Molecular Biology* 128(1):e100. doi: 10.1002/cpmb.100.

Gleditzsch, Daniel, Patrick Pausch, Hanna Müller-Esparza, Ahsen Özcan, Xiaohan Guo, Gert Bange, and Lennart Randau. 2019. "PAM Identification by CRISPR-Cas Effector Complexes: Diversified Mechanisms and Structures." *RNA Biology* 16(4):504–17. doi: 10.1080/15476286.2018.1504546.

Guo, Congting, Xiaoteng Ma, Fei Gao, and Yuxuan Guo. 2023. "Off-Target Effects in CRISPR/Cas9 Gene Editing." *Frontiers in Bioengineering and Biotechnology* 11(March):1–11. doi: 10.3389/fbioe.2023.1143157.

Guo, Zheng-Jun, Lang Yang, Feng Qian, Yan-Xia Wang, Xi Yu, Cheng-Dong Ji, Wei Cui, Dong-Fang Xiang, Xia Zhang, Peng Zhang, Ji Ming Wang, You-Hong Cui, and Xiu-Wu Bian. 2016. "Transcription Factor RUNX2 Up-Regulates Chemokine Receptor CXCR4 to Promote Invasive and Metastatic Potentials of Human Gastric Cancer." *Oncotarget* 7(15):20999–12. doi: 10.18632/oncotarget.8236.

Gupta, Rajat M., and Kiran Musunuru. 2014. "The Emergence of Genome-Editing Technology." *The Journal of Clinical Investigation* 124(10):4154–61. doi: 10.1172/JCI72992.transcription.

Haapaniemi, Emma, Sandeep Botla, Jenna Persson, Bernhard Schmierer, and Jussi Taipale. 2018. "CRISPR-Cas9 Genome Editing Induces a P53-Mediated DNA Damage Response." *Nature Medicine* 24(7):927–30. doi: 10.1038/s41591-018-0049-z.

Hille, Frank, and Emmanuelle Charpentier. 2016. "CRISPR-Cas: Biology, Mechanisms and Relevance." *Philosophical Transactions of the Royal Society of London. Series B, Biological Sciences* 371(1707). doi: 10.1098/rstb.2015.0496.

Hinnen, A., J. B. Hicks, and G. R. Fink. 1978. "Transformation of Yeast." *Proceedings of the National Academy of Sciences of the United States of*

America 75(4):1929–33. doi: 10.1073/pnas.75.4.1929.

Hiranniramol, Kasidet, Yuhao Chen, Weijun Liu, and Xiaowei Wang. 2020. "Generalizable SgRNA Design for Improved CRISPR/Cas9 Editing Efficiency." *Bioinformatics (Oxford, England)* 36(9):2684–89. doi: 10.1093/bioinformatics/btaa041.

Hojo, Hironori. 2023. "Emerging RUNX2-Mediated Gene Regulatory Mechanisms Consisting of Multi-Layered Regulatory Networks in Skeletal Development." *International Journal of Molecular Sciences* 24(3). doi: 10.3390/ijms24032979.

Hong, Cheol-hwa, Hyun-jung Sohn, Hyun-joo Lee, Hyun-il Cho, and Tai-gyu Kim. 2017. "Antigen Presentation by Individually Transferred HLA Class I Generated Using the Multiplex CRISPR-Cas9 System." *J. Immunother* 40(6):201–10.

Hong, Taeyeon, Seung Min Bae, Gwonhwa Song, and Whasun Lim. 2024. "Guide for Generating Single-Cell–Derived Knockout Clones in Mammalian Cell Lines Using the CRISPR/Cas9 System." *Molecules and Cells* 47(7):100087. doi: 10.1016/j.mocell.2024.100087.

Hsu, Patrick D., David A. Scott, Joshua A. Weinstein, F. Ann Ran, Silvana Konermann, Vineeta Agarwala, Yinqing Li, Eli J. Fine, Xuebing Wu, Ophir Shalem, Thomas J. Cradick, Luciano A. Marraffini, Gang Bao, and Feng Zhang. 2013. "DNA Targeting Specificity of RNA-Guided Cas9 Nucleases." *Nature Biotechnology* 31(9):827–32. doi: 10.1038/nbt.2647.

Huang, Ningshu, Zhenglan Huang, Miao Gao, Zhenhong Luo, Fangzhu Zhou, Lin Liu, Qing Xiao, Xin Wang, and Wenli Feng. 2018. "Induction of Apoptosis in Imatinib Sensitive and Resistant Chronic Myeloid Leukemia Cells by Efficient Disruption of Bcr-Abl Oncogene with Zinc Finger Nucleases." *Journal of Experimental & Clinical Cancer Research : CR* 37(1):62. doi: 10.1186/s13046-018-0732-4.

Hunt, Mary C., Marina I. Siponen, and Stefan E. H. Alexson. 2012. "The Emerging Role of Acyl-CoA Thioesterases and Acyltransferases in Regulating Peroxisomal Lipid Metabolism." *Biochimica et Biophysica Acta* 1822(9):1397–1410. doi: 10.1016/j.bbadis.2012.03.009.

Hwang, Gue-Ho, Beomjong Song, and Sangsu Bae. 2021. “Current Widely-Used Web-Based Tools for CRISPR Nucleases, Base Editors, and Prime Editors.” *Gene and Genome Editing* 1(April):100004. doi: 10.1016/j.ggedit.2021.100004.

Ishino, Y., H. Shinagawa, K. Makino, M. Amemura, and A. Nakata. 1987. “Nucleotide Sequence of the Iap Gene, Responsible for Alkaline Phosphatase Isozyme Conversion in Escherichia Coli, and Identification of the Gene Product.” *Journal of Bacteriology* 169(12):5429–33. doi: 10.1128/jb.169.12.5429-5433.1987.

Ishizuka, Mitsuru, Yoshiro Toyama, Hiroyuki Watanabe, Yukio Fujiki, Arata Takeuchi, Sho Yamasaki, Shigeki Yuasa, Masaru Miyazaki, Nobuyuki Nakajima, Shinsuke Taki, and Takashi Saito. 2004. “Overexpression of Human Acyl-CoA Thioesterase Upregulates Peroxisome Biogenesis.” *Experimental Cell Research* 297(1):127–41. doi: 10.1016/j.yexcr.2004.02.029.

Jansen, Ruud, Jan D. A. van Embden, Wim Gaastra, and Leo M. Schouls. 2002. “Identification of Genes That Are Associated with DNA Repeats in Prokaryotes.” *Molecular Microbiology* 43(6):1565–75. doi: 10.1046/j.1365-2958.2002.02839.x.

Jin, Ben, Sayed Ala Moududee, Dongxia Ge, Pengbo Zhou, Alun R. Wang, Yao Zhong Liu, and Zongbing You. 2024. “SCFFBXW11 Complex Targets Interleukin-17 Receptor A for Ubiquitin–Proteasome-Mediated Degradation.” *Biomedicines* 12(4). doi: 10.3390/biomedicines12040755.

Jinek, Martin, Krzysztof Chylinski, Ines Fonfara, Michael Hauer, Jennifer A Doudna, and Emmanuelle Charpentier. 2012. “A Programmable Dual-RNA-Guided DNA Endonuclease in Adaptive Bacterial Immunity.” *Science (New York, N.Y.)* 337(6096):816–21. doi: 10.1126/science.1225829.

Joung, J. Keith, and Jeffry D. Sander. 2013. “TALENs: A Widely Applicable Technology for Targeted Genome Editing.” *Nature Reviews. Molecular Cell Biology* 14(1):49–55. doi: 10.1038/nrm3486.

Joung, Julia, Silvana Konermann, Jonathan S. Gootenberg, Omar O. Abudayyeh, Randall J. Platt, Mark D. Brigham, Neville E. Sanjana, and Feng Zhang.

2017. “Genome-Scale CRISPR-Cas9 Knockout and Transcriptional Activation Screening.” *Nature Protocols* 12(4):828–63. doi: 10.1038/nprot.2017.016.

Jurtz, Vanessa, Sinu Paul, Massimo Andreatta, Paolo Marcatili, Bjoern Peters, and Morten Nielsen. 2017. “NetMHCpan-4.0: Improved Peptide–MHC Class I Interaction Predictions Integrating Eluted Ligand and Peptide Binding Affinity Data.” *The Journal of Immunology* 199(9):3360–68. doi: 10.4049/jimmunol.1700893.

Kahaki, Seyed Alireza Mousavi, Nayereh Ebrahimzadeh, Hossein Fahimi, and Arfa Moshiri. 2024. “Development of an Optimized Protocol for Generating Knockout Cancer Cell Lines Using the CRISPR/Cas9 System, with Emphasis on Transient Transfection.” *PLoS ONE* 19(11 November):1–24. doi: 10.1371/journal.pone.0310368.

Kainulainen, Markus, Simone Lau, Charles E. Samuel, Veit Hornung, and Friedemann Weber. 2016. “NSs Virulence Factor of Rift Valley Fever Virus Engages the F-Box Proteins FBXW11 and β-TRCP1 To Degrade the Antiviral Protein Kinase PKR.” *Journal of Virology* 90(13):6140–47. doi: 10.1128/jvi.00016-16.

Karginov, Fedor V, and Gregory J. Hannon. 2010. “The CRISPR System: Small RNA-Guided Defense in Bacteria and Archaea.” *Molecular Cell* 37(1):7–19. doi: 10.1016/j.molcel.2009.12.033.

Karimi, Zahra, Ali Ahmadi, Ali Najafi, and Reza Ranjbar. 2018. “Bacterial CRISPR Regions: General Features and Their Potential for Epidemiological Molecular Typing Studies.” *The Open Microbiology Journal* 12(1):59–70. doi: 10.2174/1874285801812010059.

Karnaukhov, Vadim, Wayne Paes, Isaac B. Woodhouse, Thomas Partridge, Annalisa Nicastri, Simon Brackenridge, Dmitrii Shcherbinin, Dmitry M. Chudakov, Ivan V. Zvyagin, Nicola Ternette, Hashem Koohy, Persephone Borrow, and Mikhail Shugay. 2022. “HLA Variants Have Different Preferences to Present Proteins with Specific Molecular Functions Which Are Complemented in Frequent Haplotypes.” *Frontiers in Immunology* 13(December):1–17. doi: 10.3389/fimmu.2022.1067463.

Kaur, Gurman, Stephanie Gras, Jesse I. Mobbs, Julian P. Vivian, Adrian Cortes, Thomas Barber, Subita Balaram Kuttikkatte, Lise Torp Jensen, Kathrine E. Attfield, Calliope A. Dendrou, Mary Carrington, Gil Mcvean, Anthony W. Purcell, Jamie Rossjohn, and Lars Fugger. 2017. "Structural and Regulatory Diversity Shape HLA-C Protein Expression Levels." *Nature Communications* 8(May):1–12. doi: 10.1038/ncomms15924.

Khairkhah, Niloofar, Mohammad Reza Aghasadeghi, Ali Namvar, and Azam Bolhassani. 2020. "Design of Novel Multiepitope Constructs-Based Peptide Vaccine against the Structural S, N and M Proteins of Human COVID-19 Using Immunoinformatics Analysis." *PloS One* 15(10):e0240577. doi: 10.1371/journal.pone.0240577.

Khalil, Ahmad M. 2020. "The Genome Editing Revolution: Review." *Journal of Genetic Engineering and Biotechnology* 18(1):68. doi: 10.1186/s43141-020-00078-y.

Khan, Sikandar Hayat. 2019. "Genome-Editing Technologies: Concept, Pros, and Cons of Various Genome-Editing Techniques and Bioethical Concerns for Clinical Application." *Molecular Therapy Nucleic Acids* 16(June):326–34. doi: 10.1016/j.omtn.2019.02.027.

Komor, Alexis C., Yongjoo B. Kim, Michael S. Packer, John A. Zuris, and David R. Liu. 2016. "Programmable Editing of a Target Base in Genomic DNA without Double-Stranded DNA Cleavage." *Nature* 533(7603):420–24. doi: 10.1038/nature17946.

Kostyushev, Dmitry, Anastasiya Kostyusheva, Sergey Brezgin, Valery Smirnov, Elena Volchkova, Alexander Lukashev, and Vladimir Chulanov. 2020. "Gene Editing by Extracellular Vesicles." *International Journal of Molecular Sciences* 21(19):1–34. doi: 10.3390/ijms21197362.

Kulpa, Deanna A., and Kathleen L. Collins. 2011. "The Emerging Role of HLA-C in HIV-1 Infection." *Immunology* 134(2):116–22. doi: 10.1111/j.1365-2567.2011.03474.x.

Lamers, Susanna L., Gary B. Fogel, Elyse J. Singer, Marco Salemi, David J. Nolan, Leanne C. Huysentruyt, and Michael S. McGrath. 2012. "HIV-1 Nef in Macrophage-Mediated Disease Pathogenesis." *International Reviews of*

Immunology 31(6):432–50. doi: 10.3109/08830185.2012.737073.

Larcher, Thibaut, Aude Lafoux, Laurent Tesson, Séverine Remy, Virginie Thepenier, Virginie François, Caroline Le Guiner, Helicia Goubin, Maéva Dutilleul, Lydie Guigand, Gilles Toumaniantz, Anne De Cian, Charlotte Boix, Jean-Baptiste Renaud, Yan Cherel, Carine Giovannangeli, Jean-Paul Concordet, Ignacio Anegon, and Corinne Huchet. 2014. "Characterization of Dystrophin Deficient Rats: A New Model for Duchenne Muscular Dystrophy." *PloS One* 9(10):e110371. doi: 10.1371/journal.pone.0110371.

Lazarow, Paul B. 2011. "Viruses Exploiting Peroxisomes." *Current Opinion in Microbiology* 14(4):458–69. doi: https://doi.org/10.1016/j.mib.2011.07.009.

Lee, Jaesuk, Jiyeon Kweon, and Yongsub Kim. 2025. "Emerging Trends in Prime Editing for Precision Genome Editing." *Experimental and Molecular Medicine* (July). doi: 10.1038/s12276-025-01463-8.

Lee, Seung Hwan, and Sangsu Bae. 2016. "Structural and Dynamic Views of the CRISPR-Cas System at the Single-Molecule Level." *BMB Reports* 49(4):201–7. doi: 10.5483/bmbrep.2016.49.4.042.

Li, Hongyi, Yang Yang, Weiqi Hong, Mengyuan Huang, Min Wu, and Xia Zhao. 2020. "Applications of Genome Editing Technology in the Targeted Therapy of Human Diseases: Mechanisms, Advances and Prospects." *Signal Transduction and Targeted Therapy* 5(1). doi: 10.1038/s41392-019-0089-y.

Liang, Kai, Ningning Li, Xiao Wang, Jianye Dai, Pulan Liu, Chu Wang, Xiao Wei Chen, Ning Gao, and Junyu Xiao. 2018. "Cryo-EM Structure of Human Mitochondrial Trifunctional Protein." *Proceedings of the National Academy of Sciences of the United States of America* 115(27):7039–44. doi: 10.1073/pnas.1801252115.

Liao, Hongyu, Jiahao Wu, Nathan J. VanDusen, Yifei Li, and Yanjiang Zheng. 2024. "CRISPR-Cas9-Mediated Homology-Directed Repair for Precise Gene Editing." *Molecular Therapy Nucleic Acids* 35(4):102344. doi: 10.1016/j.omtn.2024.102344.

Liu, Chang, Li Zhang, Hao Liu, and Kun Cheng. 2017. "Delivery Strategies for CRISPR-Cas9 Gene-Editing Systems." *J Control Release* 266(816):17–26. doi: 10.1016/j.jconrel.2017.09.012.Delivery.

Liu, Guanqing, Yong Zhang, and Tao Zhang. 2020. “Computational Approaches for Effective CRISPR Guide RNA Design and Evaluation.” *Computational and Structural Biotechnology Journal* 18:35–44. doi: 10.1016/j.csbj.2019.11.006.

Liu, L. X., F. Margottin, S. Le Gall, O. Schwartz, L. Selig, R. Benarous, and S. Benichou. 1997. “Binding of HIV-1 Nef to a Novel Thioesterase Enzyme Correlates with Nef-Mediated CD4 down-Regulation.” *The Journal of Biological Chemistry* 272(21):13779–85. doi: 10.1074/jbc.272.21.13779.

Liu, Qi, Jianhui Yang, Yumeng Xing, Yu Zhao, and Yang Liu. 2023. “Development of Delivery Strategies for CRISPR-Cas9 Genome Editing.” *BMEMat* 1(3). doi: 10.1002/bmm2.12025.

Lotfi, Malihe, Dorsa Morshedi Rad, Samaneh Sharif Mashhadi, Atefeh Ashouri, Majid Mojarrad, Sina Mozaffari-Jovin, Shima Farrokhi, Maryam Hashemi, Marzieh Lotfi, Majid Ebrahimi Warkiani, and Mohammad Reza Abbaszadegan. 2023. “Recent Advances in CRISPR/Cas9 Delivery Approaches for Therapeutic Gene Editing of Stem Cells.” *Stem Cell Reviews and Reports* 19(8):2576–96. doi: 10.1007/s12015-023-10585-3.

Lu, Yaoyao, Cedric Happi Mbakam, Bo Song, Eli Bendavid, and Jacques P. Tremblay. 2022. “Improvements of Nuclease and Nickase Gene Modification Techniques for the Treatment of Genetic Diseases.” *Frontiers in Genome Editing* 4(July):1–14. doi: 10.3389/fgeed.2022.892769.

Makarova, Kira S., Yuri I. Wolf, Jaime Iranzo, Sergey A. Shmakov, Omer S. Alkhnbashi, Stan J. J. Brouns, Emmanuelle Charpentier, David Cheng, Daniel H. Haft, Philippe Horvath, Sylvain Moineau, Francisco J. M. Mojica, David Scott, Shiraz A. Shah, Virginijus Siksnys, Michael P. Terns, Česlovas Venclovas, Malcolm F. White, Alexander F. Yakunin, Winston Yan, Feng Zhang, Roger A. Garrett, Rolf Backofen, John van der Oost, Rodolphe Barrangou, and Eugene V Koonin. 2020. “Evolutionary Classification of CRISPR–Cas Systems: A Burst of Class 2 and Derived Variants.” *Nature Reviews Microbiology* 18(2):67–83. doi: 10.1038/s41579-019-0299-x.

Mangeot, Philippe E., Valérie Risson, Floriane Fusil, Aline Marnef, Emilie Laurent, Juliana Blin, Virginie Mournetas, Emmanuelle Massouridès,

Thibault J. M. Sohier, Antoine Corbin, Fabien Aubé, Marie Teixeira, Christian Pinset, Laurent Schaeffer, Gaëlle Legube, François Loïc Cosset, Els Verhoeyen, Théophile Ohlmann, and Emiliano P. Ricci. 2019. "Genome Editing in Primary Cells and in Vivo Using Viral-Derived Nanoblades Loaded with Cas9-SgRNA Ribonucleoproteins." *Nature Communications* 10(1):1–15. doi: 10.1038/s41467-018-07845-z.

Manrique, Santiago, Daniel Sauter, Florian A. Horenkamp, Sebastian Lülf, Hangxing Yu, Dominik Hotter, Kanchan Anand, Frank Kirchhoff, and Matthias Geyer. 2017. "Endocytic Sorting Motif Interactions Involved in Nef-Mediated Downmodulation of CD4 and CD3." *Nature Communications* 8(1):442. doi: 10.1038/s41467-017-00481-z.

Mark, Pekka, and Lennart Nilsson. 2001. "Structure and Dynamics of the TIP3P , SPC , and SPC / E Water Models at 298 K." 9954–60. doi: 10.1021/jp003020w.

Miller, Jeffrey C., Michael C. Holmes, Jianbin Wang, Dmitry Y. Guschin, Ya-Li Lee, Igor Rupniewski, Christian M. Beausejour, Adam J. Waite, Nathaniel S. Wang, Kenneth A. Kim, Philip D. Gregory, Carl O. Pabo, and Edward J. Rebar. 2007. "An Improved Zinc-Finger Nuclease Architecture for Highly Specific Genome Editing." *Nature Biotechnology* 25(7):778–85. doi: 10.1038/nbt1319.

Mills, Clarence, Andrew Riching, Ashleigh Keller, Jesse Stombaugh, Amanda Haupt, Elena Maksimova, Sarah M. Dickerson, Emily Anderson, Kevin Hemphill, Chris Ebmeier, John A. Schiel, Josien Levenga, Matthew Perkett, Anja van Brabant Smith, and Zaklina Strezoska. 2022. "A Novel CRISPR Interference Effector Enabling Functional Gene Characterization with Synthetic Guide RNAs." *The CRISPR Journal* 5(6):769–86. doi: 10.1089/crispr.2022.0056.

Mohr, Stephanie E., Yanhui Hu, Benjamin Ewen-Campen, Benjamin E. Housden, Raghuvir Viswanatha, and Norbert Perrimon. 2016. "CRISPR Guide RNA Design for Research Applications." *The FEBS Journal* 283(17):3232–38. doi: 10.1111/febs.13777.

Mojica, F. J., G. Juez, and F. Rodríguez-Valera. 1993. "Transcription at Different

Salinities of Haloferax Mediterranei Sequences Adjacent to Partially Modified PstI Sites." *Molecular Microbiology* 9(3):613–21. doi: 10.1111/j.1365-2958.1993.tb01721.x.

Moscou, Matthew J., and Adam J. Bogdanove. 2009. "A Simple Cipher Governs DNA Recognition by TAL Effectors." *Science (New York, N.Y.)* 326(5959):1501. doi: 10.1126/science.1178817.

Motoche-Monar, Cristofer, Julián E. Ordoñez, Oscar Chang, and Fernando A. Gonzales-Zubiate. 2023. "GRNA Design: How Its Evolution Impacted on CRISPR/Cas9 Systems Refinement." *Biomolecules* 13(12):1–21. doi: 10.3390/biom13121698.

Mundlos, S. 1999. "Cleidocranial Dysplasia: Clinical and Molecular Genetics." *Journal of Medical Genetics* 36(3):177–82.

Nakagawa, Ryoya, Soumya Kannan, Han Altae-Tran, Satoru N. Takeda, Atsuhiro Tomita, Hisato Hirano, Tsukasa Kusakizako, Tomohiro Nishizawa, Keitaro Yamashita, Feng Zhang, Hiroshi Nishimasu, and Osamu Nureki. 2022. "Structure and Engineering of the Minimal Type VI CRISPR-Cas13bt3." *Molecular Cell* 82(17):3178-3192.e5. doi: 10.1016/j.molcel.2022.08.001.

Navarro, Carla, María P. Díaz, Pablo Duran, Ana Castro, Andrea Díaz, Clímaco Cano, Ana Karina Carbonell-Zabaleta, Donny Sabrith Solano-Jimenez, Diego Rivera-Porras, Julio César Contreras-Velásquez, and Valmore Bermúdez. 2025. "CRISPR-Cas Systems: A Functional Perspective and Innovations." *International Journal of Molecular Sciences* 26(8). doi: 10.3390/ijms26083645.

Neefjes, J. J., and H. L. Ploegh. 1988. "Allele and Locus-Specific Differences in Cell Surface Expression and the Association of HLA Class I Heavy Chain with Beta 2-Microglobulin: Differential Effects of Inhibition of Glycosylation on Class I Subunit Association." *European Journal of Immunology* 18(5):801–10. doi: 10.1002/eji.1830180522.

Neisig, A., C. J. Melief, and J. Neefjes. 1998. "Reduced Cell Surface Expression of HLA-C Molecules Correlates with Restricted Peptide Binding and Stable TAP Interaction." *Journal of Immunology (Baltimore, Md. : 1950)* 160(1):171–79.

Nelson, James W., Peyton B. Randolph, Simon P. Shen, Kelcee A. Everette, Peter J. Chen, Andrew V. Anzalone, Meirui An, Gregory A. Newby, Jonathan C. Chen, Alvin Hsu, and David R. Liu. 2022. "Engineered PegRNAs Improve Prime Editing Efficiency." *Nature Biotechnology* 40(3):402–10. doi: 10.1038/s41587-021-01039-7.

Nilsson, Jonas Birkelund, Jason Greenbaum, Bjoern Peters, and Morten Nielsen. 2025. "NetMHCpan-4.2: Improved Prediction of CD8+ Epitopes by Use of Transfer Learning and Structural Features." *Frontiers in Immunology* 16(August):1–14. doi: 10.3389/fimmu.2025.1616113.

Nishimasu, Hiroshi, Xi Shi, Soh Ishiguro, Linyi Gao, Seiichi Hirano, Sae Okazaki, Taichi Noda, Omar O. Abudayyeh, Jonathan S. Gootenberg, Hideto Mori, Seiya Oura, Benjamin Holmes, Mamoru Tanaka, Motoaki Seki, Hisato Hirano, Hiroyuki Aburatani, Ryuichiro Ishitani, Masahito Ikawa, Nozomu Yachie, Feng Zhang, and Osamu Nureki. 2018. "Engineered CRISPR-Cas9 Nuclease with Expanded Targeting Space." *Science (New York, N.Y.)* 361(6408):1259–62. doi: 10.1126/science.aas9129.

O'Huigin, Colm, Smita Kulkarni, Yunping Xu, Zhihui Deng, Judith Kidd, Kenneth Kidd, Xiaojiang Gao, and Mary Carrington. 2011. "The Molecular Origin and Consequences of Escape from MiRNA Regulation by HLA-C Alleles." *American Journal of Human Genetics* 89(3):424–31. doi: 10.1016/j.ajhg.2011.07.024.

Palmeira, Julys da Fonseca, Gustavo A. Argañaraz, Guilherme Xavier Lyra Malcher de Oliveira, and Enrique R. Argañaraz. 2019. "Physiological Relevance of ACOT8-Nef Interaction in HIV Infection." *Reviews in Medical Virology* 29(5):1–7. doi: 10.1002/rmv.2057.

Parolini, Francesca, Priscilla Biswas, Michela Serena, Francesca Sironi, Valentina Muraro, Elisabetta Guizzardi, Lucia Cazzoletti, Maria Teresa Scupoli, Davide Gibellini, Elisabetta Ugolotti, Roberto Biassoni, Alberto Beretta, Mauro Malnati, Maria Grazia Romanelli, and Donato Zipeto. 2018. "Stability and Expression Levels of HLA-C on the Cell Membrane Modulate HIV-1 Infectivity." *Journal of Virology* 92(1):1–17. doi: 10.1128/jvi.01711-17.

Perez, Elena E., Jianbin Wang, Jeffrey C. Miller, Yann Jouvenot, Kenneth A. Kim, Olga Liu, Nathaniel Wang, Gary Lee, Victor V Bartsevich, Ya-Li Lee, Dmitry Y. Guschin, Igor Rupniewski, Adam J. Waite, Carmine Carpenito, Richard G. Carroll, Jordan S. Orange, Fyodor D. Urnov, Edward J. Rebar, Dale Ando, Philip D. Gregory, James L. Riley, Michael C. Holmes, and Carl H. June. 2008. "Establishment of HIV-1 Resistance in CD4+ T Cells by Genome Editing Using Zinc-Finger Nucleases." *Nature Biotechnology* 26(7):808–16. doi: 10.1038/nbt1410.

Pons-Fuster, Eduardo, Enrique Bernal, Concepción F. Guillamón, Lourdes Gimeno, María V. Martínez-Sánchez, Inmaculada Ruiz-Lorente, José A. Campillo, Diana Ceballos, Ana Torres, Cristina Tomás, Ángeles Muñoz, Antonia Alcaraz, Pedro Selma, Carlos Ruiz-Nicolas, Manuel Muro, and Alfredo Minguela. 2024. "HLA-C*07 Is Associated with Symptomatic HIV-1-Associated Neurocognitive Disorders (HAND) and Immune Dysregulation." *Infectious Diseases* 56(10):818–29. doi: 10.1080/23744235.2024.2351047.

Puria, Rekha, Shakti Sahi, and Vikrant Nain. 2012. "HER2+ Breast Cancer Therapy: By CPP-ZFN Mediated Targeting of MTOR?" *Technology in Cancer Research & Treatment* 11(2):175–80. doi: 10.7785/tcrt.2012.500247.

Qasim, Waseem, Hong Zhan, Sujith Samarasinghe, Stuart Adams, Persis Amrolia, Sian Stafford, Katie Butler, Christine Rivat, Gary Wright, Kathy Somana, Sara Ghorashian, Danielle Pinner, Gul Ahsan, Kimberly Gilmour, Giovanna Lucchini, Sarah Inglott, William Mifsud, Robert Chiesa, Karl S. Peggs, Lucas Chan, Farzin Farzeneh, Adrian J. Thrasher, Ajay Vora, Martin Pule, and Paul Veys. 2017. "Molecular Remission of Infant B-ALL after Infusion of Universal TALEN Gene-Edited CAR T Cells." *Science Translational Medicine* 9(374). doi: 10.1126/scitranslmed.aaj2013.

Qi, Lei S., Matthew H. Larson, Luke A. Gilbert, Jennifer A. Doudna, Jonathan S. Weissman, Adam P. Arkin, and Wendell A. Lim. 2013. "Repurposing CRISPR as an RNA-Guided Platform for Sequence-Specific Control of Gene Expression." *Cell* 152(5):1173–83. doi: 10.1016/j.cell.2013.02.022.

Ran, F. Ann, Patrick D. Hsu, Jason Wright, Vineeta Agarwala, David A. Scott,

and Feng Zhang. 2013. “Genome Engineering Using the CRISPR-Cas9 System.” *Nature Protocols* 8(11):2281–2308. doi: 10.1038/nprot.2013.143.

Rasmussen, Michael, Emilio Fenoy, Mikkel Harndahl, Anne Bregnballe Kristensen, Ida Kallehauge Nielsen, Morten Nielsen, and Søren Buus. 2016. “Pan-Specific Prediction of Peptide-MHC Class I Complex Stability, a Correlate of T Cell Immunogenicity.” *Journal of Immunology (Baltimore, Md. : 1950)* 197(4):1517–24. doi: 10.4049/jimmunol.1600582.

Rath, Devashish, Lina Amlinger, Archana Rath, and Magnus Lundgren. 2015. “The CRISPR-Cas Immune System: Biology, Mechanisms and Applications.” *Biochimie* 117:119–28. doi: https://doi.org/10.1016/j.biochi.2015.03.025.

Rees, Holly A., and David R. Liu. 2018. “Base Editing: Precision Chemistry on the Genome and Transcriptome of Living Cells.” *Nature Reviews. Genetics* 19(12):770–88. doi: 10.1038/s41576-018-0059-1.

Reynisson, Birkir, Bruno Alvarez, Sinu Paul, Bjoern Peters, and Morten Nielsen. 2021. “NetMHCpan-4.1 and NetMHCIIpan-4.0: Improved Predictions of MHC Antigen Presentation by Concurrent Motif Deconvolution and Integration of MS MHC Eluted Ligand Data.” *Nucleic Acids Research* 48(W1):W449–54. doi: 10.1093/NAR/GKAA379.

Le Rhun, Anaïs, Andrés Escalera-Maurer, Majda Bratovič, and Emmanuelle Charpentier. 2019. “CRISPR-Cas in Streptococcus Pyogenes.” *RNA Biology* 16(4):380–89. doi: 10.1080/15476286.2019.1582974.

Richter, Michelle F., Kevin T. Zhao, Elliot Eton, Audrone Lapinaite, Gregory A. Newby, B. W. Thuronyi, Christopher Wilson, Luke W. Koblan, Jing Zeng, Daniel E. Bauer, Jennifer A. Doudna, and David R. Liu. 2020. “Phage-Assisted Evolution of an Adenine Base Editor with Improved Cas Domain Compatibility and Activity.” *Nature Biotechnology* 38(7):883–91. doi: 10.1038/s41587-020-0453-z.

Roe, Daniel R., and Thomas E. 3rd Cheatham. 2013. “PTRAJ and CPPTRAJ: Software for Processing and Analysis of Molecular Dynamics Trajectory Data.” *Journal of Chemical Theory and Computation* 9(7):3084–95. doi: 10.1021/ct400341p.

Rouillon, Christophe, Januka S. Athukoralage, Shirley Graham, Sabine Grüschow, and Malcolm F. White. 2018. “Control of Cyclic Oligoadenylate Synthesis in a Type III CRISPR System.” *ELife* 7. doi: 10.7554/eLife.36734.

Saeed, Kamran, Faisal Ayub, Muhammad Arshad Durrani, and Muhammad Mujahid. 2025. “CRISPR Cas Systems: From Bacterial Defense Mechanisms to Revolutionary Tools Reshaping Genetic Research and Translation Therapeutics.” *Microbe (Netherlands)* 7(November 2024). doi: 10.1016/j.microb.2025.100344.

Saito, Akiko, Akio Ooki, Takashi Nakamura, Shoko Onodera, Kamichika Hayashi, Daigo Hasegawa, Takahito Okudaira, Katsuhito Watanabe, Hiroshi Kato, Takeshi Onda, Akira Watanabe, Kenjiro Kosaki, Ken Nishimura, Manami Ohtaka, Mahito Nakanishi, Teruo Sakamoto, Akira Yamaguchi, Kenji Sueishi, and Toshifumi Azuma. 2018. “Targeted Reversion of Induced Pluripotent Stem Cells from Patients with Human Cleidocranial Dysplasia Improves Bone Regeneration in a Rat Calvarial Bone Defect Model.” *Stem Cell Research and Therapy* 9(1):1–10. doi: 10.1186/s13287-017-0754-4.

Sarantis, Panagiotis, Evangelos Koustas, Adriana Papadimitropoulou, Athanasios G. Papavassiliou, and Michalis V. Karamouzis. 2020. “Pancreatic Ductal Adenocarcinoma: Treatment Hurdles, Tumor Microenvironment and Immunotherapy.” *World Journal of Gastrointestinal Oncology* 12(2):173–81. doi: 10.4251/wjgo.v12.i2.173.

Sarkizova, Siranush, Susan Klaeger, Phuong M. Le, Letitia W. Li, Giacomo Oliveira, Hasmik Keshishian, Christina R. Hartigan, Wandi Zhang, David A. Braun, Keith L. Ligon, Pavan Bachireddy, Ioannis K. Zervantonakis, Jennifer M. Rosenbluth, Tamara Ouspenskaia, Travis Law, Sune Justesen, Jonathan Stevens, William J. Lane, Thomas Eisenhaure, Guang Lan Zhang, Karl R. Clauser, Nir Hacohen, Steven A. Carr, Catherine J. Wu, and Derin B. Keskin. 2020. “A Large Peptidome Dataset Improves HLA Class I Epitope Prediction across Most of the Human Population.” *Nature Biotechnology* 38(2):199–209. doi: 10.1038/s41587-019-0322-9.

Schaefer, Malinda R., Maya Williams, Deanna A. Kulpa, Pennelope K. Blakely, Anna Q. Yaffee, and Kathleen L. Collins. 2008. “A Novel Trafficking Signal

within the HLA-C Cytoplasmic Tail Allows Regulated Expression upon Differentiation of Macrophages." *Journal of Immunology (Baltimore, Md. : 1950)* 180(12):7804–17. doi: 10.4049/jimmunol.180.12.7804.

Selim, Heba Mohammed Refat M., Fatma Alzahraa M. Gomaa, Mohammad Y. Alshahrani, and Khaled M. Aboshanab. 2025. "Role of CRISPR-Cas System as a New Approach in Fighting the Antimicrobial Resistance of Bacterial and Viral Pathogens." *Infectious Diseases & Immunity* 5(2).

Serena, Michela, Alejandro Giorgetti, Mirko Busato, Francesca Gasparini, Erica Diani, Maria Grazia Romanelli, and Donato Zipeto. 2016. "Molecular Characterization of HIV-1 Nef and ACOT8 Interaction: Insights from in Silico Structural Predictions and in Vitro Functional Assays." *Scientific Reports* 6(February):1–13. doi: 10.1038/srep22319.

Severi, Ali Alizadeh, and Bahman Akbari. 2024. "CRISPR-Cas9 Delivery Strategies and Applications: Review and Update." *Genesis (United States)* 62(3). doi: 10.1002/dvg.23598.

Shen, Yue, Jerry M. Parks, and Jeremy C. Smith. 2023. "HLA Class I Supertype Classification Based on Structural Similarity." *The Journal of Immunology* 210(1):103–14. doi: 10.4049/jimmunol.2200685.

Sheriff, Adam, Ina Guri, Paulina Zebrowska, Virginia Llopis-Hernandez, Imogen R. Brooks, Stavroula Tekkela, Kavita Subramaniam, Ruta Gebrezgabher, Gaetano Naso, Anastasia Petrova, Katarzyna Balon, Alexandros Onoufriadis, Dorota Kujawa, Martyna Kotulska, Gregory Newby, Łukasz Łaczmański, David R. Liu, John A. McGrath, and Joanna Jacków. 2022. "ABE8e Adenine Base Editor Precisely and Efficiently Corrects a Recurrent COL7A1 Nonsense Mutation." *Scientific Reports* 12(1):1–16. doi: 10.1038/s41598-022-24184-8.

Sibilio, Leonardo, Aline Martayan, Andrea Setini, Elisa Lo Monaco, Elisa Tremante, Richard H. Butler, and Patrizio Giacomini. 2008. "A Single Bottleneck in HLA-C Assembly." *Journal of Biological Chemistry* 283(3):1267–74. doi: 10.1074/jbc.M708068200.

Silva, George, Laurent Poirot, Roman Galetto, Julianne Smith, Guillermo Montoya, Philippe Duchateau, and Frederic Paques. 2011. "Meganucleases

and Other Tools for Targeted Genome Engineering: Perspectives and Challenges for Gene Therapy." *Current Gene Therapy* 11(1):11–27. doi: 10.2174/156652311794520111.

Smirnikhina, Svetlana A., Milyausha I. Zaynitdinova, Vasilina A. Sergeeva, and Alexander V Lavrov. 2022. "Improving Homology-Directed Repair in Genome Editing Experiments by Influencing the Cell Cycle." *International Journal of Molecular Sciences* 23(11). doi: 10.3390/ijms23115992.

Stefani, Chiara, Antonella Sangalli, Elena Locatelli, Tania Federico, Giovanni Malerba, Maria Grazia Romanelli, Gustavo Adolfo Argañaraz, Bosco Christiano Maciel Da Silva, Alberto Jose Duarte Da Silva, Jorge Casseb, Enrique Roberto Argañaraz, Alessandra Ruggiero, and Donato Zipeto. 2022. "Increased Prevalence of Unstable HLA-C Variants in HIV-1 Rapid-Progressor Patients." *International Journal of Molecular Sciences* 23(23):1–9. doi: 10.3390/ijms232314852.

Stoddard, Barry L. 2011. "Homing Endonucleases: From Microbial Genetic Invaders to Reagents for Targeted DNA Modification." *Structure* 19(1):7–15. doi: https://doi.org/10.1016/j.str.2010.12.003.

Taha, Eman A., Joseph Lee, and Akitsu Hotta. 2022. "Delivery of CRISPR-Cas Tools for in Vivo Genome Editing Therapy: Trends and Challenges." *Journal of Controlled Release* 342(January):345–61. doi: 10.1016/j.jconrel.2022.01.013.

Taylor, Hannah N., Eric Laderman, Matt Armbrust, Thomson Hallmark, Dylan Keiser, Joseph Bondy-Denomy, and Ryan N. Jackson. 2021. "Positioning Diverse Type IV Structures and Functions Within Class 1 CRISPR-Cas Systems." *Frontiers in Microbiology* 12:671522. doi: 10.3389/fmicb.2021.671522.

Tekcham, Dinesh Singh, Di Chen, Yu Liu, Ting Ling, Yi Zhang, Huan Chen, Wen Wang, Wuxiyar Otkur, Huan Qi, Tian Xia, Xiaolong Liu, Hai Long Piao, and Hongxu Liu. 2020. "F-Box Proteins and Cancer: An Update from Functional and Regulatory Mechanism to Therapeutic Clinical Prospects." *Theranostics* 10(9):4150–67. doi: 10.7150/thno.42735.

Thaweesapphithak, Sermporn, Kittipat Termteerapornpimol, Siriwong

Wongsirisuwan, Soranun Chantarangsu, and Thantrira Porntaveetus. 2024. “The Impact of RUNX2 Gene Variants on Cleidocranial Dysplasia Phenotype: A Systematic Review.” *Journal of Translational Medicine* 22(1). doi: 10.1186/s12967-024-05904-2.

Thomas, K. R., and M. R. Capecchi. 1987. “Site-Directed Mutagenesis by Gene Targeting in Mouse Embryo-Derived Stem Cells.” *Cell* 51(3):503–12. doi: 10.1016/0092-8674(87)90646-5.

Tian, Chuan, Koushik Kasavajhala, Kellon A. A. Belfon, Lauren Raguette, He Huang, Angela N. Migues, John Bickel, Yuzhang Wang, Jorge Pincay, Qin Wu, and Carlos Simmerling. 2020. “Ff19SB: Amino-Acid-Specific Protein Backbone Parameters Trained against Quantum Mechanics Energy Surfaces in Solution.” *Journal of Chemical Theory and Computation* 16(1):528–52. doi: 10.1021/acs.jctc.9b00591.

Tsai, Shengdar Q., Nhu T. Nguyen, Jose Malagon-Lopez, Ved V Topkar, Martin J. Aryee, and J. Keith Joung. 2017. “CIRCLE-Seq: A Highly Sensitive in Vitro Screen for Genome-Wide CRISPR–Cas9 Nuclease off-Targets.” *Nature Methods* 14(6):607–14. doi: 10.1038/nmeth.4278.

Tsai, Shengdar Q., Zongli Zheng, Nhu T. Nguyen, Matthew Liebers, Ved V Topkar, Vishal Thapar, Nicolas Wyvekens, Cyd Khayter, A. John Iafrate, Long P. Le, Martin J. Aryee, and J. Keith Joung. 2015. “GUIDE-Seq Enables Genome-Wide Profiling of off-Target Cleavage by CRISPR-Cas Nucleases.” *Nature Biotechnology* 33(2):187–97. doi: 10.1038/nbt.3117.

Tu, Tianxiang, Zongming Song, Xiaoyu Liu, Shengxing Wang, Xiaoxue He, Haitao Xi, Jiahua Wang, Tong Yan, Haoran Chen, Zhenwu Zhang, Xiujuan Lv, Jineng Lv, Xiu Feng Huang, Junzhao Zhao, Chao Po Lin, Caixia Gao, Jinwei Zhang, and Feng Gu. 2022. “A Precise and Efficient Adenine Base Editor.” *Molecular Therapy* 30(9):2933–41. doi: 10.1016/j.ymthe.2022.07.010.

Udenwobele, Daniel Ikenna, Ruey-Chyi Su, Sara V Good, Terry Blake Ball, Shailly Varma Shrivastav, and Anuraag Shrivastav. 2017. “Myristoylation: An Important Protein Modification in the Immune Response.” *Frontiers in Immunology* 8:751. doi: 10.3389/fimmu.2017.00751.

Urnov, Fyodor D., Edward J. Rebar, Michael C. Holmes, H. Steve Zhang, and Philip D. Gregory. 2010. “Genome Editing with Engineered Zinc Finger Nucleases.” *Nature Reviews Genetics* 11(9):636–46. doi: 10.1038/nrg2842.

Vigón, Lorena, Miguel Galán, Montserrat Torres, Antonio J. Martín-Galiano, Sara Rodríguez-Mora, Elena Mateos, Magdalena Corona, Rosa Malo, Cristina Navarro, María Aránzazu Murciano-Antón, Valentín García-Gutiérrez, Vicente Planelles, Jorge Martínez-Laso, María Rosa López-Huertas, Mayte Coiras, Esther Alonso Herrador, Pablo Amich Alemany, Victoria Bosch Martos, Sandra Chamorro, Belén Comeche, Lorena Cordova Castaño, Susana Domínguez-Mateos, Aurora Expósito Mora, Valle Falcones, María Mercedes Gea Martinez, Alberto Gomez Bonilla, María Victoria Leon Gomez, Gema Lora Rey, Alejandro Luna de Abia, Patricia Mínguez, Maria Luisa Muñoz Balsa, Javier Pérez Gonzalez, Sandra Pérez-Santos, Jose Sanchez Hernández, Cruz Soriano, and Andrea Vinssac Rayado. 2022. “Association between HLA-C Alleles and COVID-19 Severity in a Pilot Study with a Spanish Mediterranean Caucasian Cohort.” *PLoS ONE* 17(8 August):1–20. doi: 10.1371/journal.pone.0272867.

Wang, Haifeng, Marie La Russa, and Lei S. Qi. 2016. “CRISPR/Cas9 in Genome Editing and Beyond.” *Annual Review of Biochemistry* 85:227–64. doi: 10.1146/annurev-biochem-060815-014607.

Wang, Meng, Lukasz Kurgan, and Min Li. 2023. “A Comprehensive Assessment and Comparison of Tools for HLA Class I Peptide-Binding Prediction.” *Briefings in Bioinformatics* 24(3). doi: 10.1093/bib/bbad150.

Wang, Xiaoqing, Honghao Song, Junyu Liang, Yang Jia, and Yongfei Zhang. 2022. “Abnormal Expression of HADH, an Enzyme of Fatty Acid Oxidation, Affects Tumor Development and Prognosis (Review).” *Molecular Medicine Reports* 26(6):1–8. doi: 10.3892/mmr.2022.12871.

Watanabe, H., T. Shiratori, H. Shoji, S. Miyatake, Y. Okazaki, K. Ikuta, T. Sato, and T. Saito. 1997. “A Novel Acyl-CoA Thioesterase Enhances Its Enzymatic Activity by Direct Binding with HIV Nef.” *Biochemical and Biophysical Research Communications* 238(1):234–39. doi: 10.1006/bbrc.1997.7217.

Wienert, Beeke, Stacia K. Wyman, Christopher D. Richardson, Charles D. Yeh, Pinar Akcakaya, Michelle J. Porritt, Michaela Morlock, Jonathan T. Vu, Katelynn R. Kazane, Hannah L. Watry, Luke M. Judge, Bruce R. Conklin, Marcello Maresca, and Jacob E. Corn. 2019. "Unbiased Detection of CRISPR Off-Targets in Vivo Using DISCOVER-Seq." *Science (New York, N.Y.)* 364(6437):286–89. doi: 10.1126/science.aav9023.

Wysokinski, Daniel, Janusz Blasiak, and Elzbieta Pawlowska. 2015. "Role of RUNX2 in Breast Carcinogenesis." *International Journal of Molecular Sciences* 16(9):20969–93. doi: 10.3390/ijms160920969.

Xu, Fang, Caiyan Zheng, Weihui Xu, Shiyao Zhang, Shanshan Liu, Xiaopeng Chen, and Kai Yao. 2024. "Breaking Genetic Shackles: The Advance of Base Editing in Genetic Disorder Treatment." *Frontiers in Pharmacology* 15(March):1–39. doi: 10.3389/fphar.2024.1364135.

Xu, Huaigeng, Bo Wang, Miyuki Ono, Akihiro Kagita, Kaho Fujii, Noriko Sasakawa, Tatsuki Ueda, Peter Gee, Misato Nishikawa, Masaki Nomura, Fumiyo Kitaoka, Tomoko Takahashi, Keisuke Okita, Yoshinori Yoshida, Shin Kaneko, and Akitsu Hotta. 2019. "Targeted Disruption of HLA Genes via CRISPR-Cas9 Generates IPSCs with Enhanced Immune Compatibility." *Cell Stem Cell* 24(4):566-578.e7. doi: 10.1016/j.stem.2019.02.005.

Yan, Jun, Paul Oyler-Castrillo, Purnima Ravisankar, Carl C. Ward, Sébastien Levesque, Yangwode Jing, Danny Simpson, Anqi Zhao, Hui Li, Weihao Yan, Laine Goudy, Ralf Schmidt, Sabrina C. Solley, Luke A. Gilbert, Michelle M. Chan, Daniel E. Bauer, Alexander Marson, Lance R. Parsons, and Britt Adamson. 2024. "Improving Prime Editing with an Endogenous Small RNA-Binding Protein." *Nature* 628(8008):639–47. doi: 10.1038/s41586-024-07259-6.

Yao, Jing, Jun Yang, Zhe Yang, Xin-Ping Wang, Tong Yang, Bing Ji, and Zheng-Yun Zhang. 2021. "FBXW11 Contributes to Stem-Cell-like Features and Liver Metastasis through Regulating HIC1-Mediated SIRT1 Transcription in Colorectal Cancer." *Cell Death & Disease* 12(10):930. doi: 10.1038/s41419-021-04185-7.

Yeo, Nan Cher, Alejandro Chavez, Alissa Lance-Byrne, Yingleong Chan, David

Menn, Denitsa Milanova, Chih-Chung Kuo, Xiaoge Guo, Sumana Sharma, Angela Tung, Ryan J. Cecchi, Marcelle Tuttle, Swechchha Pradhan, Elaine T. Lim, Noah Davidsohn, Mo R. Ebrahimkhani, James J. Collins, Nathan E. Lewis, Samira Kiani, and George M. Church. 2018. "An Enhanced CRISPR Repressor for Targeted Mammalian Gene Regulation." *Nature Methods* 15(8):611–16. doi: 10.1038/s41592-018-0048-5.

Yin, Jiang An, Lukas Frick, Manuel C. Scheidmann, Tingting Liu, Chiara Trevisan, Ashutosh Dhingra, Anna Spinelli, Yancheng Wu, Longping Yao, Dalila Laura Vena, Britta Knapp, Jingjing Guo, Elena De Cecco, Kathi Ging, Andrea Armani, Edward J. Oakeley, Florian Nigsch, Joel Jenzer, Jasmin Haegele, Michal Pikusa, Joachim Täger, Salvador Rodriguez-Nieto, Vangelis Bouris, Rafaela Ribeiro, Federico Baroni, Manmeet Sakshi Bedi, Scott Berry, Marco Losa, Simone Hornemann, Martin Kampmann, Lucas Pelkmans, Dominic Hoepfner, Peter Heutink, and Adriano Aguzzi. 2025. "Arrayed CRISPR Libraries for the Genome-Wide Activation, Deletion and Silencing of Human Protein-Coding Genes." *Nature Biomedical Engineering* 9(1):127–48. doi: 10.1038/s41551-024-01278-4.

Zhao, Zhihan, Peng Shang, Prarthana Mohanraju, and Niels Geijsen. 2023. "Prime Editing: Advances and Therapeutic Applications." *Trends in Biotechnology* 41(8):1000–1012. doi: 10.1016/j.tibtech.2023.03.004.

Zhu, Yanfei, Yin Zou, Qian Yu, Huijun Sun, Sixuan Mou, Shuhua Xu, and Min Zhu. 2018. "Combined Surgical-Orthodontic Treatment of Patients with Cleidocranial Dysplasia: Case Report and Review of the Literature." *Orphanet Journal of Rare Diseases* 13(1):217. doi: 10.1186/s13023-018-0959-3.

Zipeto, Donato, Michela Serena, Simona Mutascio, Francesca Parolini, Erica Diani, Elisabetta Guizzardi, Valentina Muraro, Emanuela Lattuada, Sebastiano Rizzardo, Marina Malena, Massimiliano Lanzafame, Giovanni Malerba, Maria Grazia Romanelli, Stefano Tamburin, and Davide Gibellini. 2018. "HIV-1-Associated Neurocognitive Disorders: Is HLA-C Binding Stability to β(2)-Microglobulin a Missing Piece of the Pathogenetic Puzzle?" *Frontiers in Neurology* 9:791. doi: 10.3389/fneur.2018.00791.

7. ACKNOWLEDGMENTS

First of all, I would like to express my deepest gratitude to my supervisor, Prof. Donato Zipeto, for welcoming me into his laboratory, for the continuous scientific discussions, and for the trust he gave me by involving me in stimulating projects.

I would also like to sincerely thank my co-supervisor Dr. Alessandra Ruggiero, who has always been available and supportive during these years, helping me overcome different challenges encountered during my PhD.

I would also like to really thank Prof. Marianne Carlon (KU Leuven, Belgium) for giving me the opportunity to join her laboratory during my PhD mobility period, and for her constant guidance and discussions on the projects. I am equally grateful to Dr. Lidia Laudonia Dipalo, who supervised and guided me through all the experimental work during my months abroad.

I would like to thank all the collaborators I worked with during my PhD: Prof. Maria Teresa Valenti (University of Verona) for allowing me to contribute to the development of edited osteosarcoma cells and prime editing projects; Prof. Daniela Cecconi (University of Verona) for the collaboration on edited pancreatic tumour cells; Prof. Monica Neagu and her PhD student Georgiana Dobre ("Victor Babes" National Institute of Pathology, Romania) for our joint work on melanoma cell lines; and Prof. Giovanni Grazioso (University of Milan) for participating in the project on HLA-C stability.

A sincere thank you also goes to my colleagues and friends Michele, Elisa and Carola, who have shared these years in the laboratory with me, always offering collaboration, support and friendship, and contributing in a concrete way to various experimental aspects of the projects.

Finally, a special thank you to my family, my girlfriend Silvia and all my friends who have been close to me during these years of study and research, supporting me with affection and constant encouragement.

8. ATTACHMENTS

Below is a series of attachments (papers, abstracts, posters, conference participation) that were produced during my PhD.

frontiers | Frontiers in Immunology

TYPE Original Research
PUBLISHED 11 December 2025
DOI 10.3389/fimmu.2025.1703026

OPEN ACCESS

EDITED BY
Simone Agostini,
Fondazione Don Carlo Gnocchi Onlus (IRCCS), Italy

REVIEWED BY
Nobubelo Ngandu,
South African Medical Research Council, South Africa
Pengcheng Wei,
Guangxi University, China

*CORRESPONDENCE
Donato Zipeto
donato.zipeto@univr.it

RECEIVED 10 September 2025
REVISED 25 November 2025
ACCEPTED 26 November 2025
PUBLISHED 11 December 2025

CITATION
Voi M, Sangalli A, Milano EG, De Martinis C, Orlandi E, Tamburin S, Mantovani E, Federico A, Lanzafame M, Lattuada E, Argañaraz GA, Da Silva BCM, Da Silva Duarte AJ, Casseb J, Argañaraz ER, Malena M, Albani M, Ruggiero A, Romanelli MG, Valenti MT, Grazioso G and Zipeto D (2025) Computational characterization of peptide binding stability to HLA-C allotypes and its association with HIV-1 infection progression and HIV-1 related neurocognitive impairment. *Front. Immunol.* 16:1703026. doi: 10.3389/fimmu.2025.1703026

Computational characterization of peptide binding stability to HLA-C allotypes and its association with HIV-1 infection progression and HIV-1 related neurocognitive impairment

Mauro Voi[1], Antonella Sangalli[1], Erica Ginevra Milano[2], Carola De Martinis[1], Elisa Orlandi[1], Stefano Tamburin[1], Elisa Mantovani[1], Angela Federico[1], Massimiliano Lanzafame[3,4], Emanuela Lattuada[3], Gustavo Adolfo Argañaraz[5], Bosco Christiano Maciel Da Silva[6], Alberto Jose Da Silva Duarte[6], Jorge Casseb[7], Enrique Roberto Argañaraz[5], Marina Malena[8], Marco Albani[2], Alessandra Ruggiero[1], Maria Grazia Romanelli[1], Maria Teresa Valenti[1], Giovanni Grazioso[2] and Donato Zipeto[1*]

[1]Department of Neurosciences, Biomedicine and Movement Sciences, University of Verona, Verona, Italy, [2]Department of Pharmaceutical Sciences, University of Milan, Milan, Italy, [3]Unit of Infectious Diseases, Santa Chiara Hospital, Azienda Provinciale per i Servizi Sanitari, Trento, Italy, [4]Centre for Medical Sciences (CISMED), University of Trento, Trento, Italy, [5]Laboratory of Molecular Neurovirology, Department of Pharmacy, Faculty of Health Science, University of Brasilia, Brasilia, Brazil, [6]Medical Investigation Laboratory Unit 56 (LIM/56), Faculdade de Medicina FMUSP, University of São Paulo, São Paulo, Brazil, [7]Faculty of Medicine, Institute of Tropical Medicine, University of São Paulo, São Paulo, Brazil, [8]U.O.S. Infectious Diseases, Santa Maria della Misericordia Hospital AULSS5, Rovigo, Italy

Background: HLA-C molecules play a critical role in the immune response, particularly in antigen presentation and immune modulation.
Methods: To investigate the effect of the most common HLA-C allotypes on the stability of the HLA-C-β-2 microglobulin-peptide complex, we used the NetMHCpan-4.2 bioinformatic tool that predicts peptide binding to MHC class I molecules. This allowed us to predict the probability of a broad set of peptides to be naturally processed, presented on each HLA-C allotype, and ultimately recognised by the immune system, measured by EL-score. By plotting the EL-score against the percentile of the peptide's stability rank position, curves were drawn to illustrate the relative stability of the binding interaction of each HLA-C allotype tested, and the area under the curve was calculated to determine a stability score for each HLA-C variant.
Results: This approach permits us to greatly improve the classification of HLA-C allotypes according to their stability, overcoming the previous coarse stable and unstable binary classification. Analysis of two well-characterised HIV-1 patient cohorts, one focused on disease progression and the other on neurocognitive

impairment, demonstrated a significant association between unstable HLA-C alleles, faster disease progression, and worse HIV-associated neurocognitive outcomes.
Conclusions: These findings underscore the role of HLA-C stability in AIDS progression, suggesting that profiling HLA-C stability may serve as a predictive tool for HIV-1 disease management and assessing neurocognitive risk, with potential implications in personalised medicine.

KEYWORDS

HLA-C, HIV-1, antigen presentation, immune response, neurocognitive disorders, HAND, peptide-binding stability, personalized medicine

Introduction

The human leukocyte antigen (HLA) system is a key component of the innate and adaptive immune responses, playing a critical role in antigen presentation (1, 2). HLA-C is a class I major histocompatibility complex (MHC-I) molecule involved in the immune surveillance against infections and malignancies. Unlike HLA-A and HLA-B, HLA-C exhibits lower surface expression and distinct peptide-binding properties due to less efficient assembly and cell membrane expression (3–5), making its functional stability a critical aspect of immune response regulation (6). Despite its historically perceived lower relevance, emerging evidence has demonstrated that HLA-C plays a significant role in modulating immune responses, particularly in HIV-1 infection, influencing viral replication, immune escape mechanisms, and disease progression (7).

HLA-C is central to antigen presentation to CD8+ T cells and immune surveillance. Its genetic variability influences disease susceptibility and transplant compatibility (1, 2). Furthermore, the stability of the HLA-C-β-2 microglobulin (β_2m)-peptide complex determines antigen presentation efficiency, with less stable variants linked to impaired immune responses, increased infection risk, and reduced immunotherapy efficacy (7–9).

HLA-C expression varies significantly among individuals (10) and is modulated by genetic factors, including promoter polymorphisms, microRNA interactions, and alternative splicing (9, 11–13). Single-nucleotide polymorphisms (SNPs) in the 3' untranslated region (3'UTR) of the HLA-C gene affect its expression levels, particularly through regulation by miR-148a (14). Furthermore, HLA-C upregulation has been linked to greater immune pressure on HIV-1, driving viral evolution and immune escape mutations (10).

The efficiency of antigen presentation is directly linked to the stability of the HLA-C/peptide complex, which varies across alleles and can impact immune recognition and viral control. Unlike HLA-A and HLA-B, HLA-C displays more selective peptide-binding preferences, which impact its effectiveness in presenting viral antigens. HLA-C allotypes display considerable variation in their peptide-binding clefts, which directly influences peptide binding stability (9). These differences affect the capacity of HLA-C molecules to stabilize peptide-MHC complexes and maintain antigen presentation on the cell surface. While allotypes like HLA-C*05 and HLA-C*08 are characterized by higher binding stability, others, such as HLA-C*07, are more prone to peptide dissociation and degradation (6). Sibilio and colleagues evaluated the post-assembly stability of HLA-C variants using pulse-labelling assays in homozygous cell lines expressing eight serologically defined HLA-C alleles. Their findings revealed that some HLA-C variants, such as HLA-C*05, C*06, C*08, exhibit stronger binding to β_2m, whereas others, including HLA-C*04 and C*07, display weaker β_2m association and reduced complex stability (15).

The extensive polymorphism of HLA alleles presents challenges for experimentally characterizing HLA/peptide stability across variants *in vitro*. To overcome this limitation, several computational tools have been developed to predict the interaction between HLA and peptides (16), among which NetMHCpan stands out for its high predictive accuracy (17). This model incorporates multiple parameters, including binding affinity, stability, length, processing and presentation pathways, to estimate peptide presentation and immunogenicity (17). NetMHCpan uses artificial neural networks trained on experimental binding affinity and mass spectrometry-eluted ligand (EL) data to significantly improve the accuracy of peptide-binding predictions across different HLA alleles. Evolving through versions 4.0, 4.1 and most recently 4.2, it incorporates enhanced machine learning techniques and new training datasets to improve performance in identifying immunogenic peptides (17–19). A key innovation in recent versions is the integration of structural features to enhance the predictive power of the algorithm (18), as well as the EL-score (19), which incorporates data on naturally processed and presented peptides obtained via mass spectrometry-based ligand elution assays (20). This overcomes the limitations of the traditional IC50-based calculation of binding affinity. Therefore, the EL-score represents a composite measure that integrates binding affinity (BA), the traditional indicator of peptide-MHC interaction strength, with eluted ligand data from naturally presented peptides, enhancing biological relevance. It also incorporates peptide stability and processing parameters, reflecting the likelihood that a bound

peptide remains stably displayed on the cell surface. The EL-score aims to predict the likelihood that a peptide will be naturally processed, presented on an MHC class I molecule, and ultimately trigger immunity. Studies have shown that the EL-score provides a better correlation with immunogenicity than BA alone. For instance, Harndahl et al. demonstrated that peptide-MHC stability is a stronger predictor of T cell activation than affinity, supporting the inclusion of EL data in prediction models (8). Similarly, Rasmussen et al. reported that combining affinity and stability scores improves the identification of CTL epitopes, reinforcing NetMHCpan's value in epitope discovery for vaccine development (21). Recent improvements using deep learning frameworks and large-scale mass spectrometry have further refined EL-score predictions, supporting it as a robust metric linking computational models to experimental outcomes.

HLA-C expression levels and the stability of its association with β_2m and peptide are key factors influencing antiviral immunity. Certain HLA-C alleles are linked to better control of HIV-1 replication (10). Variations in viral load associated with different HLA-C alleles are thought to result from differences in their capacity to present HIV-derived peptides to CD8+ T cells and NK cells—key players in targeting infected cells (22). Moreover, research has shown that HLA-C expression levels and peptide-binding stability are critical determinants of immune control (23).Unstable HLA-C variants have also been linked to increased HIV-1 infectivity. Previous findings from our group indicate that these variants may dissociate from β_2m, forming free heavy chains that interact with the HIV-1 envelope glycoprotein (Env), enhancing viral infectivity (24). In contrast, stable HLA-C variants remain bound to β_2m and retain strong antigen-presenting functions, which are associated with better immune control. Thus, binding stability to peptides confers to HLA-C the ability to act as a conventional molecule involved in cellular immunity, or as an accessory factor modulating HIV-1 infectivity (25).

HIV-associated neurocognitive disorders (HAND) encompass a spectrum of subjective and objective cognitive impairments, from mild to severe, that occur in approximately 50% of HIV-infected individuals and persist despite effective antiretroviral therapy, suggesting that host genetic factors influence their onset and progression (26). HLA-C polymorphism also plays a role in HAND (27, 28). Unstable HLA-C variants may contribute to higher levels of free β_2m in cerebrospinal fluid, leading to chronic neuroinflammation and neuronal damage (29). This mechanism is supported by associations between high β_2m levels and neurodegenerative conditions, including Alzheimer's disease (30). Additionally, HLA-C*07 has been specifically linked to a higher incidence of HAND in HIV-positive individuals, further supporting the hypothesis that HLA-C variation plays a role in neurocognitive impairment (31).

In this study, we sought to thoroughly investigate HLA-C stability to evaluate its relevance to HIV-1 clinical outcomes. To these aims, we integrated bioinformatic predictions with clinical progression and neurocognitive outcomes.

Materials and methods

Molecular dynamics analysis

Starting from the crystal structures of five human allelic variants of HLA-C currently available on Protein Data Bank (specifically: HLA-C*03:04 - PDB ID: 1EFX; HLA-C*04:01 – PDB ID: 1QQD; HLA-C*05:01 – PDB ID: 5VGD; HLA-C*06:02 – PDB ID: 5W6A; HLA-C*07:02 – PDB ID: 5VGE), single point mutations were introduced on the co-crystallized nonapeptides using Maestro's Workspace tool 'Mutate Residue' (release 2021–2, Schrödinger, LLC, New York, NY, USA). Subsequently, ff19SB force field (32) were applied on the systems using the "Protein Preparation Wizard" available in Maestro (release 2021–2, Schrödinger, LLC, New York, NY, USA), then the complexes were immersed in TIP3P (33) water cubic boxes and their geometry was energy minimized, allowing the remainder of the system (HLA-C and β_2m) to adapt to the newly introduced oligopeptide sequences. Then, Molecular Dynamics (MD) simulations were accomplished on these systems, using the Amber24. The parameters for these MD simulations were configured as follows: 300 ns, 300 K, and 1 atm. For each system, we carried out three independent replicas. The attained trajectories were clustered, by means of Amber24's cpptraj tool (34), to identify the different families of complex conformations and to identify the most populated ones. On these, the Molecular Mechanics-Generalized Born Surface Area (MM-GBSA) approach was applied to decompose the pairwise binding energetic contributions within the HLA/β_2m interactions.

Peptide and HLA-C stability binding analysis

Peptides binding to the 21 most frequent HLA-C allotypes in the human population (C*01:02, C*02:02, C*03:02, C*03:03, C*03:04, C*04:01, C*04:03, C*05:01, C*06:02, C*07:01, C*07:02, C*07:04, C*08:01, C*08:02, C*12:02, C*12:03, C*14:02, C*14:03, C*15:02, C*16:01, C*17:01) were experimentally validated by Sarkizova et al. (35). The final number of selected peptides was 36070, with a median of 1403 (range 730-3311) (Table 1). Their database cumulatively covers 95.8% of individuals worldwide based on allele frequencies. For our analysis, we focused on peptides of 8–12 amino acids, as they comprised most of the initial list and were the ones preferentially bound by MHC-I complexes (36). Allele frequencies were reported according to Sarkizova et al. (35). The Eluted Ligand (EL) score for each peptide binding to its specific HLA-C allotype was determined using NetMHCpan-4.2 (https://services.healthtech.dtu.dk/services/NetMHCpan-4.2/) with default parameters. Peptides were then ranked by NetMHCpan-4.2 EL-score for each HLA-C allele. The ranking was expressed in percentiles (% Ranking) to account for different peptide pool sizes. The resulting EL-score versus % Ranking curves were used to calculate the area under the curve (AUC) to determine a stability score for each HLA-C allotype considered (Figure 1).

TABLE 1 The most frequent human HLA-C allotypes and their calculated stability score.

Allotype	Peptides number	Frequency	Stability score (AUC)	Weighted average
C*01:02	1357	0.085	63.87	–
C*02:02	930	0.028	56.76	–
C*03:02	1194	0.025	65.09	*65.52*
C*03:03	2123	0.056	63.17	
C*03:04	2356	0.091	67.08	
C*04:01	1854	0.112	67.28	*68.06*
C*04:03	1038	0.019	72.67	
C*05:01	1442	0.026	84.84	-
C*06:02	1324	0.062	56.13	-
C*07:01	808	0.069	29.74	*40.96*
C*07:02	1072	0.131	50.45	
C*07:04	730	0.015	9.70	
C*08:01	1802	0.045	35.23	-
C*08:02	3148	0.020	78.34	-
C*12:02	1403	0.032	52.20	-
C*12:03	2175	0.020	50.34	-
C*14:02	1371	0.025	77.80	*76.05*
C*14:03	2784	0.015	73.12	
C*15:02	3311	0.034	57.39	–
C*16:01	2883	0.024	51.12	–
C*17:01	965	0.019	55.18	–

For the 21 most frequent HLA-C allotypes (first column), the number of specific binding peptides (8-12mer) identified by Sarkizova et al. (35) is reported (second column) alongside their frequency in the human population (third column). The area under the curve (AUC) calculation (fourth column) provides a stability score for each allotype. When second-digit typing was not possible, an average stability score weighted by frequencies was calculated (fifth column).

Patient cohorts

Two groups of HIV-1 infected individuals were enrolled in this study and categorized based on disease progression and neurocognitive status.

The first cohort included 47 patients classified as progressors (P; >10,000 copies HIV genome/mm^3, and ≤200 CD4+ T lymphocytes/mm^3) and 37 patients classified as long-term non-progressors (LTNPs; <10,000 copies HIV genome/mm^3, and ≥400 CD4+ T lymphocytes/mm^3). HIV viral-load measurements were obtained periodically throughout each patient's follow-up period (defined as the interval between initial infection detection and the end of monitoring). LTNPs were followed for a minimum of seven years. Progressors were observed until their CD4$^+$ T-cell count declined to ≤200 cells/mm^3, at which point antiretroviral treatment was initiated and sample collection was discontinued. All subjects gave informed consent, and the research protocols were approved by the relevant institutional review boards and research ethics committees (Ethics Committee of the Health Department of the Federal District (#066/07); and the Ethics Committee for Analysis of the public network of the Federal District, Brazil; and the Ethics Committee for Analysis of Research Projects (CAPPesq) of Hospital das Clínicas HCFMUSP (#CAPPesq #0306/10, Online registration #5867), from the Faculty of Medicine at the University of São Paulo, Brazil. The cohort is unique since the study participants had not received any treatment at the time of sampling. Further details on the patient cohort are reported in our previous study (37).

The second cohort included 57 patients referred by the Infectious Diseases Outpatient Clinics of the Verona University Hospital a) aged < 67 years, b) on dual/triple antiretroviral therapy regimens, and with c) stable suppressed plasma viremia. Participants with a history of recurrent drug abuse, current drug addiction, or other neurological diseases (e.g., history of cerebrovascular events) that could cause cognitive decline were excluded. Each patient underwent a comprehensive neuropsychological test battery designed to measure the cognitive domains recommended by the three main diagnostic guidelines (i.e., attention, executive function, learning and memory, language, speed of processing, complex motor skills) (26). The impact of cognitive difficulties on the ability to perform everyday activities was also assessed. As neuropsychiatric symptoms frequently occur alongside HIV infection, anxiety and depression were evaluated.

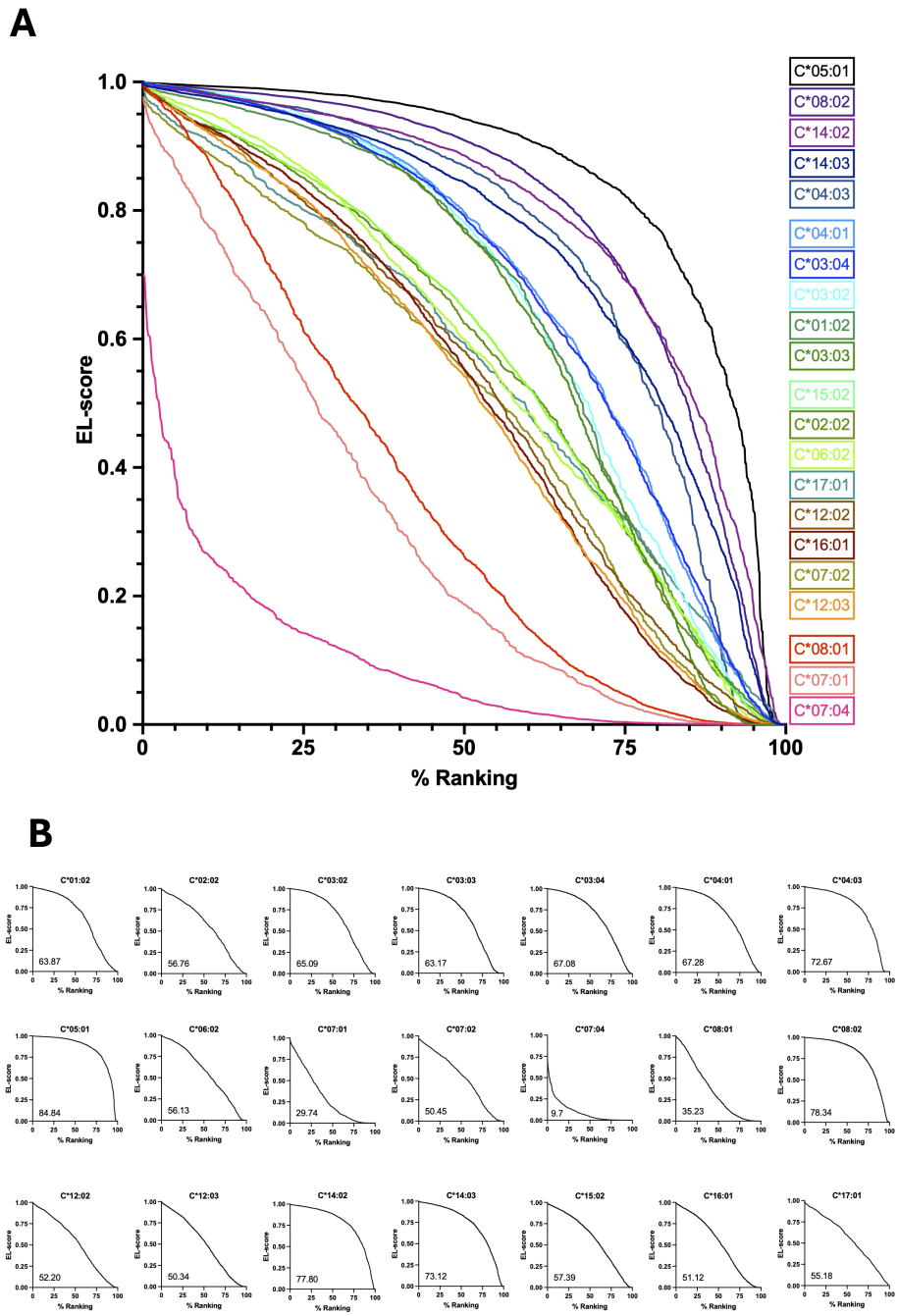

FIGURE 1
EL-score vs percentile ranking curves for each HLA-C/peptide pool. Individual EL-score values of each specific HLA-C allotype and its corresponding peptides, as predicted by NetMHCpan-4.2, were ranked and plotted against the percentile of the peptides' ranking position, resulting in distinct stability distribution profiles for each HLA-C allele. HLA-C *05:01, C*08:02, C*14:02, C*14:03 and C*04:03 clearly show a strong binding trend with most peptides, whereas HLA-C*07:04, C*07:01 and C*08:01 exhibit the lowest EL-score values for most peptides. The curves are shown overlapped in **(A)**, where each curve is color-coded according to the corresponding HLA-C allotype, and separately in **(B)**, where the area under the curve for each HLA-C allotype is reported in the lower left corner of each plot.

The Frascati criteria (38) were used as the gold standard for diagnosing HIV-associated neurocognitive disorders (HAND) and for dividing patients into HAND-positive (n=16) and HAND-negative (n=41) groups. Patients reporting subjective cognitive complaints were added to the first group, in line with the most recent recommendations provided by the International HIV-Cognition Working Group, which highlight the importance of changes in cognition that have been noticed by the individual or an observer, even in the absence of impact on daily functioning (39). All patients signed an informed consent for the study that was

conducted according to the Declaration of Helsinki and approved by the Institutional Ethics Committee of Verona and Rovigo (Italy) (#2459 CESC).

HLA-C genotyping and sequencing

DNA samples from all patients were extracted from peripheral blood lymphocytes and subjected to allele-specific polymerase chain reaction (AS-PCR) and Sanger sequencing to determine HLA-C allotypes as described in our previous study (37). HLA-C allotypes C*01, C*02, C*05, C*06, C*12, C*14, C*15, C*16 and C*17 were typed at one digit resolution, since less common allotypes were mostly clustering in the same subgroup according to Shen et al. (40). Allele-specific PCR was used to type C*12:03 and C*16:01. Sequencing analysis of the HLA-C region between exons 2 and 3 was utilized to further characterize HLA-C*03:02, C*03:03, C*03:04, C*04:01, C*04:03, C*07:01, C*07:02, C*07:04, C*08:01 and C*08:02 variants at second digit resolution, by performing sequence alignments at the Immuno Polymorphism Database (IPD https://www.ebi.ac.uk/ipd/index.html).

Determination of patient-specific HLA-C stability score

A stability score was determined for each patient based on their HLA-C genotype by multiplying the allotype stability scores (determined by the AUC of the corresponding allotypes). For HLA-C alleles typed at the first-digit resolution, the stability score of the most frequent allotype was used.

For HLA-C*14, the two most common allotypes (C*14:02 and C*14:03) have similar frequencies (35) and are clustered within the same subgroup, according to Shen et al. (40). In this case, the allotype stability score was determined by calculating the frequency-weighted mean. Similarly, when a patient's DNA was insufficient for second-digit genotyping, the frequency-weighted mean was calculated.

Finally, since allele-specific PCR for HLA-C*12 only identifies the common subtype C*12:03 at the second-digit, the stability score of the other most frequent C*12 allotype (C*12:02) was assigned when C*12 typing did not match C*12:03.

Statistical analysis

Statistical analyses were performed using GraphPad Prism (version 10). Comparisons between independent patient groups (LTNP vs P; HAND- vs HAND+) were performed using the two-tailed Mann–Whitney U test. A p-value < 0.05 was considered statistically significant.

Results

HLA-C allotypes exhibit different binding stability with their specific peptides

The analysis of the EL-score distribution revealed significant variations in HLA-C binding stability. Indeed, allele C*05:01 showed a strong binding for most peptides, while peptides specifically binding allele C*07:04 presented much lower binding prediction values. The determination of a stability score by calculating the AUC allowed a clear identification of different stability values describing the binding of each allele to its own peptide pool. Accordingly, some alleles, such as HLA-C*07:04, C*07:01 and C*08:01, displayed weak binding interactions, while others, such as HLA-C*05:01, C*08:02 and C*14, exhibited strong binding stability (Figure 1). Notably, we identified discrepancies within allele subtypes that challenged previous classifications of stability. For example, HLA-C*07, previously considered an unstable allele (37), showed subtype-dependent variability, with C*07:02 demonstrating a greater stability score than C*07:01 and C*07:04. Similarly, HLA-C*08, considered a stable allele, presented a similar subtype variability, with C*08:02 among the variants with the highest stability, but C*08:01 among those with the lowest. The considered HLA-C allotypes and the calculated stability scores are reported in Table 1.

The HLA-C complex stability is determined by the interactions with the peptide

Computational studies were performed to acquire atomistic details on the interaction between HLA-C/peptide and β_2m. Analyses were performed after selecting a group of HLA-C variants for which the crystal structures were available in the Protein Data Bank (www.rcsb.org). We randomly selected two 9-mer peptides specific for each allotype tested. After accomplishing MD simulations of the selected peptides in complex with the HLA-C/β_2m heterodimer, the analysis of the MD trajectories and the data retrieved from the pairwise energy decomposition revealed that there was a clear recurring pattern in β_2m's "hot spot" residues involved in the interaction with HLA-C. In fact, the trend of the residues mainly contributing and their energetic contributions' values were superimposable within the different allelic variants, but also amongst the different peptides (Table 2). On average (Figure 2 and Table 2), our analysis revealed that a) β_2m-Trp80 and -Trp61 give the main energetic contribution in each considered complex, since their energetic contribution's values are always among -9 and -12 kcal/mol; b) β_2m-Phe76 always stands in second position, with values around -5/-6 kcal/mol; c) The β_2m-Tyr30 residue is another key contributor to the interaction, providing a consistent energetic contribution of around -4 to -5 kcal/mol across all complexes.

10.3389/fimmu.2025.1703026

TABLE 2 Energetic contributions of β_2m residues to HLA-C complex stability.

Allotype	Peptide	EL-score	% Ranking	β2m residue	ΔG [kcal/mol]
C*03:04	QATMPHLSM	0.610	64.941	Trp80	-10.1
				Phe76	-5.8
	TITDIISAL	0.712	57.598	Trp80	-10.5
				Phe76	-5.7
C*04:01	YHDKNIVLL	0.813	48.220	Trp80	-10.7
				Phe76	-4.7
	TFESLVAKL	0.533	70.712	Trp61	-9.4
				Phe76	-5.2
C*05:01	NLDQPPAFF	0.924	56.380	Trp80	-9.3
				Phe76	-5.6
	NAEAKITKL	0.621	88.141	Trp 61	-10.3
				Phe76	-5.5
C*06:02	FKMTIPLLV	0.490	59.063	Trp80	-11.7
				Phe76	-6.1
	VYYLKNREV	0.563	53.852	Trp80	-9.8
				Phe76	-6.5
C*07:02	LRHPVCVEL	0.439	61.007	Trp80	-10.4
				Phe76	-5.8
	FYRVTTEQY	0.499	55.877	Trp80	-10.7
				Phe76	-5.6

Binding free energy values (ΔG) of β_2m residues that are functionally important for interaction were analyzed for five different HLA-C allotypes for which crystallographic structures are available in the Protein data bank (www.rcsb.org). The analysis was performed on the trimeric complex consisting of the HLA-C heavy chain, β_2m, and peptide. Two randomly chosen peptides specific to each allotype were analyzed. The β_2m residues primarily involved in interacting with HLA-C were Trp80 and Phe76. These residues formed comparable contacts and exhibited similar ΔG values across different HLA-C allotypes.

These data clearly indicate that β_2m maintains an invariant binding pattern with HLA-C heavy chain molecules, with consistent binding affinity and interacting residues, regardless of the bound peptide or HLA-C subtype.

Lower HLA-C stability scores are associated with HIV-1 progression and HIV-1-related neurocognitive impairment

Peptide specificity is determined by interactions of peptide side chains with six binding pockets in the HLA-C peptide-binding site (41). Kangueane et al. (42) assigned common HLA-C alleles to 18 different sub-supertypes, with variants within the same sub-supertype generally binding a highly shared set of peptides. It is thus possible to predict peptide binding of other members of a supertype using experimental results based on just one member of the type (42). A more recent classification by Shen et al. (40) proposed three main subtypes for HLA-C (C7 includes various C*07 alleles; C1 includes C*05, C*17 and most of C*01 and C*15; C2 includes C*02, C*06, C*14, C*16). Because structural clustering of the peptide-binding region correlates with binding specificity (40), according to the supertype classification by Shen et al., we adopted typing at the second-digit level for structurally divergent alleles belonging to different subtypes (for instance C*03:02 to C2, while C*03:03 and C*03:04 to C1) or to different subgroups within C1 (C*04:03 and C*04:01, or C*08:01 and C*08:02), C7 (C*07:01, C*07:02 and C*07:04) and C2 (C*12:02 and C*12:03) subtypes, in order to obtain a more precise identification of the specific allotype. Based on these considerations, HLA-C typing made it possible to calculate a stability score related to each patient's genotype and to correlate this value to different outcomes of HIV-1 infection. The stability scores calculated based on the HLA-C genotype of each HIV-1 patient considered are shown in Table 3 and Table 4.

We found that Progressors (P) exhibited significantly lower stability scores compared to Long Term Non Progressors (LTNP) ($p = 0.0143$), supporting the hypothesis that unstable HLA-C alleles are associated with more severe disease outcomes (Figure 3A).

The examination of neurocognitive outcomes showed that HAND-positive patients had a higher prevalence of unstable alleles, with a statistically significant difference in stability scores compared to HAND-negative patients ($p = 0.0221$) (Figure 3B).

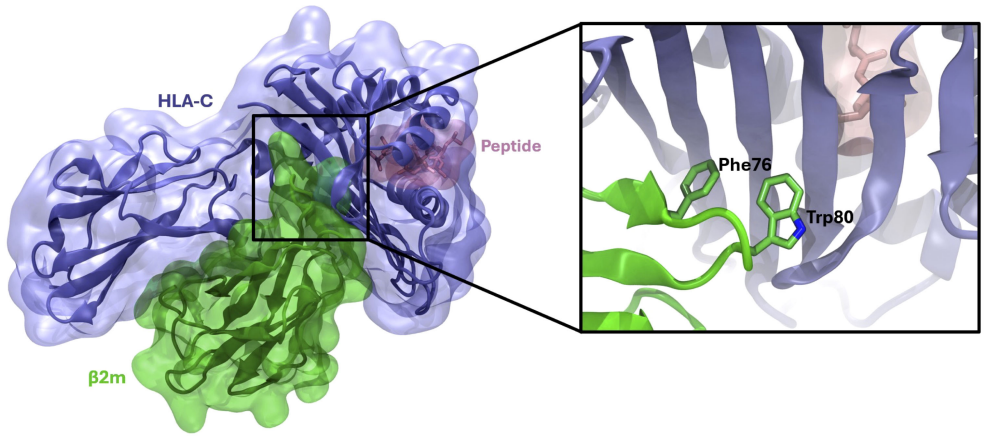

FIGURE 2
HLA-C/β_2m/peptide complex. A 3D representation of the HLA-C/β_2m/peptide complex, as obtained at the end of MD simulations, is shown on the left. On the right, a detailed visualization of the HLA-C/β_2m interface, highlighting residues critical for mediating protein-protein interactions, is shown.

Discussion

We explored HLA-C stability by means of advanced computational techniques and found that HLA-C stability influenced HIV-1 progression and cognitive outcomes. The identification of allele subtypes with different stability levels challenges traditional classifications of HLA-C as simply "stable" or "unstable," highlighting the advantages of a more precise and individualized approach in assessing HLA-C function. Moreover, our findings provide compelling evidence that HLA-C stability may contribute to shaping both immune responses and neurological outcomes in HIV-1 infected individuals.

HLA-C function is related to its stability

HLA-C stability is significantly influenced by genetic variations, which can either enhance or reduce its functionality within the immune response system (43, 44). HLA-C molecules exhibit differential stability based on genetic variations in their promoter regions, affecting their expression levels and antigen presentation efficiency. Some alleles, e.g., HLA-C*05, exhibit high stability and remain on the cell surface for prolonged surface expression, whereas others, e.g., HLA-C*07, display lower stability, impairing peptide loading and presentation (9). These observations are consistent with previous findings showing that inefficient peptide binding contributes to lower surface expression of HLA-C compared to HLA-A and HLA-B (6), likely due to its greater selectivity for peptide binding (3).

Several experimental and computational methodologies have been employed to assess HLA-C peptide binding stability. Mass spectrometry-based ligand elution assays have been used to profile naturally processed peptides, revealing a preference for 9-mer peptides in HLA-C binding (35, 36). Computational tools such as NetMHCpan and MHCflurry have demonstrated increased predictive accuracy in assessing binding affinities and stability of peptide-HLA interactions (19). Notably, peptide-MHC stability, rather than binding affinity alone, has been identified as a better predictor of T-cell immunogenicity (8). Additionally, computational tools like NetMHCpan and mass spectrometry-based ligand profiling have significantly improved the prediction and validation of HLA-C peptide-binding stability (19). These methodologies may provide insights into how stability affects immune function, disease progression, and therapeutic outcomes.

Recent studies have shown that HLA-C expression varies widely in an allele-specific manner, with higher expression levels exerting greater selection pressure on HIV-1, leading to virus-mediated downregulation of HLA-C (9). Certain single-nucleotide polymorphisms (SNPs) in the promoter and 3' untranslated region (UTR) of HLA-C, such as rs9264942 (located in the 5' UTR of the HLA-C gene), have been correlated with HIV viral load and disease progression (45). Additionally, the 3'UTR of HLA-C is a target for microRNA regulation (miR-148a), which influences HLA-C surface expression (14). This regulatory mechanism plays a crucial role in determining antigen presentation efficiency and immune escape strategies employed by HIV-1.

Our computational analysis supports evidence that HLA-C allotypes differ in their ability to bind and stabilize peptides, influencing their expression levels on the cell surface. Structural studies have demonstrated that HLA-C*07 has a deeper and narrower antigen-binding cleft, while HLA-C*05 has a relatively flat peptide-binding groove, allowing it to bind a broader range of peptides and remain more stably expressed on the cell membrane (9). These findings align with our stability analysis, which demonstrated that HLA-C*07:04 is the most unstable allele, while HLA-C*05:01 exhibits the highest stability. Importantly, the inefficient association of certain HLA-C variants with β_2m leads to the accumulation of misfolded HLA-C heavy chains, further affecting antigen presentation efficiency (6, 15).

10.3389/fimmu.2025.1703026

TABLE 3 HLA-C stability scores in HIV-1 patients according to AIDS progression.

Sample code	HIV-1 progression	Sex	Age	HLA-C genotype and stability scores				Stability score
				1st allele	Score (1st)	2nd allele	Score (2nd)	
PR1	LTNP	M	42	*03	*65.52*	*08:02	78.34	5132.84
PR2	LTNP	M	29	*03	*65.52*	*03	*65.52*	4292.87
PR3	LTNP	F	36	*06	56.13	*07:02	50.45	2831.76
PR4	LTNP	M	54	*02	56.76	*12:03	50.34	2857.30
PR5	LTNP	F	47	*07:02	50.45	*12	52.20	2633.49
PR6	LTNP	M	23	*05	84.84	*05	84.84	7197.83
PR7	LTNP	M	55	*05	84.84	*06	56.13	4762.07
PR8	LTNP	M	35	*02	56.76	*06	56.13	3185.94
PR9	LTNP	M	58	*05	84.84	*08:02	78.34	6646.37
PR10	LTNP	M	46	*07:02	50.45	*14	*76.05*	3836.72
PR11	LTNP	M	32	*07:02	50.45	*12:03	50.34	2539.65
PR12	LTNP	M	26	*05	84.84	*12:03	50.34	4270.85
PR13	LTNP	M	33	*02	56.76	*15	57.39	3257.46
PR14	LTNP	M	52	*07:01	29.74	*08:02	78.34	2329.83
PR15	LTNP	M	42	*04:01	67.28	*07:01	29.74	2000.91
PR16	LTNP	M	34	*04:01	67.28	*07:02	50.45	3394.28
PR17	LTNP	M	44	*04:01	67.28	*08:02	78.34	5270.72
PR18	LTNP	M	55	*01	63.87	*12	52.20	3334.01
PR19	LTNP	M	32	*14	*76.05*	*08:02	78.34	5957.76
PR20	LTNP	M	49	*04:01	67.28	*08:02	78.34	5270.72
PR21	LTNP	F	42	*04:01	67.28	*16:01	51.12	3439.35
PR22	LTNP	F	54	*07:01	29.74	*12	52.20	1552.43
PR23	LTNP	M	51	*04:01	67.28	*08:02	78.34	5270.72
PR24	LTNP	F	58	*01	63.87	*07:02	50.45	3222.24
PR25	LTNP	F	77	*01	63.87	*04:01	67.28	4297.17
PR26	LTNP	M	39	*04:01	67.28	*06	56.13	3776.43
PR27	LTNP	M	40	*04:01	67.28	*12	52.20	3512.02
PR28	LTNP	F	43	*05	84.84	*02	56.76	4815.52
PR29	LTNP	F	47	*04:01	67.28	*06	56.13	3776.43
PR30	LTNP	M	28	*07:01	29.74	*05	84.84	2523.14
PR31	LTNP	F	49	*03	*65.52*	*02	56.76	3718.92
PR32	LTNP	M	53	*07	*40.96*	*16:01	51.12	2093.88
PR33	LTNP	M	30	*03:02	65.09	*06	56.13	3653.50
PR34	LTNP	M	49	*05	84.84	*06	56.13	4762.07
PR35	LTNP	F	43	*01	63.87	*06	56.13	3585.02
PR36	LTNP	M	27	*05	84.84	*12:03	50.34	4270.85
PR37	LTNP	M	57	*06	56.13	*12:03	50.34	2825.58

(Continued)

10.3389/fimmu.2025.1703026

TABLE 3 Continued

Sample code	HIV-1 progression	Sex	Age	HLA-C genotype and stability scores				Stability score
				1st allele	Score (1st)	2nd allele	Score (2nd)	
PR38	P	M	45	*04:01	67.28	*07:02	50.45	3394.28
PR39	P	M	57	*03	*65.52*	*07:01	29.74	1948.56
PR40	P	M	28	*06	56.13	*07:01	29.74	1669.31
PR41	P	M	41	*07:02	50.45	*12	52.20	2633.49
PR42	P	M	40	*02	56.76	*04:01	67.28	3818.81
PR43	P	M	42	*04:01	67.28	*07:01	29.74	2000.91
PR44	P	M	25	*04:01	67.28	*08:02	78.34	5270.72
PR45	P	M	23	*05	84.84	*07:01	29.74	2523.14
PR46	P	M	30	*03:02	65.09	*04	*68.06*	4430.03
PR47	P	M	30	*05	84.84	*07:01	29.74	2523.14
PR48	P	M	28	*07:02	50.45	*12:03	50.34	2539.65
PR49	P	M	31	*03	*65.52*	*07:01	29.74	1948.56
PR50	P	M	39	*02	56.76	*04:01	67.28	3818.81
PR51	P	M	37	*04:01	67.28	*07:02	50.45	3394.28
PR52	P	M	26	*03	*65.52*	*02	56.76	3718.92
PR53	P	M	36	*04:01	67.28	*04:01	67.28	4526.60
PR54	P	M	51	*07:04	9.7	*15	57.39	556.68
PR55	P	F	47	*04	*68.06*	*16	51.12	3479.23
PR56	P	M	28	*04:01	67.28	*06	56.13	3776.43
PR57	P	M	65	*07:04	9.7	*15	57.39	556.68
PR58	P	M	61	*07	*40.96*	*07	*40.96*	1677.72
PR59	P	F	30	*07:01	29.74	*04:01	67.28	2000.91
PR60	P	M	57	*04:01	67.28	*12:03	50.34	3386.88
PR61	P	M	41	*03:02	65.09	*07:02	50.45	3283.79
PR62	P	M	54	*07:02	50.45	*07:02	50.45	2545.20
PR63	P	M	24	*04	*68.06*	*05	84.84	5774.21
PR64	P	M	31	*03:02	65.09	*06	56.13	3653.50
PR65	P	M	30	*07:02	50.45	*08:02	78.34	3952.25
PR66	P	M	64	*01	63.87	*02	56.76	3625.26
PR67	P	M	48	*04:01	67.28	*15	57.39	3861.20
PR68	P	F	55	*07	*40.96*	*05	84.84	3475.05
PR69	P	F	41	*06	56.13	*16	51.12	2869.37
PR70	P	F	50	*07:02	50.45	*16:01	51.12	2579.00
PR71	P	M	30	*04:01	67.28	*08:02	78.34	5270.72
PR72	P	M	49	*03	*65.52*	*06	56.13	3677.64
PR73	P	F	32	*04:01	67.28	*06	56.13	3776.43
PR74	P	M	61	*03	*65.52*	*07:01	29.74	1948.56

(Continued)

10.3389/fimmu.2025.1703026

TABLE 3 Continued

Sample code	HIV-1 progression	Sex	Age	HLA-C genotype and stability scores				Stability score
				1st allele	Score (1st)	2nd allele	Score (2nd)	
PR75	P	M	29	*03:02	65.09	*07:02	50.45	3283.79
PR76	P	F	53	*04:01	67.28	*06	56.13	3776.43
PR77	P	M	57	*04	*68.06*	*12	52.20	3552.73
PR78	P	F	57	*04	*68.06*	*07:04	9.70	660.18
PR79	P	M	33	*07:01	29.74	*07:02	50.45	1500.38
PR80	P	M	32	*03	*65.52*	*15	57.39	3760.19
PR81	P	F	39	*04	*68.06*	*12:03	50.34	3426.14
PR82	P	F	32	*07	*40.96*	*16:01	51.12	2093.88
PR83	P	M	63	*06	56.13	*07:02	50.45	2831.76
PR84	P	F	50	*07	*40.96*	*17	55.18	2260.17

HIV-1 infected individuals who showed either slow (Long Term Non Progressors, LTNP) or rapid progression (P) to AIDS were genotyped for HLA-C alleles. The stability values corresponding to each allotype were multiplied together to give a final HLA-C stability score for each patient. Allele scores calculated using a frequency-weighted average are reported in italics. Patient code, sex (M, male; F, female), HLA-C alleles and their corresponding stability scores, and the final calculated stability scores are reported.

In addition, we noted that some very unstable variants, such as C*07:01 or C*07:04, are also the lowest expressed variants, whereas some more stable variants, such as C*05:01 or C*14:02, are among the most highly expressed alleles. While numerous factors contribute to the regulation of HLA-C expression levels, the peptide-binding capacity of different HLA-C variants is also recognized as a key determinant influencing their surface expression (46). Therefore, it is plausible that inefficient peptide binding may contribute to the lower expression of certain HLA-C variants on the cell membrane (9), suggesting a potential correlation between stability and expression levels.

Our analysis improved the definition of the stability of HLA-C allotypes, overcoming the previous binary classification, which was too simplistic and inaccurate. The in-depth characterization of binding stability to peptides specific to the most common variants in the human population was carried out using pools of experimentally validated peptides known to bind to the main allotypes (35). This approach enabled obtaining a "stability coefficient" for each of these HLA-C variants and thereby quantified the overall stability profile of each HLA-typed individual based on the combination of their specific allotype stability coefficients.

HLA-C stability influences HIV-1 infection progression

HLA-C stability plays a critical role in modulating defense mechanisms against HIV-1. Unstable alleles may increase HIV-1 progression, suggesting that by influencing antigen presentation efficiency, they may alter the ability of CD8+ T cells to recognize and eliminate infected cells, in keeping with previous findings indicating that HLA-C expression levels directly affect HIV-1 immune control (10). Additionally, in our previous studies (24, 25) we reported that stable HLA-C alleles are associated with lower viral loads and more effective immune responses, supporting our finding that unstable alleles contribute to a faster progression to AIDS.

To assess the correlation between stability metrics and progression of HIV-1 infection, we re-analyzed a population of HIV-1 positive, treatment-naïve subjects described and characterized in our previous study (37). In the original analysis, the different allotypes were binary divided into stable and unstable, revealing a significant correlation between rapid progression to AIDS and the presence of unstable HLA-C variants. In the present study, we refined the analysis by performing high-resolution typing of the second digit for divergent subtypes and assessing a quantitative stability coefficient based on their HLA-C allotype combination. This enhanced approach confirmed and strengthened our earlier findings, showing a robust and highly significant correlation between accelerated disease progression and a higher burden of unstable HLA-C allotypes.

HLA-C stability impact on HIV-associated neurocognitive outcomes

The association between unstable HLA-C alleles and HAND is particularly noteworthy. Previous studies have suggested that unstable HLA-C variants may lead to increased levels of free β_2m, contributing to neuroinflammation and neuronal damage (29). Additionally, a recent study has specifically linked HLA-C*07 to HAND in HIV patients (31).

To test the clinical relevance of the specific stability coefficient for each major HLA-C allotype on neurological outcomes in HIV-1 infection, we analyzed a population of HIV-positive subjects with subjective report or objective evidence of cognitive impairment and compared them to cognitively unimpaired ones. We observed a

10.3389/fimmu.2025.1703026

TABLE 4 HLA-C stability scores in HIV-1–infected patients with and without neurocognitive impairment.

Sample code	Neurocognitive status	Sex	Age	HLA-C genotype and stability scores				Stability score
				1st allele	Score (1st)	2nd allele	Score (2nd)	
H1	HAND +	M	42	*01	63.87	*06	56.13	3585.02
H2	HAND +	F	46	*03:02	65.09	*07:02	50.45	3283.79
H3	HAND +	M	60	*02	56.76	*16:01	51.12	2901.57
H4	HAND +	M	59	*03:02	65.09	*04:01	67.28	4379.26
H5	HAND +	F	52	*07:02	50.45	*07:04	9.70	489.37
H6	HAND +	M	66	*03:02	65.09	*16:01	51.12	3327.40
H7	HAND +	M	40	*06	56.13	*07:01	29.74	1669.31
H8	HAND +	M	63	*01	63.87	*07:01	29.74	1899.49
H9	HAND +	M	56	*04:01	67.28	*07:01	29.74	2000.91
H10	HAND +	F	53	*06	56.13	*12:03	50.34	2825.58
H11	HAND +	M	52	*05	84.84	*07:01	29.74	2523.14
H12	HAND +	M	56	*04:01	67.28	*12:03	50.34	3386.88
H13	HAND +	M	51	*07:01	29.74	*07:01	29.74	884.47
H14	HAND +	F	65	*02	56.76	*07:01	29.74	1688.04
H15	HAND +	M	58	*07:01	29.74	*12:03	50.34	1497.11
H16	HAND +	M	64	*07:01	29.74	*08:02	78.34	2329.83
H17	HAND -	M	57	*07:01	29.74	*07:02	50.45	1500.38
H18	HAND -	M	58	*07:01	29.74	*15	57.39	1706.78
H19	HAND -	F	54	*07:01	29.74	*14	*76.05*	2261.73
H20	HAND -	M	45	*04:01	67.28	*15	57.39	3861.20
H21	HAND -	M	31	*07:01	29.74	*12:03	50.34	1497.11
H22	HAND -	F	53	*02	56.76	*12:03	50.34	2857.30
H23	HAND -	M	39	*03:02	65.09	*12:03	50.34	3276.63
H24	HAND -	F	56	*04:01	67.28	*06	56.13	3776.43
H25	HAND -	M	41	*04:01	67.28	*12:03	50.34	3386.88
H26	HAND -	M	55	*04:01	67.28	*04:01	67.28	4526.60
H27	HAND -	F	56	*05	84.84	*12:03	50.34	4270.85
H28	HAND -	NA	NA	*04:01	67.28	*07:01	29.74	2000.91
H29	HAND -	M	62	*05	84.84	*07:01	29.74	2523.14
H30	HAND -	F	57	*07:02	50.45	*12:03	50.34	2539.65
H31	HAND -	M	47	*07:02	50.45	*15	57.39	2895.33
H32	HAND -	M	60	*02	56.76	*15	57.39	3257.46
H33	HAND -	M	60	*06	56.13	*07:01	29.74	1669.31
H34	HAND -	M	62	*03:02	65.09	*07:02	50.45	3283.79
H35	HAND -	M	59	*08:02	78.34	*17	55.18	4322.80
H36	HAND -	M	65	*01	63.87	*14	*76.05*	4857.31
H37	HAND -	M	62	*06	56.13	*12:03	50.34	2825.58

(Continued)

10.3389/fimmu.2025.1703026

TABLE 4 Continued

Sample code	Neurocognitive status	Sex	Age	HLA-C genotype and stability scores				Stability score
				1st allele	Score (1st)	2nd allele	Score (2nd)	
H38	HAND -	M	37	*01	63.87	*07:01	29.74	1899.49
H39	HAND -	M	54	*02	56.76	*08:02	78.34	4446.58
H40	HAND -	F	64	*04:01	67.28	*07:02	50.45	3394.28
H41	HAND -	M	59	*04:01	67.28	*06	56.13	3776.43
H42	HAND -	M	46	*07:02	50.45	*14	*76.05*	3836.72
H43	HAND -	M	64	*04:01	67.28	*06	56.13	3776.43
H44	HAND -	F	54	*05	84.84	*16:01	51.12	4337.02
H45	HAND -	M	58	*05	84.84	*07:01	29.74	2523.14
H46	HAND -	M	54	*07:01	29.74	*07:02	50.45	1500.38
H47	HAND -	M	55	*03:02	65.09	*14	*76.05*	4950.09
H48	HAND -	M	54	*06	56.13	*06	56.13	3150.58
H49	HAND -	M	47	*04:01	67.28	*07:02	50.45	3394.28
H50	HAND -	M	60	*04:01	67.28	*06	56.13	3776.43
H51	HAND -	M	51	*03:02	65.09	*12:03	50.34	3276.63
H52	HAND -	M	64	*04:01	67.28	*04:01	67.28	4526.60
H53	HAND -	M	65	*03:02	65.09	*12:03	50.34	3276.63
H54	HAND -	M	47	*04:01	67.28	*05	84.84	5708.04
H55	HAND -	M	48	*04:01	67.28	*16:01	51.12	3439.35
H56	HAND -	M	45	*07:01	29.74	*15	57.39	1706.78
H57	HAND -	M	53	*04:01	67.28	*07:01	29.74	2000.91

HIV-infected individuals presenting (HAND-positive, HAND+) on not presenting (HAND-negative, HAND-) neurocognitive impairment were genotyped for HLA-C alleles. For each patient, the stability score of each allele was multiplied to obtain the final HLA-C stability score. Allele scores calculated using a weighted average are reported in italics. Patient code, sex (M, male; F, female; NA, not available), HLA-C alleles and their respective stability scores, and the final calculated stability scores are reported.

significantly higher presence of unstable HLA-C variants in HAND-positive subjects than in HAND-negative ones, further confirming our preliminary observation on a small case series (29). Our findings confirm this association, suggesting that HLA-C instability may exacerbate neurocognitive decline by promoting chronic immune activation and neuroinflammatory processes. Extensive scientific evidence supports the notion that genetic determinants of immune function are critical in shaping disease outcomes in HIV-1. In particular, previous studies have emphasized the role of HLA alleles in HIV-1 replication and progression (7, 10, 24, 25). Our findings extend this knowledge by highlighting the relevance of HLA-C allele stability at a more granular level. The association between HLA-C stability and neurocognitive disorders also aligns with research on β_2m in neurodegeneration (29), providing a potential molecular framework for future investigations into HIV-associated neurocognitive impairment.

HLA-C stability: towards a precision medicine approach

A major advantage of this refined stability analysis is the ability to calculate a personalized HLA-C stability score for each patient. By integrating computational stability assessments, such as EL-scores and AUC-derived stability coefficients, with patient-specific genetic data, it is possible to develop a predictive model that can help stratify patients based on their risk of rapid disease progression or neurocognitive complications. This approach aligns with the broader movement toward personalized medicine, where treatments and monitoring strategies are tailored to an individual's genetic profile. From a clinical perspective, the ability to predict disease progression based on HLA-C stability could lead to more targeted interventions. For instance, patients identified as having unstable HLA-C variants could be prioritized for early

10.3389/fimmu.2025.1703026

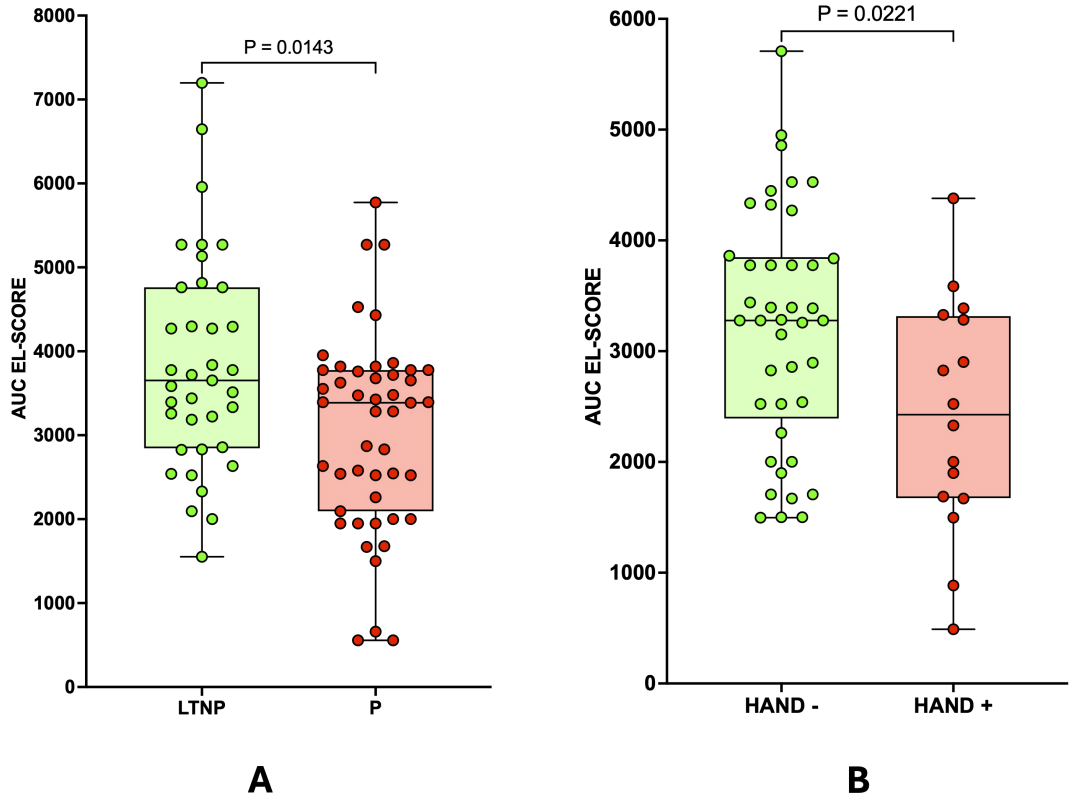

FIGURE 3
Association of patient HLA-C stability scores with HIV-1 progression and HIV-1-related neurocognitive impairment. **(A)** HIV-1 patients who experience rapid disease progression (Progressors, P, n=47) exhibit lower stability scores than those with slower progression (Long Term Non Progressors, LTNP, n=37). **(B)** HIV-1 patients presenting neurocognitive impairment (HAND+, n=16) have lower stability scores than cognitively normal patients (HAND-, n=41). Statistical analyses were performed using the two-tailed Mann-Whitney U test; $p < 0.05$ was considered statistically significant.

intervention strategies, including more intensive monitoring, earlier initiation of antiretroviral therapy, or adjunctive therapies targeting immune modulation. Furthermore, understanding the link between HLA-C instability and HAND could open new therapeutic avenues, such as early interventions targeting neuroinflammatory pathways. The use of HLA-C genotyping could improve personalized treatment strategies, identifying individuals at higher risk of rapid disease progression or HAND.

The study of HLA-C peptide binding stability is critical for understanding immune regulation and its implications in infectious diseases, cancer, and autoimmunity. Advances in computational modelling and experimental methodologies provide valuable insights into the structural and functional aspects of HLA-C stability. Future research should focus on refining predictive models, defining clinically relevant stability thresholds and exploring therapeutic interventions aimed at enhancing HLA-C-mediated immune responses.

The main limitation of the study was the inability to perform more precise typing at the second digit for several biological samples due to insufficient DNA for testing. This reduced the accuracy of the data obtained, necessitating the use of a frequency-weighted average of stability scores in some cases.

Conclusions

HLA-C plays a crucial and multifaceted role in HIV-1 infection, influencing immune recognition, disease progression, and neurocognitive outcomes. Despite its lower surface expression compared to HLA-A and HLA-B, HLA-C contributes significantly to both adaptive and innate immune responses. Advances in genomic and immunological research continue to reveal the complex interactions between HLA-C and HIV-1, providing valuable insights into potential therapeutic and vaccine strategies. By using an innovative cutting-edge bioinformatic pipeline, we demonstrated that reduced HLA-C stability is associated with faster HIV-1 disease progression and a higher prevalence of HIV-associated neurocognitive disorders. Overall, the findings from this study emphasize that HLA-C stability analysis should become an integral part of HIV-1 disease management and research. Future studies should focus on refining predictive models for personalized stability scoring, validating these findings in larger, independent cohorts, to early identify those at greater risk of progression or developing neurocognitive symptoms and intervene early with the most appropriate treatment approaches to improve patient outcomes.

Data availability statement

The original contributions presented in the study are included in the article/supplementary material. Further inquiries can be directed to the corresponding author.

Ethics statement

The studies involving humans were approved by Ethics Committee of the Health Department of the Federal District (#066/07) from hospitals of the public network of the Federal District. Brazil; Ethics Committee for Analysis of Research Projects (CAPPesq) of Hospital das Clínicas HCFMUSP (#CAPPesq #0306/10, online registration #5867) Faculdade de Medicina da Universidade de Sao Paulo, Brazil Institutional Ethics Committee of Verona and Rovigo (Italy) (#2459 CESC). The studies were conducted in accordance with the local legislation and institutional requirements. The participants provided their written informed consent to participate in this study.

Author contributions

MV: Conceptualization, Data curation, Formal analysis, Investigation, Methodology, Software, Validation, Writing – original draft, Writing – review & editing. AS: Investigation, Methodology, Validation, Writing – review & editing. EGM: Investigation, Methodology, Software, Writing – review & editing. CDM: Investigation, Methodology, Writing – review & editing. EO: Investigation, Methodology, Writing – review & editing. ST: Conceptualization, Data curation, Methodology, Supervision, Validation, Writing – original draft, Writing – review & editing. EM: Data curation, Investigation, Validation, Writing – review & editing. AF: Data curation, Formal analysis, Investigation, Methodology, Writing – review & editing. ML: Data curation, Formal analysis, Investigation, Methodology, Validation, Writing – review & editing. EL: Data curation, Methodology, Validation, Writing – review & editing. GAA: Data curation, Methodology, Validation, Writing – review & editing. BCMDS: Data curation, Methodology, Validation, Writing – review & editing. AJDSD: Data curation, Methodology, Validation, Writing – review & editing. JC: Data curation, Methodology, Validation, Writing – review & editing. ERA: Data curation, Investigation, Methodology, Supervision, Writing – original draft, Writing – review & editing. MM: Data curation, Methodology, Writing – review & editing. MA: Data curation, Formal analysis, Investigation, Methodology, Software, Writing – review & editing. AR: Conceptualization, Supervision, Visualization, Writing – review & editing. MGR: Conceptualization, Supervision, Visualization, Writing – review & editing. MTV: Conceptualization, Supervision, Visualization, Writing – review & editing. GG: Conceptualization, Investigation, Methodology, Software, Supervision, Validation, Writing – original draft, Writing – review & editing. DZ: Conceptualization, Data curation, Formal analysis, Funding acquisition, Investigation, Project administration, Software, Supervision, Writing – original draft, Writing – review & editing.

Funding

The author(s) declared that financial support was received for this work and/or its publication. This study was financially supported by the Gilead Fellowship Program, 2019 Edition, by the Federal District Research Support Foundation (FAPDF), Bench Amendment No. 7108001, and by the Italian Ministry of Research (MUR) as part of the Excellence Project 2023-2027 of the Department of Neuroscience, Biomedicine and Movement Sciences of the University of Verona.

Acknowledgments

The study was conducted in accordance with the Declaration of Helsinki and approved by the Ethics Committee of the Health Department of the Federal District (#066/07) from hospitals of the public network of the Federal District. Brazil; Ethics Committee for Analysis of Research Projects (CAPPesq) of Hospital das Clínicas HCFMUSP (#CAPPesq #0306/10, online registration #5867) Faculdade de Medicina da Universidade de Sao Paulo, Brazil and the Institutional Ethics Committee of Verona and Rovigo (Italy) (#2459 CESC). We acknowledge the contribution of Brazilian, Canadian, and US patients who agreed to participate in this study. We thank INDACO for providing high-performance computing resources and support.

Conflict of interest

The authors declare that the research was conducted in the absence of any commercial or financial relationships that could be construed as a potential conflict of interest.

Generative AI statement

The author(s) declare that no Generative AI was used in the creation of this manuscript.

Any alternative text (alt text) provided alongside figures in this article has been generated by Frontiers with the support of artificial intelligence and reasonable efforts have been made to ensure accuracy, including review by the authors wherever possible. If you identify any issues, please contact us.

Publisher's note

References

1. Robinson J, Guethlein LA, Cereb N, Yang SY, Norman PJ, Marsh SGE, et al. Distinguishing functional polymorphism from random variation in the sequences of >10,000 HLA-A, -B and -C alleles. *PloS Genet*. (2017) 13:e1006862. doi: 10.1371/journal.pgen.1006862

2. Parham P. MHC class I molecules and kirs in human history, health and survival. *Nat Rev Immunol*. (2005) 5:201–14. doi: 10.1038/nri1570

3. Neisig A, Melief CJ, Neefjes J. Reduced cell surface expression of HLA-C molecules correlates with restricted peptide binding and stable TAP interaction. *J Immunol*. (1998) 160:171–9. doi: 10.4049/jimmunol.160.1.171

4. Zemmour J, Parham P. Distinctive polymorphism at the HLA-C locus: implications for the expression of HLA-C. *J Exp Med*. (1992) 176:937–50. doi: 10.1084/jem.176.4.937

5. McCutcheon JA, Gumperz J, Smith KD, Lutz CT, Parham P. Low HLA-C expression at cell surfaces correlates with increased turnover of heavy chain mRNA. *J Exp Med*. (1995) 181:2085–95. doi: 10.1084/jem.181.6.2085

6. Blais ME, Dong T, Rowland-Jones S. HLA-C as a mediator of natural killer and T-cell activation: spectator or key player? *Immunology*. (2011) 133:1–7. doi: 10.1111/j.1365-2567.2011.03422.x

7. Zipeto D, Beretta A. HLA-C and HIV-1: friends or foes? *Retrovirology*. (2012) 9:39. doi: 10.1186/1742-4690-9-39

8. Harndahl M, Rasmussen M, Roder G, Dalgaard Pedersen I, Sørensen M, Nielsen M, et al. Peptide-MHC class I stability is a better predictor than peptide affinity of CTL immunogenicity. *Eur J Immunol*. (2012) 42:1405–16. doi: 10.1002/eji.201141774

9. Kaur G, Gras S, Mobbs JI, Vivian JP, Cortes A, Barber T, et al. Structural and regulatory diversity shape HLA-C protein expression levels. *Nat Commun*. (2017) 8:15924. doi: 10.1038/ncomms15924

10. Apps R, Qi Y, Carlson JM, Chen H, Gao X, Thomas R, et al. Influence of HLA-C expression level on HIV control. *Science*. (2013) 340:87–91. doi: 10.1126/science.1232685

11. Kulkarni S, Qi Y, O'HUigin C, Pereyra F, Ramsuran V, McLaren P, et al. Genetic interplay between HLA-C and MIR148A in HIV control and Crohn disease. *Proc Natl Acad Sci U.S.A*. (2013) 110:20705–10. doi: 10.1073/pnas.1312237110

12. Vince N, Li H, Ramsuran V, Naranbhai V, Duh FM, Fairfax BP, et al. HLA-C level is regulated by a polymorphic oct1 binding site in the HLA-C promoter region. *Am J Hum Genet*. (2016) 99:1353–8. doi: 10.1016/j.ajhg.2016.09.023

13. Goodson-Gregg FJ, Rothbard B, Zhang A, Wright PW, Li H, Walker-Sperling VE, et al. Tuning of NK-specific HLA-C expression by alternative mRNA splicing. *Front Immunol*. (2019) 10:3034. doi: 10.3389/fimmu.2019.03034

14. O'Huigin C, Kulkarni S, Xu Y, Deng Z, Kidd J, Kidd K, et al. The molecular origin and consequences of escape from miRNA regulation by HLA-C alleles. *Am J Hum Genet*. (2011) 89:424–31. doi: 10.1016/j.ajhg.2011.07.024

15. Sibilio L, Martayan A, Setini A, Monaco EL, Tremante E, Butler RH, et al. A single bottleneck in HLA-C assembly. *J Biol Chem*. (2008) 283:1267–74. doi: 10.1074/jbc.M708068200

16. Wang M, Kurgan L, Li M. A comprehensive assessment and comparison of tools for HLA class I peptide-binding prediction. *Briefings Bioinf*. (2023) 24(3):1-9. doi: 10.1093/bib/bbad150

17. Jurtz V, Paul S, Andreatta M, Marcatili P, Peters B, Nielsen M. NetMHCpan-4.0: improved peptide–MHC class I interaction predictions integrating eluted ligand and peptide binding affinity data. *J Immunol*. (2017) 199:3360–8. doi: 10.4049/jimmunol.1700893

18. Nilsson JB, Greenbaum J, Peters B, Nielsen M. NetMHCpan-4.2: improved prediction of CD8+ epitopes by use of transfer learning and structural features. *Front Immunol*. (2025) 16:1616113. doi: 10.3389/fimmu.2025.1616113

19. Reynisson B, Alvarez B, Paul S, Peters B, Nielsen M. NetMHCpan-4.1 and NetMHCIIpan-4.0: improved predictions of MHC antigen presentation by concurrent motif deconvolution and integration of MS MHC eluted ligand data. *Nucleic Acids Res*. (2020) 48:W449–54. doi: 10.1093/nar/gkaa379

20. Olp MD, Laufer VA, Valesano AL, Zimmerman A, Woodside KJ, Lu Y, et al. HLA-C peptide repertoires as predictors of clinical response during early SARS-coV-2 infection. *Life*. (2024) 14:1181. doi: 10.3390/life14091181

21. Rasmussen M, Fenoy E, Harndahl M, Kristensen AB, Nielsen IK, Nielsen M, et al. Pan-specific prediction of peptide–MHC class I complex stability, a correlate of T cell immunogenicity. *J Immunol*. (2016) 197:1517–24. doi: 10.4049/jimmunol.1600582

22. Malnati MS, Ugolotti E, Monti MC, Battista D, Vanni I, Bordo D, et al. Activating Killer Immunoglobulin Receptors and HLA-C: a successful combination providing HIV-1 control. *Sci Rep*. (2017) 7:42470. doi: 10.1038/srep42470

23. The International HIV Controllers Study. The major genetic determinants of HIV-1 control affect HLA class I peptide presentation. *Science*. (2010) 330:1551–7. doi: 10.1126/science.1195271

24. Serena M, Parolini F, Biswas P, Sironi F, Blanco Miranda A, Zoratti E, et al. HIV-1 Env associates with HLA-C free-chains at the cell membrane modulating viral infectivity. *Sci Rep*. (2017) 7:40037. doi: 10.1038/srep40037

25. Parolini F, Biswas P, Serena M, Sironi F, Muraro V, Guizzardi E, et al. Stability and expression levels of HLA-C on the cell membrane modulate HIV-1 infectivity. *J Virol*. (2018) 92. doi: 10.1128/JVI.01711-17

26. Tierney SM, Sheppard DP, Kordovski VM, Faytell MP, Avci G, Woods SP. A comparison of the sensitivity, stability, and reliability of three diagnostic schemes for HIV-associated neurocognitive disorders. *J Neurovirol*. (2017) 23:404–21. doi: 10.1007/s13365-016-0510-z

27. Kallianpur AR, Levine AJ. Host genetic factors predisposing to HIV-associated neurocognitive disorder. *Curr HIV/AIDS Rep*. (2014) 11:336–52. doi: 10.1007/s11904-014-0222-z

28. Leslie S, Donnelly P, McVean G. A statistical method for predicting classical HLA alleles from SNP data. *Am J Hum Genet*. (2008) 82:48–56. doi: 10.1016/j.ajhg.2007.09.001

29. Zipeto D, Serena M, Mutascio S, Parolini F, Diani E, Guizzardi E, et al. HIV-1-associated neurocognitive disorders: is HLA-C binding stability to beta(2)-microglobulin a missing piece of the pathogenetic puzzle? *Front Neurol*. (2018) 9:791. doi: 10.3389/fneur.2018.00791

30. McArthur JC, Nance-Sproson TE, Griffin DE, Hoover D, Selnes OA, Miller EN, et al. The diagnostic utility of elevation in cerebrospinal fluid beta 2-microglobulin in HIV-1 dementia. Multicenter AIDS Cohort Study. *Neurology*. (1992) 42:1707–12. doi: 10.1212/wnl.42.9.1707

31. Pons-Fuster E, Bernal E, Guillamón CF, Gimeno L, Martínez-Sánchez MV, Ruiz-Lorente I, et al. HLA-C*07 is associated with symptomatic HIV-1-associated neurocognitive disorders (HAND) and immune dysregulation. *Infect Dis-Nor*. (2024) 56:818–29. doi: 10.1080/23744235.2024.2351047

32. Tian C, Kasavajhala K, Belfon KAA, Raguette L, Huang H, Migues AN, et al. ff19SB: amino-acid-specific protein backbone parameters trained against quantum mechanics energy surfaces in solution. *J Chem Theory Comput*. (2020) 16:528–52. doi: 10.1021/acs.jctc.9b00591

33. Mark P, Nilsson L. Structure and dynamics of the TIP3P, SPC, and SPC/E water models at 298 K. *J Phys Chem A*. (2001) 105:9954–60. doi: 10.1021/jp003020w

34. Roe DR, Cheatham TE. III, PTRAJ and CPPTRAJ: software for processing and analysis of molecular dynamics trajectory data. *J Chem Theory Comput*. (2013) 9:3084–95. doi: 10.1021/ct400341p

35. Sarkizova S, Klaeger S, Le PM, Li LW, Oliveira G, Keshishian H, et al. A large peptidome dataset improves HLA class I epitope prediction across most of the human population. *Nat Biotechnol*. (2019) 38:199–209. doi: 10.1038/s41587-019-0322-9

36. Karnaukhov V, Paes W, Woodhouse IB, Partridge T, Nicastri A, Brackenridge S, et al. HLA variants have different preferences to present proteins with specific molecular functions which are complemented in frequent haplotypes. *Front Immunol*. (2022) 13:1067463. doi: 10.3389/fimmu.2022.1067463

37. Stefani C, Sangalli A, Locatelli E, Federico T, Malerba G, Romanelli MG, et al. Increased prevalence of unstable HLA-C variants in HIV-1 rapid-progressor patients. *Int J Mol Sci*. (2022) 23:14852. doi: 10.3390/ijms232314852

38. Antinori A, Arendt G, Becker JT, Brew BJ, Byrd DA, Cherner M, et al. Updated research nosology for HIV-associated neurocognitive disorders. *Neurology*. (2007) 69:1789–99. doi: 10.1212/01.WNL.0000287431.88658.8b

39. Nightingale S, Ances B, Cinque P, Dravid A, Dreyer AJ, Gisslen M, et al. Cognitive impairment in people living with HIV: consensus recommendations for a new approach. *Nat Rev Neurol*. (2023) 19:424–33. doi: 10.1038/s41582-023-00813-2

40. Shen Y, Parks JM, Smith JC. HLA class I supertype classification based on structural similarity. *J Immunol*. (2023) 210:103–14. doi: 10.4049/jimmunol.2200685

41. Nguyen AT, Szeto C, Gras S. The pockets guide to HLA class I molecules. *Biochem Soc Trans*. (2021) 49:2319–31. doi: 10.1042/bst20210410

42. Kangueane P, Sakharkar MK, Rajaseger G, Bolisetty S, Sivasekari B, Zhao B, et al. A framework to sub-type HLA supertypes. *Front Biosci*. (2005) 10:879–86. doi: 10.2741/1582

43. Liu Q, Yang M, Zhong P, Wei Q, Jiao H, Meng J, et al. Micropolymorphism outside the peptide-binding groove of human leukocyte antigen (HLA)-C*14 modulates structural stability and shapes immune responses. *Int J Biol Macromol*. (2025) 309:142772. doi: 10.1016/j.ijbiomac.2025.142772

44. Yang M, Zhong P, Liu Q, Jiao H, Lei J, Wei P. Biochemical and structural insights into position 97 micropolymorphisms in human leukocyte antigen (HLA)-C*12 allotypes and their differential disease associations. *Int J Biol Macromol*. (2025) 306:141681. doi: 10.1016/j.ijbiomac.2025.141681

45. Fellay J, Shianna KV, Ge D, Colombo S, Ledergerber B, Weale M, et al. A whole-genome association study of major determinants for host control of HIV-1. *Science*. (2007) 317:944–7. doi: 10.1126/science.1143767

46. Dendrou CA, Petersen J, Rossjohn J, Fugger L. HLA variation and disease. *Nat Rev Immunol*. (2018) 18:325–39. doi: 10.1038/nri.2017.143

Scientific Foundation SPIROSKI, Skopje, Republic of North Macedonia
South East European Journal of Immunology. 2025 Mar 31; 8(CITIM): 065.
https://doi.org/10.3889/seejim.2025.6121
eISSN: 1857-9388
Category: *CITIM - Cancer Immunotherapy & Immunomonitoring (CITIM2025)*
Section: *Invited lectures*

Investigating RUNX2 KO in B16 melanoma cells as a potential strategy to enhance in vivo tumor response to therapeutic approaches

Elena-Georgiana Dobre*[1], Mauro Voi[2], Elisa Orlandi[2], Carola de Martinis[2], Carolina Constantin[1], Donato Zipeto[2], Maria-Teresa Valenti[2], Monica Neagu[1]

[1]*Immunology Laboratory, "Victor Babes" National Institute of Pathology, Bucharest, Romania*
[2]*Department of Neurosciences, Biomedicine and Movement Sciences, University of Verona, Verona, Italy*

Citation: Dobre EG, Voi M, Orlandi E, de Martinis C, Constantin C, Zipeto D, Valenti MT, Neagu M. Investigating RUNX2 KO in B16 melanoma cells as a potential strategy to enhance in vivo tumor response to therapeutic approaches. SEE J Immunol. 2025 Mar 27;8(CITIM):065. https://doi.org/10.3889/seejim.2025.6121.
Keywords: Cutaneous melanoma (CM); RUNX2 KO generation; immunotherapies
***Correspondence:** Elena Georgiana Dobre. Immunology Laboratory, "Victor Babes" National Institute of Pathology, Bucharest, Romania.
E-mail: dobregeorgiana_95@yahoo.com
Received: 01-Mar-2025
Accepted: 25-Mar-2025

Funding: This research did not receive any financial support
Competing Interests: The authors have declared that no competing interests exist

Abstract

Background: Cutaneous melanoma (CM) is a heterogeneous and highly metastatic disease with unpredictable clinical behaviour, for which the most effective pharmacological strategies are still being sought. In the present study, we describe the workflow for RUNX2 KO generation in B16 melanoma cells, an approach that according to preliminary data from international databases may contribute to defusing CM resistance to targeted and immunotherapies.
Methods: The role of the RUNX2 gene in CM was investigated using the TIMER2.0 (http://timer.cistrome.org/) and TISIDB (http://cis.hku.hk/TISIDB/) databases. Two gRNAs targeting exon 4 of RUNX2 were designed and cloned into the px459v2.0 plasmid, as previously described[1]. The B16 melanoma cells were transfected with 2.5 µg of plasmid DNA using Lipofectamine 3000 in DMEM (without antibiotics). After one day, cells were selected with complete DMEM containing 1 µg/ml puromycin for six days. Cells were further subjected to monoclonal cell isolation by seeding 0.3 cells/well in 96-well plates. Genomic DNA was extracted from the transfected bulk cell population and isolated clones and PCR-amplified with primers spanning the gRNA-target region. RUNX2 KO was confirmed by Western blot.
Results: According to the TIMER2.0 and TISIDB databases, RUNX2 shows positive correlations with the most notorious immune inhibitors within the CM tumour microenvironment and is overexpressed in CM patients unresponsive to immune and targeted therapies. Therefore, we hypothesize that orchestrating RUNX2 KO in melanoma may be a promising strategy to improve tumour response to therapeutic approaches. Five B16 clones were subjected to Sanger sequencing and all showed editing events. In particular, they showed an in-frame deletion within the Runt domain of the RUNX2 gene. In addition, these five clones showed no RUNX2 protein expression by Western blot.
Conclusions: Our study presents the workflow for obtaining genetically engineered melanoma cells that can be further exploited to dissect the biological roles of RUNX2 in syngeneic B16 melanoma mouse models.
References:
[1]Deiana M. et al., 2018. New insights into the Runt Domain of RUNX2 in melanoma cell proliferation and migration. *Cells*. 7(11):220.

jove

Pseudotyped Viruses As a Molecular Tool to Monitor Humoral Immune Responses Against SARS-CoV-2 Via Neutralization Assay

Tobia Fantoni[*,1], **Michele Bissoli**[*,1], **Chiara Stefani**[1], **Mauro Voi**[1], **Alexandrina Dabija**[1], **Rebecca Casula**[1], **Domenico Luca Minafra**[1], **Julys da Fonseca Palmeira**[2], **Enrique Roberto Argañaraz**[2], **Martin Mayora-Neto**[3], **Nigel J. Temperton**[3], **Donato Zipeto**[1], **Alessandra Ruggiero**[1]

[1] Department of Neuroscience, Biomedicine and Movement, University of Verona [2] Laboratory of Molecular Neurovirology, Faculty of Health Science, University of Brasília [3] Viral Pseudotype Unit, Medway School of Pharmacy, Universities of Kent and Greenwich at Medway

[*] These authors contributed equally

Corresponding Author

Alessandra Ruggiero
Alessandra.Ruggiero@univr.it

Citation

Fantoni, T., Bissoli, M., Stefani, C., Voi, M., Dabija, A., Casula, R., Minafra, D.L., da Fonseca Palmeira, J., Argañaraz, E.R., Mayora-Neto, M., Temperton, N.J., Zipeto, D., Ruggiero, A. Pseudotyped Viruses As a Molecular Tool to Monitor Humoral Immune Responses Against SARS-CoV-2 Via Neutralization Assay. *J. Vis. Exp.* (201), e65658, doi:10.3791/65658 (2023).

Date Published

November 21, 2023

DOI

10.3791/65658

URL

jove.com/video/65658

Abstract

Pseudotyped viruses (PVs) are molecular tools that can be used to study host-virus interactions and to test the neutralizing ability of serum samples, in addition to their better-known use in gene therapy for the delivery of a gene of interest. PVs are replication defective because the viral genome is divided into different plasmids that are not incorporated into the PVs. This safe and versatile system allows the use of PVs in biosafety level 2 laboratories. Here, we present a general methodology to produce lentiviral PVs based on three plasmids as mentioned here: (1) the backbone plasmid carrying the reporter gene needed to monitor the infection; (2) the packaging plasmid carrying the genes for all the structural proteins needed to generate the PVs; (3) the envelope surface glycoprotein expression plasmid that determines virus tropism and mediates viral entry into the host cell. In this work, SARS-CoV-2 Spike is the envelope glycoprotein used for the production of non-replicative SARS-CoV-2 pseudotyped lentiviruses.

Briefly, packaging cells (HEK293T) were co-transfected with the three different plasmids using standard methods. After 48 h, the supernatant containing the PVs was harvested, filtered, and stored at -80 °C. The infectivity of SARS-CoV-2 PVs was tested by studying the expression of the reporter gene (luciferase) in a target cell line 48 h after infection. The higher the value for relative luminescence units (RLUs), the higher the infection/transduction rate. Furthermore, the infectious PVs were added to the serially diluted serum samples to study the neutralization process

of pseudoviruses' entry into target cells, measured as the reduction in RLU intensity: lower values corresponding to high neutralizing activity.

Introduction

Pseudotyped viruses (PVs) are molecular tools used in microbiology to study host-virus and pathogen-pathogen interactions[1,2,3,4]. PVs consist of an inner part, the viral core that protects the viral genome, and an outer part, the envelope glycoproteins on the surface of the virus that defines the tropism[5]. A pseudovirus is replication-incompetent in the target cell because it does not contain all the genetic information to generate new viral particles. This combination of peculiar features makes PVs a safe alternative to a wildtype virus. Wildtype viruses, on the other hand, are highly pathogenic and cannot be used in BSL 2 laboratories for analysis[6].

The infectivity of PVs can be monitored by a reporter gene, usually coding for a fluorescent protein (GFP, RFP, YFP) or an enzyme that produces chemiluminescent products (luciferase). This is contained in one of the plasmids used for PV production and incorporated in the genome of the pseudovirus[7].

Several types of PV cores currently exist, including lentiviral-derived particles based on the HIV-1 genome. The great advantage of HIV-1-based PVs over other platforms is their intrinsic integration process in the target cell genome[8]. Although HIV-1 is a highly contagious virus and is the causative agent of AIDS, these lentiviral vectors are safe to use because of the extensive optimization steps over the years. Optimal safety conditions were achieved with the introduction of 2nd-generation lentiviral vectors, in which viral genes were depleted without influencing transduction capabilities[9]. The 3rd and 4th generations contributed to the increased safety of lentiviral vector handling with the further splitting of the viral genome into separate plasmids[10, 11]. The latest generations of PVs are generally employed to produce lentiviral vectors for gene therapy.

PVs can be used to study interactions between viruses and host cells, during both the production and the infection phases. PVs are especially employed in pseudovirus neutralization assays (PVNA). PVNAs are widely validated to assess the neutralization potential of serum or plasma by targeting the viral glycoprotein on the PV's envelope[12,13]. Neutralization activity, expressed as the inhibitory concentration 50 (IC50), is defined as the dilution of serum/plasma that blocks 50% of viral particle entry[14]. In this protocol, we described the set-up of a PVNA to test the antibody activity against Severe Acute Respiratory Syndrome - Coronavirus 2 (SARS-CoV-2) in sera collected before and after receiving a booster vaccine dose.

Protocol

The present protocol has been approved by and follows the guidelines of the Ethical Committee of the University of Verona (approval protocol number 1538). Informed written consent was obtained from the human subjects participating in the study. Whole blood samples were collected from healthcare worker (HCW) volunteers who were in the process of receiving anti-SARS-CoV-2 vaccines. These samples were collected in plastic tubes containing anticoagulants for the subsequent isolation of serum[15].

All the following processes must be performed in a Class-2 biological hood, working under sterile conditions. Virus handling must be performed with care, and all waste products must be neutralized in a diluted bleach solution. An overview of the protocol is displayed in **Figure 1**.

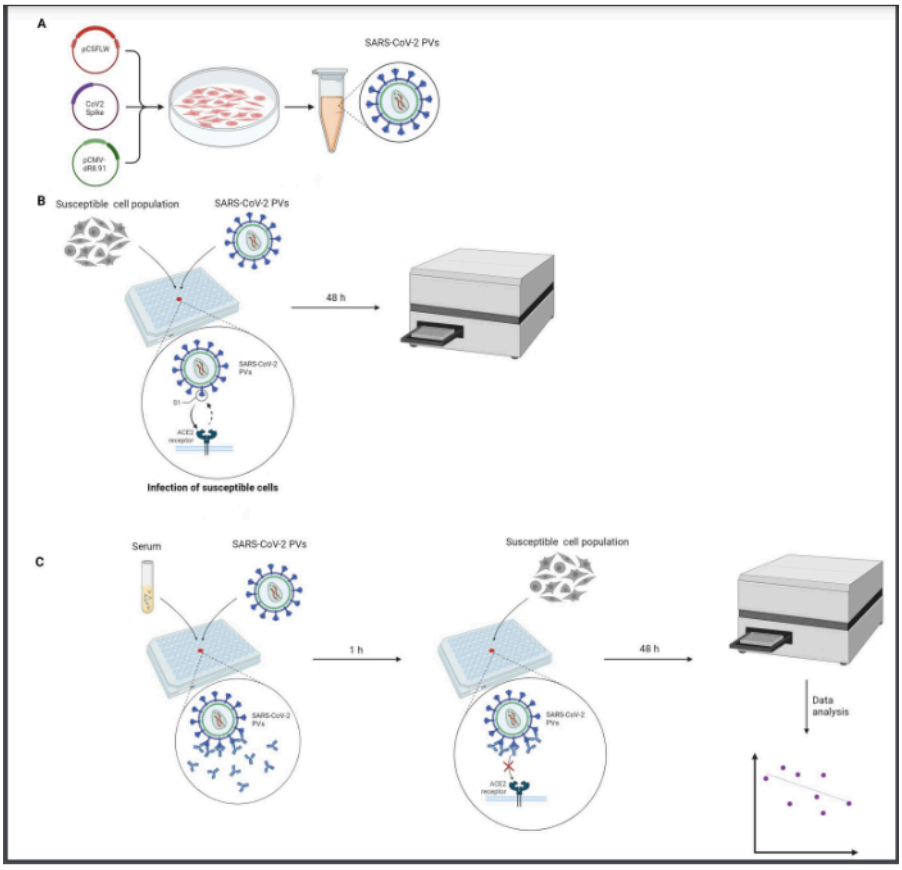

Figure 1: Graphical representation of a neutralization assay. (**A**) PV production, (**B**) PV titration, and (**C**) neutralization assay. All the procedures are performed in a class-2 biological hood under sterile conditions. Titration step (B) needs to be performed to standardize the infectivity levels of PVs before use in the neutralization assay (C). This figure was created with BioRender. Please click here to view a larger version of this figure.

1. SARS-CoV-2 PVs production and infectivity test

1. Seed 5 x 10^5 HEK293T cells in complete Dulbecco's Modified Eagle Medium (DMEM, high-glucose, 10% foetal bovine serum (FBS), 1% L-glutamine, 1% penicillin/streptomycin) in a 6-well plate (6WP) to reach a suitable cell density compatible with the transfection reagent used. In the case of performing transfection with polyehtylenimine (PEI) (prepare the reagent following the manufacturer instructions), ensure that the cells reach 40-60% density on the day of transfection (step 1.3). Keep the cells in a humidified incubator at 37 °C and 5% CO_2.

2. Prior to transfection, replace the spent cell medium with fresh medium without antibiotics (DMEM, high-glucose, 10% FBS, 1% L-glutamine) to achieve higher transfection efficiency.
   NOTE: The day after seeding, HEK293T cells are ready to be transfected.
3. Transfect adherent HEK293T cells with a suitable transfection reagent according to the manufacturer's instructions. If using PEI, prepare two mixes and follow the steps below.
   1. To prepare mix A, add 500 ng of pCMV-dR8.91 packaging plasmid[16], 750 ng of pCSFLW reporter plasmid[16], and 450 ng of SARS-CoV-2 Spike expressing plasmid in 100 µL of reduced serum medium.
   2. To prepare mix B, add 17.5 µL of PEI (concentration: 1 mg/mL) to 100 µL of the reduced serum medium.
   3. Allow both mixes to incubate at room temperature (RT) for 5 min. Next, mix the contents of both tubes together by adding the PEI mix B to DNA mix A.
   4. Incubate the tube for 20-30 min at RT. Flick the tube gently every 3-4 min to enhance the mixing. Finally, add the mixture to the HEK293T cells.
4. 16-20 h after the transfection, replace the culture medium with fresh, complete DMEM. Incubate at 37 °C and 5% CO_2, to allow for the production of PVs by transfected cells.
5. 72 h after the transfection, harvest the supernatant containing PVs. Then centrifuge at 1600 x *g* for 7 min at room temperature to remove cell debris and dead cells and filter it through a 0.45 µm cellulose acetate filter.
6. OPTIONAL STEP: To increase the final yield of PV titer, perform multiple transfections, pool the cell media containing PVs, and concentrate it using concentrating tubes.
7. Proceed directly with the next steps ("PVs titration", section 2) or aliquot the PV-containing medium in suitable tubes to store at -80 °C until use. Prepare an additional aliquot (400-500 µL) to be used for titration.
   NOTE: Making multiple aliquots will guarantee reproducibility between experiments by avoiding excessive thaw-freeze cycles.

2. PVs titration

1. Use the fresh PV-containing medium for the next steps or thaw the testing aliquot (step 1.7) to perform the titration of the new viral stock. Freezing aliquots of the same PV stock will guarantee reproducibility.
2. Add 50 µL of complete DMEM (or complete medium compatible with the target cell line in usage) in all the wells of a 96 well-plate (96WP) necessary to test in duplicate the PV stock, leaving row "A" empty. Add 100 µL of PVs stock to row "A". Based on the number of preparations to be tested, leave one column without the virus as a "cell only" control (**Figure 2**).
3. Pipette 50 µL from row A to row B and repeat this process up to row G to obtain serial dilutions of the initial stock. Discard the excess volume from the last row.
4. Detach cellsusing trypsin/ethylenediaminetetraacetic acid 1x (EDTA) in Dulbecco's phosphate buffer saline 1x (DPBS 1x), after removing the spent medium and washing cells with DPBS 1x twice. Prepare cells to a density of 4 x 10^5 cells/mL.

NOTE: In this protocol, PVs infection was tested on the susceptible cell line HEK293T/ACE2; such cells were derived from HEK293T, transduced using a lentiviral vector to express ACE2 receptor.

5. Add 50 µL of the cell suspension into each well to ensure a cell count of 2 x 10^4 cells per well.
6. Incubate at 37 °C and 5% CO_2, for 48 h.
7. After the incubation, perform the Luciferase assay to obtain the reading as per the manufacturer's instructions. Add 100 µL of the luciferase reagent to the wells and incubate in the dark at RT for 2 min. Move the content of each well to a black 96 well plate (compatible with the available plate reader) and read the plates in a 96 well plate reader.

NOTE: The luminometer used for the luciferase readout will produce a spreadsheet file with the raw, unprocessed data that will be used for downstream analysis (in this case, an Excel file). The virus' infectivity will be expressed as relative luminescence units (RLU) (described in paragraph 4.1).

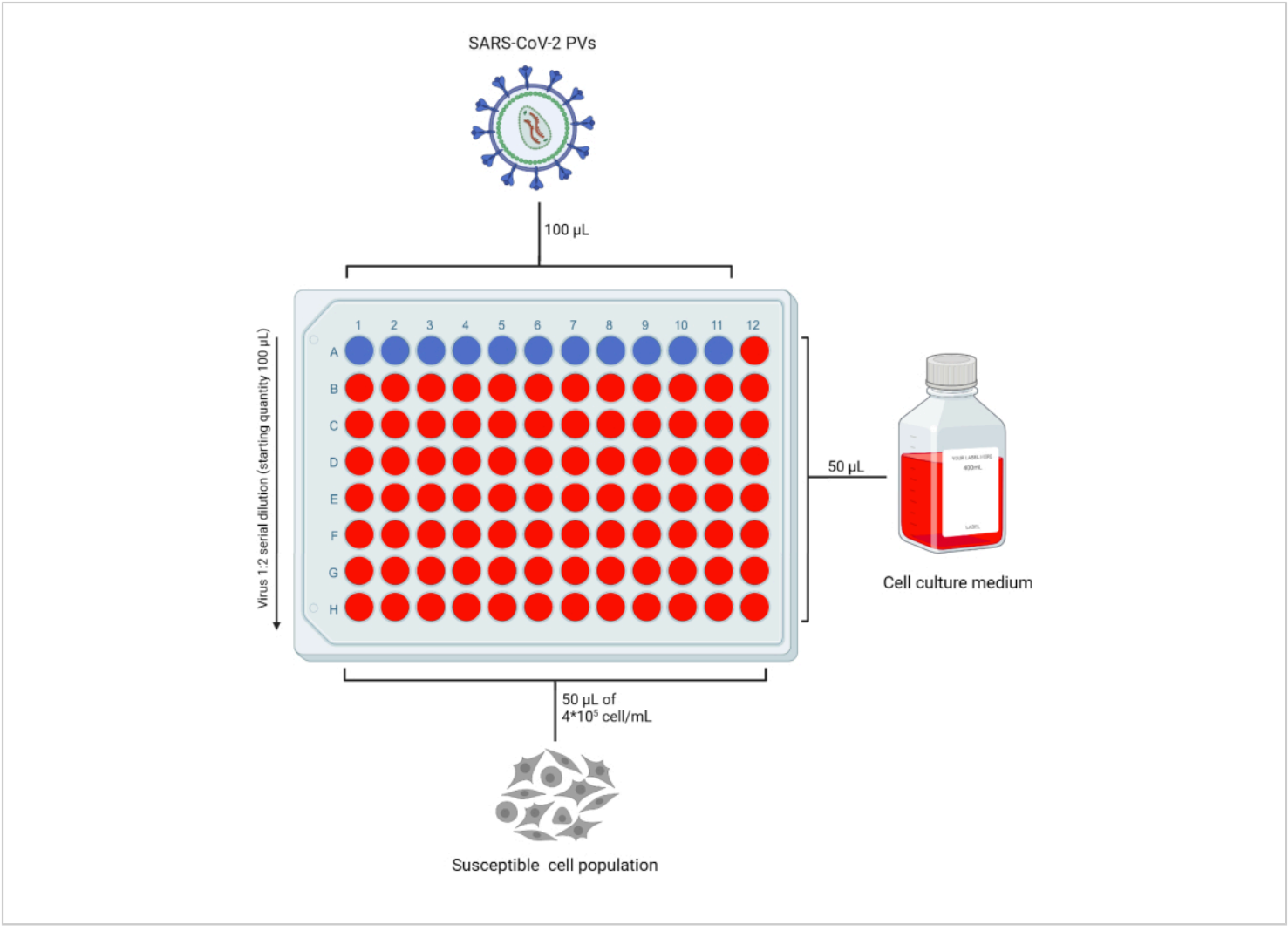

Figure 2: Representative layout of a 96 well plate for PVs titration. A fixed volume of PV-containing supernatant is added to row A, columns 1-11, and serially diluted. The last column is left as the "cell only" control. This figure was created with BioRender. Please click here to view a larger version of this figure.

3. Neutralization assay

1. Thaw patients' sera on ice. Inactivate serum samples by incubating them at 56 °C for 30 min.
2. In a 96 well plate, add 50 µL of the fresh, complete DMEM (or complete medium compatible with the target cell line used)in each of the following wells: from row B (columns 1-10) to row H (columns 1-10). Put 95 µL of the fresh, complete DMEM in row A (columns 1-10). Add 50 µL and 100 µL of complete DMEM into the wells of columns 11 and 12, respectively. These will be the infected (virus control, or VC) and uninfected (cell only, or CC) controls, respectively (**Figure 3**).
3. Add 5 µL of heat-inactivated serum/plasma samples in row A (columns 1-10). Each sample will be in duplicate. With a multichannel pipette, mix the samples in the first row and move 50 µL of medium containing serum from row A to row B. Repeat this process up to the last row (**Figure 3**). Discard the remaining 50 µL.
4. Thaw the necessary number of PVs' aliquots and dilute to ≥ 10^4 RLU/mL. Add 50 µL of the diluted PV-containing medium to each well (from column 1 to column 11) using a multichannel pipette to reach a 1:1 dilution of heat inactivated serum/plasma to virus. Incubate at 37 °C and 5% CO_2, for 1 h to allow the antibodies in the serum samples to bind to the SARS-CoV-2 spike protein on the PVs.
5. Prepare at least 5 mL suspension of susceptible cells (HEK293T/ACE2) at a cell density of 4 x 10^5 cells/mL. Add 50 µL of the cell suspension to each well and incubate at 37 °C and 5% CO_2, for 48 h.
6. After the incubation, perform the luciferase assay reading according to the manufacturer's instructions, as described in step 2.7.

   NOTE: The luminometer used for luciferase readout will produce a spreadsheet file (in this case, .xlsx) with the raw, unprocessed data that will be used for downstream analysis (the Luciferase assay file).

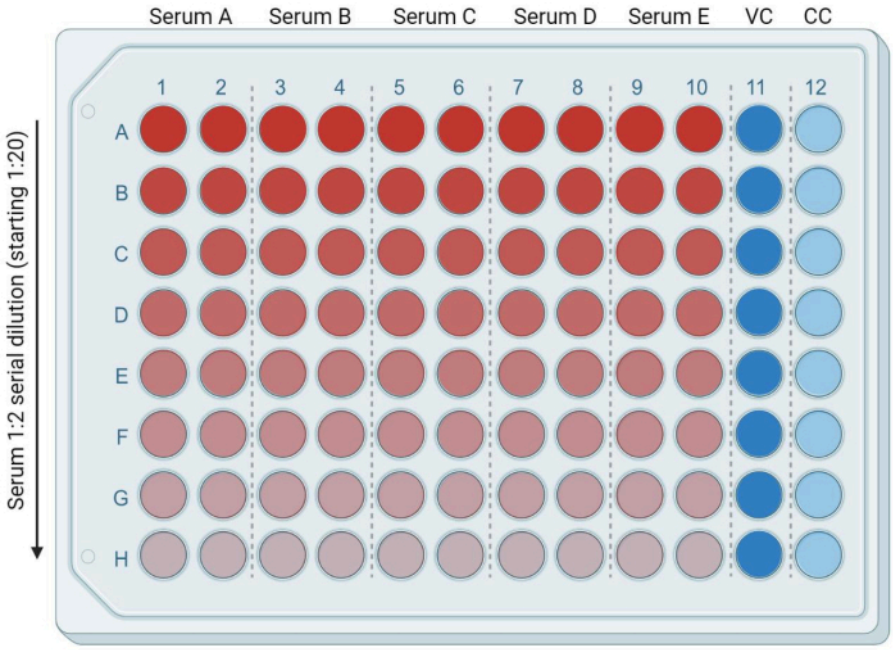

Figure 3: Plate representation based on serum dilution. Bright red corresponds to a higher quantity of serum, and bright blue lane (column 11) corresponds to infected cell control (VC, virus control). Light blue lane (column 12) corresponds to uninfected cells (CC, cell control). This figure was created with BioRender. Please click here to view a larger version of this figure.

4. Titration analysis

1. On the Luciferase assay file, assign the names/titles to the corresponding samples.
2. Multiply the RLU measure by the dilution factors (from the top to the bottom of the grid: 20x, 40x, 80x, 160x, 320x, 640x, 1,280x, 2,560x) to obtain RLU/mL. If different dilution factors are used, change the multiplication factors accordingly.
3. Calculate the average RLU/mL for each PV preparation.

5. PVs neutralization assay analysis

1. On the Luciferase assay spreadsheet file (in this case, .xlsx), assign the corresponding titles to the tested samples. Enter the dilution factor of the sample (40s, 80x, 160x, 320x, 640x, 1,280x, 2,560x, 5,120x). Calculate the Log10 of the dilution factors.
2. Calculate the average RLU of uninfected and infected control (**Figure 3**, columns 11 and 12, respectively). These values will be useful for the normalization in step 5.5.

3. Open a new document for data analysis. Select **X/Y analysis**, input X as **Numbers** and Y as **Enter 2 replicate values in side-by-side sub-columns**.
4. Enter Log10 (dilution) values as X numbers. Enter the duplicate RLU of the samples.
5. Go to **Analyze > Normalize > Flag all** the samples on the same sheet. Input the average VC and CC values in **How is 0% defined?**, and **How is 100% defined?**, respectively. Click **OK**.
6. On the normalized data sheet, go to **Analyze > XY analyses > Nonlinear analyses (curve fit)**. Flag all the samples and click **OK**. For the **Dose-response - Inhibition**, select **log(inhibitor) vs normalized response - variable slope**.
7. Under **Constrain**, change **HillSlope** to **Must be less than 0**.
8. Under **Output**, flag **Create summary table and graph**. Click on **OK** to obtain the final analyses. A working sheet with a template for the analysis is provided in **Supplementary File 1**.

Representative Results

This protocol describes the production of SARS-CoV-2 PVs and a downstream application of these PVs to analyze the neutralization activity of serum/plasma of subjects receiving anti-COVID-19 vaccination[17]. Furthermore, this protocol can be applied to produce pseudotypes of each SARS-CoV-2 variant of concern (VOC) to test the evolution of the neutralizing response. Despite this protocol facilitating the study of humoral immune response after COVID-19 vaccination, it can be adapted to easily test the neutralization of different sera/plasma against different viruses[13,18,19].

Figure 4A represents the increment of the dilution of serum (Log(dilution)) corresponding to the increase of the RLU signal. Thus, the higher the dilution of the sample, the less blocked the virus entry is (**Figure 4A**). This is further expressed as a percentage of neutralization (**Figure 4B**).

The IC50 result shows the neutralization capacity of a single vaccine serum over time. In the example reported in **Figure 4C**, the subject developed a strong humoral activity against the virus at four weeks after vaccination; however, after 16 weeks the IC50 is similar to the one prior to vaccine administration. In this case, the PVNA showed the loss of neutralization potential over time.

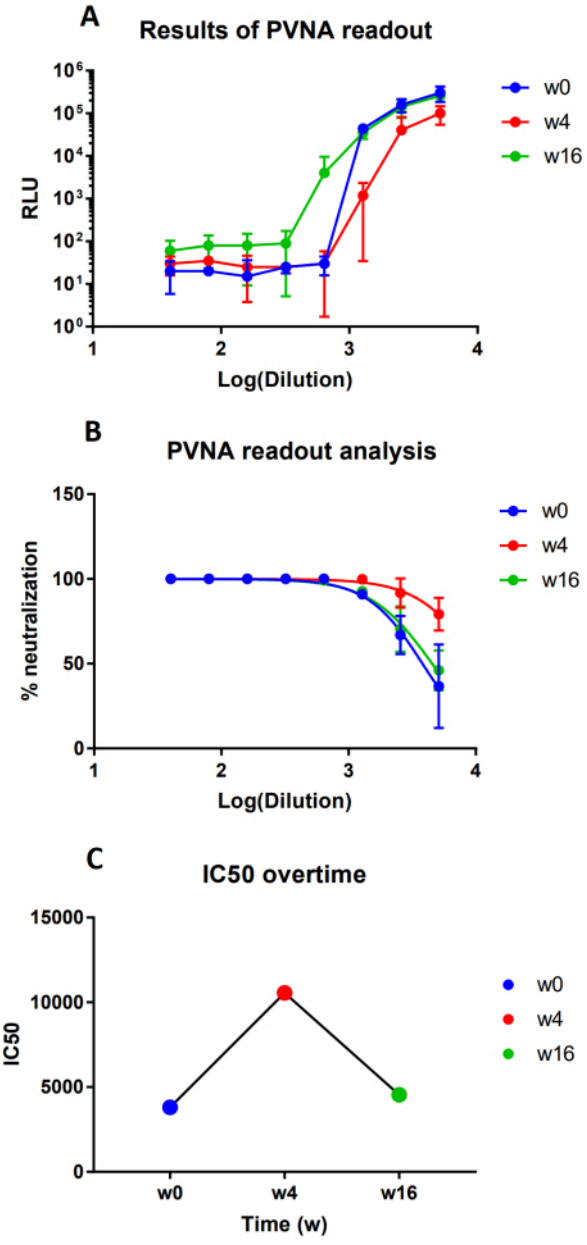

Figure 4: Representative results of PVNA. (**A**) Infectivity (RLU, and (**B**) percentage of neutralization are shown at week 0 (W0, before the vaccination); W4 (four weeks after vaccination); W16 (sixteen weeks after W0). (**C**) IC50 values at the same time points. Please click here to view a larger version of this figure.

Supplementary File 1: Neutralization analysis template. A working sheet with a template for conducting the neutralization analysis. Please click here to download this File.

Discussion

Although using a wildtype virus simulates the actual infection, lentiviral PVs are a safer option to study the mechanisms associated with viral entry and infection without the strict safety requirements necessary to work with pathogenic viruses[4,20,21]. PVs are composed of a replication-defective viral core surrounded by the surface envelope glycoprotein of a pathogenic virus which is the objective of the study.

HIV-1-based PVs are one of the most widely used platforms and these have been employed in this protocol for the production of SARS-CoV-2 pseudoviral particles. The reporter gene can be different as per the use of the PVs; in this case, the choice of the luciferase reporter gene provides an easy, fast, and sensitive readout of the infectivity of the produced PVs.

PVs based on lentiviruses are widely applied to study anti-HIV-1 humoral response[22]. The PV technology was instantly applied during the recent COVID-19 pandemic, caused by SARS-CoV-2. SARS-CoV-2 is a highly pathogenic human *Betacoronavirus*, identified for the first time in China (Wu Han) which became rapidly pandemic, causing more than 6 million deaths worldwide[23,24]. Because of the validation of vaccine strategies, the pandemic has been largely controlled; nonetheless, in most vulnerable people, such as cancer patients or people living with HIV, it does still pose a risk[25,26,27]. In this context, there is still a need for validated assays to monitor the anti-vaccine humoral response in terms of neutralizing activity. In this article we have described a simple protocol that can be easily be performed in laboratories with no access to category-3 containment. Furthermore, the PV platform is a versatile system to study different SARS-COV-2 virus variants. Indeed, by changing the envelope-expressing plasmid with different spikes, it is possible to generate PVs of SARS-CoV-2 new variants or of any other coronaviruses[28]. These virus portfolios can be used to assess the reactivity of vaccine-induced humoral response against the different variants of concern[15, 29,30,31,32]. This information can guide the generation of new and more effective vaccines.

Three major obstacles could be encountered while following this protocol concerning transfection conditions, titration failure and/or neutralization assay. First, the packaging cells may not be sufficiently confluent at the time of transfection. This may be due to the lack of nutrients. Ensure that step 1.1. is properly followed. Otherwise, perform seeding in the morning of the day before transfection and transfect the packaging cells later the next day to increase the growth time. A recurring problem is the potential contamination of the cell medium between transfection and medium replacement the next day. In this case, repeat the procedure by increasing the sterilization procedure before use when working under the BSL2 hood or include antibiotics to avoid unwanted contaminations. Second, an undetected luciferase signal may occur that can be attributed to various stages of PVs production or the characteristics of the target cell line. Plasmids should be extracted with endotoxin-free kits. The transfection step is critical for the outcome of the protocol. PEI reagent must be prepared at the correct concentration of 1 mg/mL. Gently flicking the tube during the preparation of transfection mixes enhances the formation of DNA-PEI complexes. To verify that the cells have been transfected correctly, it is recommended to perform the luciferase assay immediately after harvesting the cells. In addition, include a control virus envelope glycoprotein such as VSV: VSV-PVs give strong RLU signals on human cell lines. Moreover, it is necessary to mention that the target cell line must express

the receptor, which is easily verified via western blot or flow cytometry.

This method has been previously optimized[16] with respect to the experimental conditions, including the selection of the transfection reagent, the determination of the ratios between the different plasmids needed for the generation of the PV, and the selection of the target cell lines, the use of luciferase as reporter genes. Nonetheless, each laboratory will need to validate the proposed methods according to the available equipment. For example, (step 2.7) requires the addition of 100 µL of Luciferase substrate as suggested by the producer: this is optimal for the readout of the luciferase assay with the plate reader that is currently available. On the other hand, other laboratories that are equipped with a different plate reader may adapt the protocol using different luciferase substrates or volumes of the reagent[33]. Furthermore, other authors have proposed the use of the green fluorescent protein (GFP) as a reporter gene instead of the luciferase. This could be considered if a laboratory is fully equipped for GFP readout but not luciferase[34,35].

To conclude, PVs are a flexible and straightforward system that allows quantifying the infection by using a simple detection method. It represents a cost-effective approach that is more accessible for many research groups and allows avoiding the use of pathogenic viruses that require a biosafety level 3 laboratory[21]. The use of PVs represents a well-characterized and safe approach to studying antibody-mediated neutralization in individuals who experienced SARS-CoV-2 infection and/or vaccination.

Disclosures

The authors declare to have no conflict of interest.

Acknowledgments

We acknowledge the contribution of the health-care workers volunteers. This project was supported by the Department of Excellence 2023/2027, MUR, Italy. AR and DZ were supported by PRIN2022 (EU fundings; NextGenerationEU)

References

1. Ozaki, D. A. et al. International technology transfer of a GCLP-compliant HIV-1 neutralizing antibody assay for human clinical trials. *Plos One.* **7** (1), e30963 (2012).
2. Pouget, M. et al. Generation of liposomes to study the effect of Mycobacterium tuberculosis lipids on HIV-1 cis- and trans-infections. *International Journal of Molecular Sciences.* **22** (4), 1945 (2021).
3. McKay, L. G. A. et al. The HCV envelope glycoprotein down-modulates NF-κB signalling and associates with stimulation of the host endoplasmic reticulum stress pathway. *Frontiers in Immunology.* **13**, 831695 (2022).
4. Xiang, Q., Li, L., Wu, J., Tian, M., Fu, Y. Application of pseudovirus system in the development of vaccine, antiviral-drugs, and neutralizing antibodies. *Microbiological Research.* **258**, 126993 (2022).
5. Li, Q., Liu, Q., Huang, W., Li, X., Wang, Y. Current status on the development of pseudoviruses for enveloped viruses. *Reviews in Medical Virology.* **28** (1), e1963 (2018).
6. D'Apice, L. et al. Comparative analysis of the neutralizing activity against SARS-CoV-2 Wuhan-Hu-1 strain and variants of concern: Performance evaluation of a pseudovirus-based neutralization assay. *Frontiers in Immunology.* **13**, 981693 (2022).

7. Falzarano, D., Groseth, A., Hoenen, T. Development and application of reporter-expressing mononegaviruses: current challenges and perspectives. *Antiviral Research.* **103**, 78-87 (2014).
8. Gutierrez-Guerrero, A., Cosset, F.-L., Verhoeyen, E. Lentiviral vector pseudotypes: Precious tools to improve gene modification of hematopoietic cells for research and gene therapy. *Viruses.* **12** (9), 1016 (2020).
9. Zufferey, R., Nagy, D., Mandel, R. J., Naldini, L., Trono, D. Multiply attenuated lentiviral vector achieves efficient gene delivery in vivo. *Nature Biotechnology.* **15** (9), 871-875 (1997).
10. Dull, T. et al. A third-generation lentivirus vector with a conditional packaging system. *Journal of Virology.* **72** (11), 8463-8471 (1998).
11. Berkhout, B. A Fourth generation lentiviral Vector: Simplifying genomic gymnastics. *Molecular Therapy.* **25** (8), 1741-1743 (2017).
12. Wu, X. et al. Development and evaluation of a pseudovirus-luciferase assay for rapid and quantitative detection of neutralizing antibodies against Enterovirus 71. *Plos One.* **8** (6), e64116 (2013).
13. Ferrara, F. et al. Development of lentiviral vectors pseudotyped with Influenza B hemagglutinins: application in vaccine immunogenicity, mAb potency, and sero-surveillance studies. *Frontiers in Immunology.* **12**, 661379 (2021).
14. Hu, J. et al. Development of cell-based pseudovirus entry assay to identify potential viral entry inhibitors and neutralizing antibodies against SARS-CoV-2. *Genes & Diseases.* **7** (4), 551-557 (2020).
15. Dalle Carbonare, L. et al. Serology study after BTN162b2 vaccination in participants previously infected with SARS-CoV-2 in two different waves versus naïve. *Communications Medicine.* **1** (1), 38 (2021).
16. Di Genova, C. et al. Production, titration, neutralisation, storage and lyophilisation of severe acute respiratory syndrome coronavirus 2 (SARS-CoV-2) lentiviral pseudotypes. *Bio-protocol.* **11** (21), e4236 (2021).
17. Chmielewska, A. M., Czarnota, A., Bieńkowska-Szewczyk, K., Grzyb, K. Immune response against SARS-CoV-2 variants: The role of neutralization assays. *NPJ Vaccines.* **6** (1), 1-8 (2021).
18. Chen, Q. et al. Development and optimization of a sensitive pseudovirus-based assay for HIV-1 neutralizing antibodies detection using A3R5 cells. *Human Vaccines & Immunotherapeutics.* **14** (1), 199-208 (2018).
19. Gauger, P. C., Vincent, A. L. Serum virus neutralization assay for detection and quantitation of serum neutralizing antibodies to influenza A virus in swine. *Methods in Molecular Biology (Clifton, N.J.).* **2123**, 321-333 (2020).
20. Miglietta, R., Pastori, C., Venuti, A., Ochsenbauer, C., Lopalco, L. Synergy in monoclonal antibody neutralization of HIV-1 pseudoviruses and infectious molecular clones. *Journal of Translational Medicine.* **12** (1), 346 (2014).
21. Chen, M., Zhang, X.-E. Construction and applications of SARS-CoV-2 pseudoviruses: A mini review. *International Journal of Biological Sciences.* **17** (6), 1574-1580 (2021).
22. Zipeto, D. et al. Induction of human immunodeficiency virus neutralizing antibodies using fusion complexes. *Microbes and Infection.* **8** (6), 1424-1433 (2006).

23. *WHO Coronavirus (COVID-19) Dashboard.* at <https://covid19.who.int>. (2023).
24. Zhou, P. et al. A pneumonia outbreak associated with a new coronavirus of probable bat origin. *Nature.* **579** (7798), 270-273 (2020).
25. Chen, X., Huang, H., Ju, J., Sun, R., Zhang, J. Impact of vaccination on the COVID-19 pandemic in U.S. states. *Scientific Reports.* **12** (1), 1554 (2022).
26. Stefani, C., Fantoni, T., Bissoli, M., Thomas, J., Ruggiero, A. HIV and SARS-CoV-2 Co-Infection: From Population Study Evidence to In Vitro Studies. *Life.* **12** (12), 2089 (2022).
27. Watson, O. J. et al. Global impact of the first year of COVID-19 vaccination: a mathematical modelling study. *The Lancet Infectious Diseases.* **22** (9), 1293-1302 (2022).
28. Cantoni, D. et al. Analysis of antibody neutralisation activity against SARS-CoV-2 variants and seasonal human coronaviruses NL63, HKU1, and 229E induced by three different COVID-19 vaccine olatforms. *Vaccines.* **11** (1), 58 (2023).
29. Siracusano, G. et al. Different decay of antibody response and VOC sensitivity in naïve and previously infected subjects at 15 weeks following vaccination with BNT162b2. *Journal of Translational Medicine.* **20** (1), 22 (2022).
30. Ruggiero, A. et al. SARS-CoV-2 vaccination elicits unconventional IgM specific responses in naïve and previously COVID-19-infected individuals. *eBioMedicine.* **77** (2022).
31. Piubelli, C. et al. Subjects who developed SARS-CoV-2 specific IgM after vaccination show a longer humoral immunity and a lower frequency of infection. *eBioMedicine.* **89**, 104471 (2023).
32. Zhang, G. F. et al. Infectivity of pseudotyped SARS-CoV-2 variants of concern in different human cell types and inhibitory effects of recombinant spike protein and entry-related cellular factors. *Journal of Medical Virology.* **95** (1), e28437 (2023).
33. da Costa, K. A. S. et al. Influenza A (N1-N9) and Influenza B (B/Victoria and B/Yamagata) neuraminidase pseudotypes as tools for pandemic preparedness and improved influenza vaccine design. *Vaccines.* **10** (9), 1520 (2022).
34. Condor Capcha, J. M. et al. Generation of SARS-CoV-2 spike pseudotyped virus for viral entry and neutralization assays: a 1-week protocol. *Frontiers in Cardiovascular Medicine.* **7**, 618651 (2021).
35. Diomede, L. et al. Doxycycline inhibition of a pseudotyped virus transduction does not translate to inhibition of SARS-CoV-2 infectivity. *Viruses.* **13** (9), 1745 (2021).

A precise characterisation of peptide binding stability to HLA-C alleles and correlation with the progression of HIV-1 infection and HIV-1 related neurocognitive impairment

Mauro Voi[1], A. Sangalli[1], E.G. Milano[2], C. De Martinis[1], E. Orlandi[1], S. Tamburin[1], E. Mantovani[1], A. Federico[1], M. Lanzafame[3,4], E. Lattuada[3], G. A. Arganaraz[5], B.C.M. Da Silva[6], A.J. Duarte Da Silva[6], J. Casseb[7], E.R. Arganaraz[5], A. Ruggiero[1], M.T. Valenti[1], G. Grazioso[2], D. Zipeto[1]

[1]Department of Neurosciences, Biomedicine and Movement Sciences, University of Verona, Verona, Italy
[2]Department of Pharmaceutical Sciences, University of Milan, Milan, Italy.
[3]Unit of Infectious Diseases, Santa Chiara Hospital, Azienda Provinciale per i Servizi Sanitari, Trento, Italy
[4]Centre for Medical Sciences (CISMED), University of Trento, Trento, Italy
[5]Lab of Molecular Neurovirology, Faculty of Health Science, University of Brasilia, Brasilia, Brazil
[6]Medical Investigation Laboratory Unit 56 (LIM/56), Faculdade de Medicina FMUSP, University of São Paulo, São Paulo,Brazil
[7]Faculty of Medicine, Institute of Tropical Medicine, University of São Paulo, São Paulo, Brazil

Background. The molecular binding stability of HLA-C to the β2-microglobulin/peptide complex influences HIV-1 progression and HIV-1 association with neurocognitive impairment.
Materials and Methods. The NetMHCpan4.1 tool was used to predict the binding affinity of peptides specific to the most common human HLA-C allotypes, expressed as Eluted Ligand score (EL-score). The EL-score was plotted against the peptide ranking percentile, and a stability score was determined by calculating the area under the curve (AUC) for each HLA-C allele.
Naïve, HIV-1 infected subjects showing a different rate of HIV-1 progression and HIV-1 subjects presenting or not neurocognitive impairment were genotyped for HLA-C. Each patient's stability score was calculated and analysed for correlations with HIV-1 progression and neurocognitive impairment.
Results. The peptide binding score curves relative to ranking percentage highlighted differences in HLA-C allele stability. C*05:01 and C*08:02 were the most stable among the considered alleles, while C*07:04, C*07:01, and C*08:01 were the least stable. Individuals with slower progression to AIDS had significantly higher HLA-C stability scores than those with rapid HIV-1 progression ($P = 0.0113$). Furthermore, HIV-infected patients with neurocognitive impairment exhibited significantly lower HLA-C stability scores than those without ($P = 0.0074$).
Conclusion. Peptide binding analysis and AUC calculations provided an effective method for classifying HLA-C stability, overcoming the previous stable-unstable binary classification. The observed correlation between HLA-C stability scores and HIV-1 disease progression revealed that lower stability scores were associated with both accelerated progression to AIDS and the presence of neurocognitive impairment. These findings highlight the potential prognostic value of HLA-C stability in HIV-1 infection and suggest that targeting HLA-C-peptide interactions could be explored as a novel therapeutic approach.

Abstract

20th SIBBM Seminar Frontiers in Molecular Biology

Naples, Italy • 17-19 June 2025

Editing RUNX2 KO in B16 melanoma cells with Crispr-Cas9 as a potential strategy to enhance *in vivo* tumor response to therapeutic approaches

Carola De Martinis[1], E.G. Dobre[2], M. Voi[1], E. Orlandi[1], M. Bissoli[1], C. Constantin[2], M. Neagu[2], D. Zipeto[1], M. T. Valenti[1]
[1]Department of Neurosciences, Biomedicine and Movement Sciences, University of Verona, Verona, Italy
[2]Immunology Laboratory, "Victor Babes" National Institute of Pathology, Bucharest, Romania

Background: Cutaneous melanoma (CM) is a heterogeneous and highly metastatic disease with variable clinical behavior, for which the most effective pharmacological strategies are still being sought.
RUNX2 is a transcription factor involved in many pathways, such as apoptosis, Epithelial-Mesenchymal Transition (EMT), and stem cell function, affecting WNT, NOTCH, BMP, and RAS signaling.
The present study presents the workflow for RUNX2 knockout (KO) generation in B16 melanoma cells, an approach that may contribute to defusing CM resistance to targeted and immune therapy.
Material and methods: Two gRNAs targeting exon 4 of RUNX2 were designed and cloned into pX459v2.0 plasmid. The B16 melanoma cells were transfected with 2.5 µg of plasmid DNA by Lipofectamine 3000 in DMEM (w/o antibiotics). After 24 hours, cells were selected with complete DMEM containing 1µg/mL puromycin for six days. Cells were further subjected to monoclonal cell isolation by seeding 0.3 cells/well into 96-well plates. Genomic DNA was extracted from isolated clones, PCR-amplified with primers spanning the gRNA-targeting region and subjected to Sanger sequencing. RUNX2 KO was confirmed by Western blot.
Results: Clones with a 108 bp-deletion showed by PCR were selected for Sanger sequencing and western blot analysis. Seven B16 clones showed editing events by sequencing. In particular, four clones showed in-frame deletion within the Runt domain of the RUNX2 gene. Three clones displayed heterozygous editing. These seven clones showed no RUNX2 protein expression by western blot.
Conclusions: Our study presents the workflow for obtaining genetically engineered melanoma cells that may be further exploited to dissect the biological roles of RUNX2 in B16 melanoma syngeneic mouse models.

Abstract
20th SIBBM Seminar Frontiers in Molecular Biology
Naples, Italy • 17-19 June 2025

CRISPR/Cas9-mediated generation of HADHA KO PANC-1 cells to study the role of HADHA in pancreatic cancer stemness

Mauro Voi[1], A. Dezhgir[1], G. Siragusa[2], A. Ruggiero[1], D. Cecconi[2], D. Zipeto[1]
[1]Department of Neurosciences, Biomedicine and Movement Sciences, University of Verona, Verona, Italy
[2]Department of Biotechnology, University of Verona, Verona, Italy

Background. The CRISPR/Cas9 technique was applied to generate HADHA KO PANC-1 cells to depict the role of HADHA in stemness of pancreatic cancer stem cells (PCSCs).
Methods. Two different gRNAs targeting exon 1 of the HADHA gene were designed and cloned into Cas9-expressing plasmids. Parental PANC-1 (P) cells were transfected with Cas9/gRNA plasmids to generate HADHA-KO cells. Individual clones were isolated and analysed by Western Blot and Sanger sequencing of the edited region. To obtain PCSCs, P cells were cultured in a specific "stem selective medium." Tumoursphere formation was imaged after 5,10,15 days using the EVOS FL Imaging System.
Results. Different transfection protocols were tested on PANC-1 cells, with Lipofectamine3000 giving the best results of transfection efficiency, albeit moderate. We identified a clone (C8E12) showing the absence of the HADHA protein by Western Blot. Sanger sequencing revealed a heterozygous editing on the gRNA-targeted region, with a 124-bp and a 78-bp deletion on the two different alleles. Induction of dedifferentiation on the KO clone showed that HADHA knockout does not alter the stemness of the pancreatic cancer cell line: the KO clone is still able to grow in suspension and to remain undifferentiated. HADHA KO-PCSCs exhibited the formation of more compacted and denser tumourspheres than WT-PCSCs.
Conclusion. The low transfection efficiency on PANC-1 cells led to the identification of a single HADHA KO clone after the application of the CRISPR/Cas9 technique. The effect of the absence of HADHA expression was evaluated on PCSC morphology. KO cells retain the ability to form spheres, although morphologically they appear more compact and show denser structures than their WT counterpart. However, the effects of HADHA knockout on PCSC proliferation, chemoresistance, and tumour migration should be further investigated to understand its role in PCSCs biology and its potential as therapeutic target in pancreatic cancer.

Abstract

19th SIBBM Seminar Frontiers in Molecular Biology

Trento, Italy • 17-19 June 2024

The absence of the human thioesterase ACOT8 negatively affects HIV-1 infectivity *in vitro*

Michele Bissoli[1], M. Voi[1], A. Dezhgir[1], A. Campese[1], C. Stefani[1], J.F. Palmeira[2], E.R. Argañaraz[2], A. Ruggiero[1], D. Zipeto[1]
[1]Department of Neurosciences, Biomedicine and Movement Sciences, School of Medicine - University of Verona, Italy
[2]Laboratory of Molecular Neurovirology, Faculty of Health Science, University of Brasilia, Brazil

During the replicative cycle of HIV-1, a broad spectrum of interactions between viral and host proteins occurs. Among these, the thioesterase ACOT8 has been reported to interact with the HIV-1 Nef protein. Here we study the effect of ACOT8 depletion on HIV-1 infectivity.
CRISPR/Cas9 was used to knock-out ACOT8 gene in HEK293T cells. Knock-out was verified by Sanger sequencing and Western blot. Off-target analysis was performed by Cas-OFFinder web tool, and the most likely sites were amplified by PCR followed by Sanger sequencing. HIV-1 pseudotyped viruses were produced in wild type and ACOT8 knock-out HEK293T cells and titrated by HIV-1 p24 quantification. The same viral input was used to infect the TZM-bl cell line, allowing quantification of viral infectivity by Luciferase detection. A rescue experiment was performed by transfecting the knock-out cells with a plasmid encoding for ACOT8 to further verify the absence of off-target due to CRISPR/Cas9. The Mann-Whitney test was used to detect statistically significant differences between the viral infectivity in presence or absence of ACOT8.
HEK293T knock-out clones obtained exhibit non-in-frame deletions in the ACOT8 region. The absence of protein expression was verified by Western blot. Knock-out clones show no modifications in the predicted off-target sites.
HIV-1 pseudotyped viruses showed lower infectivity when produced in absence of ACOT8 than when produced in its presence (p-value<0.0001). In contrast, no significant differences were observed using the control envelope of VSV. Pseudotyped virus produced in knock-out cells in which ACOT8 expression was restored showed comparable levels of infectivity to virus produced in HEK293T wild type cells.
Our preliminary data suggest that ACOT8 absence in cells producing HIV-1 pseudotyped virus is associated with reduced viral infectivity. Further experiments are underway to characterize the mechanisms modulating infectivity and other factors involved in this interaction.

Abstract

19th SIBBM Seminar Frontiers in Molecular Biology

Trento, Italy • 17-19 June 2024

Human thioesterase ACOT8 has an impact on *in vitro* HIV-1 infectivity

Michele Bissoli[1], C. Stefani[1], M. Voi[1], R. Casula[1], A. Corsi[1], M.G. Romanelli[1], E.R. Argañaraz[2], J.F. Palmeira[2], A. Ruggiero[1], D. Zipeto[1]

[1]Dept of Neurosciences, Biomedicine and Movement Sciences, School of Medicine - University of Verona, Italy

[2]Laboratory of Molecular Neurovirology, Faculty of Health Science, University of Brasilia, Brazil

Introduction. HIV-1 establishes a broad spectrum of interactions with host proteins, including the cellular thioesterase ACOT8, presumably mediated by interactions with the HIV-1 Nef protein. This work investigates the impact on HIV-1 infectivity of ACOT8 depletion during HIV-1 viral particle production.

Methods. CRISPR/Cas9 technology was used to knock-out the ACOT8 gene in HEK293T and TZM-bl cells. HEK293T wild type and knock-out cells were used to produce HIV-1 pseudotyped viruses with different HIV-1 envelopes (the CCR5 tropic QHO, AC-10 and pRHPA and the CXCR4 tropic LAI). Virus titers were assessed by quantification of HIV-1 p24 and the same input was used for infections on TZM-bl wild type and ACOT8 knock-out cell lines; infectivity was evaluated as Relative Luminescence Units (RLU). The Mann-Whitney test was applied to detect statistically significant differences between the infectivity of pseudotyped virus produced in the presence or absence of ACOT8, and in the presence of absence of Nef.

Results. The different HIV-1 envelopes tested showed higher infectivity when pseudotyped viruses were produced in the presence of ACOT8 rather than when they were produced in its absence (QHO, $p= 0.0011$), even when Nef was not present (QHO, p-value<0.0001, AC10, $p=0.0019$, pRHPA, $p<0.0001$, LAI, $p<0.0001$). In contrast, no difference was observed with the VSV envelope control. No differences were found by infecting TZM-bl target cells with or without ACOT8. This suggests that ACOT8 might play a role in increasing HIV infectivity at the pre-entry level.

Conclusions. Our preliminary data suggest that expression of ACOT8 in cells producing HIV-1 pseudotyped virus is associated with increased viral infectivity. Further experiments are needed to better define the mechanisms that modulate virion infectivity and any other factors involved in this interaction.

Abstract

18th SIBBM Seminar Frontiers in Molecular Biology

Bari, Italy • 26-28 June 2023

A precise characterization of peptide binding stability to HLA-C alleles and correlation with the progression of HIV-1 infection and HIV-1 related neurocognitive impairment

Mauro Voi[1], A. Sangalli[1], E. G. Milano[2], C. De Martinis[1], E. Orlandi[1], S. Tamburin[1], E. Mantovani[1], A. Federico[1], M. Lanzafame[3,4], E. Lattuada[3], G. A. Arganaraz[5], B. C. M. Da Silva[6], A. J. Duarte Da Silva[6], J. Casseb[7], E. R. Arganaraz[5], A. Ruggiero[1], M. T. Valenti[1], G. Grazioso[2], D. Zipeto[1]

[1] Department of Neurosciences, Biomedicine and Movement Sciences, University of Verona, Verona, Italy.
[2] Department of Pharmaceutical Sciences, University of Milan, Milan, Italy.
[3] Unit of Infectious Diseases, Santa Chiara Hospital, Azienda Provinciale per i Servizi Sanitari, Trento, Italy.
[4] Centre for Medical Sciences (CISMED), University of Trento, Trento, Italy.
[5] Lab of Molecular Neurovirology, Faculty of Health Science, University of Brasilia, Brasilia, Brazil.
[6] Medical Investigation Laboratory Unit 56 (LIM/56), Faculdade de Medicina FMUSP, University of São Paulo, São Paulo,Brazil
[7] Faculty of Medicine, Institute of Tropical Medicine, University of São Paulo, São Paulo, Brazil

Introduction

HLA-C is a highly polymorphic gene encoding the alpha chain of the HLA class I C molecule, a component of the major histocompatibility complex (MHC). Within the complex, the α chain is associated with beta-2-microglobulin (β_2m) and an antigenic peptide and plays a central role in immunity, especially against viral infections[1] (Fig.1). Each HLA-C allele may present a different degree of binding stability to the β_2m/peptide complex and this may have an impact on the immunological response[2]. Here, we analysed the binding affinity of specific peptide pools for 21 of the most frequent HLA-C allotypes and defined stability scores for each of them. The scores were then correlated with the HLA-C genotype of HIV-1 infected patients.

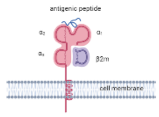

Figure 1. MHC-I complex. HLA-C molecule (in red) is expressed on cell membrane, and it binds with β2m and an antigenic peptide. Created with Biorender.

Workflow

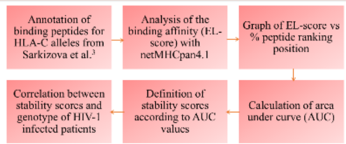

Figure 2. Bioinformatic and experimental workflow.

Materials and methods

Calculation of HLA-C stability score

Peptides 8–12 amino acids in length, specifically binding to the most prevalent human HLA-C allotypes, were identified by Sarkizova et al.[3]. The binding affinity scores (EL-score) of each peptide for the corresponding HLA-C allotype were calculated using NetMHCpan4.1 (https://services.healthtech.dtu.dk/services/NetMHCpan-4.1/) and plotted against the percentage of the peptide ranking position. The stability score for each of the considered HLA-C alleles was determined by calculating the corresponding Area Under the Curve (AUC).

Genotyping of HIV-1-infected patients

For our analysis, we considered two cohorts of HIV-1–positive patients. The first, previously analyzed by Stefani et al.[2], includes individuals with varying degrees of HIV-1 disease progression (Long Term Non Progressors, LTNP, n = 37; Progressors, P, n = 47), while the second cohort comprises individuals with or without neurocognitive impairment (ANI/HAD, n = 16; normal cognition, n = 41). Genomic DNA from patient-derived peripheral blood lymphocytes was analyzed by AS-PCR and Sanger sequencing to determine HLA-C allotypes at one-digit resolution, as previously described[2], and second-digit resolution for structurally divergent alleles (*03, *04, *07, *08, *12). A patient-specific HLA-C stability score was then calculated by multiplying the allele-specific AUC-derived scores and correlated with HIV-1 disease progression or the presence of neurocognitive impairment.

Results

1. Analysis of HLA-C alleles and binding peptides

A dataset of 36,070 experimentally validated peptides specifically binding to the 21 most frequent HLA-C allotypes was retrieved from Sarkizova et al.[3] For each HLA-C/peptide pool, binding predictions values (EL-score) were obtained using NetMHCpan-4.1 and then plotted against the percentage of peptide ranking position. From the generated curves, the area under the curve (AUC) was calculated to determine a stability score for each HLA-C variant.

ALLOTYPE	PEPTIDES NUMBER	FREQUENCY	Stability score (AUC)
C*01:02	1257	0.082	55.02
C*02:02	950	0.038	57.5
C*03:02	1194	0.025	57.14
C*03:03	2123	0.056	51.51
C*03:04	2235	0.081	54.75
C*04:01	1851	0.113	61.42
C*04:03	1098	0.019	55.32
C*05:01	1442	0.026	82
C*06:02	1124	0.063	55.74
C*07:01	858	0.090	30.79
C*07:02	1072	0.131	30.61
C*07:04	720	0.012	30.52
C*08:01	1002	0.046	34.84
C*08:02	1148	0.02	77.41
C*12:02	1403	0.032	49.58
C*12:03	2175	0.02	47.84
C*14:02	1371	0.025	71.03
C*14:03	2781	0.015	66.71
C*15:02	2221	0.034	57.09
C*16:01	2883	0.024	48.64
C*17:01	965	0.019	45.87

Table 1. The most frequent human HLA-C allotypes with the calculated stability score based on the binding to specific peptides.

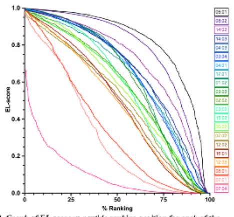

Figure 3. Graph of EL-score vs peptide ranking position for each of the considered HLA-C alleles.

The analysis of the EL-score distribution highlighted significant variations in HLA-C binding stability. Strong binders included C*05:01, C*08:02, and C*14:02, while C*07:04, C*07:01, and C*08:01 displayed low stability. Curves of HLA-C stability and the calculated stability scores are shown in Figure 3 and Table 1.

2. Correlation between HLA-C stability and HIV-1 progression

HLA-C typing enabled the calculation of a stability score linked to each patient's genotype, obtained by multiplying the stability values for each allotype, which was then correlated with different outcomes of HIV-1 infection. Specifically, clinical analysis confirmed a strong association between HLA-C stability and HIV-1 disease progression. HIV-1 individuals with a rapid progression to AIDS disease (Progressors, P) showed significantly lower stability scores than those with slower progression (Long Term Non Progressors, LTNP) ($p = 0.0113$, *Mann Whitney test*), supporting the hypothesis that unstable HLA-C alleles are linked to more severe disease outcomes (Fig. 4).

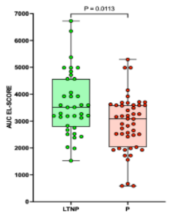

Figure 4. Correlation of patient HLA-C stability scores with HIV-1 progression .

3. Correlation between HLA-C stability and HIV-1 related neurocognitive impairment

The calculation of a patient-specific HLA-C stability score was used to correlate HLA-C stability with the presence of neurocognitive disorder in HIV-1 positive patients. In particular, subjects presenting neurocognitive impairment (ANI/HAD) showed reduced stability scores compared to cognitively normal patients (normal) ($p = 0.0164$, *Mann Whitney test),* supporting the hypothesis of a correlation between HLA-C stability and the development of neurological problems (Fig.5).

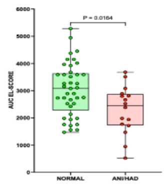

Figure 5. Correlation of patient HLA-C stability scores with HIV-1 related neurocognitive impairment.

Discussion

Different HLA-C variants show a different degree of association with β_2m/peptide complex, and this may have an influence with the response to certain viral infections, such as HIV-1. In this study, we selected 21 of the most frequent alleles and analysed their ability to bind specific peptides to each of them, to determine a stability score. This allowed us to give a more rigorous classification in the stability definition of the alleles considered, overcoming the previous coarse stable and unstable binary classification.

Analysis of two well-characterised cohorts of HIV-1 patients (evaluating progression to AIDS and neurocognitive impairment) showed a significant correlation between unstable HLA-C alleles, faster disease progression, and increased incidence of HIV-associated neurocognitive disorders. In this context, assigning a stability value to each HLA-C allotype enabled the calculation of a precise score for every patient based on their HLA-C genotype, paving the way for the use of the HLA-C profile as a clinical predictive marker for HIV-1 disease progression and neurocognitive risk assessment. A more comprehensive understanding may be achieved by increasing the number of patients in each group and by evaluating additional factors, such as HLA-C expression levels, which may correlate with the stability of the HLA-C/β2m/peptide complex and provide valuable clinical insights for future studies.

References

[1] Kulpa DA, Collins KL. The emerging role of HLA-C in HIV-1 infection. Immunology. 2011 Oct;134(2):116-22. doi: 10.1111/j.1365-2567.2011.03474.x.

[2] Stefani C, Sangalli A, Locatelli E, Federico T, Malerba G, Romanelli MG, Argañaraz GA, Da Silva BCM, Da Silva AJD, Casseb J, Argañaraz ER, Ruggiero A, Zipeto D. Increased Prevalence of Unstable HLA-C Variants in HIV-1 Rapid-Progressor Patients. Int J Mol Sci. 2022 Nov 27;23(23):14852. doi: 10.3390/ijms232314852.

[3] Sarkizova S, Klaeger S, Le PM, Li LW, Oliveira G, Keshishian H, Hartigan CR, Zhang W, Braun DA, Ligon KL, Bachireddy P, Zervantonakis IK, Rosenbluth JM, Ouspenskaia T, Law T, Justesen S, Stevens J, Lane WJ, Eisenhaure T, Lan Zhang G, Clauser KR, Hacohen N, Carr SA, Wu CJ, Keskin DB. A large peptidome dataset improves HLA class I epitope prediction across most of the human population. Nat Biotechnol. 2020 Feb;38(2):199-209. doi: 10.1038/s41587-019-0322-9.

mauro.voi@univr.it

Poster

20th SIBBM Seminar Frontiers in Molecular Biology

Naples, Italy • 17-19 June 2025

A precise characterization of peptide binding stability to HLA-C alleles and correlation with the progression of HIV-1 infection

Mauro Voi[1], Antonella Sangalli[1], Melania La Conca[1], Enrique Roberto Argañaraz[2], Donato Zipeto[1]

[1]Department of Neurosciences, Biomedicine and Movement Sciences, University of Verona, Verona, Italy
[2]Lab of Molecular Neurovirology, Faculty Of Health Science, University of Brasilia, Brasilia, Brasil.

PhD programme in Applied Life and Health Sciences
Cycle XXXVIII

Introduction

HLA-C is a highly polymorphic gene that encodes for the alpha chain of the major histocompatibility complex class I (MHC-I). Within the complex, the α chain is associated with beta-2-microglobulin (β_2-m) and an antigenic peptide and plays a central role in the immune system, especially against viral infections[1] (Fig.1). Each HLA-C allele may present a different degree of binding stability to the β_2m/peptide complex and this may have an impact on the immunological response[2]. Here, we analysed the binding affinity of specific peptide pools for each HLA-C allele and defined stability scores for 21 of the most frequent HLA-C alleles. We then correlated stability scores with the HLA-C genotype of HIV-1 infected patients.

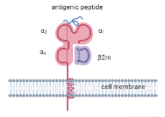

Figure 1. MHC-I complex. HLA-C molecule (in red) is expressed on cell membrane, and it binds with β_2-m and an antigenic peptide. *Created with Biorender*

Workflow

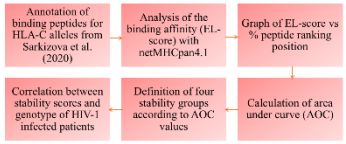

Figure 2. Bioinformatic and experimental workflow.

Materials and methods

Calculation of HLA-C stability score

Peptides specifically binding each of the most frequent human HLA-C allotypes were determined by Sarkizova et al. (2020)[3]. The binding affinity scores of each peptide for the corresponding HLA-C allotype were calculated using NetMHCpan4.1 and plotted against the percentage of the peptide ranking position. The stability score for each of the considered HLA-C alleles was determined by calculating the corresponding Area Under the Curve (AUC).

Genotyping of HIV-1-infected patients

A cohort of HIV-1-infected patients was previously characterized by Stefani et al. (2022)[2] based on immunovirological parameters, with different degrees of HIV-1 progression (LTNPs, Long Term Non Progressors; Ps, Progressors). Individuals with alleles other than those reported in Sarkizova et al. (2020) were not considered in this analysis. The final number of considered subjects was 77 (36 LTNPs, 41 Ps). For some of the already characterized allotype groups (HLA-C*07 and HLA-C*08), Sanger sequencing allowed the characterization of the HLA-C gene at the second digit. The AUC score for each HLA-C allele was multiplied and used to calculate the HLA-C stability score of each patient, and it was correlated with HIV-1 progression.

Results

1. Analysis of HLA-C alleles and binding peptides

A pool of binding peptides for each of 21 HLA-C alleles covering at least one allele in 95% of worldwide population was defined by Sarkizova et al. (2020). By plotting the peptide affinity score (EL-score) of each allele against the percentage of the peptide ranking position, we observed a different distribution for each HLA-C allele, reflecting a different range of stability (Fig.3).

HLA-C 03:03, 03:04 and 14:02, 14:03 were considered part of the same group as they possess the same binding affinity for the same peptides.

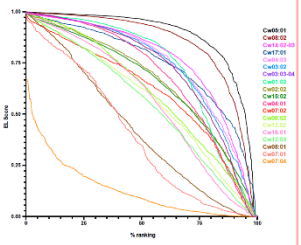

Figure 3. Graph of EL-score vs peptide ranking position for each of the considered HLA-C alleles.

2. Definition of four groups for HLA-C stability

AUC was calculated from the graph shown in figure 1 for each HLA-C allele.

The calculation of AUC allowed us to define four main groups (stable, S – mid stable, MS – mid unstable, MU – unstable, U) showing a different degree of stability.

The C*05:01 and C*08:02 HLA-C alleles were classified as the most stable, while the C*07:04, C*07:01 and C*08:01 alleles presented the lowest stability scores. Based on this classification, the C*12:02, C*12:03 and C*16:01 alleles were also grouped as unstable, while the rest of the alleles presented intermediate stability scores.

HLA-C allele	AUC	Stability groups
C*05:01	88.35	S
C*08:02	84.65	S
C*14:02 – 14:03	76.39	MS
C*17:01	74.70	MS
C*04:03	74.27	MS
C*03:02	73.82	MS
C*03:02	72.87	MS
C*03:03 – 03:04	72.17	MS
C*04:01	68.59	MU
C*02:02	65.73	MU
C*15:02	65.37	MU
C*07:02	60.82	MU
C*06:02	60.79	MU
C*12:02	57.09	U
C*16:01	56.56	U
C*12:03	54.95	U
C*08:01	42.36	U
C*07:01	39.19	U
C*07:04	13.18	U

Table 1. Classification into four stability groups according to AUC values. *HLA-C alleles were subdivided into four stability groups according to the following criteria: AUC>80 (stable, S), 70<AUC<80 (mid stable, MS), 70<AUC<60 (mid unstable, MS); AUC<60 (unstable U).*

3. Correlation between HLA-C stability and HIV-1 progression

HIV-1-infected patients with slower progression to AIDS (long-term non-progressors, LTNPs) show significantly higher (P=0.019, *Mann Whitney test*) AUC stability scores than subjects with faster HIV-1 progression (progressors, Ps), meaning that the presence of stable variants is associated to a slower progression of the disease (Fig. 4). The distribution of the different stability classes of HLA-C alleles between the two groups (LTNP and P) is statistically significant (P=0.0070, *chi-square test*).

Stability classification	LTNP	P
S	15	4
MS	6	10
MU	12	12
U	4	13
Total alleles	57	59

Table 2. Presence of HLA-C alleles belonging to the four different stability classes in the HIV-1 infected patients.

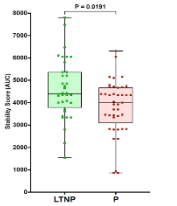

Figure 4. Correlation between stability scores and genotype of HIV-1 infected patients.

Discussion

Different HLA-C variants may show a different degree of association with β_2m/peptide complex, and this may have an influence with the response to certain viral infections, such as HIV-1. In this study, we selected 21 of the most frequent alleles and analysed their ability to bind specific peptides to each of them, to determine a stability score. This allowed us to give a more rigorous classification in the stability definition of the alleles considered, finding a significant correlation between HLA-C stability score and HIV-1 progression, with LTNP subjects having a genotype with higher stability score with respect to P patients. Greater statistical power can be achieved by increasing the number of subjects tested for each class, taking into account, however, that most alleles present an intermediate degree of stability with their own peptides. For some other allotype groups, as HLA-C*04, characterization of HLA-C allele at the second digit will be performed to better discriminate the stability class of each allele in the genotype of HIV-1 infected subjects.

References

[1] Kulpa DA, Collins KL. The emerging role of HLA-C in HIV-1 infection. Immunology. 2011 Oct;134(2):116-22. doi: 10.1111/j.1365-2567.2011.03474.x.

[2] Stefani C, Sangalli A, Locatelli E, Federico T, Malenba G, Romanelli MG, Argañaraz GA, Da Silva BCM, Da Silva AJD, Casseb J, Argañaraz ER, Ruggiero A, Zipeto D. Increased Prevalence of Unstable HLA-C Variants in HIV-1 Rapid-Progressor Patients. Int J Mol Sci. 2022 Nov 27;23(23):14852. doi: 10.3390/ijms232314852.

[3] Sarkizova S, Klaeger S, Le PM, Li LW, Oliveira G, Keshishian H, Hartigan CR, Zhang W, Braun DA, Ligon KL, Bachireddy P, Zervantonakis IK, Rosenbluh JM, Ouspenskaia T, Law T, Justesen S, Stevens J, Lane WJ, Eisenhaure T, Lan Zhang G, Clauser KR, Hacohen N, Carr SA, Wu CJ, Keskin DB. A large peptidome dataset improves HLA class I epitope prediction across most of the human population. Nat Biotechnol. 2020 Feb;38(2):199-209. doi: 10.1038/s41587-019-0322-9.

mauro.voi@univr.it

Poster

PhD Day - University of Verona – 26 September 2024

CRISPR/Cas9 generation of HADHA KO PANC-1 cells to study the role of HADHA in pancreatic cancer stemness

Mauro Voi[1], A. Dezhgir[1], G. Siragusa[2], A. Ruggiero[1], D. Cecconi[2], D. Zipeto[1]

[1] Department of Neurosciences, Biomedicine and Movement Sciences, University of Verona, Verona, Italy.
[2] Department of Biotechnology, University of Verona, Verona, Italy.

PhD programme in Applied Life and Health Sciences
Cycle XXXVIII

Introduction

CRISPR/Cas9 has rapidly changed the genome editing field and it has been widely applied to generate gene knockout cell lines, useful to understand the biological consequences of gene silencing in selected cell lines. The technique relies on the use of guide RNAs (gRNAs) and an endonuclease (Cas9) that mediate double strand break on a specific gRNA-targeted genomic region[1,2]. Here, we select the Hydroxyacyl-CoA Dehydrogenase Trifunctional Multienzyme Complex Subunit Alpha (HADHA) gene as target to knockout in human pancreatic cancer cells (PANC-1). The gene was found to be overexpressed in pancreatic cancer stem cells (PCSCs)[3]. Therefore, CRISPR/Cas9 was used to generate HADHA KO PANC-1 cells. The knockout cell line was then used to obtain pancreatic cancer stem cells (PCSCs) and the effect of HADHA absence was evaluated on the ability to form tumourspheres. While HADHA knockout did not alter the stemness of pancreatic cancer cells, HADHA KO-PCSCs display the formation of denser tumourspheres than WT-PCSCs.

Workflow

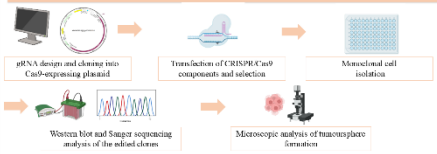

Figure 1. Experimental workflow.

Materials and methods

CRISPR/Cas9 generation of knockout cells

Two gRNAs targeting exon 1 of the HADHA gene were designed by using CRISPRscan and separately cloned into Cas9-expressing plasmids. GFP transfection was firstly used to assess transfection efficiency with Lipofectamine3000, Transit-LT1 and nucleofection. Both gRNA/Cas9 plasmids were then transfected into parental PANC-1 (P) cells by Lipofectamine3000, after optimization of the DNA:reagents ratio. After selection with puromycin, single cell cloning was performed by seeding 0.3 cells/well in 96-well plates. Individual clones were then tested by Western blot with anti-HADHA monoclonal murine antibody. Genomic DNA was extracted and Sanger sequencing was performed on the PCR-amplified gRNA-targeted region. The TOPO® TA Expression Kit was used to clone PCR products into the TOPO® vector and, following bacterial transformation, Sanger sequencing was performed on six isolated colonies. Final sequences were aligned with the reference WT sequence by EMBOSS Needle software. For each gRNA, the most probable off-target sites were selected by COSMID web tool. These top-ranked off-target genomic sites were then PCR-amplified, Sanger sequenced and aligned to the reference WT sequence.

Tumoursphere formation assay

PCSCs were obtained by culturing P cells in a specific "stem selective medium". Images of tumoursphere formation were taken after 5, 10, 15 days using the EVOS FL Imaging System. Only cell clusters >40µm were considered.

Results

1. Transfection optimization on PANC-1 cells

Transfection efficiency was tested by transfecting pEGFP plasmid into PANC-1 cells with Lipofectamine3000, Transit-LT1 and nucleofection. Lipofectamine3000 displays the best transfection efficiency, even if moderate (Fig.2).

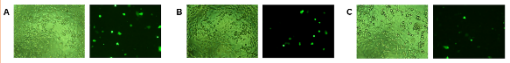

Figure 2. GFP transfection on PANC-1 cells. Lipofectamine3000 (A) shows a greater transfection efficiency than Transit-LT1 (B) and nucleofection (C).

Different Lipofectamine3000-based transfection conditions were evaluated in order to find the optimal one (Fig.3). Cells transfected with conditions 6 (1.5:4:1, ratio Lipofectamine 3000 – p3000 – DNA, with 5 µg DNA) and 8 (1.25:2:1, ratio Lipofectamine 3000 – p3000 – DNA, with 3 µg DNA) exhibit the best survival rate after puromycin selection and they were therefore subjected to single cell cloning, along with conditions 7-9 (pooled together) that display a lower survival percentage.

Figure 3. Lipofectamine3000 transfection optimization. *In each ratio, the first value refers to the amount of Lipofectamine3000 reagent, the second value to the amount of p3000 reagent, and the third value to the amount of DNA. In parentheses, the total amount of DNA is expressed in µg.*

2. Generation of HADHA KO PANC-1 cells

Western blot showed absence of the HADHA protein band in one (C8E12) of the tested clones (Fig.4).

The knockout was confirmed by Sanger sequencing, showing a 124-bp frameshift deletion on the first allele removing part of exon 1 and intron 1 and a 78-bp deletion on the second allele disrupting almost entirely exon 1 (Fig.5). Off-target analysis was conducted by selecting the two most probable off-target sites for each gRNA. All the off-target sites in the KO clone (C8E12) correspond to the WT sequence, meaning that no unintended off-target events have occurred in the predicted off-target sites (Fig.6).

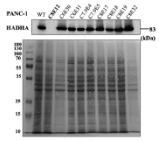

Figure 4. WB on the isolated clones. *Only one clone (C8E12) showed absence of the HADHA protein.*

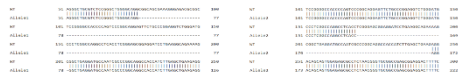

Figure 5. Alignment of the edited sample to the WT. *Allele 1 shows a 124bp-deletion, while allele 2 has a 78bp-deletion.*

Figure 6. Alignment of off-target sites of KO clone to the WT. *No off-target events occurred in the selected genomic sites.*

3. Tumoursphere formation of HADHA KO PCSCs

After induction of dedifferentiation, HADHA KO clone still retains the ability to grow in suspension and to remain undifferentiated, demonstrating that the absence of HADHA does not affect the stemness of this pancreatic cancer cell line. Microscopic analysis shows that KO-PCSCs tend to form larger and more compact tumourspheres than the WT-PCSCs (Fig.7).

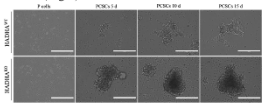

Figure 7. *Bright-field microscopic images of WT and HADHA KO P cells and PCSCs, at different days (5-10-15).*

Discussion

Since HADHA gene was found to be overexpressed in PCSCs, we generated HADHA KO PANC-1 cells to evaluate the effect of HADHA absence on pancreatic cancer stemness. PANC-1 cells appeared difficult to transfect, with Lipofectamine3000 yielding the best transfection efficiency results, albeit moderate. Among several tested clones, one resulted HADHA KO, as confirmed by Western Blot analysis and Sanger sequencing. KO cells do not lose the ability to undergo undifferentiation, meaning that the absence of HADHA does not alter the stemness of the pancreatic cancer cell line. However, the HADHA KO-PCSCs form denser and more compact structures than the WT-PCSCs. Starting from these preliminary results at the morphological level, the effect of the absence of HADHA will be next evaluated on proliferation, chemoresistance and tumour migration of PCSCs to better define HADHA role in PCSCs biology or its potential involvement as therapeutic target in pancreatic cancer.

References

[1] Ran, F. A. *et al.* (2013) 'Genome engineering using the CRISPR-Cas9 system.', *Nature protocols*, 8(11), pp. 2281–2308. doi: 10.1038/nprot.2013.143.

[2] Giuliano, C. J. *et al.* (2019) 'Generating Single Cell–Derived Knockout Clones in Mammalian Cells with CRISPR/Cas9', *Current Protocols in Molecular Biology*, 128(1). doi: 10.1002/cpmb.100.

[3] Di Carlo, C. *et al.* (2021) 'Integrated lipidomics and proteomics reveal cardiolipin alterations, upregulation of HADHA and long chain fatty acids in pancreatic cancer stem cells', *Scientific Reports*, 11(1), pp. 1–13. doi: 10.1038/s41598-021-92752-5.

mauro.voi@univr.it

Poster

19th SIBBM Seminar Frontiers in Molecular Biology

Trento, Italy • 17-19 June 2024

Application of CRISPR/Cas9 to generate knockout cell lines

Mauro Voi, Ali Dezhgir, Domenico Luca Minafra, Arianna Minoia, Giuliana Siragusa, Daniela Cecconi, Maria Teresa Valenti, Alessandra Ruggiero, Donato Zipeto.

PhD programme in Applied Life and Health Sciences

Cycle XXXVIII

Introduction

CRISPR/Cas9 is one of the most effective genome editing approaches to generate gene knockout cell lines, that can be used to investigate the biological consequences of gene knockout in selected cell lines[1]. The efficacy of the technique depends on several factors, as the good design of gRNA-targeting genes, transfectability of the chosen cell line and optimized conditions for the delivery of the CRISPR/Cas9 components. Here, we described CRISPR/Cas9 application to generate different KO cell lines by targeting genes that are involved in various biological processes. In particular, we applied CRISPR/Cas9 to knockout the ACOT8 gene in HEK293T that will be used to better depict the role of ACOT8 in HIV-1-host interaction[2]. HADHA was the targeted gene in PANC-1 cells aiming at studying the effect of this gene knockout on the growth of pancreatic cancer stem cells[3]. KO of FBXW11 will be investigated in osteosarcoma MG63 cells[4].

Workflow

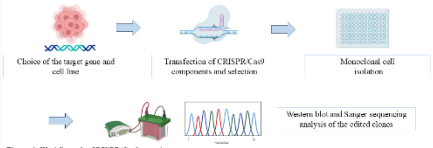

Figure 1. Workflow of a CRISPR/Cas9 experiment.

Materials and methods

CRISPR/Cas9 on different cell lines

Three gRNAs targeting exon 1 of the **ACOT8** gene, two gRNAs targeting exon 1 of **HADHA**, three gRNAs targeting exons 1, 2 and 5 of **FBXW11** were designed and separately cloned into Cas9-expressing plasmids. HEK293T were transfected with each single ACOT8-gRNA and with a pool of the 3gRNA-targeting ACOT8 by TransIT-LT1 (Mirus). Cells were selected with 0.5ug/ml puromycin. Single cell cloning was then performed by single cell dilutions. Genomic DNA was extracted and PCR-amplified with sequencing primers spanning a 244 bp-fragment encompassing the target region of the three gRNAs. Amplicons were then analysed by Sanger sequencing to verify the presence of indels.
PANC-1 cells were transfected with 2gRNA-targeting HADHA by Lipofectamine3000 and selected with 2 ug/ml puromycin for 5 days. Single cell cloning was then performed by single cell dilutions in order to isolate monoclonal cells. Western Blot was performed on cell lysates of clones to evaluate the absence of the protein product. PCR on edited clones was performed with sequencing primers that amplify a 347-bp fragment surrounding the target region of the two gRNAs. Sanger sequencing was carried out on the purified amplicon.
Transfection efficiency on MG63 cells was firstly evaluated by GFP transfection by using Lipofectamine3000, TransIT-LT1, nucleofection.
MG63 cells and HEK293T were then transfected with 3gRNA-targeting FBXW11 by TransIT-LT1 and Sanger sequencing was performed on the cell pool.

Results

1. Generation of ACOT8 KO HEK293T cells

We analysed 15 clones derived from single and pooled ACOT8-gRNA transfection (3 gRNA_1-, 2 gRNA_2-, 7 gRNA_3-, 3 gRNA_pooled - derived clones). For these 15 clones, Sanger sequencing showed homozygous editing for 7 clones (46,7%), heterozygous editing for 8 clones (53,3 %), while none of them was WT (0%).
4 homozygous-edited clones presenting frameshift deletions were selected for further analysis. Figure 2 shows clone C7, presenting a 2bp-deletion resulting in a premature stop codon on exon 1.

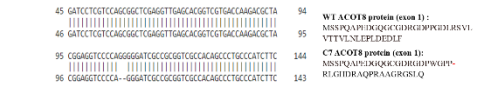

Figure 2. Alignment of C7 clone to the WT and protein translation. Clone C7 shows a 2bp-deletion resulting in a premature stop codon on exon 1.

2. Generation of HADHA KO PANC-1 cells

Among different clones tested by Western blot, only one (C8E12) showed absence of the HADHA protein band (Fig. 3).

The effective knockout was confirmed by Sanger sequencing that revealed a 124-bp frameshift deletion on the first allele removing part of exon 1 and intron 1 and a 78-bp deletion on the second allele eliminating almost entirely exon 1, including disruption of start codon and Kozak sequence. Alignment of the edited sample with reference WT sequence is shown in Figure 4.

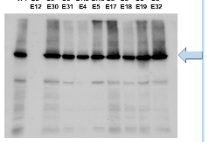

Figure 3. WB on the isolated clones. Only one clone (C8E12) showed absence of the HADHA protein.

Figure 4. Alignment of the edited sample to the WT. Allele 1 shows a 124bp-deletion, while allele 2 has a 78-deletion.

3. CRISPR/Cas9 on FBXW11 gene for MG63 cells

Transfection efficiency on MG63 cells was tested with GFP plasmid after transfection with Lipofectamine3000, TransIT-LT1 and nucleofection. All the tested conditions gave good efficiency results (Fig. 5).

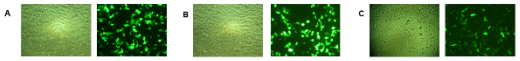

Figure 5. Transfection efficiency on MG63 cells. GFP transfection with Lipofectamine (A), TransIT-LT1 (B) and nucleofection (C) showed a good efficiency.

Sanger sequencing on pool MG63 and HEK293T after TransIT-LT1 transfection with 3gRNA-targeting FBXW11 showed no CRISPR/Cas9 genome editing for MG63 in any of the guide-targeted region, while HEK293T showed the desidered modifications.

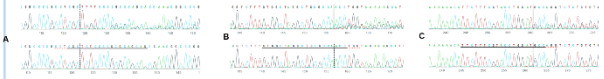

Figure 6. Sanger sequencing on pool MG63 and HEK293T. No editing events were observed for MG63 cells (second lane), while HEK293T appear edited (first lane) for any of gRNA targeted exons 1, 2 and 5 (A,B,C respectively) of FBXW11 gene.

Discussion

HEK293T cells were transfected at a great efficiency, resulting in several edited clones. ACOT8 KO clones presenting homozygous and frameshift indels will be used for better depicting HIV-1-host cell interaction.
Among different PANC-1 clones, only one resulted KO for HADHA gene. The absence of the HADHA protein on the growth of pancreatic cancer stem cells will be evaluated.
Despite a good efficiency after transfection with the GFP-plasmid, MG63 did not show genomic editing events in any of the guide-targeted regions. In a CRISPR/Cas9 experiment, it is also possible that transfected cells undergo apoptosis due to knockout of essential genes or activation of p53-related pathways after double-strand breaks. Since HEK293T have been successfully edited for this gene and MG63 cells are reported to be p53-defective[5], the lack of genome editing should mostly be attributed to an inefficient transfection. Lentiviral transduction will be considered to generate FBXW11 KO MG63 cells, that will be used to study the role of FBXW11 in osteosarcoma.

References

[1] Giuliano, C. J. *et al.* (2019) 'Generating Single Cell–Derived Knockout Clones in Mammalian Cells with CRISPR/Cas9', *Current Protocols in Molecular Biology*, 128(1). doi: 10.1002/cpmb.100

[2] Sereda, M. *et al.* (2016) 'Molecular characterization of HIV-1 Nef and ACOT8 interaction: Insights from in silico structural predictions and in vitro functional assays', *Scientific Reports*, 6(February), pp. 1–13. doi: 10.1038/srep22319.

[3] Di Carlo, C. *et al.* (2021) 'Integrated lipidomics and proteomics reveal cardiolipin alterations, upregulation of HADHA and long chain fatty acids in pancreatic cancer stem cells', *Scientific Reports*, 11(1), pp. 1–13. doi: 10.1038/s41598-021-92752-5.

[4] Dalle Carbonare, L. *et al.* (2023) 'Expression of FBXW11 in normal and disease-associated osteogenic cells', *Journal of Cellular and Molecular Medicine*, 27(11), pp. 1580–1591. doi: 10.1111/jcmm.17767.

[5] Hu, X. *et al.* (2010) 'The expression and significance of IDH1 and p53 in osteosarcoma', *Journal of Experimental and Clinical Cancer Research*, 29(1), pp. 1–10. doi: 10.1186/1756-9966-29-13.

mauro.voi@univr.it

PhD Day - University of Verona – 25 September 2023

CRISPR Medicine Media Aps, Kong Georgs Vej 12, 2000 Frederiksberg, Denmark

jbock@crisprmedicinenews.com, +45 24207221, DK-39130327

The CRISPR MEDiCiNE Conference 2025

Certificate of Attendance at CRISPRMED25 for Mauro Voi

University of Verona, Italy

2025-04-22

To whom it concerns,

On behalf of the organisers of The CRISPR MEDiCiNE Conference 2025, CRISPRMED25, which was held virtually (online) on 7th April 2025, and in-person at Øksnehallen, Halmtorvet 11, 1700, Copenhagen, Denmark, phone +45 33 29 80 00, from April 8 – 11, 2025, I confirm Mauro Voi's attendance in the CRISPRMED25 virtual event on 7th April 2025.

The conference brought together an international group of scientists from the gene-editing community to exchange information in both oral and poster presentations, as well as networking and social events.

For more information about the conference, see:

https://event.fourwaves.com/crisprmed25/pages

Sincerely,

Jens-Ole Bock

Jens-Ole Bock

Founder of CRISPR Medicine News, CMN and Organiser of CRISPRMED25

CRISPR Medicine Media Aps

Kong Georgs Vej 12, Frederiksberg, Denmark

Company number: DK-39130327

Phone Number: +45 24207221 | Email: jbock@crisprmedicinenews.com

Certificate of attendance –

CRISPRMED25 – 7 April 2025

Certificate of participation – CRISPR-Cas Genome Editing: Workflow, Tools and Techniques - Workshop – 28-30 November 2023